

University of Massachusetts Medical School

eScholarship@UMMS

GSBS Dissertations and Theses

Graduate School of Biomedical Sciences

2015-06-11

Identifying, Targeting, and Exploiting a Common Misfolded, Toxic Conformation of SOD1 in ALS: A Dissertation

Melissa S. Rotunno

University of Massachusetts Medical School

Let us know how access to this document benefits you.

Follow this and additional works at: https://escholarship.umassmed.edu/gsbs_diss



Part of the [Biochemistry, Biophysics, and Structural Biology Commons](#), [Genetics and Genomics Commons](#), [Nervous System Diseases Commons](#), and the [Neuroscience and Neurobiology Commons](#)

Repository Citation

Rotunno MS. (2015). Identifying, Targeting, and Exploiting a Common Misfolded, Toxic Conformation of SOD1 in ALS: A Dissertation. GSBS Dissertations and Theses. <https://doi.org/10.13028/M2M59V>.

Retrieved from https://escholarship.umassmed.edu/gsbs_diss/781

This material is brought to you by eScholarship@UMMS. It has been accepted for inclusion in GSBS Dissertations and Theses by an authorized administrator of eScholarship@UMMS. For more information, please contact Lisa.Palmer@umassmed.edu.

**IDENTIFYING, TARGETING AND EXPLOITING A COMMON MISFOLDED,
TOXIC CONFORMATION OF SOD1 IN ALS**

A Dissertation Presented

By

Melissa S. Rotunno

Submitted to the Faculty of the

University of Massachusetts Graduate School of Biomedical Sciences, Worcester

in partial fulfillment of the requirements for the degree of

DOCTOR OF PHILOSOPHY

June 11, 2015

Biochemistry and Molecular Pharmacology

**IDENTIFYING, TARGETING AND EXPLOITING A COMMON MISFOLDED,
TOXIC CONFORMATION OF SOD1 IN ALS**

A Dissertation Presented By
Melissa S. Rotunno

The signatures of the Dissertation Defense Committee signify
completion and approval as to style and content of the Dissertation

Daryl A. Bosco, Ph.D., Thesis Advisor

Robert H. Brown Jr., Ph.D., MD, Member of Committee

William Royer, Ph.D., Member of Committee

Haining Zhu, Ph.D., Member of Committee

The signature of the Chair of the Committee signifies that the written dissertation
meets the requirements of the Dissertation Committee

Jill Zitzewitz, Ph.D., Chair of Committee

The signature of the Dean of the Graduate School of Biomedical Sciences
signifies that the student has met all graduation requirements of the school.

Anthony Carruthers, Ph.D.,
Dean of the Graduate School of Biomedical Sciences

Biochemistry and Molecular Pharmacology
June 11, 2015

For my husband, who not only turned me on to science many years ago but who has supported, helped and encouraged me throughout this journey.

ACKNOWLEDGEMENTS

First and foremost, I would like to thank my mentor, Daryl Bosco, who consistently guided and pushed me to my full potential as a scientist. I am incredibly lucky to have stumbled upon her lab. I am forever grateful to her for her insight and constructive criticism. She is a strong, passionate scientist who I hope to emulate. I could not have asked for a better mentor.

Second, I would like to thank the entire Bosco lab for their constant support, Catherine Ward, Reddy Sama, Laura Kaushansky, Sivakumar Boopathy, Maeve Tischbein, and Desiree Baron. I am thankful to have pursued my doctorate in a lab environment where troubleshooting is a group effort, input is constantly offered, and ideas are shared freely.

I would like to thank my TRAC, Zuoshang Xu, William Royer, Robert H. Brown, and my chair, Jill Zitzewitz. Their helpful suggestions and discussions over the years have been very beneficial, to say the least. From the beginning, they were vested in my project with a willingness to devote their time and/or resources to advance my research. Thank you to Haining Zhu as well for taking the time to participate in my defense.

I would also like to thank Jared Auclair (Northeastern University) and the UMass Proteomics and Mass Spectrometry Facility, specifically Kristin Boggio, John Leszyk, and Scott Shaffer. They have always offered help and taken time out of their day to explain detailed methods and data interpretation without

hesitation. Although I have plenty more to learn, by devoting their time to me, they have given me a solid mass spec base to expand on in the future.

Lastly, I would like to thank my family and friends for their support over the years. I would especially like to thank my mom whose love and encouragement was welcomed at every turn.

ABSTRACT

Amyotrophic lateral sclerosis (ALS) is a neurodegenerative disease characterized by a loss of voluntary movement over time, leading to paralysis and death. While 10% of ALS cases are inherited or familial (FALS), the majority of cases (90%) are sporadic (SALS) with unknown etiology. Approximately 20% of FALS cases are genetically linked to a mutation in the anti-oxidizing enzyme, superoxide dismutase (SOD1). SALS and FALS are clinically indistinguishable, suggesting a common pathogenic mechanism exists for both types. Since such a large number of genetic mutations in *SOD1* result in FALS (>170), it is reasonable to suspect that non-genetic modifications to SOD1 induce structural perturbations that result in ALS pathology as well. In fact, misfolded SOD1 lacking any genetic mutation was identified in end stage spinal cord tissues of SALS patients using misfolded SOD1-specific antibodies. In addition, this misfolded WT SOD1 found in SALS tissue inhibits axonal transport *in vitro*, supporting the notion that misfolded WT SOD1 exhibits toxic properties like that of FALS-linked SOD1. Indeed, aberrant post-translational modifications, such as oxidation, cause WT SOD1 to mimic the toxic properties of FALS-linked mutant SOD1. Based on these data, I hypothesize that modified, misfolded forms of WT SOD1 contribute to SALS disease progression in a manner similar to FALS-linked mutant SOD1 in FALS. The work presented in this dissertation supports this hypothesis. Specifically, one common misfolded form of SOD1 is defined and exposure of this toxic region is shown to enhance SOD1 toxicity. Preventing

exposure, or perhaps stabilization, of this “toxic” region is a potential therapeutic target for a subset of both familial and sporadic ALS patients. Further, the possibility of exploiting this misfolded SOD1 species as a biomarker is explored. For example, an over-oxidized SOD1 species was identified in peripheral blood mononuclear cells (PBMCs) from SALS patients that is reduced in controls. Moreover, 2-dimensional gel electrophoresis revealed a more negatively charged species of SOD1 in PBMCs of healthy controls greatly reduced in SALS patients. This species is hypothesized to be involved in the degradation of SOD1, further implicating both misfolded SOD1 and altered protein homeostasis in ALS pathogenesis.

TABLE OF CONTENTS

APPROVAL	II
DEDICATION	III
ACKNOWLEDGEMENTS	IV
ABSTRACT	VI
TABLE OF CONTENTS	VIII
LIST OF TABLES	X
LIST OF FIGURES	XI
LIST OF ABBREVIATIONS	XIV
PREFACE	XV
CHAPTER I: INTRODUCTION	1
AMYOTROPHIC LATERAL SCLEROSIS (ALS)	1
<i>Clinical Overview</i>	1
<i>Genetic and Environmental Factors</i>	2
<i>Insights into Disease Pathogenesis and Mechanism</i>	4
CU, ZN-SUPEROXIDE DISMUTASE (SOD1)	9
<i>Structure and Function of the SOD1 Holoenzyme</i>	9
<i>Normal Post-translational Modifications of SOD1</i>	10
<i>A Role for SOD1 in Cell Signaling</i>	14
MECHANISMS OF SOD1 IN FAMILIAL ALS	16
<i>Evidence of Misfolding in FALS-linked Mutant SOD1</i>	16
<i>Toxic Functions of FALS-linked SOD1</i>	19
SOD1 AND SPORADIC ALS	23
<i>Evidence for a Role of SOD1 in SALS</i>	23
<i>Loss of native SOD1 PTMs Results in WT SOD1 Misfolding</i>	27
<i>Aberrant Post-Translational Modifications Induce WT SOD1 Misfolding</i>	29
<i>Misfolded WT SOD1 Proteins are Toxic and Mimic FALS-linked SOD1</i>	30
SUMMARY	34
CHAPTER II: IDENTIFICATION OF A MISFOLDED REGION IN SOD1 THAT IS EXPOSED IN ALS	36
INTRODUCTION	36
RESULTS	38
<i>C4F6 is selective for misfolded forms of SOD1 over native wild-type SOD1</i>	38
<i>Hot-spots for C4F6 cross-linking are located within the electrostatic and zinc binding loops of misfolded SOD1 variants</i>	40
<i>Misfolding of loops IV and VII within ALS-linked SOD1 variants exposes the C4F6 epitope</i>	47

<i>Exposure of the C4F6 epitope within SOD1 correlates with microglial activation....</i>	50
<i>Enhancing the metal occupancy of SOD1 reduces exposure of the C4F6 epitope.</i>	54
<i>Identification of key SOD1 residues required for C4F6 binding.....</i>	57
DISCUSSION.....	64
MATERIALS AND METHODS	68
CHAPTER III: EXPLOITING SOD1 AS A POTENTIAL BIOMARKER.....	78
INTRODUCTION.....	78
RESULTS	79
<i>C4F6 ELISA detects misfolded SOD1</i>	79
<i>SOD1 protein is elevated in the CSF of ALS patients.....</i>	82
<i>A subset of SALS patients' sera harbors misfolded SOD1.....</i>	84
<i>SOD1 isolated from SALS patients displays toxic properties</i>	86
<i>No conformational differences in SOD1 from SALS patients detected by limited proteolysis.....</i>	87
<i>A subpopulation of SOD1 is greatly reduced in SALS.....</i>	91
<i>An over-oxidized SOD1 species is present in SALS PBMCs</i>	100
DISCUSSION.....	111
MATERIALS AND METHODS	120
CHAPTER IV: DISCUSSION.....	127
SOD1-BASED THERAPEUTICS	129
<i>Immunization Strategies Targeting SOD1</i>	131
<i>Decreasing Expression of SOD1</i>	133
<i>Small Molecules Targeting Misfolded SOD1</i>	136
OTHER PROMISING FUTURE THERAPEUTICS.....	137
PROTEIN MISFOLDING AND ALS.....	141
<i>Evidence of Altered Protein Homeostasis.....</i>	141
<i>The Additive Effect of Aging.....</i>	142
CONCLUSION	144
APPENDIX I: INVESTIGATING A CAUSATIVE ROLE FOR WT SOD1 IN SPORADIC ALS.....	147
APPENDIX II: REVERTING THE ALS-LINKED MISFOLDED SOD1 TO ITS NON-TOXIC WILD-TYPE CONFORMATION.....	164
APPENDIX III: POST-TRANSLATIONAL MODIFICATION BY CYSTEINE PROTECTS CU/ZN-SUPEROXIDE DISMUTASE FROM OXIDATIVE DAMAGE.	178
APPENDIX IV: CYSTEINYLATION OF SOD1 MAY PROTECT AGAINST MISFOLDED SOD1	188
REFERENCES.....	190

LIST OF TABLES

Chapter I

Table I-1 – Antibodies that recognize misfolded conformations of SOD1

Chapter II

Table II-1 – Apparent dissociation constants (K_d) of the C4F6/SOD1 interaction as determined by the OCTET system

Table II-2 – Amino acids that cross-link in the C4F6/SOD1 complex

Chapter III

Table III-1 – Characteristics of participants providing blood for SOD1 analysis

Table III-2 – Relative abundance of SOD1 peptides identified by Mass Spectrometry

Appendix II

Table AII-1 – Promising compounds identified in C4F6-ELISA LOPAC Screen

Appendix III

Table AIII-1 – Amount of SOD1 Cysteinylylated Using Different Purification Procedures and from Different Sources

LIST OF FIGURES

Chapter I: Introduction

Figure I-1 – Structural features of SOD1

Figure I-2 – The putative normal function of the native WT SOD1 protein

Figure I-3 – Conformation specific antibodies highlight regions exposed in SOD1 upon misfolding

Figure I-4 – The toxic properties shared by ALS-linked mutant SOD1 and modified WT-SOD1

Chapter II: Identification of a Misfolded Region in SOD1 that is Exposed in ALS

Figure II-1 – C4F6 specifically cross-links to misfolded SOD1 in the presence of DSP or EDC

Figure II-2 – C4F6 cross-links to loops IV and VII within misfolded SOD1

Figure II-3 – Metal analyses reveal deficient metal coordination in ALS-linked and loop-deletion SOD1 variants

Figure II-4 – Deletion of loops IV and VII exposes the C4F6 epitope

Figure II-5 – Exposure of the C4F6 epitope correlates with elevated SOD1-mediated microglial activation

Figure II-6 – The metallation status of SOD1 inversely correlates with C4F6 reactivity

Figure II-7 – Amino acids D92 and D96 in SOD1^{ΔIV/ΔVII} are required for C4F6 binding

Figure II-8 – Amino acids D92 and D96 in full-length SOD1 variants are required for C4F6 binding

Chapter III: Exploiting SOD1 as a Potential Biomarker

Figure III-1 – Detection of misfolded SOD1 utilizing a C4F6-based ELISA

Figure III-2 – Quantification of SOD1 in Cerebrospinal fluid by ELISA

Figure III-3 – Quantification of misfolded SOD1 in sera by ELISA

Figure III-4 – SOD1 immunopurified from brain and spinal cord of sporadic ALS patients inhibits axonal transport

Figure III-5 – Unaltered digestion patterns of SOD1 purified from SALS and control human tissue

Figure III-6 – Human red blood cells (RBC) contain modified SOD1 protein

Figure III-7 – Phosphorylation and deamidation are present on SOD1 isolated from RBCs

Figure III-8 – PBMCs isolated from control cases harbor an SOD1 species greatly reduced in SALS

Figure III-9 – Immunoprecipitated SOD1 from Control PBMCs contains Spot 2

Figure III-10 – Tryptophan oxidation at residue 32 of SOD1 is elevated in SALS PBMCs

Figure III-11 – Histidine oxidation to 2-oxo-histidine is present on PBMCs isolated from control and SALS samples

Figure III-12 – Histidine oxidation to aspartic acid is unique to SOD1 in PBMCs isolated from controls

Chapter IV: Discussion

Figure IV-1 – PTM-linked and FALS-linked SOD1 share a common misfolded conformation

Figure IV-2 – Therapeutic Strategies for SOD1-linked ALS

Figure IV-3 – Protein Misfolding, aging, and ALS

Appendix I: Investigating a Causative Role for WT SOD1 in Sporadic ALS

Figure AI-1 – Schematic of SOD1 activity assay

Figure AI-2 – SOD1 proteins are stable for up to 28 days in osmotic pumps

Figure AI-3 – SOD1 proteins retain activity for 28 days in osmotic pumps

Figure AI-4 – Oxidized SOD1 exhibits reduced activity compared to WT SOD1

Figure AI-5 – Mass spectrometry identifies Fluoro488-tagged species of SOD1

Figure AI-6 – Osmotic pumps effectively deliver SOD1 protein to the spinal cord of implanted mice

Figure AI-7 – No decline in mass is observed for mice treated with SOD1 variants

Appendix II: Reverting the ALS-linked Misfolded SOD1 to its Non-toxic Wild-Type Conformation

Figure AII-1 – Initial small molecule screen, LOPAC®1280, identifies six compounds capable of reducing C4F6-ELISA signal

Figure AII-2 – Independent verification of lead compounds with a Dose-Response analysis

Figure AII-3 – Verification of the lead compound, MRS2211, using an alternative sandwich ELISA approach

Figure AII-4 – MRS2211 attenuates C4F6 reactivity in all ALS-linked SOD1 variants tested

Figure AII-5 – Optimized C4F6-ELISA identifies 6 potential compounds to repair misfolded SOD1

Appendix III: Post-translational modification by cysteine protects Cu/Zn-superoxide dismutase from oxidative damage

Figure AIII-1 – Cysteinylation, a prevalent post-translational modification of SOD1 in human nervous tissue

Figure AIII-2 – Cysteinylation and peroxide-mediated oxidations accounting for the majority of observed SOD1, purified from human tissue, post-translational modifications

Figure AIII-3 – Cysteinylation protecting SOD1 from oxidation

Figure AIII-4 – SOD1 Cys111, the site of cysteinylation

Appendix IV: Cysteinylation of SOD1 may protect against misfolded SOD1

Figure AIV-1 – Cysteinylation of recombinant SOD1 results in a decrease in C4F6 reactivity

LIST OF ABBREVIATIONS

2D-GE – 2-dimensional gel electrophoresis
ALS – Amyotrophic lateral sclerosis
ALSFR – ALS functional rating score
CCS – copper chaperone for SOD1
CD – circular dichroism
CID – collision induced dissociation
CNS – central nervous system
CSF – Cerebrospinal Fluid
Ctl – Control
DSF – differential scanning fluorimetry
DSP – dithiobis[succinimidyl propionate]
EDC – 1-ethyl-3-[3-dimethylaminopropyl]carbodiimide hydrochloride
ERAD – ER-associated degradation
FALS – Familial amyotrophic lateral sclerosis
FAT – fast axonal transport
FTLD – frontotemporal lobar dementia
H/D exchange – hydrogen/deuterium exchange
HCD – higher-energy collisional dissociation
ITC – isothermal titration calorimetry
Loop IV– Zinc Binding loop
Loop VII – Electrostatic loop
LPS – lipopolysaccharide
NMR – nuclear magnetic resonance
PBMCs – Peripheral Blood Mononuclear Cells
PBS – phosphate buffered saline
PET – positron emission tomography
PSD – post-source decay
PTM – Post Translational Modification
RBCs – Red Blood Cells
SALS – Sporadic amyotrophic lateral sclerosis
SAT – slow axonal transport
SOD1 – Cu/Zn superoxide dismutase 1
SOD1_{ox} – Oxidized SOD1
SOD1^{ΔIV/ΔVII} – SOD1 lacking the zinc binding and electrostatic loops
TDP-43 – transactive response DNA protein 43 kDa
TNF α – tumor necrosis factor alpha
UPR – Unfolded Protein Response
UPS – Ubiquitin proteasome system

PREFACE

Parts of this dissertation appeared in:

Rotunno, M.S., Auclair, J.R., Maniatis, S., Shaffer, S.A., Agar, J., Bosco, D.A., "Identification of a Misfolded Region in Superoxide Dismutase 1 that is Exposed in Amyotrophic Lateral Sclerosis." *Journal of Biological Chemistry*. 2014, 289, 28527-28538.

Rotunno, M.S., Bosco, D.A., "An emerging role for misfolded wild-type SOD1 in sporadic ALS pathogenesis." *Frontiers in Cellular Neuroscience*. 2013, 7, 253.
Invited review.

Auclair, J.R., Johnson, J.L., Liu, Q., Salisbury, J.P., Rotunno, M.S., Petsko, G.A., Ringe, D., Brown Jr., R.H., Bosco, D.A., Agar, J.N. "Post-translational Modification by Cysteine Protects Cu/Zn-Superoxide Dismutase from Oxidative Damage." *Biochemistry*. 2013, 52, 6137-44.

PREFACE TO CHAPTER I:**Parts of this chapter appeared in:**

Rotunno, M.S., Bosco, D.A., "An emerging role for misfolded wild-type SOD1 in sporadic ALS pathogenesis." *Frontiers in Cellular Neuroscience*. 2013, 7, 253. Invited review.

CHAPTER I: INTRODUCTION

Amyotrophic Lateral Sclerosis (ALS)

Clinical Overview

Amyotrophic Lateral Sclerosis (ALS) is a debilitating neurodegenerative disease with 5,000 new cases diagnosed each year in the United States (<http://wwwn.cdc.gov/ALS/>). Conditions begin mildly, with onset occurring either as bulbar or limb with a slight male preference (1.5:1, (Yoshida et al. 1986)). Bulbar onset starts with difficulty swallowing and/or chewing as where limb onset tends to be realized when the patient trips and/or falls from muscle weakness in the legs (Kiernan et al. 2011). The mild muscle weakness quickly progresses to a gross loss of voluntary muscle movement (e.g., walking, speaking, breathing). Like Alzheimer's disease, ALS primarily effects the aging population with an average onset of 60, but there are also earlier documented cases with an onset as young as 25 years of age. Some patients can live for decades with this disease, but typically ALS progresses fast, with death occurring within 3-5 years of diagnosis.

An overlooked aspect of the disease is the intense pain that the majority of patients experience during progression. This pain is a side effect of the neuronal death and muscle wasting known to occur in ALS pathogenesis and is caused by such symptoms as joint inflammation and muscle cramping (Handy et al. 2011). Medication directed at calming muscle spasms, such as Baclofen are prescribed in some cases. Unfortunately, even though medications are prescribed to deal

with many of the symptoms associated with ALS, such as depression, sialorrhea, muscle cramping and stiffness, studies directed at finding better treatments for these symptoms are lacking (Radunovic et al. 2007, Nakamura et al. 2012). The only FDA approved drug aimed directly at slowing the progression of ALS is Riluzole, extending survival by a mere 3 months (Miller et al. 2012). The ALS community is starving for more effective treatments of this devastating disease.

Genetic and Environmental Factors

Approximately 10% of cases are inherited, or familial (FALS), while the remaining 90% are sporadic (SALS), the majority with unknown etiology. However, the genetic causes of FALS cases are largely known. These FALS-linked genetic mutations are found in genes such as *C9ORF72* (40%, (Dejesus-Hernandez et al. 2011, Renton et al. 2011)), *SOD1* (15%, (Rosen et al. 1993)), *TARDBP* (4%,(Sreedharan et al. 2008)), and *FUS* (4%, (Kwiatkowski et al. 2009, Vance et al. 2009, Renton et al. 2014)). The first genetic link to ALS, discovered in 1993, were mutations in *SOD1* on chromosome 21. Currently, the most prevalent genetic mutation that results in FALS pathology is hexanucleotide expansions in *C9ORF72*, which is thought to contribute to ~40% of FALS cases (Dejesus-Hernandez et al. 2011, Renton et al. 2011). This mutation is an intronic repeat with multiple modes of disease pathogenicity proposed, such as an unknown loss of function mechanism, unconventional repeat associated non-ATG (RAN) translation of the expansion and toxicity of the dipeptide product, and RNA toxicity via RNA foci sequestering RNA binding proteins (Rohrer et al.

2015). C9orf72 hexanucleotide expansions are also the cause of a subset of frontotemporal lobar dementia (FTLD) cases. Why in some cases this expansion results in ALS, some FTLD, and some both is unknown at this time (Cruts et al. 2013). Even within the same family, some members can develop FTLD while others present with ALS, highlighting the complexity of disease pathogenesis.

A “two hit” hypothesis has been put forward for the development of both SALS and FALS. This hypothesis proposes that some individuals have a predisposition to develop ALS, but require a “second hit” such as brain injury, environmental toxins, etc. to develop disease. A debated issue in the field is whether or not traumatic brain injury increases the likelihood of developing ALS in the future (Pearce et al. 2015). Multiple studies have shown a link between repeated brain injury in sports, e.g., football, soccer and boxing, and the development of ALS (Lehman et al. 2012, Kuwahara and Sato 2013). There have also been contradicting reports that show no correlation between brain injury and ALS (Beghi et al. 2010, Turner M. R. et al. 2010). In fact, it has been postulated that the link between professional athletes and ALS may be more tightly linked to the performance enhancing drugs frequently used among them and not the head injury itself (Pearce et al. 2015).

Supporting the “two hit” hypothesis, there are subpopulations with higher frequency of ALS occurrence, likely due to exposure to environmental chemical toxins. One such example is the Gulf War veterans deployed in the Gulf Region

who had a 2-fold increase in the likelihood of developing ALS (Haley 2003a, Horner et al. 2003). The increased susceptibility of Gulf War veterans to develop disease extended far beyond ALS, with 21% experiencing some type of military-linked disease (Haley 2003b). One theory proposed for this increase is exposure to chemical warfare agents such as sarin, an organophosphate nerve agent (Haley et al. 1999, Haley 2003b). This theory has been supported by data showing altered concentrations of paraoxanases in sera of these veterans, which are a group of enzymes involved in hydrolysis of organophosphates (Haley et al. 1999).

Insights into Disease Pathogenesis and Mechanism

ALS is a multifaceted disease involving among others, mitochondrial dysfunction, protein aggregation, protein clearance deficits, chronic inflammation, oxidative stress and excitotoxicity (Barber and Shaw 2010, Sreedharan and Brown 2013). Pinpointing the aspects that are causative in disease, and not simply a byproduct or coping mechanism, has proved challenging. ALS is characterized by severe neuronal loss in the spinal cord and motor cortex (Kawamata et al. 1992). Ubiquitinated inclusions are typically found in end-stage neuronal tissue, specifically in neurons and surrounding glia (Nakano et al. 2004, Mackenzie and Feldman 2005, Mendonca et al. 2006). P62, a ubiquitin binding protein, localizes to these inclusions as well (Nakano et al. 2004, Maekawa et al. 2009, Braak et al. 2010). The presence of both ubiquitin and p62 implicate defective protein clearance mechanisms in disease, as both proteins are

associated with targeting proteins for degradation. Another common component of these inclusions found in ALS is TDP-43 (Maekawa et al. 2009). TDP-43-containing inclusions are not unique to ALS, but are also found in the closely linked FTLD. In fact, approximately 5% of ALS patients have FTLD as well (Neumann et al. 2006, Maekawa et al. 2009), with evidence of some level of cognitive impairment seen in 50% of ALS patients (Ringholz et al. 2005, Rusina et al. 2010, Rohrer et al. 2015).

A chronic state of inflammation is evident both in biofluids, such as CSF and blood (Zhang R. et al. 2005, Kuhle et al. 2009, Zhang R. et al. 2009, Fiala et al. 2010) as well as in the CNS of patients (Turner M. R. et al. 2004). For example, spinal cord tissue from end-stage ALS patients show enhanced microglia activation (Kawamata et al. 1992). In fact, PET imaging technologies are able to detect an increase in microglial activation in the brain of living ALS patients (Turner M. R. et al. 2004). Further, CD4+ and CD8+ lymphocytes are increased in the brain of ALS patients (Kawamata et al. 1992). In the CSF, the proinflammatory cytokines MCP-1 and IL-8 are upregulated (Kuhle et al. 2009). In sera, the proinflammatory cytokine IL-17A is upregulated (Fiala et al. 2010). The cause of this state of chronic inflammation is unknown, but there is evidence for an increase in the endotoxin level in the plasma of ALS patients (Zhang R. et al. 2009), which is a potent activator of the immune system. Interestingly, the chronic injection of endotoxin decreases survival in an ALS mouse model (Nguyen et al. 2004), suggesting the presence of endotoxin in ALS patients may

exacerbate disease. Moreover, FALS-linked proteins are prone to misfold and aggregate which, in turn, induces pro-inflammatory responses both *in vitro* and in ALS mouse models (Di Giorgio et al. 2008, Zhao et al. 2010, Haidet-Phillips et al. 2011, Butovsky et al. 2012). These data suggest that FALS-linked proteins may directly induce the chronic neuroinflammation observed in patients.

ALS mouse models show increased survival when treated with inflammatory modulators, arguing for a link between chronic inflammation and ALS progression (Tikka et al. 2001, Drachman et al. 2002, Kriz et al. 2002, Van Den Bosch et al. 2002). Minocycline, for example, inhibits microglia activation and proliferation and extends survival in ALS mouse models (Tikka et al. 2001, Kriz et al. 2002, Van Den Bosch et al. 2002). Disheartening clinical trials of minocycline treatment in patients, however, failed to recapitulate the mouse models and, in contrast, seemed to exacerbate disease (Gordon et al. 2007). Nonetheless, glial cells, such as astrocytes and microglia, activated by ALS-linked proteins have proved toxic to motor neurons *in vitro* (Di Giorgio et al. 2008, Zhao et al. 2010, Haidet-Phillips et al. 2011), supporting the notion that gliosis is involved in pathogenesis. Alternatively, the state of neuroinflammation in ALS could be a protective mechanism. Astrocytes are involved in supporting and maintaining the extracellular environment of the CNS (Rothstein et al. 1996). Microglia are thought of as the “macrophage” of the CNS, where they protect the neuronal network through constant perusal and clearance of cellular debris and/or foreign material through phagocytosis. In their activated state, microglia

function as antigen-presenting cells that jumpstart the immune response and even promote repair of neuronal tissue in their post-inflammatory state (Graeber 2010). In support of this, wild-type bone marrow transplanted into ALS mouse models lacking myeloid and lymphoid cell lineages extends survival by providing functional microglia (Beers et al. 2006). In fact, it is quite likely that the initial state of neuroinflammation is protective and switches to neurotoxic at later stages of disease (Liao et al. 2012).

It is becoming increasingly clear that ALS occurs via a non-cell autonomous mechanism where non-neuronal cell types, such as glia, are implicated in pathogenesis. Transgenic mouse models with selective expression of ALS-linked SOD1 in different cell types elucidate the non cell-autonomous nature of ALS pathogenesis. A huge limit of developing mouse models with cell type-specific expression, however, is the dynamic nature of SOD1. SOD1 is a secreted protein, and as such, expression in a single cell type does not translate to mutant SOD1 being present only in that cell type (Mondola et al. 1996, Mondola et al. 1998, Cimini et al. 2002, Mondola et al. 2003). Conversely, excluding a specific cell type from SOD1 expression does not necessarily mean that the cell type is not exposed to SOD1. In the case of SOD1, this is exceedingly clear since multiple cell types have the ability to both secrete and uptake extracellular SOD1 (Mondola et al. 1996, Mondola et al. 1998, Cimini et al. 2002, Mondola et al. 2003, Turner B. J. et al. 2005, Grad et al. 2011, Munch et al. 2011, Sundaramoorthy et al. 2013). This could be one reason exclusive

expression in the skeletal muscle, for example, is adequate for inducing muscle atrophy, neuron degeneration and oxidative stress (Dobrowolny et al. 2008, Wong M. and Martin 2010). However, sole expression of ALS-linked mutant SOD1 in astrocytes of transgenic mice does not induce an ALS-like phenotype, although mild astrogliosis is observed (Gong et al. 2000). In contrast, when ALS-linked SOD1 expression is reduced in the astrocytes of ALS mouse models, survival is extended by 60 days (Yamanaka et al. 2008). The protection observed appears to be through the reduction of microgliosis, as astrogliosis is unaltered in this model. Astrocytes and microglia expressing ALS-linked proteins have been shown to be toxic to cultured neurons *in vitro* (Di Giorgio et al. 2007, Nagai et al. 2007). These data support that glia are not the only culprit in this complex disease, but are actively involved in disease progression (Rossi et al. 2008, Yamanaka et al. 2008).

In the healthy CNS, a protective role for astrocytes in neuronal survival has been well established (Rothstein et al. 1996). Astrocytes are actively involved in protection from neuronal death by excitotoxicity (Rothstein et al. 1996, Schousboe and Waagepetersen 2005, Yi and Hazell 2006), a function that might be lacking in ALS-linked astrocytes. Excitotoxicity, which is a toxic calcium influx caused by the overstimulation of cells by excessive glutamate, is heavily implicated in ALS pathogenesis. GLT-1 (a.k.a. EAAT2), a glutamate transporter preferentially expressed by astrocytes in the CNS that is responsible for the majority of glutamate uptake (Danbolt et al. 1992, Rothstein et al. 1995), is

involved in maintaining neuronal integrity and survival (Rothstein et al. 1996, Tanaka et al. 1997). Animal models lacking GLT-1 have severe neurological deficits (Rothstein et al. 1996, Tanaka et al. 1997). Reduced levels and activity of GLT-1 are seen in ALS patients, likely through a mechanism involving aberrant RNA processing (Rothstein et al. 1992, Rothstein et al. 1995, Lin et al. 1998). Moreover, an increase of glutamate, a side effect of reduced GLT-1 expression, has been found in the CSF of a subset of ALS patients (Shaw P. J. et al. 1995, Spreux-Varoquaux et al. 2002), supporting the notion that excitotoxicity is involved in disease.

Cu, Zn-Superoxide Dismutase (SOD1)

Structure and Function of the SOD1 Holoenzyme

Long before SOD1 was identified as a causative factor in FALS (Rosen et al. 1993), the anti-oxidizing and catalytic properties of native SOD1 were being investigated (McCord and Fridovich 1969). While the role of SOD1 as an anti-oxidizing enzyme is well known and accepted, the role of SOD1 as a signaling molecule has been relatively underappreciated. Herein we discuss what is known regarding the normal functions of SOD1 in the context of both anti-oxidation and signaling. The normal physiological properties of SOD1 are discussed in order to establish a foundation for the following sections that describe how both FALS-linked mutations and post-translational modifications alter the structure and function of the protein.

Copper,zinc- superoxide dismutase-1 (SOD1) is a member of the human SOD family of proteins, which also includes SOD2 and SOD3. While all three proteins function as anti-oxidizing enzymes that catalyze the dismutation of superoxide radicals ($O_2\cdot^-$) to hydrogen peroxide (H_2O_2), they are distinct proteins with unique characteristics (Zelko et al. 2002). SOD1 is highly abundant, comprising ~1% of total protein in the cell (Pardo et al. 1995), and resides mainly in the cytosol with some degree of localization in the mitochondrial inner membrane space (Fukai and Ushio-Fukai 2011). The mitochondrion is also home to SOD2, which is localized to the mitochondrial matrix. In contrast to both SOD1 and SOD2, SOD3 is predominately located outside the cell in the extracellular matrix. Other key differences amongst the SOD proteins include their quaternary structures and mechanism of superoxide dismutation: SOD1 is a homodimer while SOD2 and SOD3 are homotetrameric proteins; SOD1 and SOD3 catalyze the dismutation of $O_2\cdot^-$ through the alternate reduction and reoxidation of Cu^{2+} , whereas SOD2 utilizes manganese (Mn) as a redox active transition metal for this purpose. The role of SOD in FALS, which will be discussed in detail below, is specific to the SOD1 isoform as there is no compelling evidence supporting the involvement of either SOD2 or SOD3 in FALS pathogenesis (Tomkins et al. 2001).

Normal Post-translational Modifications of SOD1

While coordination of copper to SOD1 is required for dismutation of $O_2\cdot^-$, other post-translational modifications, such as Zn^{2+} coordination (Kayatekin et al. 2008)

and disulfide oxidation, help create a mature and structurally stable protein. The 32 kDa homodimeric SOD1 protein adopts an eight-stranded Greek key beta-barrel structural motif (**Fig. I-1**). Two functional loops are present in SOD1: the electrostatic loop that guides superoxide into the redox active site where Cu^{2+} is located and the zinc-binding loop. All told, each SOD1 molecule coordinates two copper and two zinc atoms, one of each per subunit. A unique functional feature of SOD1 is the presence of an intrasubunit disulfide bond between Cys57 and Cys146 (C57-C146), which is unusual for proteins that reside in the highly reducing environment of the cytosol. Both copper coordination and formation of C57-C146 is facilitated by the cytosolic copper carrier protein CCS (copper chaperone for SOD1) (Furukawa et al. 2004, Seetharaman et al. 2009). A recent study utilizing both electrospray ionization mass spectrometry (ESI-MS) and nuclear magnetic resonance (NMR) spectroscopy support a step-wise model for SOD1 maturation: i) SOD1 is loaded with Zn, ii) heterodimerization between SOD1 and CCS, iii) Cu is transferred from CCS to SOD1, iv) C57-C146 is formed and v) SOD1 homodimerization (Banci et al. 2012b). Together these post-translational modifications produce a highly stable protein, as evidenced by a high melting temperature (T_m) of $\sim 92^\circ\text{C}$ and resistance to denaturation in both 6 M GdmCl and 4% SDS (Forman and Fridovich 1973, Bartnikas and Gitlin 2003, Chattopadhyay and Valentine 2009). Demetallation of SOD1 and/or reduction of C57-C146 destabilizes the protein and drastically decreases the melting

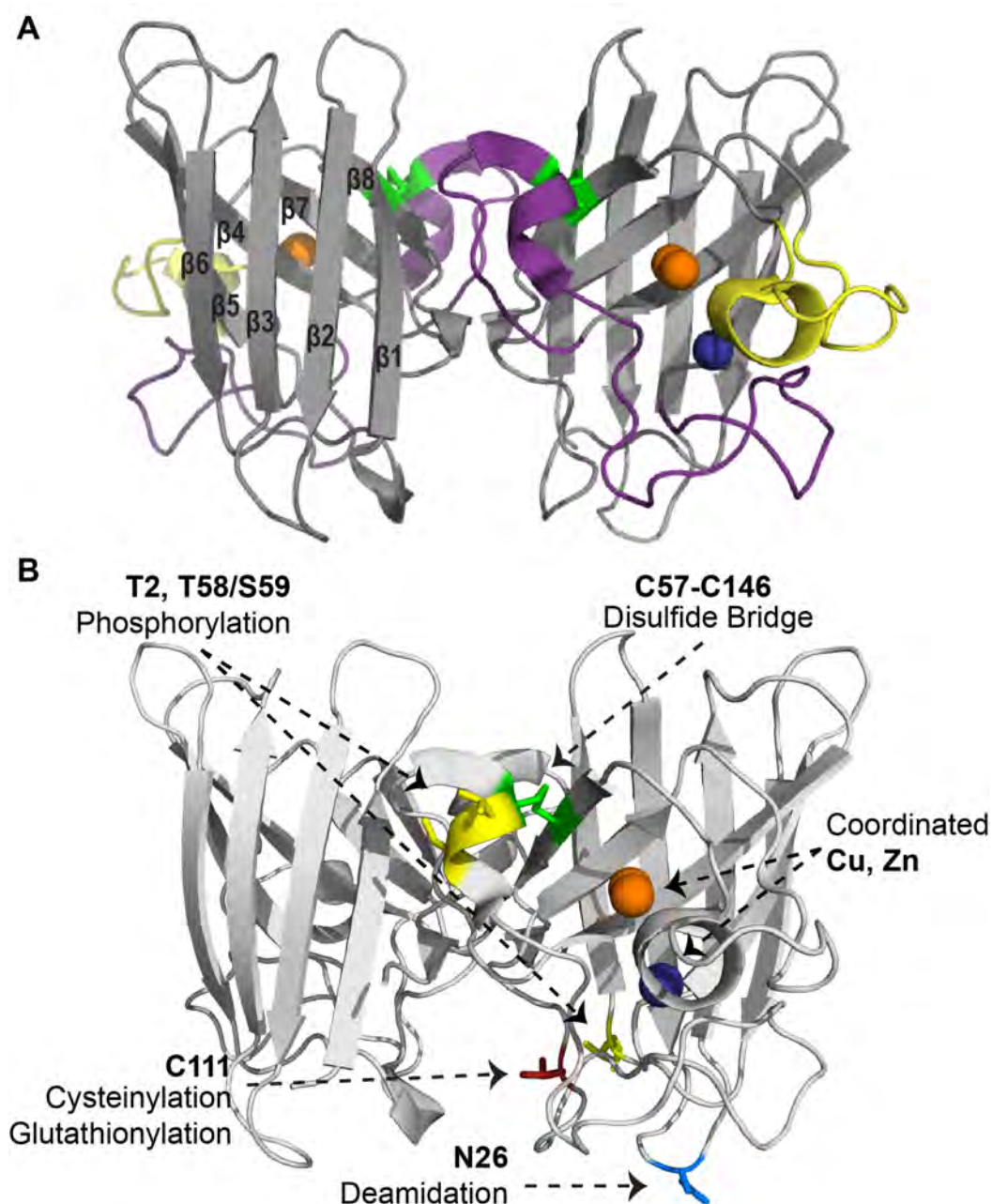


Figure I-1. Structural features of SOD1. (A,B) SOD1 is a homodimer with 1 copper (orange sphere) and one zinc (blue sphere) per subunit (PDB:2C9V). SOD1 consists of 8 beta sheets that form the beta barrel core. An intramolecular disulfide bond (C57-C146; green) stabilizes the protein structure. (A) The major functional loops are the zinc binding loop (purple; residues 49-81) and electrostatic loop (yellow; residues 124-139). (B) Additional modifications that have been identified within native human WT SOD1 include phosphorylation (yellow), deamidation (blue), and cysteinylation/glutathionylation (red).

temperature (Forman and Fridovich 1973, Potter and Valentine 2003, Furukawa and O'Halloran 2005, Chattopadhyay and Valentine 2009). As will be discussed below, these post-translational modifications (PTMs) are compromised by both FALS-linked mutations and oxidation, which in turn destabilize SOD1 in the context of disease.

In addition to PTMs that are directly linked to a mature, functional protein, other modifications have been observed within subpopulations of wild-type SOD1, although their functional importance has not been well established. These PTMs include phosphorylation, glutathionylation, cysteinylolation, and deamidation (**Fig. I-1B**). Phosphorylation, a modification typically involved in switching a protein from an “active” to “inactivate” state, or vice versa, has been observed in SOD1 isolated from erythrocytes (Wilcox et al. 2009). Although the downstream effects of this modification have yet to be established, the history of phosphorylation events in the context of other proteins suggests a functional role.

Evidence supports a destabilization effect with the introduction of glutathionylation onto the side-chain of Cys111 of SOD1 (Wilcox et al. 2009). Glutathionylation promotes monomerization, which is thought to be a precursor of aggregation (Rakhit et al. 2004, Svensson et al. 2010, Redler et al. 2011). Nonetheless, it is found on WT SOD1 isolated from human erythrocytes from non-diseased individuals (Wilcox et al. 2009). In contrast, cysteinylolation of Cys111, a modification identified within SOD1 isolated from human spinal cord

homogenates, protects SOD1 from subsequent oxidation (Auclair et al. 2013b). Although the effect of cysteinylaton on inducing SOD1 aggregation has yet to be determined, the seemingly protective effects of cysteinylaton are likely due to the smaller size of cysteine (121 Da), compared to the larger glutathione (307 Da) that impedes the beta-barrel fold and/or the dimer interface.

A Role for SOD1 in Cell Signaling

The physiological relevance of SOD1 catalysis extends beyond oxidative stress protection (as discussed in (Rotunno and Bosco 2013)). In a zinc deficient environment, for example, SOD1 is implicated in regulating the ER stress response through a mechanism involving Derlin-1 (Homma et al. 2013). Moreover, SOD1 catalysis plays a key role in signal transduction, a function that is largely underappreciated compared to its role as an anti-oxidizing enzyme (**Fig. I-2**, Reviewed in (Rotunno and Bosco 2013)). For instance, H_2O_2 generated by SOD1 can reversibly and specifically react with proteins, generally by oxidizing Cys residues. Cys oxidation in turn alters the biochemical and functional properties of those proteins in a redox dependent manner (Georgiou 2002). A variety of signal transduction pathways are modulated by H_2O_2 , including but not limited to gene expression, cell proliferation, differentiation and death (Rhee 2006, Brown D. I. and Griendling 2009), implicating SOD1 in these pathways as well. NADPH oxygenases (Nox) function as upstream regulators of these signal transduction pathways through the production of $O_2^{\bullet-}$, which is either converted to H_2O_2 spontaneously or catalytically by SOD1. SOD1 comes into

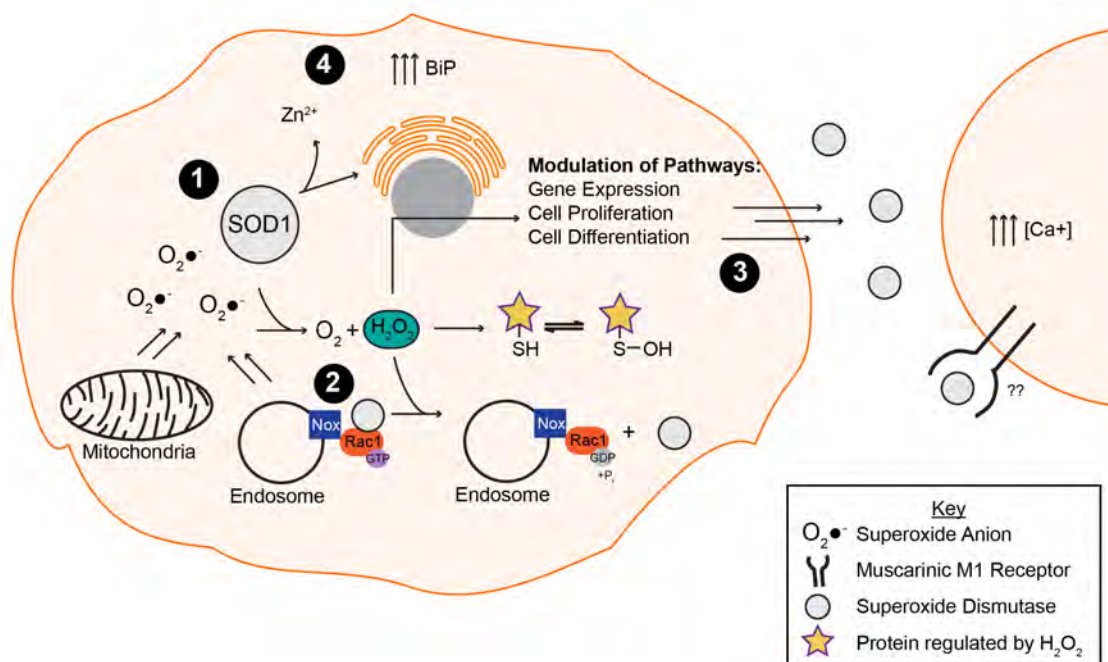


Figure I-2. The putative normal function of the native WT SOD1 protein. (1) SOD1 is responsible for converting the toxic superoxide anion ($O_2^{\bullet-}$) into oxygen (O_2) and hydrogen peroxide (H_2O_2), the latter of which is involved in the modulation of multiple pathways through oxidation of exposed thiols. (2) SOD1 binds and stabilizes Rac1 in its active, GTP bound state, resulting in Nox2 (Nox) activation and superoxide production. The hydrogen peroxide by-product of the dismutase reaction of SOD1 and superoxide anion promotes the disassociation of SOD1 from the Rac1 complex, resulting in Nox inactivation. (3) Secreted SOD1 plays a role in extracellular signaling processes. The presence of extracellular SOD1 leads to an increase in intracellular calcium via a mechanism involving the phospholipase C/protein kinase C pathway. (4) In a zinc deficient environment, SOD1 is involved in activating the ER Stress response (reviewed in (Rotunno and Bosco 2013)).

close proximity with Nox2-derived $O_2^{\bullet-}$ at the surface of endosomes in response to proinflammatory cytokines (Harraz et al. 2008). A report by Harraz et al. demonstrated that SOD1 not only acts downstream of Nox2 but can also modulate Nox function through an interaction with Rac1 (Harraz et al. 2008). SOD1 directly binds and stabilizes the active form of Rac1 in its GTP-bound state, leading to Nox2 activation and $O_2^{\bullet-}$ production. Interestingly, H_2O_2 generated by SOD1 serves as a negative feedback of Nox2 activity: H_2O_2 induces the dissociation of the SOD1/Rac1 complex, thereby inactivating Rac1 and Nox2 (Harraz et al. 2008). The mechanism for how H_2O_2 disrupts the interaction between SOD1 and Rac1 has not been elucidated. One possibility is that the H_2O_2 generated by SOD1, which is in close proximity to Rac1, oxidatively modifies Cys residues within Rac1 in such a way that disrupts the SOD1/Rac1 binding interaction.

Mechanisms of SOD1 in Familial ALS

Evidence of Misfolding in FALS-linked Mutant SOD1

Mutations in the *SOD1* gene, located on chromosome 21, are linked to an estimated 20% of FALS and 3% of SALS cases. Amino acid substitutions in the translated protein, Cu/Zn superoxide dismutase (SOD1) are the most common consequence of these genetic mutations (<http://alsod.iop.kcl.ac.uk/>). Since the majority of ALS-linked mutant-SOD1 proteins maintain their dismutase activity, disease is thought to develop through a gain of a toxic function as opposed to loss of normal function. Support of this hypothesis is evident in mouse models

overexpressing mutant SOD1 that develop ALS-like phenotype in the presence of endogenous mouse SOD1 (Gurney et al. 1994, Dal Canto and Gurney 1995, Bruijn et al. 1997, Dal Canto and Gurney 1997, Watanabe et al. 2001). Moreover, mouse models lacking SOD1 do not develop an ALS-like phenotype, but do show signs of excessive sensitivity to neuronal damage (Reaume et al. 1996), reduced fertility (Ho et al. 1998), and liver cancer (Elchuri et al. 2005).

Currently, more than 170 mutations in *SOD1* have been identified as causative in FALS pathology (<http://alsod.iop.kcl.ac.uk/>). These point mutations span the entire primary sequence of the SOD1 protein arguing for a global susceptibility of SOD1 to cause disease. The gain of toxic function involved in disease pathogenesis remains to be determined, but is likely a result of its inclination to misfold and aggregate due to the destabilization ALS-linked mutations impose on the protein. Molecular mechanisms involving the proteasome system and HDAC6 compete with accumulating aggregates *in vivo*, and in their absence, enhanced aggregation is detected (Gal et al. 2013, Kitamura et al. 2014).

Supporting the notion that FALS-linked SOD1 is destabilized, a reduction in T_m relative to WT SOD1 is observed (Stathopoulos et al. 2006, Vassall et al. 2006). In fact, FALS-linked SOD1 mutants are further destabilized when normal post-translational modifications such as Cu/Zn coordination and C57-C146 oxidation are impaired (Furukawa and O'Halloran 2005, Rodriguez et al. 2005,

Kayatekin et al. 2010, Svensson et al. 2010), demonstrating interconnection between normal post-translational modifications and the stability of SOD1. Additionally, mutant SOD1 exhibits an altered tertiary structure, evidenced by enhanced hydrophobicity compared to WT SOD1 (Tiwari et al. 2005, Munch and Bertolotti 2010). While X-ray crystallography has failed to reveal significant structural differences between WT- and mutant-SOD1 proteins, (Hart et al. 1998, Elam et al. 2003, Hough et al. 2004, Cao et al. 2008, Galaleldeen et al. 2009), solution-based structural studies indicate that FALS-linked mutations induce some degree of SOD1 unfolding, or “misfolding” within the electrostatic and/or zinc loops. For example, NMR relaxation experiments reveal an overall increase in protein dynamics for SOD1 G93A compared to WT SOD1 (Shipp et al. 2003). The region proximal to the G93A mutation, termed the “ β -barrel plug”, as well as residues within the zinc-binding loop exhibited the greatest increase in mobility, whereas the dynamics within the electrostatic loop were comparable between SOD1 G93A and WT (Shipp et al. 2003). Similarly, β -strands 3 and 4, which contain the β -barrel plug, displayed high deuterium exchange rates as assessed by mass spectrometry for several demetallated mutant forms of SOD1 (Durazo et al. 2009). In a separate study using similar methodology but with metallated forms of SOD1, only 1 out of the 13 mutants exhibited relatively high deuterium exchange rates in the β -barrel plug (Molnar et al. 2009). However, this study detected a 10-31% increase in deuterium exchange within the electrostatic loop for 7 out of 8 “WT-like” ALS-linked SOD1 mutants (i.e., mutant-SOD1 proteins

that coordinate Cu and Zn), including G93A. Deuterium exchange increased within both the electrostatic and zinc binding loops for those SOD1 mutants with impaired metal binding (Molnar et al. 2009).

Toxic Functions of FALS-linked SOD1

The structural perturbations present in FALS-linked SOD1 have been hypothesized to induce a more promiscuous protein, promoting aberrant protein-protein interactions. In fact, multiple proteins have been identified that uniquely bind or demonstrate enhanced binding for FALS-linked SOD1 variants over WT SOD1. These “toxic” interactions result in altered signaling pathways, neuroinflammation, apoptosis, axonal transport inhibition, ER stress, and calcium dysregulation.

As discussed above in “A Role for SOD1 in Cell Signaling”, WT SOD1 is involved in the regulation of Nox2 function (Harraz et al. 2008). Altered regulation of Nox2 is a consequence of FALS-linked SOD1 variants. SOD1 FALS-linked mutants (L8Q, G93A) interfere with this process by exhibiting a tighter association with Rac1-GTP thereby preventing GTP hydrolysis. The prevention of GTP hydrolysis results in constitutively activated Rac1 and an increase in Nox2 activation (Harraz et al. 2008). In turn, the cellular response to proinflammatory cytokines (Harraz et al. 2008) that utilizes this regulation mechanism, may be compromised.

Throughout the course of disease in SOD1 G93A transgenic mice, there is an increase in SOD1 associated with Bcl-2, an anti-apoptotic protein (Pasinelli et al. 2004). Moreover, overexpression of Bcl-2 in SOD1 G93A transgenic mice extends survival (Kostic et al. 1997). A study by Pedrini et al. demonstrated mutant SOD1-mediated mitochondrial damage only in the presence of Bcl-2 through exposure of the toxic BH3 domain (Pedrini et al. 2010). When the BH3 domain is exposed, Bcl-2 switches from its normal anti-apoptotic function to pro-apoptotic, an effect likely washed out by the presence of excess anti-apoptotic Bcl-2 as seen in the overexpressing rescue in the G93A mouse model (Kostic et al. 1997).

Transgenic mice expressing SOD1 G93A also exhibit alterations in axonal transport. These models have diminished fast (FAT) and slow axonal transport (SAT) with cargo specificity (Zhang B. et al. 1997, Williamson and Cleveland 1999, Kieran et al. 2005, Shi P. et al. 2010). These axonal transport defects are seen at very early stages, as early as 13 days of gestation (Kieran et al. 2005) arguing for an active role of transport inhibition in the neurodegeneration observed during disease progression. One study utilized time lapse microscopy to analyze FAT in motor neurons derived from SOD1 G93A transgenic mice and found an 80% increase in retrograde axonal transport of mitochondria along with a corresponding decrease in anterograde axonal transport. Additionally, the study showed an inhibition of FAT of membrane bound organelles in both anterograde and retrograde axonal transport (De Vos et al. 2007). The dynein

complex, responsible for retrograde transport, was found to interact with FALS-linked SOD1, and not the wild-type protein (Zhang F. et al. 2007). Moreover, isolated squid axoplasm perfused with mutant SOD1 (H46R, G93A, G85R) inhibits anterograde FAT through a mechanism involving p38 kinase (Morfini G. A. et al. 2013). An increase in phosphorylated p38 is evident in axoplasms exposed to mutant SOD1 (G93A, G85R) compared to normal WT SOD1 (Morfini G. A. et al. 2013). This phosphorylated p38 directly inhibits Kinesin-1, a motor known to be involved with anterograde transport (Morfini G. A. et al. 2013).

Neuronal cultures from SOD1 G93A transgenic mice show signs of UPR activation, a pathway activated in response to ER stress. These signs of UPR activation include activated ATF6 α and spliced XBP1 (Prell et al. 2012). In addition, mammalian cells expressing mutant SOD1 (A4V, G93A, G85R) *in vitro* induce ER stress via an enhanced interaction with Derlin-1 and direct inhibition of ER-associated degradation (ERAD). This interaction traps protein substrates headed for degradation by the UPS in a complex with Derlin-1, which prevents both ubiquitination and translocation to the cytosol (Nishitoh et al. 2008). It should be noted that intracellular expression of mutant SOD1 is not required to cause ER Stress. Another study showed extracellular WT SOD1 and SOD1 G93A are taken up by cultured cells, the latter resulting in ER stress (Munch et al. 2011, Sundaramoorthy et al. 2013). The combination of mutant-SOD1 uptake and intracellular expression in neurons could exacerbate ER stress, thereby causing a switch from the UPR coping pathway to apoptosis *in vivo* (Mondola et

al. 1998, Turner B. J. et al. 2005, Urushitani et al. 2006, Polazzi et al. 2012).

Another adverse side effect of misfolded, FALS-linked mutant SOD1 is altered calcium homeostasis. WT SOD1 has been shown to participate in calcium modulation in multiple cell culture models, even acting as a neuroprotectant in some instances (Carri et al. 1997, Mondola et al. 2004, Allen et al. 2011, Polazzi et al. 2012). Neuroblastoma cells exposed to FALS-linked SOD1 results in a greater increase in intracellular calcium levels compared to cells exposed to WT SOD1 (Carri et al. 1997, Allen et al. 2011). FALS-linked SOD1 has been proposed to modulate intracellular calcium by binding to the membrane surface and forming aberrant ion channels (Mondola et al. 2004, Allen et al. 2011). Moreover, in SOD1 G93A transgenic mice, spinal cord motor neurons have a higher level of intracellular calcium compared to non-affected neurons, such as oculomotor neurons (Siklos et al. 1998). Motor neurons are more sensitive to increased calcium levels in part because of their low cytosolic calcium buffering capacity coupled with a decrease in calcium binding proteins compared to neurons not affected throughout disease (reviewed in (von Lewinski and Keller 2005)). Since motor neurons are more sensitive to changes in calcium levels, and FALS-linked SOD1 alters these levels to a greater extent than WT SOD1, loss of calcium homeostasis could be responsible for the select vulnerability of motor neurons in ALS.

FALS-linked SOD1 has been implicated in inducing chronic neuroinflammation. Direct activation of microglia, the macrophage of the CNS,

via extracellular mutant SOD1 has been observed *in vitro* (Urushitani et al. 2006, Ezzi et al. 2007, Zhao et al. 2010). The mechanism of activation involves binding of mutant-SOD1 to the CD14/TLR receptor, the same pathway used by a known proinflammatory microglia activator, LPS (Zhao et al. 2010). This activation results in a proinflammatory activation state (i.e. increased levels of TNF α and IL-1 β), and toxicity toward cultured motor neurons (Urushitani et al. 2006, Zhao et al. 2010).

SOD1 and Sporadic ALS

Evidence for a Role of SOD1 in SALS

Sporadic ALS has no known etiology and is likely caused by a complex interplay of both genetic and environmental factors. Familial (FALS) and Sporadic (SALS) ALS are clinically indistinguishable, a fact that could be explained by a similar toxic mechanism shared between them. Evidence in other neurodegenerative disease supports the crossover of familial linked proteins to sporadic cases such as phosphorylation of α -synuclein in Parkinson's (Beyer and Ariza 2013) and phosphorylation of tau in Alzheimer's disease (Mandelkow et al. 1996).

Since mutations in SOD1 account for such a large portion of FALS, 20% of cases, we hypothesize that SOD1 plays an active role in sporadic ALS pathology as well. The causative role of SOD1 in FALS has been well established, but its role in sporadic ALS remains controversial. Accumulating evidence from human patient samples, however, supports a role for WT SOD1 in

disease. SOD1 purified from spinal cord tissue of SALS patients, for example, inhibits axonal transport *in vitro* (Bosco et al. 2010). SOD1 is also implicated by the presence of a hyperoxidized SOD1 species in patient derived lymphoblast cell lines (Guareschi et al. 2012). Further, elevated levels of antibodies toward anti-SOD1ox, have been detected in sera from a subset of SALS cases that directly correlates with survival (van Blitterswijk et al. 2011). Antibodies directed at aberrant forms of SOD1 would be expected to have a beneficial effect by neutralizing its toxic properties. Moreover, misfolded SOD1 has been detected in a subset of post-mortem spinal cord tissue slices from SALS patients lacking a mutation in SOD1 using misfolded-SOD1 specific antibodies (**Table I-1**, (Bosco et al. 2010, Forsberg et al. 2010, Pokrishevsky et al. 2012)). Many of these antibodies also recognize misfolded SOD1 induced by FALS-linked SOD1 mutations, suggesting a similar misfolded conformation is shared amongst them.

Multiple antibodies have been developed that selectively react with an altered tertiary structure present in misfolded SOD1 and not exposed in WT SOD1 (**Fig. I-3, Table I-1**). Such antibodies include C4F6 (Urushitani et al. 2006), SEDI (Rakhit et al. 2007), MS785 (Fujisawa et al. 2012), and D3H5 (Gros-Louis et al. 2010), the latter of which has extended survival in the G93A transgenic mouse model. Passive immunization therapies targeting select regions of SOD1 exposed upon misfolding have been shown to decrease the

Table I-1. Antibodies that recognize misfolded conformations of SOD1.

Antibody	SOD1 epitope (aa)	Reactive for FALS SOD1	Reactive for SALS SOD1		Therapeutic Benefits	Reference
			<i>Patient Tissue</i>	<i>Modified SOD1</i>		
B8H10⁵	57-78 ¹	+	nd ²	nd	Nd	(Gros-Louis et al. 2010, Pickles et al. 2013)
C4F6⁵	80-118	+	+	+ (ox)	Nd	(Urushitani et al. 2007, Bosco et al. 2010, Prudencio and Borchelt 2011, Brotherton et al. 2012, Pickles et al. 2013) (Fujisawa et al. 2012)
MS785	6-16	+	nd	+ ³	Nd	(Fujisawa et al. 2012)
D3H5	24-55 ¹	+	nd	+ (apo)	+	(Gros-Louis et al. 2010)
A5C3⁵	80-118 ¹	+	nd	nd	-	(Gros-Louis et al. 2010)
SEDI	143-151	+	-	+ (ox)	+ ⁴	(Rakhit et al. 2007, Liu et al. 2009, Kerman et al. 2010, Prudencio and Borchelt 2011, Liu et al. 2012, Mulligan et al. 2012)
USOD	42-48	+	-	- (ox)	Nd	(Kerman et al. 2010, Mulligan et al. 2012)
DSE2 (3H1)	125-142	+	+	nd	Nd	(Vande Velde et al. 2008, Grad et al. 2011, Pokrishevsky et al. 2012)
4-20Ra-ab	4-20	+	+	nd	Nd	(Jonsson et al. 2004, Forsberg et al. 2010)
57-72Ra-ab	57-72	+	+	nd	Nd	(Stewart et al. 2006, Forsberg et al. 2010, Forsberg et al. 2011)
131-153Ra-ab	131-153	+	+	nd	Nd	(Jonsson et al. 2004, Forsberg et al. 2010, Forsberg et al. 2011)

¹Determined using similar methodology as in C4F6 epitope mapping (Bosco et al. 2010) (unpublished data, Bosco DA).

² nd: Not Determined

³ Serum starvation in cultured cells results in SOD1 reactivity with antibody

⁴ Benefits observed from active immunization with SOD1 peptide recognized by SEDI

⁵ Commercially available

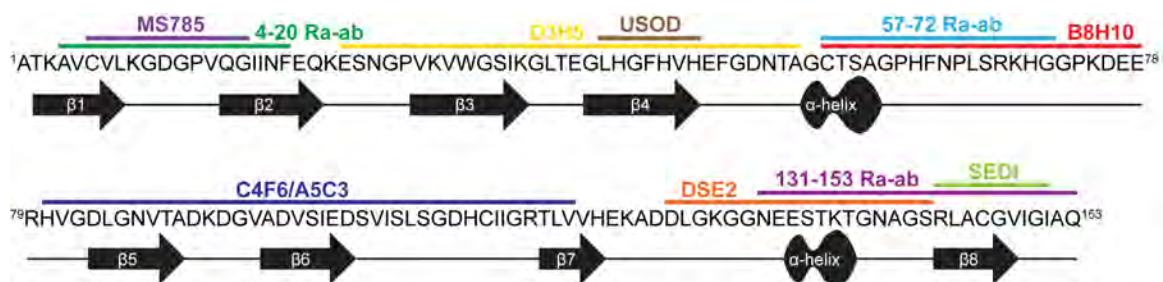


Figure I-3. Conformation specific antibodies highlight regions exposed in SOD1 upon misfolding. The primary sequence for WT SOD1 is shown with the secondary structure displayed below. The binding regions of 11 antibodies specific for misfolded SOD1 are depicted above the sequence (See **Table I-1** for antibody details).

level of misfolded SOD1 present in the spinal cord of ALS mouse models and enhance survival (Gros-Louis et al. 2010). Understanding the binding interaction between such antibodies and SOD1 will further our understanding of how aberrant SOD1 is causative in disease by painting a clearer picture of the misfolded, toxic conformation. Further, the misfolded SOD1 species itself, once identified, has the potential to be a powerful biomarker for ALS. In fact, there is evidence that soluble misfolded WT SOD1 mimics the toxic functions and toxic conformation of FALS-linked SOD1 as discussed further below.

Loss of native SOD1 PTMs Results in WT SOD1 Misfolding

As discussed above, coordination of Zn, oxidation of the C57-C146 intrasubunit disulfide bond and homodimerization of SOD1 contribute to the structural stability of the molecule. A loss in integrity of any one of these normal post-translational modifications compromises the stability of WT SOD1 and contributes to its misfolding and aggregation (**Fig. I-1**). For example, a reduction of WT SOD1 stability upon demetallation is a widely documented observation (Stathopoulos et al. 2003, Lynch et al. 2004, Furukawa and O'Halloran 2005, Ding and Dokholyan 2008). Interestingly, demetallation of WT SOD1 induces similar conformational perturbations within the zinc binding and the electrostatic loops (loops IV and VII, respectively; **Fig. I-1**) as do FALS-linked SOD1 mutations (Strange et al. 2003, Strange et al. 2007, Ding and Dokholyan 2008, Durazo et al. 2009, Molnar et al. 2009). A direct comparison of NMR backbone chemical shifts for apo dimeric WT SOD1 versus holo dimeric WT SOD1 revealed the

largest structural variations within the electrostatic loop (Banci et al. 2009). These structural alterations were accompanied by pronounced changes in backbone dynamics that further support demetallation-induced misfolding (Banci et al. 2009). Molecular dynamics (Ding and Dokholyan 2008) and H/D exchange by mass spectrometry (Durazo et al. 2009) also report enhanced flexibility within the aforementioned loops of apo WT SOD1 compared to holo SOD1, but in addition these studies also detect misfolding within the beta barrel of SOD1 upon demetallation (Ding and Dokholyan 2008, Durazo et al. 2009). Furthermore, the misfolding of WT SOD1 induced by demetallation leads to aggregation of the protein (Banci et al. 2007), which may be driven by the exposure of hydrophobic regions within misfolded SOD1 that are otherwise buried in the native protein (Tiwari et al. 2009).

In addition to demetallation, reduction of the C57-C146 disulfide bond also has a destabilizing effect on WT SOD1 that can lead to protein misfolding and aggregation in a manner similar to FALS-linked mutant SOD1 (Furukawa et al. 2008, Chan et al. 2013). Several studies have demonstrated that a reduction of C57-C146 in apo-SOD1 shifts the monomer-dimer equilibrium towards the monomeric state. Addition of zinc or oxidation of C57-C146 shifts the equilibrium back to the dimeric state, demonstrating interdependence between Zn coordination, C57-C146 bond integrity, and dimerization on the structural stability of SOD1 (Arnesano et al. 2004, Lindberg et al. 2004, Hornberg et al. 2007).

Aberrant Post-Translational Modifications Induce WT SOD1 Misfolding

In addition to alterations of the normal post-translational modifications of SOD1, WT SOD1 misfolding and aggregation can be induced by the formation of aberrant modifications. Oxidation of SOD1 side chains represents one such modification that has been postulated to play a significant causal role in both FALS and SALS (Kabashi et al. 2007). However, Shaw et al. demonstrated that FALS-linked SOD1 transgenic mouse models have miniscule amounts of modified SOD1 present in the spinal cord (Shaw B. F. et al. 2008). It should be noted that the high amount of DTT used in the analysis would likely preclude detection of certain modifications present on cysteine residues, such as cysteinylation, oxidation and glutathionylation (Shaw B. F. et al. 2008). In the context of WT SOD1, which has relevance to SALS, metal catalyzed oxidation with CuCl_2 and ascorbic acid leads to oxidative modification of SOD1 histidine residues and subsequent SOD1 aggregation (Rakhit et al. 2002, Rakhit et al. 2004). This mode of oxidation-induced SOD1 aggregation proceeds by way of SOD1 dimer dissociation/ monomer formation, demonstrating interdependence between aberrant and normal SOD1 post-translational modifications (Rakhit et al. 2004). Cys111 within SOD1 is particularly susceptible to H_2O_2 induced oxidation (**Fig. I-1B**). Prolonged exposure of SOD1 to H_2O_2 results in the irreversible conversion of the Cys111 sulfhydryl group to sulfonic acid (Fujiwara et al. 2007, Bosco et al. 2010, Auclair et al. 2013b), which may be detrimental since WT SOD1 oxidized by H_2O_2 (hereafter referred to as SOD1ox) exhibits an enhanced

propensity to misfold and aggregate (Ezzi et al. 2007, Fujiwara et al. 2007, Bosco et al. 2010, Chen X. et al. 2012b). Glutathionylation on Cys111 has a similar destabilizing effect (McAlary et al. 2013). Interestingly, modifications such as β -mercaptoethanol (Fujiwara et al. 2007), persulfide (de Beus et al. 2004) and cysteinylolation (Auclair et al. 2013b) on cysteine 111 protect SOD1 against oxidation and possibly against subsequent misfolding.

Misfolded WT SOD1 Proteins are Toxic and Mimic FALS-linked SOD1

In recent years, several reports have demonstrated a toxic effect of misfolded WT SOD1 in the context of ALS relevant pathways and processes (**Fig. I-4**). The observation that zinc depleted WT SOD1 exerts a toxic effect onto motor neurons by a mechanism involving nitric oxide provided one of the first clues that modified WT SOD1 species are toxic and may contribute to SALS pathogenesis (Estevez et al. 1999, Beckman et al. 2001). The fact that oxidation damages the zinc binding site of SOD1 and aging is known to result in increased protein oxidation, it is reasonable to suspect that zinc-deficiency plays a role in pathology (Smith C. D. et al. 1991, Sampson and Beckman 2001). In fact, zinc supplements extend survival in ALS mouse models (Ermilova et al. 2005). More recently, zinc- deficient SOD1 was shown to exhibit a toxic effect related to mitochondrial dysfunction in *Drosophila* (Bahadorani et al. 2013). That metal deficient WT SOD1 can be induced to misfold and exhibit a toxic nature analogous to FALS-linked SOD1 is supported by the immunization trial in ALS mice reported by Takeuchi et al. Low copy SOD1 G93A transgenic mice

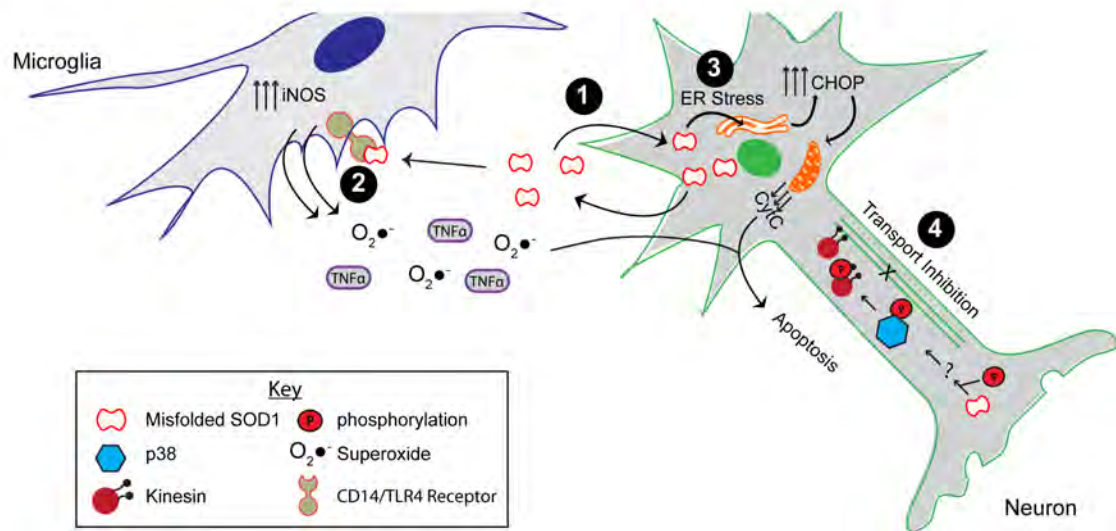


Figure I-4. The toxic properties shared by ALS-linked mutant SOD1 and modified WT SOD1. As shown, misfolded SOD1, resulting from mutations or aberrant post-translational modifications, causes the protein to engage in aberrant interactions. (1) Misfolded SOD1 is both secreted, possibly through chromogranins, and taken up from the extracellular environment. (2) Extracellular misfolded SOD1 activates microglia by binding to the CD14/TLR4 receptor, thereby elevating nitric oxide synthase (iNOS) activity as well as secretion of superoxide anion ($O_2\cdot^-$) and proinflammatory cytokines (e.g., TNF α). (3) Expression and uptake of misfolded SOD1 leads to ER stress, which elevates the pro-apoptotic CHOP protein and induces mitochondrial damage. (4) The presence of misfolded SOD1 in the axon results in axonal transport inhibition through a mechanism involving the phosphorylation of p38 and the kinesin motor. All these aberrant functions compromise the integrity of the motor neuron, and potentially contribute to both FALS and SALS pathogenesis.

vaccinated with the apo WT SOD1 immunogen exhibited delayed disease onset and prolonged survival compared to control mice injected with saline/adjuvant, and importantly, to a similar degree as mice vaccinated with apo SOD1 G93A (Takeuchi et al. 2010). This study also implicates WT SOD1 as a viable therapeutic target for SALS.

SOD1^{ox} also acquires aberrant protein-interactions that are observed for FALS-linked SOD1 mutants. For example, SOD1^{ox} interacts with the heat shock protein Hsc70 that plays a role in refolding misfolded proteins (Ezzi et al. 2007), the secretory protein chromogranin B that actively secretes misfolded forms of SOD1 (Urushitani et al. 2006, Ezzi et al. 2007), and the anti-apoptotic protein Bcl-2 in a manner that induces mitochondrial damage (Pasinelli et al. 2004, Guareschi et al. 2012). SOD1^{ox} was also shown to mimic FALS-linked SOD1 mutants in the inhibition of anterograde fast axonal transport (FAT) in squid axoplasm. These studies demonstrated that the inhibitory effect of SOD1^{ox} and mutant SOD1 was mediated by activated p38 MAPK, indicating that misfolded SOD1 can trigger kinase-dependent signaling cascades (Morfini G. A. et al. 2009, Bosco et al. 2010, Morfini G. A. et al. 2013, Song et al. 2013). Extracellular derived WT SOD1 can also induce a toxic effect onto cells. SOD1^{ox} applied to cell culture media activates immortalized microglia (Ezzi et al. 2007), which in turn may cause motor neuron death (Ezzi et al. 2007, Zhao et al. 2010). Furthermore, uptake of aggregated WT SOD1 species by

macropinocytosis in neuronal cells caused ER stress and seeded the aggregation of intracellular, endogenous SOD1 (Sundaramoorthy et al. 2013).

Studies in various SOD1 transgenic ALS mouse models have provided direct evidence for WT SOD1 mediated toxicity *in vivo*. Intriguingly, an ALS-like phenotype was only observed in transgenic mice expressing the human SOD1 A4V variant, a mutation that corresponds to an aggressive ALS phenotype in humans, when these mice expressed the human WT version of SOD1 (Deng et al. 2006). This paradoxical result may be explained by heterodimerization of WT and A4V subunits, affording a 'stabilized' and thus more toxic version of SOD1 A4V that would otherwise be degraded (Witan et al. 2008, Witan et al. 2009). A similar phenomenon was observed in double-transgenic mice expressing human SOD1 WT and G85R, where disease onset was hastened relative to single-transgenic SOD1 G85R mice (Wang L. et al. 2009). Recently, a transgenic mouse model was developed that over-expresses human WT SOD1 at similar levels to the established high-copy SOD1 G93A mouse model (Gurney et al. 1994, Graffmo et al. 2013). Compared to transgenic mice expressing fewer copies of the human WT SOD1 gene, the mice generated by Graffmo et al exhibit an ALS-like phenotype that includes significant weight loss, SOD1 aggregation, neurodegeneration, gliosis, and a shortened life-span of approximately 360 days (Graffmo et al. 2013). The authors posit that the ALS-like phenotype is not a general effect of SOD1 overexpression per se, but rather a direct consequence of a substoichiometric population of misfolded SOD1.

Although the exact mechanism for WT SOD1 mediated toxicity is not well understood in these models, and the extent to which WT SOD1 is post-translationally modified has not been addressed, these studies clearly demonstrate a link between WT SOD1 and motor neuron degeneration characteristic of ALS.

Summary

Misfolding of SOD1 induced by post-translational modifications and FALS-linked mutations converge in a common pathway with overlapping toxic downstream events. These similarities support the hypothesis that misfolded WT SOD1 plays a causative role in a subset of sporadic ALS cases. In the following chapters, I will present one common, toxic misfolded conformation shared by FALS-linked SOD1 and PTM-linked SOD1 variants that I have identified using cross-linking and mutagenesis techniques. I have also identified a species of SOD1 that is present in control peripheral blood mononuclear cells (PBMCs), but underrepresented in SALS-derived PBMCs. Further, an over-oxidized form of SOD1 was identified in SALS-derived PBMCs that was less abundant in controls. Together, these data implicate misfolded WT SOD1 in disease, suggesting therapeutics that target FALS-linked SOD1 may prove beneficial to sporadic patients lacking a genetic mutation in SOD1 as well.

PREFACE TO CHAPTER II:

Digested SOD1 peptides were injected into the mass spectrometer by Stephanie Maniatis. The preliminary sequence of the C4F6 Fab fragment was determined by John Leszyk using mass spectrometry. Prepared SOD1 samples for metal analysis were processed by Rebecca Auxier at the University of Georgia. All other work presented in this chapter was performed by Melissa S. Rotunno.

Parts of this Chapter appeared in:

Rotunno, M.S., Auclair, J.R., Maniatis, S., Shaffer, S.A., Agar, J., Bosco, D.A., "Identification of a Misfolded Region in Superoxide Dismutase 1 that is Exposed in Amyotrophic Lateral Sclerosis." *Journal of Biological Chemistry*. 2014, 289, 28527-28538.

CHAPTER II: IDENTIFICATION OF A MISFOLDED REGION IN SOD1 THAT IS EXPOSED IN ALS

Introduction

ALS is a fast-progressing, fatal neurodegenerative disorder that primarily targets motor neurons. The complex nature of ALS represents a hurdle in developing effective therapies for this incurable disease. A growing list of genes have been linked to ALS, where mutations in *SOD1*, *TDP-43*, *FUS*, *C9orf72* account for >50% of inherited, or familial ALS (FALS) (Sreedharan and Brown 2013). However, much less is known about the cause(s) of sporadic ALS (SALS) that account for the majority (90%) of ALS cases (Sreedharan and Brown 2013). FALS and SALS are clinically indistinguishable, suggesting similar mechanisms are at play for both forms of this disease.

SOD1 (Cu,Zn-superoxide dismutase) represents a factor that is common to FALS and SALS. Mutations in SOD1 likely cause FALS through a gain-of-toxic mechanism induced by a misfolded conformation of the protein (Rotunno and Bosco 2013). Importantly, aberrant post-translational modifications cause wild-type (WT) SOD1 to adopt a similar misfolded conformation (Arnesano et al. 2004, Ezzi et al. 2007, Fujiwara et al. 2007, Ding and Dokholyan 2008, Banci et al. 2009, Durazo et al. 2009, Bosco et al. 2010, Chen X. et al. 2012b, Auclair et al. 2013b). These observations support an emerging, albeit controversial, hypothesis that WT SOD1 plays a pathogenic role in a subset of SALS, analogous to the role of mutant-SOD1 in FALS (Rotunno and Bosco 2013). Over the past several years, conformation specific antibodies have been generated

that are selective for misfolded SOD1 variants over the native, WT SOD1 protein (Rakhit et al. 2007, Urushitani et al. 2007, Vande Velde et al. 2008, Forsberg et al. 2010, Gros-Louis et al. 2010, Fujisawa et al. 2012), suggesting the epitopes for these antibodies represent pathogenic motifs within misfolded SOD1. C4F6 is one such conformation specific monoclonal antibody, which is reactive for several ALS-linked SOD1 variants (Urushitani et al. 2007, Prudencio and Borchelt 2011, Brotherton et al. 2012) including an oxidized form of WT SOD1 (SOD1ox) that serves as a model protein for SALS (Bosco et al. 2010). Importantly, C4F6 detected misfolded SOD1 species within human post-mortem FALS and SALS spinal cord tissues (Bosco et al. 2010, Brotherton et al. 2012) and C4F6 reactivity correlated with disease progression in the spinal cords of SOD1 G93A transgenic mice (Brotherton et al. 2012). That C4F6 blocked the inhibitory effect of misfolded SOD1 on fast axonal transport in squid axoplasm supports the notion that the C4F6 epitope with SOD1 confers toxicity (Bosco et al. 2010). Collectively, these observations indicate that the C4F6 antibody is a reliable reporter of pathogenic SOD1 species in ALS.

Despite the evidence that C4F6 is selective for pathogenic SOD1 species, very little is known about the amino acids and structural elements that comprise this epitope. Therefore, we developed a chemical cross-linking, site-directed mutagenesis and mass spectrometry approach to define the potentially toxic C4F6 epitope within misfolded SOD1 proteins. Our analyses reveal that the zinc binding (loop IV) and electrostatic (loop VII) loops within SOD1 mask the C4F6

epitope, and support a model where ALS-linked mutations destabilize loop IV and VII (Shipp et al. 2003, Molnar et al. 2009) thereby exposing the C4F6 epitope. In support of this model, WT SOD1 lacking loops IV and VII (SOD1^{ΔIV/ΔVII}) exhibits high reactivity with C4F6 while maintaining a relatively stable tertiary-fold (Danielsson et al. 2011, Danielsson et al. 2013). Exposure of the C4F6 epitope within SOD1^{ΔIV/ΔVII} directly correlates with SOD1-mediated microglia activation, indicative of enhanced SOD1 toxicity (Ezzi et al. 2007, Zhao et al. 2010). These findings put forth loops IV and VII as well as the C4F6 epitope itself as therapeutic targets for SOD1-mediated ALS.

Results

C4F6 is selective for misfolded forms of SOD1 over native wild-type SOD1

The C4F6/SOD1 binding interaction was quantified in non-denaturing conditions using the OCTET system, which utilizes Bio-Layer Interferometry technology to accurately determine binding affinities (Broering et al. 2013). No binding interaction was detected between C4F6 and WT SOD1; thus, the apparent dissociation constant (K_d) is below the limit of detection (**Table II-1**). C4F6 exhibited the tightest binding affinity for SOD1 G93A ($K_d = 0.40 \pm 0.29 \mu\text{M}$), the immunogen for this antibody (Urushitani et al. 2007). C4F6 also recognized SOD1 A4V and G85R with K_d values of $1.46 \pm 0.41 \mu\text{M}$ and $3.00 \pm 3.83 \mu\text{M}$, respectively. Oxidation of native WT SOD1 at Cys 111 (SOD1ox) was also sufficient to produce a tight binding interaction with C4F6 ($K_d = 1.13 \pm 0.60 \mu\text{M}$). These data suggest that C4F6 recognizes an aberrant conformation shared

Table II-1. Apparent dissociation constants (K_d) of the C4F6/SOD1 interaction as determined by the OCTET system

SOD1 Variant	K_d (μM)	n
WT SOD1	NBD*	5
WT SOD1^{ΔIV}	0.72 ± 0.24	2
WT SOD1^{ΔIV/ΔVII}	0.46 ± 0.24	2
SOD1ox	1.13 ± 0.60	4
SOD1ox^{ΔIV}	1.29 ± 0.35	2
SOD1ox^{ΔIV/ΔVII}	0.32 ± 0.03	2
SOD1 G93A	0.40 ± 0.29	5
SOD1 G93A^{ΔIV}	0.28 ± 0.05	2
SOD1 G85R	3.00 ± 3.83	5
SOD1 A4V	1.46 ± 0.41	3

\pm standard deviation; NBD*, no binding detected; n denotes the number of independent experiments

amongst multiple misfolded SOD1 variants.

Hot-spots for C4F6 cross-linking are located within the electrostatic and zinc binding loops of misfolded SOD1 variants

We employed a chemical cross-linking strategy with native SOD1 proteins and C4F6 to identify the C4F6 epitope within misfolded SOD1. Both dithiobis[succinimidyl propionate] (DSP; cross-links lysines and has a 12Å spacer) and 1-ethyl-3-[3-dimethylaminopropyl]carbodiimide hydrochloride (EDC; cross-links lysines with glutamic or aspartic acid residues and has a 0Å spacer) were used independently to cross-link SOD1 proteins to the Fab fragment of C4F6. In the presence of DSP (**Fig. II-1A**) and EDC (**Fig. II-1B**), C4F6 cross-linked to all tested ALS-associated SOD1 variants and SOD1ox, but not to WT SOD1. Although the sites of ALS-linked point mutations (e.g., A4V, G85R and G93A) and oxidation (e.g., C111) are in different regions of the tertiary structure (**Fig. II-2**), C4F6 binding indicates that these SOD1 variants are misfolding in a similar manner.

To identify the amino acids involved in SOD1/C4F6 binding, the band corresponding to the cross-linked species (SOD1/C4F6*) was excised from a Coomassie-stained SDS-PAGE gel and subjected to tryptic digestion followed by mass spectrometry (MS). The amino acid sequence for the C4F6 Fab fragment was determined using both mass spectrometry and RNA sequencing (see Methods). To aid in DSP cross-link identification, samples were prepared with deuterium-labeled DSP (d₈-DSP) in parallel, resulting in cross-linked peptides

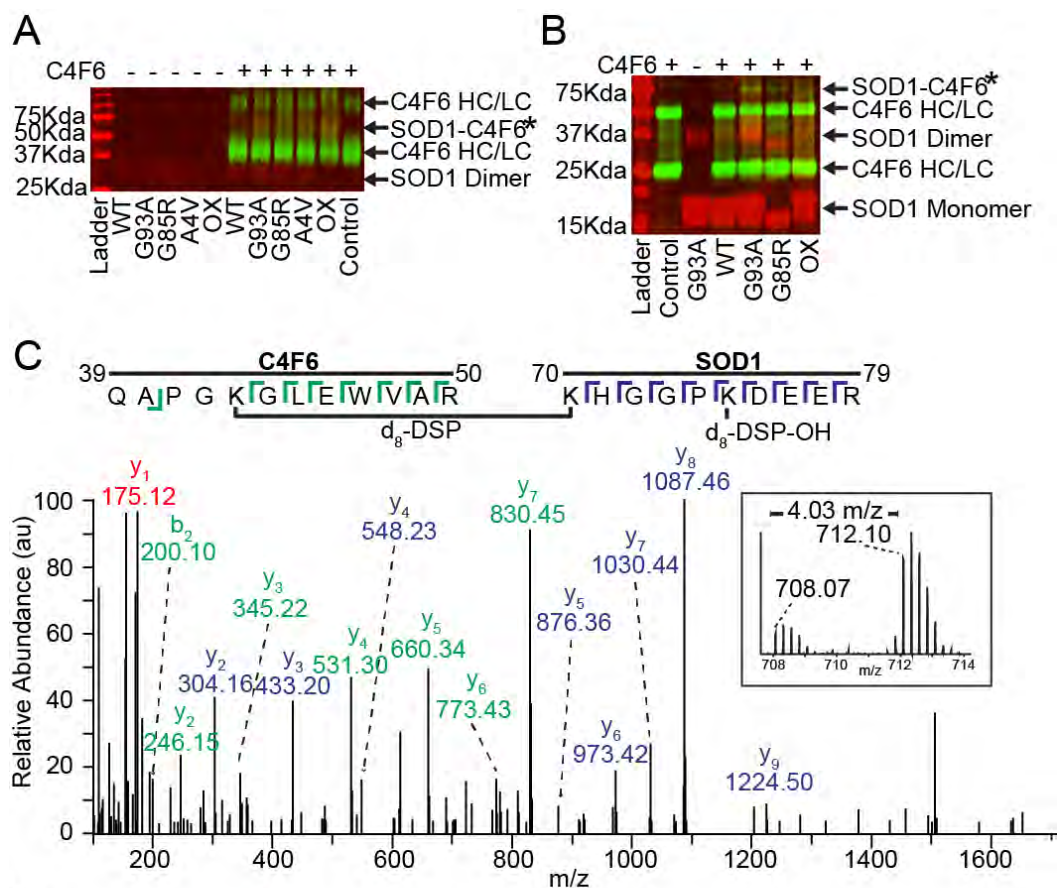


Figure II-1. C4F6 specifically cross-links to misfolded SOD1 in the presence of DSP or EDC. (A) A non-reducing western analysis with pan-SOD1 (red) and anti-Fab (green) antibodies demonstrates the specific cross-linking with DSP between misfolded SOD1 variants and C4F6 Fab (SOD1/C4F6; yellow band at 66 kDa denoted by *). HC, heavy chain; LC, light chain. (B) A band corresponding to the SOD1/C4F6 complex cross-linked with EDC (denoted by *) was detected at ~70kDa for SOD1 (G93A, G85R, ox), but not wild-type (WT) SOD1. A similar SDS-PAGE and western analysis was performed as in (A), except a 12% gel was employed under reducing conditions. (C,D) Representative cross-linked peptides from a pooled (d₈-DSP + DSP) sample where a 4.03 *m/z* shift was observed between the monoisotopic peaks (C, inset; 16.13 Da mass shift/+4 charge state = 4.03 *m/z*) 708.07 *m/z* (DSP) and 712.10 *m/z* (d₈-DSP). Both parent ions, 712.10 *m/z* (C, d₈-DSP) and 708.07 *m/z* (D, DSP), were subjected to MS/MS analysis and identified as residues 70-79 of SOD1 and residues 39-50 of C4F6.

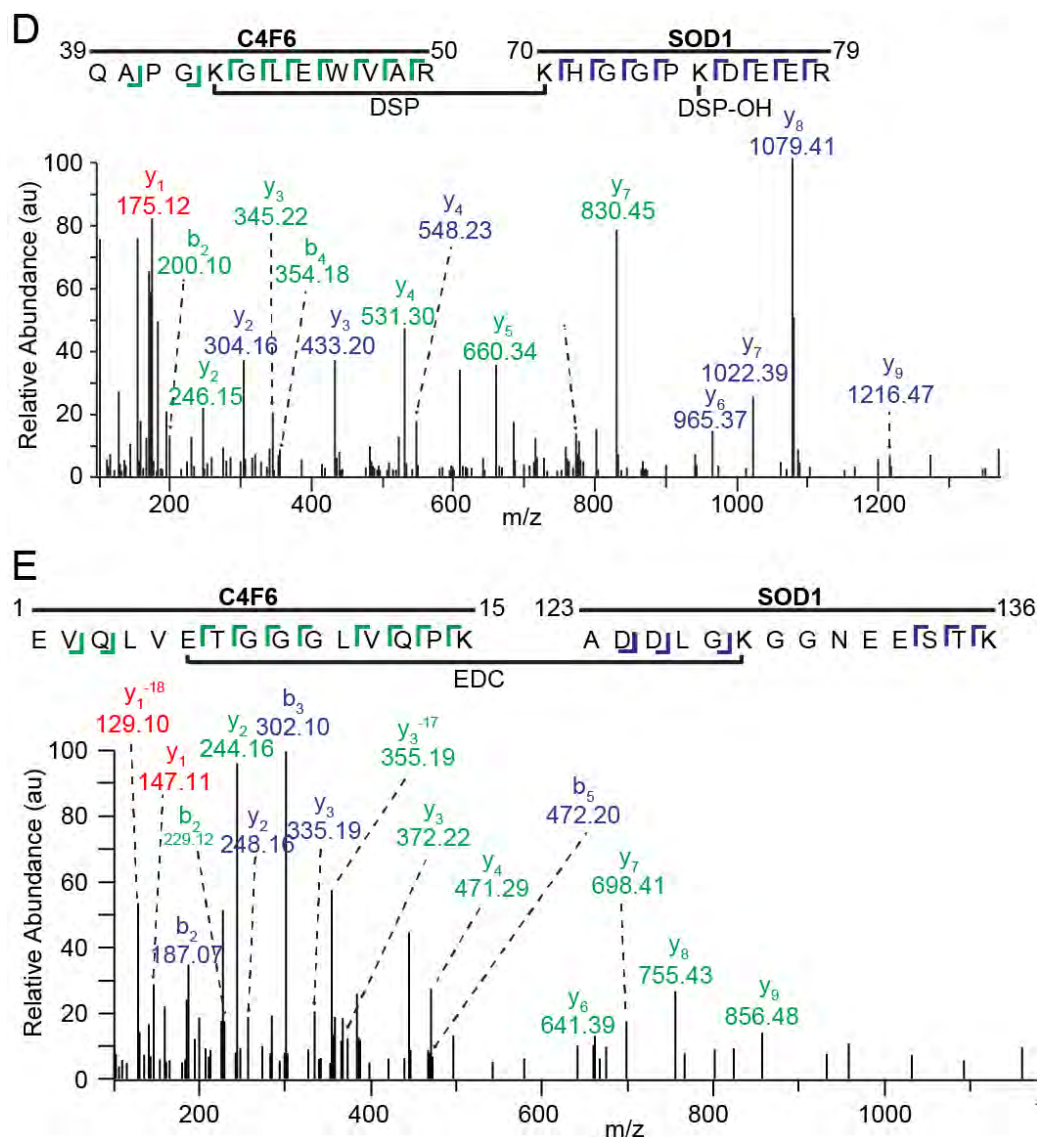


Figure II-1 continued. C4F6 specifically cross-links to misfolded SOD1 in the presence of DSP or EDC. (C,D) Representative cross-linked peptides from a pooled (d_8 -DSP + DSP) sample where a 4.03 m/z shift was observed between the monoisotopic peaks (C, inset, 16.13 Da mass shift/+4 charge state = 4.03 m/z 708.07 m/z (DSP) and 712.10 m/z (d_8 -DSP)). Both parent ions, 712.10 m/z (C, d_8 -DSP) and 708.07 m/z (D, DSP), were subjected to MS/MS analysis and identified as residues 70-79 of SOD1 and residues 39-50 of C4F6. (E) Exemplar MS/MS data (59% sequence coverage) for an EDC cross-linked peptide comprised of C4F6 (residues 1-15) and SOD1 G93A (residues 123-136). (C-E) C4F6 (green) and SOD1 (blue) ions are depicted with the corresponding sequence displayed above. Peaks with identical ions in both C4F6 and SOD1 peptides are shown in red, where -18 corresponds to a loss of a water molecule for y_1 .

with an increased mass of 8.06 Da. Pooling both DSP and d_8 -DSP samples allowed for further validation of cross-linked peptides due to a charge-state dependent shift in the observed m/z of the parent ions. A representative cross-linked peptide from a pooled (d_8 -DSP + DSP) SOD1 G93A/C4F6 sample is illustrated in **Figure II-1C** (*inset*) where a 4.03 m/z shift was observed between the monoisotopic peaks 708.07 m/z (DSP) and 712.10 m/z (d_8 -DSP). This mass-shift corresponds to the theoretical mass shift of a cross-linked peptide containing two cross-linkers, one hydrolyzed dead-end cross-linker and one directly joining the peptides, with DSP compared to d_8 -DSP (16.13 Da mass shift/+4 charge state = 4.03 m/z). Both parent ions, 712.10 m/z (d_8 -DSP) and 708.07 m/z (DSP) were subjected to MS/MS analysis and identified as residues 70-79 of SOD1 and residues 39-50 of C4F6 (**Fig. II-1C,D**). A representative cross-linked SOD1 G93A/C4F6 peptide from an EDC treated sample is illustrated in **Figure II-1E**.

In total, 10 amino acids in SOD1 G93A were found to cross-link to C4F6, the majority of which fall in the zinc binding (loop IV, residues 49-81) and electrostatic (loop VII, residues 124-139) loops of SOD1 (**Fig. II-2, Table II-2**). Both DSP and EDC cross-link these loop regions within SOD1 G93A to C4F6 (**Fig. II-2B,C, Table II-2**), demonstrating that these cross-linkers detect “hot-spots” of C4F6 binding to SOD1 G93A. Interestingly, C4F6-binding hot-spots within loops IV and VII are also detected for other misfolded SOD1 proteins, including apo-SOD1 and SOD1 (G85R, A4V, ox) variants (**Fig. II-2C, Table II-2**).

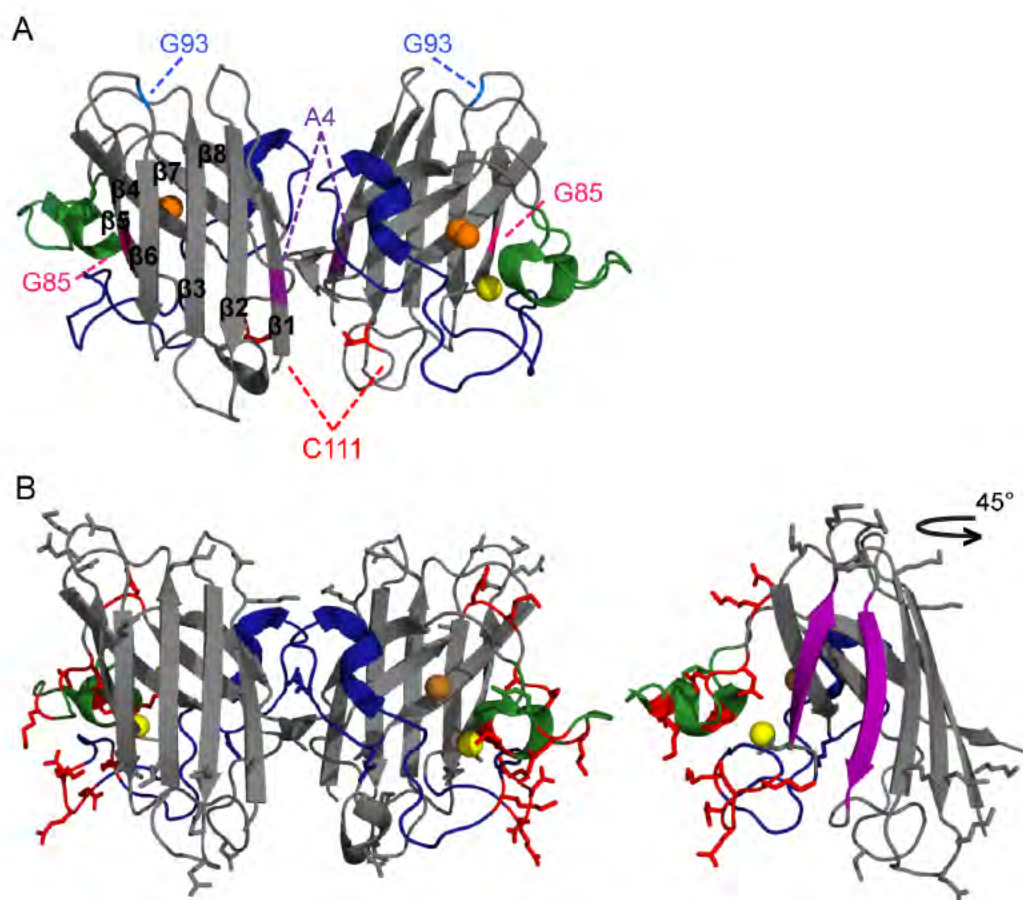


Figure II-2. C4F6 cross-links to loops IV and VII within misfolded SOD1. (A) The structure of WT SOD1 (PDB ID: 2C9V; Cu, orange; Zn, yellow) with the sites of FALS-linked mutations (A4V, G85R, and G93A) and oxidation (C111). (B) Amino acids (red) that cross-link SOD1 G93A to C4F6 with DSP or EDC are highlighted onto the structure of SOD1 G93A (PDB: 2WKO). The edge strands of $\beta 5$ and $\beta 6$ exposed upon removal of loops IV and VII are shown in purple (right). All potential side chains (K,D,E) capable of crosslinking but that were not cross-linked to C4F6 are shown in gray.



Figure II-2 continued. C4F6 cross-links to loops IV and VII within misfolded SOD1. (C) The amino acid sequences for SOD1 variants from this study are shown with the secondary structural elements illustrated below. Amino acids are highlighted as in (B); loops IV (zinc binding) and VII (electrostatic) harbor a majority of cross-linked residues. SOD1^{ΔIV/ΔVII} is denoted by ΔIV/ΔVII (loop IV, blue; loop VII, green).

Table II-2. Amino acids that cross-link in the C4F6/SOD1 complex.

SOD1 Variant	SOD1 AA	C4F6 AA	% Coverage	Efficacy	Cross linker
SOD1 G93A 94±12% ¹	K70	K43 HC	>59.1	3/4	DSP
	K70	K54 HC	66.7	1/4	DSP
	K70	D65 LC	>67.6	2/2	EDC
	K70	K112 LC	>60.0	4/4	DSP
	K75	K43 HC	68.2	1/4	DSP
	K75	K54 HC	>55.6	2/4	DSP
	K75	D68 HC	82.4	1/2	EDC
	D76/E77	K54 HC	62.5	1/2	EDC
	E77/78	K54 HC	61.5	1/2	EDC
	E121	K54 HC	58.3	1/2	EDC
	E121	K67 HC	50.0	1/2	EDC
	K122	K54 HC	60.0	1/4	DSP
	D124/125	K54 HC	>52.2	2/2	EDC
	K128	E6 HC	58.6	1/2	EDC
	E132	K54 HC	52	1/2	EDC
	K136	E6 HC	63.3	1/2	EDC
K136	D65 LC	>53.8	2/2	EDC	
K136	K215 HC	70.0	1/4	DSP	
SOD1 G85R 97±4% ¹	K70	D64 HC	60.9	1/1	EDC
	K70	D65 LC	66.7	1/1	EDC
	K70	K54 HC	55.6	1/1	DSP
	D76	K54 HC	55.6	1/1	EDC
	D76/E77/E78	K54 HC	53.9	1/1	EDC
	E121	K54 HC	54.2	1/1	EDC
	E132	K54 HC	60.0	1/1	EDC
	K136	D65 LC	50.0	1/1	EDC
SOD1 A4V 94% ¹	K70	K54 HC	55.6	1/2	DSP
	K75	K54 HC	>51.9	2/2	DSP
	K122	K54 HC	53.6	1/2	DSP
	K136	K43 HC	66.7	1/2	DSP
	K136	K54 HC	>50.0	2/2	DSP
SOD1 OX 94% ¹	K70	K43 HC	63.6	1/2	DSP
	K70	K54 HC	>70.4	2/2	DSP
	K70	K67 HC	51.9	1/2	DSP
	K70	K112 LC	86.7	1/2	DSP
	K75	K54 HC	63.0	1/2	DSP
	K136	K215 HC	70.0	1/2	DSP
Apo WT SOD1 90% ¹	K75	K54 HC	>55.6	2/2	DSP
	K70	K43 HC	59.1	1/2	DSP
SOD1^{ΔIV, VII} 65% ¹	K122 ²	K54 HC	65.6	1/2	DSP
	K122 ²	K43 HC	63.0	1/2	DSP
	K122 ²	K215 HC	65.0	1/2	DSP

¹SOD1 sequence coverage of trypsin digestion (\pm standard deviation, where applicable). Sequence coverage for the light and heavy chain of the C4F6 fab fragment were found to be 90±11% and 67±7%. It is noted that the sequence coverage for the heavy chain is low, however the sequence coverage of the variable region was consistently 100% (amino acids 1-120).

²Number corresponds to amino acid position in full-length SOD1.

DSP: Represents combined data from deuterated and nondeuterated DSP analyses.

Misfolding of loops IV and VII within ALS-linked SOD1 variants exposes the C4F6 epitope

Since loops IV and VII within SOD1 harbor the majority of amino acids involved in C4F6 binding (**Fig. II-2**), we hypothesized that the C4F6 epitope is located within these loops. It follows that removal of loops IV and VII within misfolded SOD1 should eliminate the C4F6/SOD1 interaction. Loop-deletion constructs were engineered to test this hypothesis. SOD1^{ΔIV} represents WT SOD1 with loop IV replaced by a Gly-Ala-Gly linker. The SOD1^{ΔIV/ΔVII} construct lacks loops IV and VII, both of which were replaced by Gly-Ala-Gly linkers (**Fig. II-2C**, ΔIV/ΔVII). SOD1^{ΔIV} and SOD1^{ΔIV/ΔVII} are both apo- (**Fig. II-3**) and monomeric proteins (Danielsson et al. 2011). SOD1^{ΔIV/ΔVII} is a well-folded protein as determined by X-ray crystallography (**Fig. II-4A**) (Danielsson et al. 2013), NMR, protein stability (Danielsson et al. 2011, Danielsson et al. 2013) and circular dichroism (CD) (**Fig. II-4B**) analyses.

Surprisingly, removal of loops IV and VII within SOD1 strengthened the C4F6/SOD1 interaction. Octet (**Table II-1**) and native western (**Fig. II-4C**) analyses demonstrated that removal of these loops promoted a binding interaction between WT SOD1 and C4F6. WT SOD1^{ΔIV} and WT SOD1^{ΔIV/ΔVII} bound C4F6 with a K_d of 0.72 ± 0.24 and 0.46 ± 0.24 (μM), respectively. Moreover, the affinity of SOD1^{ox} for C4F6 increased 3-fold, from 1.13 ± 0.60 to 0.32 ± 0.03 , upon deletion of loops IV and VII. Therefore, C4F6 affinity for SOD1 proteins lacking loops IV and VII is increased relative to the respective full-length protein

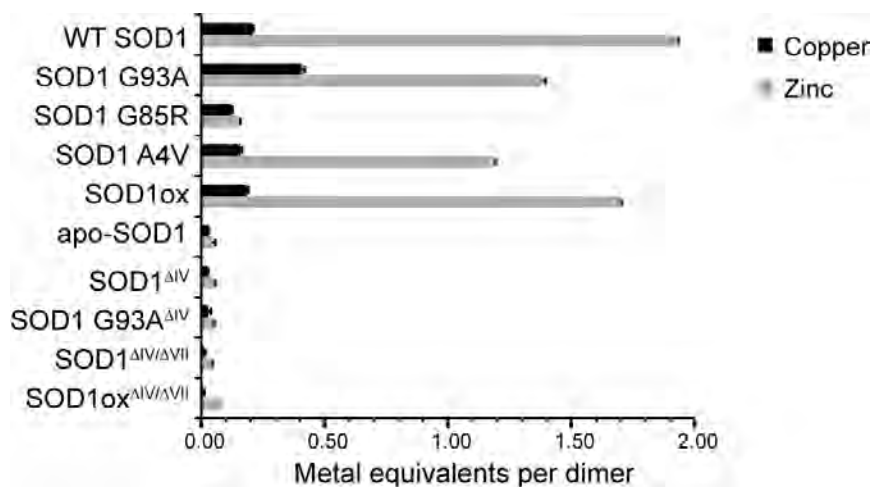


Figure II-3. Metal analyses reveal deficient metal coordination in ALS-linked and loop-deletion SOD1 variants. The metal content of as-isolated SOD1 variants determined by ICP-OES. Full-length SOD1 (G93A, G85R, A4V, ox) contain lower levels of zinc compared to WT SOD1. SOD1 (apo, WT Δ IV, G93A Δ IV, WT Δ IV/ Δ VII, and ox Δ IV/ Δ VII) are deficient in both copper and zinc. (apo refers to demetallated (see methods); Δ IV, deletion of loop IV; Δ IV/ Δ VII deletion of loops IV and VII).

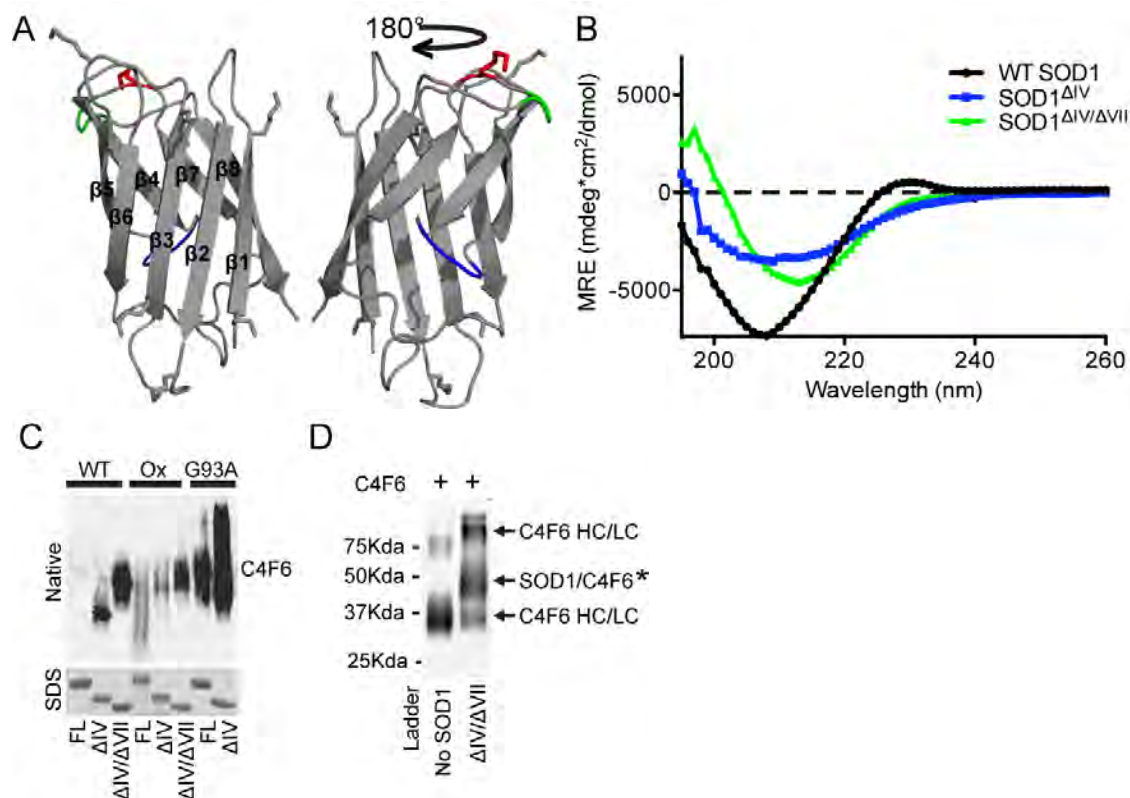


Figure II-4. Deletion of loops IV and VII exposes the C4F6 epitope. (A) The structure of SOD1^{ΔIV/ΔVII} (PDB: 4BCZ; loop IV, blue; loop VII, green; Lys122, red). (B) CD spectra of WT SOD1 revealed a minimum ellipticity at 208 nm, indicative of a mixture of both β -sheets and α -helices within the secondary structure as previously reported (Greenfield 2006, Svensson et al. 2006). A similar trend is seen for SOD1^{ΔIV}. Due to the omission of alpha-helices within loops IV and VII, the minimum ellipticity is shifted towards a longer wavelength for SOD1^{ΔIV/ΔVII} relative to WT SOD1 and SOD1^{ΔIV}. (C) The indicated recombinant SOD1 protein (FL, full-length; ΔIV , deletion of loop IV; $\Delta IV/\Delta VII$ deletion of loops IV and VII) was subjected to a native PAGE western analysis with C4F6 (top), revealing that C4F6 reactivity is enhanced when the functional loops are removed. A denaturing SDS-PAGE (stained with Coomassie) serves as a loading control. (D) WT SOD1^{ΔIV/ΔVII} cross-links to C4F6 Fab through Lys122 in the presence of DSP (as described for **Figure II-2**).

(**Table II-1**). This trend is supported by native western analyses, which show a robust increase in C4F6 reactivity for SOD1 G93A when loop IV is removed (G93A SOD1^{ΔIV/ΔVII} could not be sufficiently expressed) and for both WT SOD1 and SOD1^{ox} upon removal of loops IV and VII (**Fig. II-4C**). WT SOD1^{ΔIV/ΔVII} also cross-linked with C4F6 in the presence of DSP (**Fig. II-4D**). Despite there being 7 potential lysines available for cross-linking with DSP (**Fig. II-2C, 4A**), cross-links were only identified at Lys122 (residue number corresponds to full-length SOD1). Lys122 is the only residue that cross-linked C4F6 in the context of full-length SOD1 G93A but was not removed by deletion of loops IV and VII (**Fig. II-2C, 4A**). These results indicate that i) the remaining 6 Lys residues in WT SOD1^{ΔIV/ΔVII} are either not proximal to the C4F6 epitope or are not sufficiently positioned for cross-linking by DSP, ii) the C4F6 epitope is not within, but rather is proximal to, loops IV and VII, iii) deletion of loops IV and VII within WT SOD1 creates and/or unmask the C4F6 epitope and iv) deletion of loops IV and VII in the context of misfolded ALS-linked variants further exposes the C4F6 epitope. The latter two hypotheses seem likely given that enhanced flexibility of loop VII has been observed in a subset of FALS-linked SOD1 variants (Molnar et al. 2009).

Exposure of the C4F6 epitope within SOD1 correlates with microglial activation

If the C4F6 epitope does indeed confer toxicity, then SOD1^{ΔIV/ΔVII} proteins are expected to exhibit heightened toxicity. Chronic activation of microglia is evident in both ALS patients and mouse models (Turner M. R. et al. 2004, Liao et

al. 2012) and is tightly linked to motor neuron death (Block et al. 2007, Zhao et al. 2010). Recombinant SOD1 G93A has been shown to activate microglia *in vitro* and, in turn, confer toxicity to cultured motor neurons (Zhao et al. 2010). We utilized this sensitive assay to determine whether exposure of the C4F6 epitope exerts a disease-relevant effect onto microglia. Cultured primary murine microglia (>95% pure, as determined by CD11b/c positive cells) were exposed to SOD1 for 48h, and their activation was assessed by both cellular morphology and TNF α secretion. Treatment with all misfolded SOD1 variants employed in this study, but not WT SOD1, resulted in a similar morphological change from ramified/resting microglia to amoeboid, indicative of activation (Graeber 2010) (**Fig. II-5A**). Consistent with these observations, elevated levels of secreted TNF α was detected in the media of microglia exposed to misfolded SOD1 proteins, but not WT SOD1, with the highest levels induced by WT SOD1 Δ IV/ Δ VII (**Fig. II-5B,C**). Consistent with previous studies using FALS-linked SOD1 proteins (Zhao et al. 2010), the addition of an anti-CD14 antibody that competes with misfolded SOD1 for the CD14/TLR4 receptor in microglia partially suppressed SOD1-induced microglia activation for all SOD1 variants tested here (**Fig. II-5**). We note that suppression of SOD1 G93A and WT SOD1 Δ IV by the CD14 antibody did not achieve statistical significance, however, that an attenuation in TNF α signal was observed for all misfolded SOD1 proteins studied here indicates these proteins activate microglia through a common mechanism. Based on these data, we propose a model whereby the enhanced flexibility of

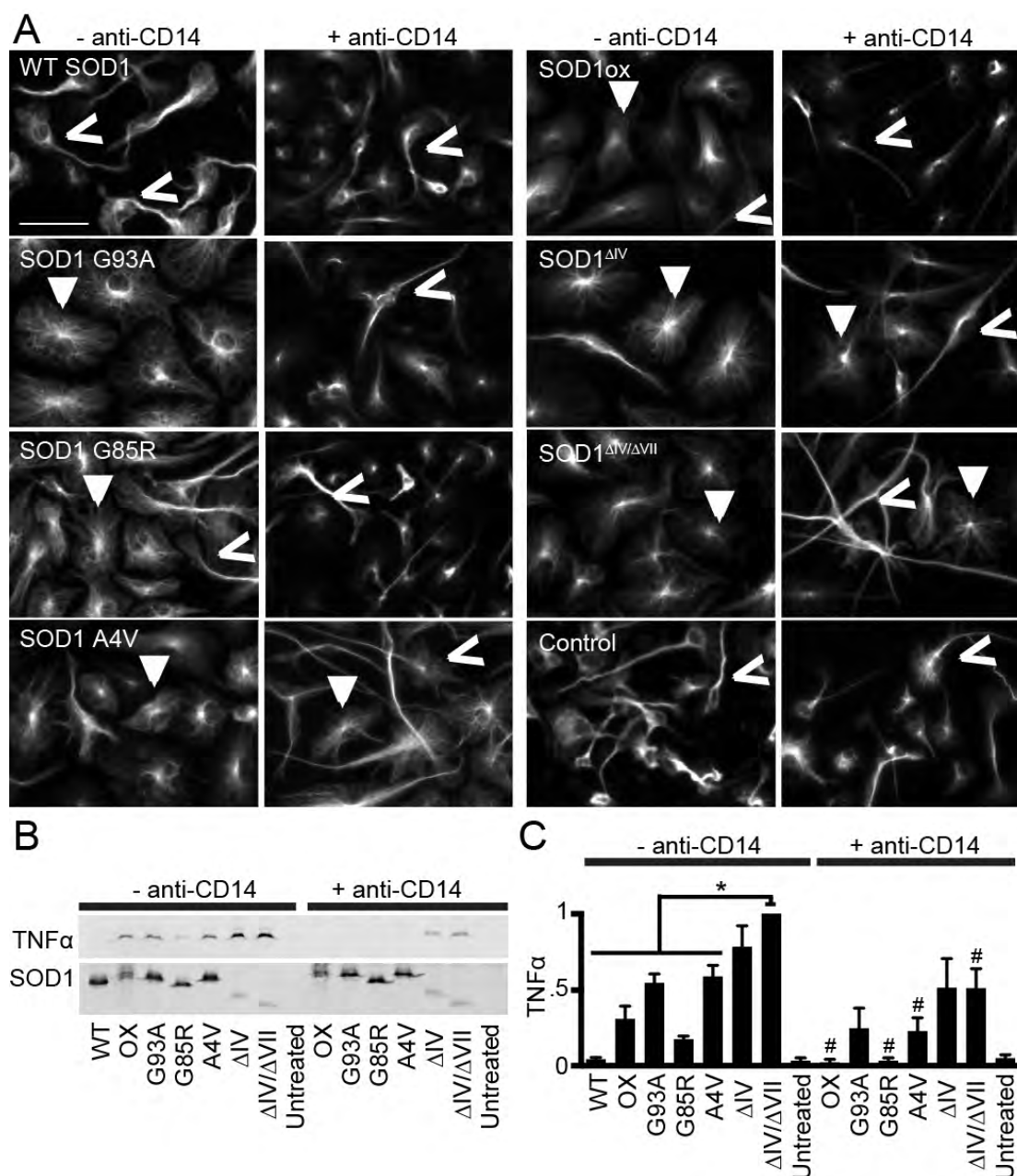


Figure II-5. Exposure of the C4F6 epitope correlates with elevated SOD1-mediated microglial activation. Primary murine microglia were incubated with the indicated SOD1 protein (2.5 μ M) for 48h prior to analysis. (A) Immunofluorescence imaging with an anti- α tubulin antibody reveals the activation status of microglia (active: closed arrows; inactive: open arrows). Pre-incubation with anti-CD14 (+ anti-CD14) attenuated microglial activation (scale= 50 microns).

Figure II-5 continued. Exposure of the C4F6 epitope correlates with elevated SOD1-mediated microglial activation. (B) Media harvested from cells treated as in (A) were probed for TNF α by western analysis (n=4); the highest signal was observed for WT SOD1 ^{Δ IV/VII} treated cells. TNF α secretion was attenuated for the + anti-CD14 condition. SOD1 proteins added to the media were assessed by western analysis with a pan-SOD1 antibody (bottom) to ensure wells were exposed to equal amounts of protein; this antibody was less reactive for the loopless constructs. (C) Densitometry analysis of (B), all SOD1 variants are significantly increased compared to WT SOD1 (p<0.05) for the -anti-CD14 condition; statistically significant comparisons with SOD1 ^{Δ IV/VII} (*, p<0.05) for the -anti-CD14 condition are indicated; SOD1 variants that exhibit a significant attenuation in microglia activation in the presence of CD14 compared to the -anti-CD14 condition are indicated (#, p<0.05).

loops IV and VII within ALS-linked variants (Shipp et al. 2003, Cao et al. 2008, Molnar et al. 2009) partially exposes a toxic domain that is recognized by C4F6, and this domain becomes fully exposed when these loops are removed.

Enhancing the metal occupancy of SOD1 reduces exposure of the C4F6 epitope

To gain further insight into the relationship between the functional loops of SOD1 and the C4F6 epitope, we assessed the effect of SOD1 metal binding on C4F6 reactivity. Inductively coupled plasma optical emission spectroscopy (ICP-OES) was used to quantify the metallation status of our recombinant SOD1 proteins (**Fig. II-3**). The WT SOD1 dimer contained approximately 1.9 equivalents of zinc and only 0.2 equivalents of copper, consistent with previous measurements (Hayward et al. 2002). SOD1 variants exhibited a relatively reduced metallation status with respect to zinc, especially SOD1 G85R (Hayward et al. 2002) (**Fig. II-3**). The dynamics within loops IV and VII are severely perturbed in metal-free SOD1 variants (Elam et al. 2003, Molnar et al. 2009), whereas coordination of copper and especially zinc stabilizes the tertiary and quaternary structures of SOD1 (Banci et al. 2003, Stathopoulos et al. 2003, Arnesano et al. 2004, Lynch et al. 2004). Since the metallation status of SOD1 correlates with its propensity to misfold, it may also influence C4F6 reactivity. In the absence of excess copper and zinc, a native western analysis of as-isolated recombinant SOD1 variants demonstrate C4F6 reactivity in the following rank order: SOD1 G85R > G93A > A4V ~ SOD1ox (**Fig. II-6A, left**). The relatively weak

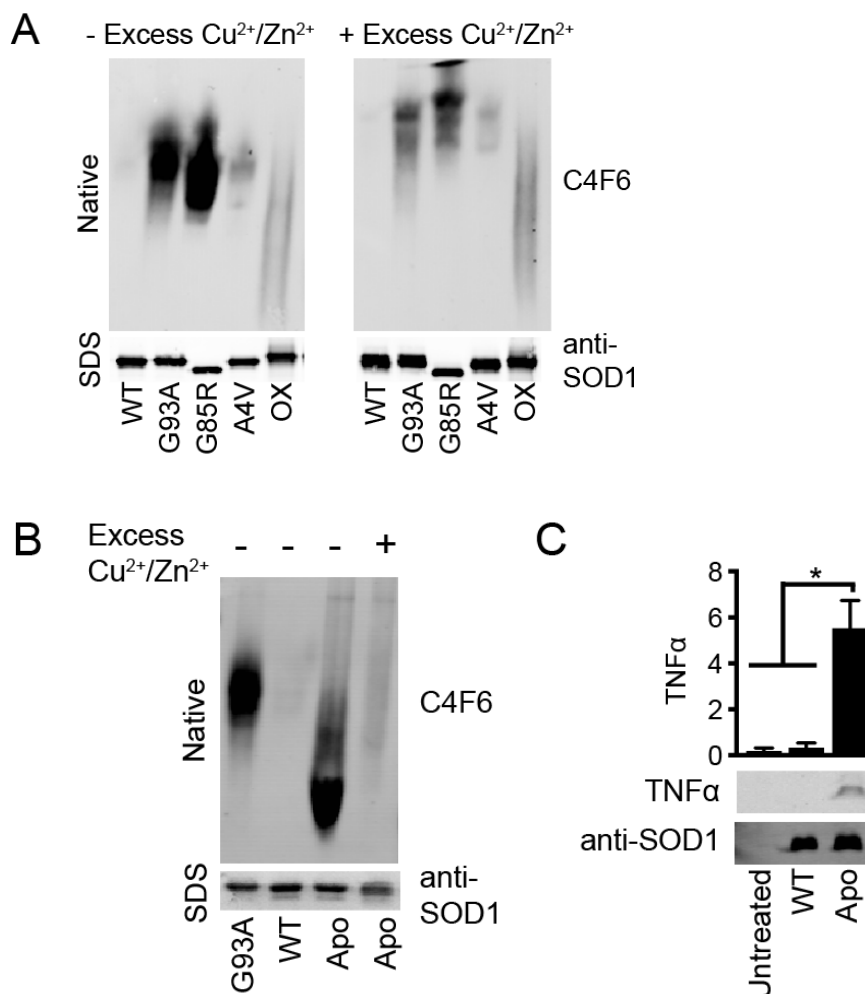


Figure II-6. The metallation status of SOD1 inversely correlates with C4F6 reactivity. SOD1 incubated for 24 h without (-) or with (+) 4-fold molar excess copper and zinc ($\text{Cu}^{2+}/\text{Zn}^{2+}$) and subjected to a native-PAGE western analysis with the C4F6 antibody. A denaturing western blot probed with a pan-SOD1 antibody (bottom) serves as a loading control. (A) C4F6 reactivity is reduced for SOD1 G93A, G85R and A4V when these proteins are incubated with excess metals. (B) Removing metals from WT SOD1, thereby generating apo-SOD1, confers reactivity with C4F6. C4F6 reactivity is attenuated when apo-SOD1 is incubated with excess $\text{Cu}^{2+}/\text{Zn}^{2+}$. (C) Apo-WT SOD1 activates primary microglia as indicated by the TNF α western analysis (gels, bottom panels; quantification, top; n=2, performed as described in **Figure II-5**). Statistically significant comparisons are indicated (*, $p < 0.05$).

reactivity of C4F6 for SOD1ox and A4V is consistent with the binding affinities measured by the OCTET, which showed a relatively tight binding interaction for the C4F6 antigen, SOD1 G93A (**Table II-1**). The strong reactivity for SOD1 G85R may stem from the low metallation status of this protein (**Fig. II-3**), as an apo-form of SOD1 G93A was used to create C4F6 (Urushitani et al. 2007). Although the binding of C4F6 for SOD1ox and A4V is weaker than SOD1 G93A and G85R, this antibody can still be used to detect these misfolded species with selectivity over the normally folded WT SOD1 protein (**Table II-1, Figs. II-1 and II-6**). In addition, C4F6 may exhibit enhanced reactivity for SOD1 A4V when this protein adopts a self-associated or aggregated form (Brotherton et al. 2012, Redler et al. 2014).

Upon incubation with excess copper chloride (II) and zinc sulfate ($\text{Cu}^{2+}/\text{Zn}^{2+}$) (Auclair et al. 2010), a change in the migration patterns of SOD1 variants (G93A, G85R, A4V) was observed, consistent with an increased positive charge and change in conformation for these proteins (Tiwari et al. 2009). A robust decrease in C4F6 reactivity was also observed by native western analyses when misfolded SOD1 species were incubated with metals (**Fig. II-6A, right**). Addition of excess metals did not have an effect on SOD1ox, and therefore an alternative strategy is necessary to “repair” this protein.

As expected, C4F6 did not recognize WT SOD1 in the absence or presence of excess $\text{Cu}^{2+}/\text{Zn}^{2+}$. However, the C4F6 epitope was exposed in full-length WT SOD1 when this protein was demetallated (**Fig. II-6B**). As observed

for the loopless constructs (**Fig. II-4**), exposure of the C4F6 epitope in apo WT SOD1 correlated with microglia activation (**Fig. II-6C**). C4F6 reactivity was attenuated when apo-SOD1 was incubated with excess metals (**Fig. II-6B**), however this attenuation was not sufficient to abolish SOD1-induced microglia activation (data not shown). Because the microglia assay is sensitive, even residual amounts of misfolded SOD1 that may have escaped remetallation are expected to induce microglia activation. An additional technical caveat of this experiment was that higher molarities of copper and zinc were used to remetallate apo-SOD1 for the microglia assay compared to the native gel analysis, potentially causing toxicity to the cells and/or causing aberrant modifications to the SOD1 protein itself (Steinebach and Wolterbeek 1993, Rakhit et al. 2002, Lemire et al. 2008). Nonetheless, the behavior of apo WT SOD1 in these experiments suggests that both C4F6 reactivity and SOD1-induced microglia activation can be modulated to some extent by the metallation status of SOD1.

Identification of key SOD1 residues required for C4F6 binding

The results of our crosslinking experiments revealed an important role for loops IV and VII in masking the C4F6 epitope, although the exact amino acids that comprise this epitope remained elusive. Therefore, a comprehensive site-directed mutagenesis strategy was employed to identify key residues within SOD1 that are involved in C4F6 binding. A series of amino acid substitutions were engineered throughout and proximal to the region corresponding to exon 4,

which was suggested to contain the C4F6 epitope in a previous study (Bosco et al. 2010). Experiments were initially performed in the SOD1^{ΔIV/ΔVII} background, as this protein exhibits the strongest interaction with C4F6 (**Fig. II-4C** and **Table II-1**). Partially purified recombinant SOD1 mutants were assessed for C4F6 binding by native and denaturing (i.e. SDS) western analyses with pan-SOD1 and C4F6 antibodies (**Fig. II-7**). Of interest were those constructs that exhibited reactivity with the pan-SOD1 antibody, but little or no reactivity with C4F6. Initially, multiple mutations were engineered to efficiently target the region within SOD1 that mediated C4F6 binding. The triple mutations V97A/I99A/D101A, D90A/D92A/V94A and D96A/S98A/D101A abolished C4F6 reactivity under both denaturing and native conditions (**Fig. II-7A**). Next, single mutations were engineered into SOD1^{ΔIV/ΔVII} to pinpoint residues that are required for the SOD1/C4F6 interaction. D92A and D96A mutations prevented C4F6 binding under both denaturing and native conditions for SOD1^{ΔIV/ΔVII}, whereas V97A prevented binding only under native conditions (**Fig. II-7B**). However, circular dichroism (CD) spectroscopy indicated that the V97A mutation severely altered the secondary structure of SOD1^{ΔIV/ΔVII} (**Fig. II-7C**). Conversely, the secondary structures as determined by CD were comparable for SOD1^{ΔIV/ΔVII} WT, D92A and D96A (**Fig. II-7C**). Further, V97A- SOD1^{ΔIV/ΔVII} appeared severely destabilized based on the melting profile acquired by differential scanning fluorimetry (DSF, **Fig. II-7D**), and thus the loss of C4F6 reactivity likely reflects a significant structural perturbation arising from this mutation. In contrast, D92A and D96A

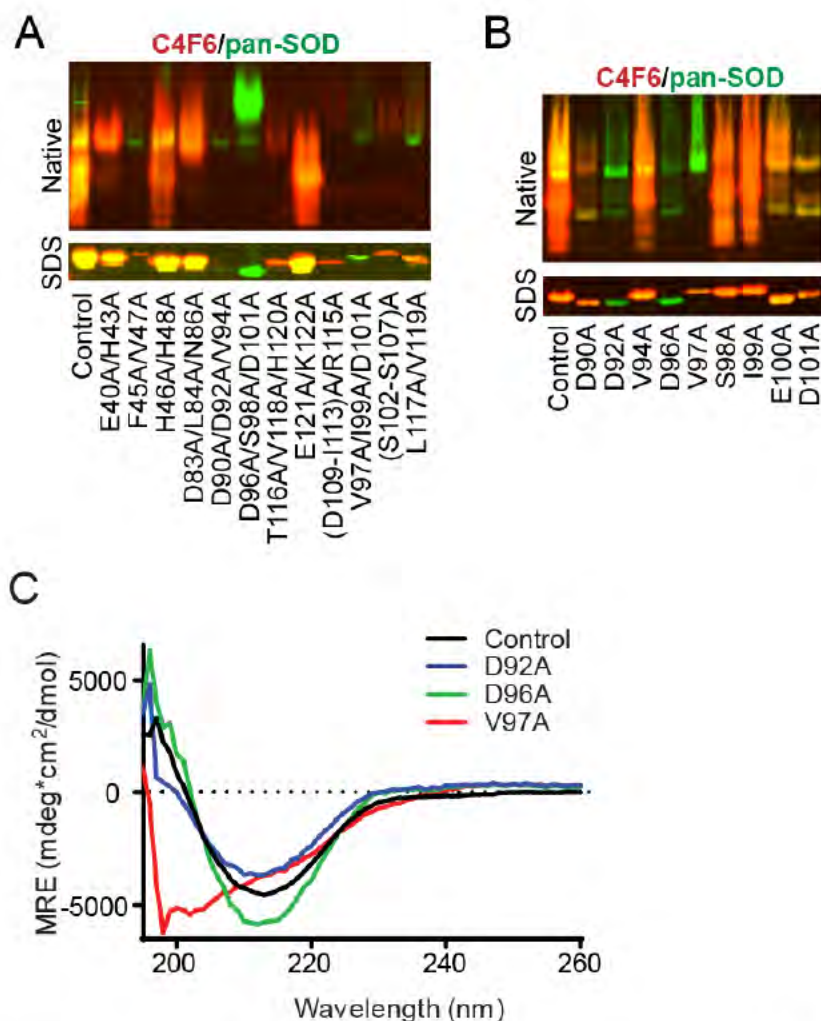


Figure II-7. Amino acids D92 and D96 in SOD1^{ΔIV/ΔVII} are required for C4F6 binding. Mutagenesis pinpoints key amino acids in misfolded SOD1 responsible for C4F6 reactivity. (A) Western analyses of SOD1^{ΔIV/ΔVII} with the indicated mutations (residue number corresponds to full-length SOD1). Pan-SOD1 (green) and C4F6 (red) antibodies were employed to assess partially purified SOD1 expression and reactivity with C4F6, respectively. Native western analysis (top) shows a loss of C4F6 reactivity for the following proteins: D90A/D92A/V94A, D96A/S98A/D101A, V97A/I99A/D101A and F45A/V47A. Denaturing western analysis (SDS) of SOD1^{ΔIV/ΔVII} variants reveal a loss of C4F6 reactivity for the triple mutations V97A/I99A/D101A, D90A/D92A/V94A and D96A/S98A/D101A. (B) The same analyses described in (A) demonstrate the D92A and D96A mutations induce a loss of C4F6 reactivity for SOD1^{ΔIV/ΔVII} under both native and denaturing conditions. (C) In contrast to D92A and D96A, the V97A mutation significantly perturbs the secondary structure of SOD1^{ΔIV/ΔVII} as indicated by circular dichroism (CD) spectroscopy (MRE, mean residue ellipticity).

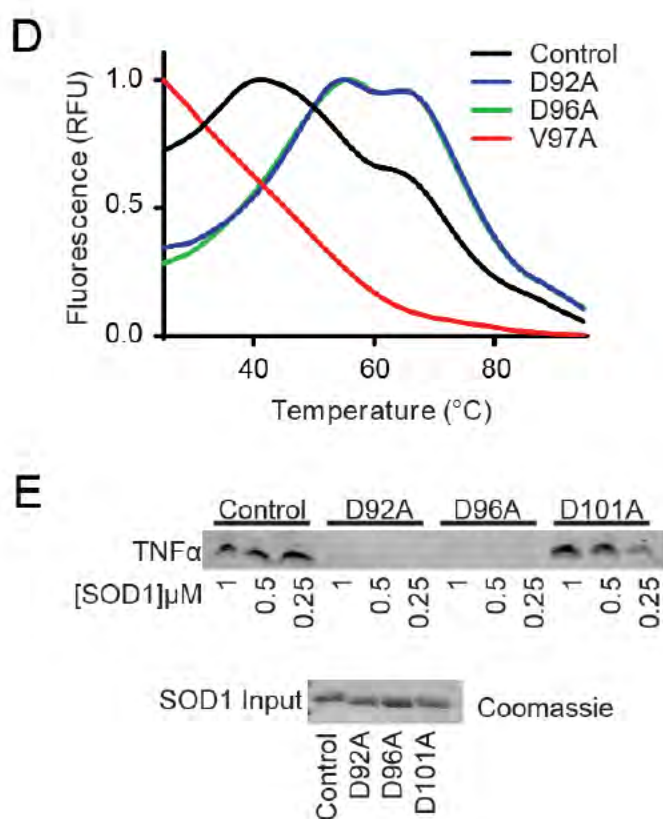


Figure II-7 continued. Amino acids D92 and D96 in SOD1 ^{Δ IV/ Δ VII} are required for C4F6 binding. (D) Differential scanning fluorimetry in the presence of SYPRO Orange demonstrates an increased thermostability for D92A-SOD1 ^{Δ IV/ Δ VII} and D96A-SOD1 ^{Δ IV/ Δ VII} of approximately 10°C compared to WT SOD1 ^{Δ IV/ Δ VII}. (E) Immortalized microglia (BV-2) cells were treated with the indicated SOD1 ^{Δ IV/ Δ VII} variant for 2 h and the media was subjected to western analysis (representative of n=3 independent experiments). In contrast to WT SOD1 ^{Δ IV/ Δ VII} (control), microglia activation is not detected upon treatment with the SOD1 ^{Δ IV/ Δ VII} (D92A and D96A) variants that show a loss of C4F6 binding (top gel). SOD1 input was analyzed by Coomassie stain as a loading control. (Control = WT SOD1 ^{Δ IV/ Δ VII}).

increased the melting temperature (T_m) of SOD1^{ΔIV/ΔVII} by at least 10 °C, indicative of a stabilizing effect for these mutations (**Fig. II-7D**). That these mutations abolish the interaction between C4F6 and mutant-SOD1 under denaturing conditions suggests residues D92 and D96 are directly involved in the binding between these proteins. For example, aspartic acid residues are charged and therefore have the potential to form ionic bonds between SOD1 and C4F6, whereas these bonds are eliminated by alanine substitutions.

Strikingly the activation of an immortalized BV-2 microglia cell line by SOD1^{ΔIV/ΔVII} was eliminated by the D92A and D96A point mutations (**Fig. II-7E**). In contrast, a variant that did not exhibit altered C4F6 reactivity (e.g., D101A, **Fig. II-7B**) was still able to activate microglia. One possibility is that the D92A and D96A mutations alter the conformations of beta strands 5 and 6 within SOD1^{ΔIV/ΔVII}, thereby reducing the exposure of these strands and thus the toxic effects they mediate (Richardson and Richardson 2002, Elam et al. 2003, Valentine and Hart 2003).

The D92A and D96A mutations also prevented C4F6 binding under both denaturing and native conditions in the context of full-length ALS-linked SOD1 variants (G93A, G85R, and A4V) (**Fig. II-8A**). To assess the role of these residues in SOD1-induced microglia activation in the context of the full-length protein, the D96A mutation was introduced into ALS-linked SOD1 (G93A, G85R, A4V) proteins. All of the D96-containing variants maintained the ability to

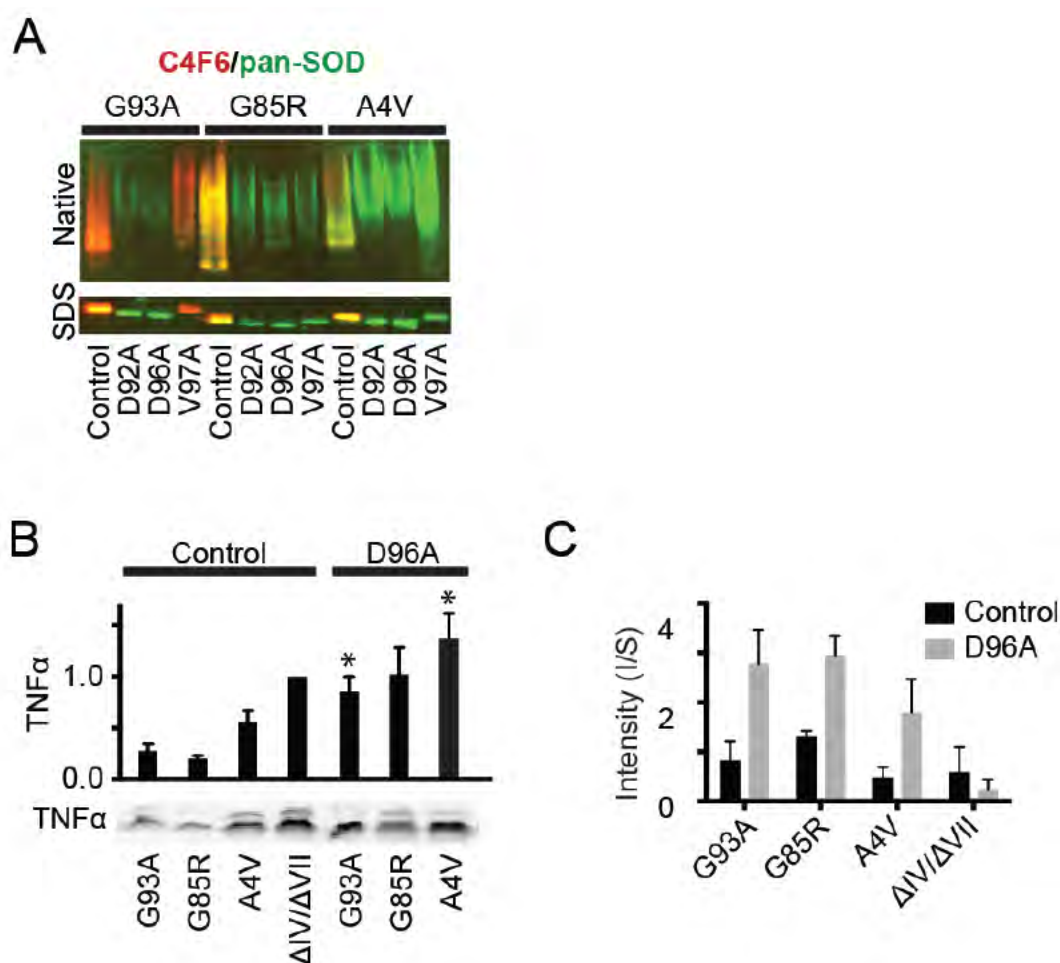


Figure II-8. Amino acids D92 and D96 in full-length SOD1 variants are required for C4F6 binding. (A) The same analyses described in Fig. II-7A demonstrate the D92A and D96A mutations induce a loss of C4F6 reactivity for full-length ALS-linked SOD1 variants under both native and denaturing (SDS) conditions. 'Control' refers to the respective variant without the additional mutation. (B) ALS-linked proteins containing the D96A mutation retain the ability to activate microglia as indicated by TNF α western analysis (bottom, performed as described in Figure II-5). Quantification of TNF α is displayed above. Statistically significant comparisons between ALS-linked SOD1 variants and their D96A counterparts are indicated (*, $p < 0.05$; $n = 2$). (C) The insoluble/soluble ratio (I/S) is enhanced for full-length ALS-linked SOD1 variants when the D96A mutation is present. Graph represents results from a western blot and densitometry analysis of lysates prepared from *E. coli* expressing the indicated SOD1 protein ($n = 2$).

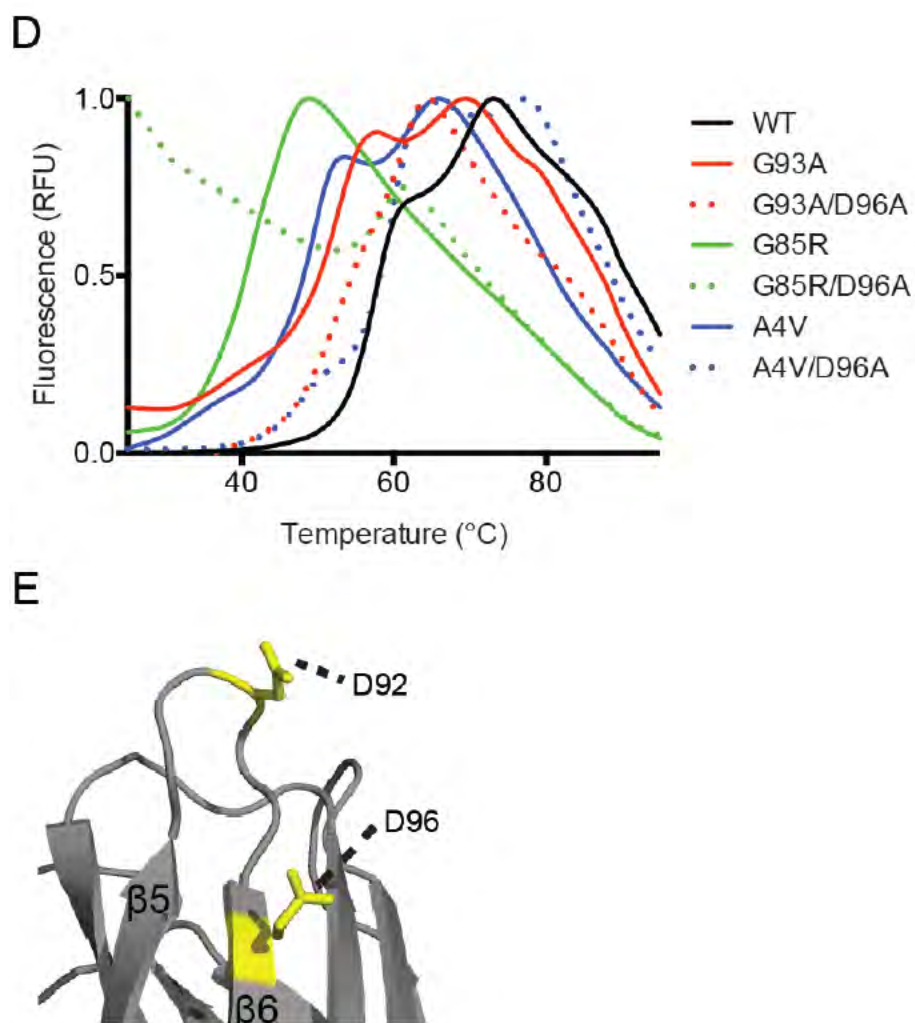


Figure II-8 continued. Amino acids D92 and D96 in full-length SOD1 variants are required for C4F6 binding. (D) The melting temperature of SOD1 variants with the additional D96A mutation as indicated by differential scanning fluorimetry in the presence of Sypro Orange demonstrates a destabilization for the SOD1 G85R variant. The remaining variants have an increase in melting temperature in the presence of D96A, likely caused by their increased aggregation propensity (C). (E) The location of amino acids D92 and D96 mapped onto SOD1 ^{Δ IV/ Δ VII} (PDB ID: 4BCZ).

activate primary microglia (**Fig. II-8B**), indicating there is still a misfolded conformation within SOD1 despite abolishing the binding interaction between SOD1 and C4F6. This misfolded conformation is likely within the zinc binding and electrostatic loops themselves, since the truncated variant, SOD1^{ΔIV/ΔVII}, lacking these loops no longer induces toxicity in the presence of the D96A mutation (**Fig. II-7E**). In fact, the D96A mutation may worsen the misfolded nature of full-length mutant SOD1 as indicated by the higher levels of TNF α for ALS-linked proteins with this mutation (**Fig. II-8B**), increased aggregation propensity (**Fig. II-8C**) and an alteration in the melting profiles as indicated by DSF (**Fig. II-8D**). While native SOD1 must be misfolded for C4F6 to bind, a loss of C4F6 binding does not require SOD1 to be properly folded. These data demonstrate that a single amino acid substitution is not sufficient to restore a wild-type like conformation in an ALS-linked SOD1 protein. Alternatively, strategies aimed at developing chemical chaperones to stabilize misfolded SOD1 and/or mask the C4F6 epitope could be pursued.

Discussion

The structural conformation(s) within misfolded SOD1 that trigger toxic events in ALS have not been defined. Based on the following observations, we posit that the C4F6 epitope represents a misfolded conformation that confers toxicity. First, C4F6 reactivity has been demonstrated in both SALS- (Bosco et al. 2010) and FALS-human spinal cord sections (Brotherton et al. 2012). Second, C4F6 preferentially binds both FALS-linked SOD1 (Urushitani et al. 2007, Bosco

et al. 2010, Prudencio and Borchelt 2011, Brotherton et al. 2012) and aberrantly modified WT SOD1 (Bosco et al. 2010) proteins (**Table II-1**). Third, C4F6 blocks the toxic effect of SOD1 derived from SALS-human spinal cord tissues in an axonal transport assay (Bosco et al. 2010). Fourth, C4F6 reactivity within spinal cord sections of SOD1 G93A transgenic mice directly correlates with disease progression (Brotherton et al. 2012).

In the present study, we quantified the disassociation constants between C4F6 and FALS-linked SOD1 mutants and demonstrated binding for all FALS-linked SOD1 variants tested. While C4F6 exhibited the lowest relative affinity for SOD1 A4V (**Table II-1** and **Fig. II-6**), this antibody is still able to detect this variant, which is both aggressive and common in North America, with clear selectivity over normally folded WT SOD1. Further, Brotherton et al. detected C4F6-positive inclusions in human FALS spinal cord tissues expressing SOD1 A4V (Brotherton et al. 2012), suggesting that C4F6 reactivity is enhanced for aggregated forms of SOD1 A4V. Information regarding the residues and structural elements that comprise the C4F6 epitope have been lacking (Bosco et al. 2010). Unfortunately, attempts to assess the SOD1/C4F6 complex by H/D exchange and to gain high-resolution information from X-ray crystallography have been unsuccessful. We attempted to co-crystallize the SOD1 G93A/C4F6 Fab complex, but crystals repeatedly contained solely the SOD1 protein (data not shown). For H/D exchange of the C4F6/SOD1 complex, the amount of antibody required to shift the majority of SOD1 molecules to the bound state resulted in an

overlapping of SOD1 and C4F6 spectra. Differentiating the spectra of SOD1 and C4F6 is pivotal for the data interpretation, and therefore prohibited the analysis (data not shown). Both of these approaches were likely hindered by the low binding affinity of SOD1 and C4F6 (**Table II-1**). Alternatively, our chemical cross-linking and mass spectrometry strategy developed here was employed to define the C4F6 epitope, leading us first to loops IV and VII within SOD1 (**Fig. II-2**). To our surprise, all loop-less constructs tested herein exhibited significantly enhanced binding affinity for C4F6 relative to their full-length SOD1 counterparts (**Fig. II-4C**). These results demonstrate that DSP and EDC report on SOD1 residues proximal to, but not directly in, the C4F6 epitope. Nonetheless, using site-directed mutagenesis we were able to pin-point residues D92 and D96 as being critical for the SOD1/C4F6 binding interaction (**Fig. II-7**). These residues are likely engaged in chemical bonding with C4F6, such that their mutagenesis precludes a C4F6/SOD1 interaction but yet retains the misfolded nature of ALS-linked SOD1. The model that emerges from these studies is one where loops IV and VII modulate the exposure of the C4F6 epitope. FALS-linked mutations, oxidation and demetallation (**Fig. II-1, II-2, and II-6**) alter the stability and conformation of these loops (Elam et al. 2003, Molnar et al. 2009). These events contribute to the formation of the C4F6 epitope, and removal of these loops allows full exposure to this region (**Fig. II-4**).

While the toxicity of misfolded SOD1 proteins is well documented in the context of different assays and model systems (Rotunno and Bosco 2013), the

current study provides insight into one region within misfolded SOD1 that may confer toxicity. We demonstrate a direct correlation between exposure of the C4F6 epitope and SOD1-induced microglial activation (**Fig. II-5**). Chronic microglia activation is a hallmark of ALS pathogenesis, and SOD1-induced microglia activation leads to motor neuron death (Zhao et al. 2010). We also note that elements of β -strands 5 and 6, including residue D96, comprise the C4F6 epitope (**Figs. II-2B** and **II-8E**). Exposure of β -strands 5 and 6 mediate oligomerization of SOD1 and similar β -strands have been shown to mediate aberrant protein-interactions (Richardson and Richardson 2002, Elam et al. 2003, Valentine and Hart 2003). This is primarily because edge strands are poised and readily available to interact with other exposed edge strands (Richardson and Richardson 2002, Elam et al. 2003). Thus, these strands may contribute to the mechanism of toxicity induced by the C4F6 epitope. Other conformation specific antibodies with SOD1 epitopes overlapping with and unique to C4F6 have been described, indicative of additional misfolded regions within ALS-linked SOD1 proteins (Rakhit et al. 2007, Vande Velde et al. 2008, Forsberg et al. 2010, Gros-Louis et al. 2010, Fujisawa et al. 2012, Pokrishevsky et al. 2012, Pickles et al. 2013). Thus, it is plausible that other misfolded regions within SOD1 confer toxicity as well. It will be important to determine which epitope is most relevant to the toxic ALS-phenotypes induced by misfolded SOD1 *in vivo*.

Importantly, we show it is possible to convert the properly folded WT SOD1 to a microglia-activating, misfolded conformation recognized by C4F6 by stripping SOD1 of both copper and zinc (**Fig. II-6**). We further show the ability to revert the misfolded conformation of SOD1 to a more “WT-like” structure, as demonstrated by the reduced accessibility of the C4F6 epitope in misfolded SOD1 upon incubation with excess metals (**Fig. II-6**). A similar outcome could potentially be achieved with chemical chaperones, which have been used to mitigate the misfolding and toxicity of other amyloidogenic proteins (Coelho et al. 2013). Either with small molecules or alternative approaches, our results advocate for concealing the C4F6 epitope and/or stabilizing loops IV and VII as rational therapeutic strategies for SOD1-mediated ALS.

Materials and Methods

SOD1 protein expression and purification- The pET3d vectors containing human *SOD1* and *SOD1* ^{Δ IV/ Δ VII} (amino acid substitutions: C6A, C111S, and C146A) were generous gifts from Dr. Jill Zitzewitz (UMMS). This vector was used to construct WT *SOD1* ^{Δ IV/ Δ VII} used in this study (amino acid substitutions: A6C, S111C and C146A). The *SOD1* ^{Δ IV} construct was generated by Genscript and inserted into the pET3d vector using standard cloning techniques. All mutations in this study were generated using standard site directed mutagenesis methods. pET3d-SOD1 was expressed in BL21(DE3) PlysS cells and protein expression was induced with 1 mM IPTG (Sigma) in the presence of 200 μ M copper (II) chloride (Sigma) and 200 μ M zinc chloride (Sigma) when the culture reached an

optical density (OD 600) between 0.6 and 0.8. The bacterial culture was induced for 3 h at 37°C (wild-type SOD1) or 30°C (FALS-linked SOD1 and SOD1^{ΔIV/ΔVII} variants). Cells were harvested and SOD1 proteins fully purified as previously described (Hayward et al. 2002). Apo SOD1 and SOD1ox were generated from purified wild-type SOD1 as previously described (Svensson et al. 2006, Bosco et al. 2010). Protein concentrations for all subsequent analyses were quantified with the Pierce BCA Protein Assay kit (Thermo) and/or A280 using the appropriate extinction coefficients for monomeric SOD1.

For the mutagenesis screen in **Figure II-7**, SOD1^{ΔIV/ΔVII} proteins were “partially purified” by ammonium sulfate precipitation of the post-sonication supernatant (Hayward et al. 2002). Ammonium sulfate precipitation was accomplished by adding 0.16 g ammonium sulfate per 500 μl of bacterial lysate, agitating the mixture on a rotating platform for 15 min at 4°C, and then pelleting the precipitate by centrifugation at 13,000 rpm for 15 min. The supernatant was collected and used as the source of SOD1 protein. The samples were subjected to a denaturing western analysis (see Immunoblots below) and probed with a pan anti-SOD1 antibody.

Circular Dichroism- SOD1 variants were analyzed at 10 μM for full-length proteins and 20 μM for loop-deletion constructs in phosphate buffered saline, pH 7.4. Circular Dichroism (CD) spectra were acquired from 195-260 nm using a 0.1 cm cuvette at 25°C. CD spectra of SOD1 variants (WT SOD1, SOD1^{ΔIV} and SOD1^{ΔIV/ΔVII}) were acquired with a Jasco J-810 spectrophotometer (5 scans). CD

spectra of SOD1 Variants (D92A- SOD1^{ΔIV/ΔVII}, D96A- SOD1^{ΔIV/ΔVII} and V97A- SOD1^{ΔIV/ΔVII}) were acquired with an AVIV Model 400 Spectrophotometer (10 scans). Mean residue ellipticity (MRE) was calculated as follows: $MRE = (\theta * 100,000) / (A * [SOD1] * L)$, where θ represents raw data in millidegrees with buffer blank subtraction, A represents the number of amino acids in the SOD1 variant, and L represents the path length in cm.

Metal Analysis- SOD1 variants were prepared for quantitative metal analysis by dialysis with LC-MS grade water (Pierce) overnight at 4°C. SOD1 samples at concentrations ranging from 40 to 110 μ M were then subjected to an elemental analysis in technical duplicate for copper and zinc using ICP-OES (Center for Applied Isotope Studies, University of Georgia). Post-dialysis LC-MS grade water was analyzed as a buffer control and subtracted from the SOD1 samples prior to analyses.

Incubation of SOD1 proteins with excess copper and zinc- SOD1 proteins (10.75 μ M) were incubated in the presence of 4-fold molar excess copper (II) chloride and zinc sulfate for 24 h at 4°C prior to native and denaturing western analysis (see Immunoblots below for details).

Immunoblots- For denaturing western analyses, samples were diluted in 6x sample buffer (Boston Bioproducts, BP-111R). Samples were separated by PAGE with 15% Tris-acrylamide gels (unless otherwise noted) in 1% SDS, 25 mM Tris, 192 mM glycine and transferred to PVDF membrane (Millipore) in 25 M Tris, 192 mM glycine. Membranes were blocked for 1 h in Odyssey blocking

buffer (LI-COR). Primary antibodies were incubated at 4°C overnight at the following dilutions: (pan-SOD1(Taylor et al. 2007), 1:500; C4F6, 0.3 µg/ml; anti-TNF α , 1:200 (Santa Cruz, sc-1351); and anti-Fab fragment, 1:1000 (Sigma, B0529)). The blots were incubated for 1h with fluorophore-conjugated secondary antibodies (LI-COR) prior to visualization by the Odyssey Infrared Imaging System (LI-COR). The Odyssey infrared imaging software (LI-COR) was used for densitometry calculations. For native western analysis, samples were diluted 1:1 with Native Sample Buffer (Bio-Rad, 161-0738), electrophoresed with a 7.5% Tris-acrylamide gel and transferred to PVDF in 25M Tris, 192 mM glycine at 4°C. Blots were processed as described above for denaturing western analyses.

C4F6 expression, purification and Fab generation- A hybridoma cell line expressing the C4F6 monoclonal antibody was a generous gift from Dr. Jean-Pierre Julien (Laval University)(Urushitani et al. 2007). C4F6 was purified with a Protein A agarose column (Pierce) according to the manufacturer's instructions. Purified C4F6 was buffer exchanged into 0.85% NaCl with PD10 G25 desalting columns (GE Healthcare). Fab fragments of C4F6 were generated from purified C4F6 antibody using immobilized papain (Thermo Scientific) in the presence of cysteine according to the manufacturer's instructions.

OCTET binding studies- Using the OCTET QK automated system (ForteBio) in a 96-well format at ambient temperature, C4F6 was immobilized onto anti-mouse IgG Fc Capture Biosensor tips (ForteBio). The extent to which SOD1 bound to C4F6 was determined using curves generated by Bio-layer Interferometry, which

is based on light interference on the biosensor tip in the presence of SOD1 compared to an internal reference. To generate binding curves, the C4F6-coated tips were immersed into wells containing 12, 15 or 25 μM of the respective SOD1 variant in phosphate buffered saline (PBS, pH 7.4) until the binding reached equilibrium (~120s) followed by immersion into PBS-containing wells for dissociation as described (Broering et al. 2013). Dissociation constants (K_d) were determined by fitting the generated curves using the Forte Bio software with a "1:1" binding model. At least two independent experiments were averaged for each SOD1 variant.

Sequencing the C4F6 antibody by mass spectrometry and RNA/DNA analysis- For mass spectrometry sequencing of the C4F6 protein, tryptic fragments of C4F6 for mass spectrometry analyses were prepared as previously described (Shevchenko et al. 2006) and subjected to matrix-assisted laser desorption/ionization (MALDI) Time-of-Flight (TOF) and liquid chromatography tandem mass spectrometry (LC-MS/MS) analyses. For MALDI-TOF/TOF, the digested peptide samples prepared above were further purified using C18 Zip Tips (Millipore) according to the manufacturer's instructions. Samples were co-applied to the MALDI sample target with alpha-cyano-4-hydroxycinnamic acid matrix (5 mg/ml). Samples were analyzed with an Axima-TOF2 MALDI mass spectrometer (Shimadzu Scientific Instruments) following external calibration. Data were acquired in the positive ion reflectron mode using both collision induced dissociation (CID) and post-source decay (PSD) fragmentation modes.

All spectra were processed and subjected to database search using Mascot (Matrix Science). For MS searches, the Peptide Mass Fingerprint program was used with a peptide mass tolerance of 100 ppm. For CID and PSD spectra the MS/MS Ion Search program was used with a Precursor tolerance of 100 ppm and a fragment tolerance of 1.5 Da.

For LC-MS/MS analysis, tryptic peptides were reconstituted in 25 μ l 0.1% (v/v) TFA and a 3 μ l aliquot was directly loaded onto a 100 μ m ID custom packed trap column packed with 2 cm of 200 \AA , 5 μ C18AQ particles (Michrom Bioresources).

Peptides were then separated on a 75 μ m ID analytical column packed with 25 cm 100 \AA , 5 μ C18AQ (Michrom) to a gravity-pulled tip. Peptides were eluted using a Proxeon Easy nanoLC (Thermo Scientific) with a linear gradient from 100% solvent A (0.1% (v/v) formic acid in 5% (v/v) acetonitrile) to 35% solvent B (0.1% formic acid in acetonitrile) over 35 min at a flow rate of 300 nl/min. Data were acquired in positive ion electrospray mode using a Thermo Scientific LTQ Orbitrap Velos Pro mass spectrometer operating in the data dependent mode over the range m/z 350-2000. MS scans were acquired in the Orbitrap at a resolving power of 60,000 followed by 10 MS/MS spectra acquired in the LTQ ion trap. Raw data files were processed with Extract_MSN (Thermo Scientific) and were searched against the mammalian index of the NCBI nr database using Mascot (ver. 2.3). Parent mass tolerances were set to 10 ppm and fragment mass tolerances were set to 0.5 Da, and variable modifications of

acetyl (protein N-term), pyroglutamic for N-terminal glutamine, carbamidomethylation of cysteine and oxidation of methionine were considered.

Further sequencing of C4F6 was accomplished by extracting total RNA from C4F6 hybridoma cells using RNeasy kit (Qiagen) and PCR amplifying C4F6 Fab RNA for both heavy and light chains. PCR primers were designed by comparing the partial C4F6 Fab sequence obtained through mass spectrometry analyses (described above) with known antibody sequences for the same isotype, IgG2a, as C4F6 (<http://www.imgt.org/>). These primers were used in a OneStep RT-PCR Kit (Qiagen) reaction to generate corresponding cDNA, which was subjected to gel purification followed by DNA sequencing (Genewiz).

Cross-linking of SOD1 proteins with C4F6 Fab- For the DSP (dithiobis[succinimidylpropionate]; Thermo Scientific) and d₈-DSP (ProteoChem) reaction, the respective SOD1 protein (20 μM) and the Fab fragment of C4F6 (5 μM) were combined in PBS and cross-linked according to the manufacturer's instructions. The samples were then mixed 1:5 with 6x non-reducing SDS loading buffer (Boston Bioproducts), heated at 90°C for 5 min and subjected to SDS PAGE with a 10% Tris-acrylamide gel followed by coomassie blue staining (50 μl reaction/well) or western analysis (as described above; 15 μl reaction/well). Tryptic (Promega) in-gel digest was performed essentially as described (Shevchenko et al. 2006). Extracted peptides were concentrated to 30 μl and combined 1:1 (DSP:d₈-DSP) prior to mass spectrometry analysis (as described below). For EDC (1-ethyl-3-[3-dimethylaminopropyl]carbodiimide hydrochloride;

Thermo Scientific) SOD1 and the Fab fragment of C4F6 were combined to a final concentration of 100 μM and 9 μM , respectively. EDC cross-linking was performed according to the manufacturer's instructions. The reaction was quenched by mixing samples 1:5 (v/v) with 6x reducing loading buffer and heating at 90°C for 5 min. Samples were analyzed as described above for DSP cross-linking.

Identification of DSP and EDC SOD1/C4F6 Fab cross-linked peptides by mass spectrometry- Tryptic digests were analyzed by LC-MS/MS as described above for sequencing the C4F6 antibody with several noted modifications. During the 120 minute gradient elution, data dependent acquisition acquired full MS scans from m/z 350-2000 in the Orbitrap Velos Pro (resolution 60000) followed by higher-energy collisional dissociation (HCD) scans on the 10 most intense parent ions acquired in the Orbitrap. Parent ions with charge states of 1+, 2+ or 3+ were excluded from the analysis. For database searching, a concatenated peptide database was generated by xComb (Panchaud et al. 2010) containing all possible EDC or DSP linked tryptic peptides (allowing up to 2 missed cleavages) of the intermolecular interactions of SOD1 and C4F6. The raw data was searched in Proteome Discoverer 1.3 against the concatenated database, with parent tolerance of 15 ppm and fragment ion tolerance of 0.05 Da. Additionally, spectra were verified manually with the use of GPMW 8.20 software (Lighthouse Data, Denmark). To minimize false positives, only cross-linked

peptides with >50% sequence coverage were included in the list of identified cross-links.

Microglial activation assays- Primary Microglia were isolated from mouse embryonic cerebral cortices and maintained as previously described (Suzumura et al. 1987, Sasabe et al. 2007). Microglia were plated at 100,000 cells/ml in a non-tissue culture treated 96-well plate (Costar). Microglia were allowed to adhere to the plate for 48 h prior to treatment with SOD1 proteins. Purified recombinant SOD1 variants were added directly to culture medium of microglia at a concentration of 2.5 μ M for 48 h prior to immunofluorescence and immunoblotting analyses. Where indicated, the anti-CD14 antibody (Cell Sciences, CPC401A) was added to wells at 1:200 dilution 24 h prior to SOD1 treatment. The animal protocol was approved by IACUC at the University of Massachusetts Medical Center in compliance with the Animal Welfare Act, U.S. Public Health Service Policy and the National Institute of Health guidelines. All statistics were determined with an unpaired, two-tailed T-test with Welch's correction.

Immunofluorescence- Cells were fixed for 5 min with 4% paraformaldehyde followed by a 30 min block in PBS, 1% BSA, 0.5% Triton (PBSAT). Primary (anti-CD11 b/c, 1:200 (Pierce, PA1-46162); anti- α tubulin, 1:100 (Sigma, T9026)) and secondary antibodies (fluorophore-conjugated, 1:2000 (Jackson ImmunoResearch Laboratories)) were added for 1 h at ambient temperature in

PBSAT followed by nuclear staining with DAPI (1:300,000; Invitrogen, D1306) and mounting with FluorSave reagent (Fisher, D00060).

PREFACE TO CHAPTER III

Patient peripheral blood mononuclear cells and red blood cells were collected and isolated by Diane McKenna-Yasek, Catherine Ward, and Peter Sapp. Samples for mass spectrometry analysis were lyophilized and injected into the mass spectrometer by Kristin Boggio. Squid axoplasm isolation and perfusion was performed by Scott Brady and colleagues. All other work presented in this chapter was performed by Melissa S. Rotunno.

CHAPTER III: EXPLOITING SOD1 AS A POTENTIAL BIOMARKER

Introduction

Finding a reliable biomarker for ALS is critical for patient stratification for clinical trials and for early diagnosis. Multiple studies have found a large number of proteins that have a unique trend for ALS patients, but are unreliable for diagnosis when analyzing data from an individual out of the healthy population (reviewed in (Robelin and Gonzalez De Aguilar 2014)). This data, although powerful at shedding light on disease mechanism, lacks the clear-cut answer required for use as a biomarker. The ALS community would greatly benefit from a biomarker that can accurately differentiate ALS from other neurological disorders with similar clinical presentations. Early diagnosis is critical for early treatment intervention when effective drugs become available and for further classification of disease stages in clinical trials. Currently, diagnosis is through progression of paralysis, which requires approximately a year of observation from symptom onset (Radunovic et al. 2007). This method impedes opportunities for early treatment and, in turn, hinders chances of slowing progression, as early treatment has proved vital in ALS mouse models (Zhu et al. 2002, Kieran et al. 2004).

Misfolded SOD1 is present in end-stage SALS patient spinal cord tissue (Bosco et al. 2010, Forsberg et al. 2010, Pokrishevsky et al. 2012), but information regarding the extent of SOD1 misfolding in other biofluids and tissues as well as the post-translational modifications that induce this misfolding have

been lacking. In addition to the spinal cord, we identify and define differentially modified forms of SOD1 present in the brain and blood of SALS patients. The findings presented here put forward these differentially modified forms of SOD1 as a potential biomarker for sporadic ALS. Specifically, we demonstrate elevated SOD1 protein in CSF from ALS patients and misfolded SOD1 in a subset of sera samples. This study also identifies an over-oxidized SOD1 species in sporadic ALS peripheral blood mononuclear cells (PBMCs) that is reduced in controls. Further, we found a species of SOD1 present in PBMCs of healthy controls that is significantly reduced in SALS patients. Together, these data support a role for altered SOD1 homeostasis in SALS, but whether SOD1 is actively involved in pathogenesis or is simply a modified bystander has yet to be determined. Either way, the differential expression of SOD1 species identified here has the potential to serve as a biomarker for ALS.

Results

C4F6 ELISA detects misfolded SOD1

C4F6 is an established tool for identifying misfolded SOD1 in mouse models, human tissue and recombinant SOD1 protein (Urushitani et al. 2006, Bosco et al. 2010, Prudencio and Borchelt 2011, Brotherton et al. 2012, Pickles et al. 2013). Since it is known that C4F6 reports on SOD1 misfolding (See **Chapter II**), we can exploit this antibody for large scale screening of biofluids for the presence of misfolded SOD1. The specificity of C4F6 binding to recombinant misfolded SOD1 variants (SOD1 G93A, G85R, A4V, and OX) over WT SOD1 in

a C4F6-based sandwich ELISA was tested. Briefly, the plates were coated with the C4F6 antibody, followed by the addition of the indicated SOD1 variant. Then, the plates were incubated with anti-SOD1 and the amount of misfolded SOD1 present was quantified with an additional HRP-conjugated secondary antibody. Consistent with native PAGE and OCTET studies described in Chapter II (**Fig. II-6, Table II-1**), SOD1 G93A exhibited the greatest reactivity with C4F6. SOD1^{ox} displayed similar reactivity, while SOD1 A4V and G85R were barely differentiated from wild-type at concentrations *in vivo* in humans (200 ng/mL; **Fig. III-1A**). However, it should be noted that the reactivity of SOD1 A4V and G85R with C4F6 are easily distinguished from WT SOD1 in this C4F6-ELISA when concentrations nearing the apparent K_d ($>2 \mu\text{g/mL}$ or $0.13 \mu\text{M}$) are employed (**Table II-1, Fig. All-4**).

To assess the specificity of C4F6 reactivity in a more complex system, HEK cells were transiently transfected with either GST-tagged WT SOD1 or SOD1 G93A at levels similar to that of endogenous SOD1 (**Fig. III-1B**). After 24 hours, the cell lysates were subjected to the C4F6-ELISA (**Fig. III-1C**). HEK cells transfected with WT SOD1 (HEK WT) had no detectable misfolded SOD1, as determined by C4F6 reactivity. Importantly, this data suggests that complex protein mixtures, such as cell lysates, do not increase the background inherent in the C4F6-ELISA protocol, demonstrating high specificity of C4F6 to misfolded SOD1. In contrast, HEK cells transfected with SOD1 G93A had high C4F6 reactivity confirming misfolded SOD1 can be identified in heterogeneous lysates.

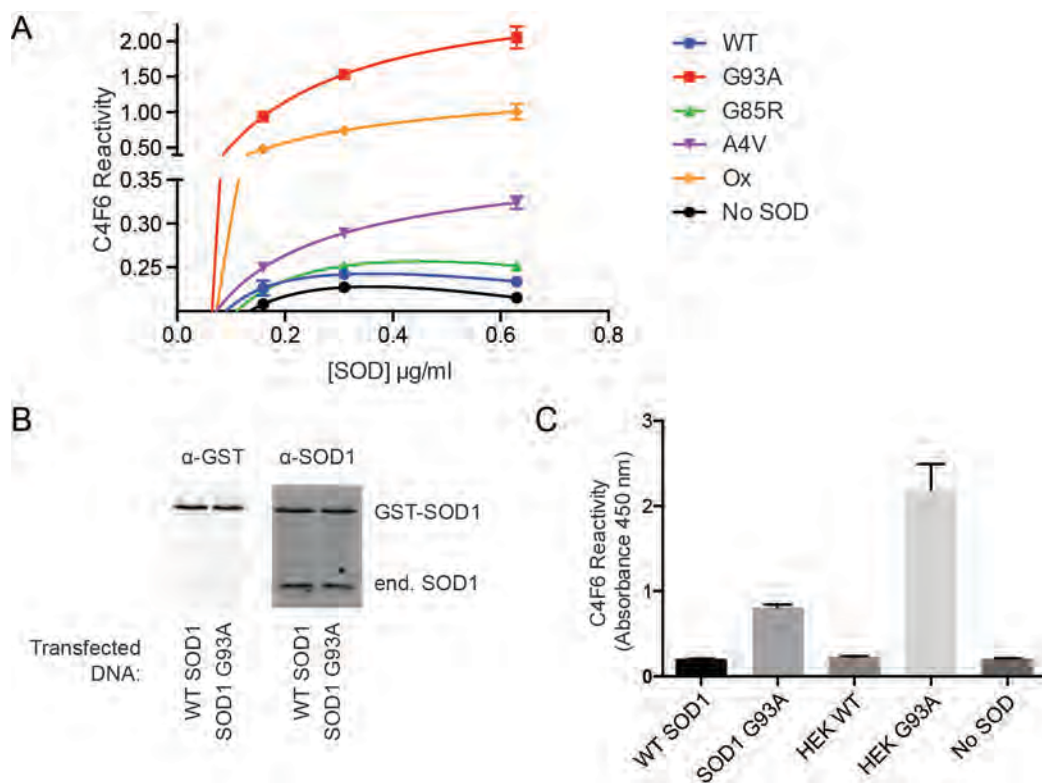


Figure III-1. Detection of misfolded SOD1 utilizing the C4F6-based ELISA. (A) The C4F6-based ELISA specifically reacts with a subset of ALS-linked SOD1 (G93A and A4V) and oxidized SOD1 (Ox) over wild-type (WT). Reactivity of ALS-linked mutant G85R has similar detection to that of WT. The graph is a representative of two independent experiments. Error bars represent SEM of a technical duplicate. (B) HEK cells were transiently transfected for 24 h with GST-tagged WT SOD1 or G93A followed by lysis with sonication. A total of 15 µg of lysate was loaded and analyzed by western blot with anti-GST (*left*) and anti-SOD1 (*right*). Both WT and G93A GST-tagged SOD1 were expressed at levels similar to endogenous SOD1 (end. SOD1). (C) A total of 150 µg HEK lysate described in (B) was analyzed with the C4F6-based ELISA. ALS-linked SOD1 G93A retains its high C4F6 reactivity when in a lysate (HEK G93A). WT SOD1 is not recognized by C4F6 when expressed transiently in HEK cells (HEK WT). Error bars represent SEM of technical duplicate. (WT SOD1, recombinant SOD1 at 100 ng/mL that serves as negative control; No SOD1, buffer control that serves as negative control; SOD1 G93A, recombinant protein at 100 ng/mL that serves as positive control).

SOD1 protein is elevated in the CSF of ALS patients

Both the C4F6-ELISA and a total-SOD1 ELISA were employed to assess the concentration and extent of misfolding of SOD1 in the CSF of ALS subjects. First, the sensitivity of the C4F6-ELISA was assessed in the context of CSF. CSF samples from i) ALS patients harboring mutations in SOD1 (FALS) and ii) control CSF with exogenous recombinant SOD1 G93A (spiked) were tested. The C4F6-ELISA was unable to detect mutant SOD1 in the SOD1 FALS-derived CSF (**Fig. III-2A**). This is not surprising, as the C4F6 reactivity to the mutations in these individuals have either not been established (I113T) or have been shown to be similar to WT SOD1 (A4V) at concentrations present in the CSF (200 ng/mL, see **Fig. III-1A**). The SOD1 G93A spiked control, however, is clearly distinguishable from that of control CSF, suggesting a subset of misfolded SOD1 species could be identified with this technique.

The C4F6-ELISA was also employed to assess the extent of SOD1 misfolding in 105 SALS patients, 39 healthy controls (HC), and 27 patients with non-ALS neurological disorders (disease controls, DC). The DC cohort included multiple sclerosis (n=9), lower motor neuron disease (n=1), peripheral neuropathy (n=3), Alzheimer's disease (n=3), and the remaining 11 were characterized as "other" neurological disorder. Despite the fact that exogenous recombinant, misfolded ALS-linked SOD1 protein was clearly detected in the CSF, no misfolded SOD1 was detected in any of these cohorts (**Fig. III-2B**). This could be due to the detection limit of the assay, as a subset of misfolded SOD1

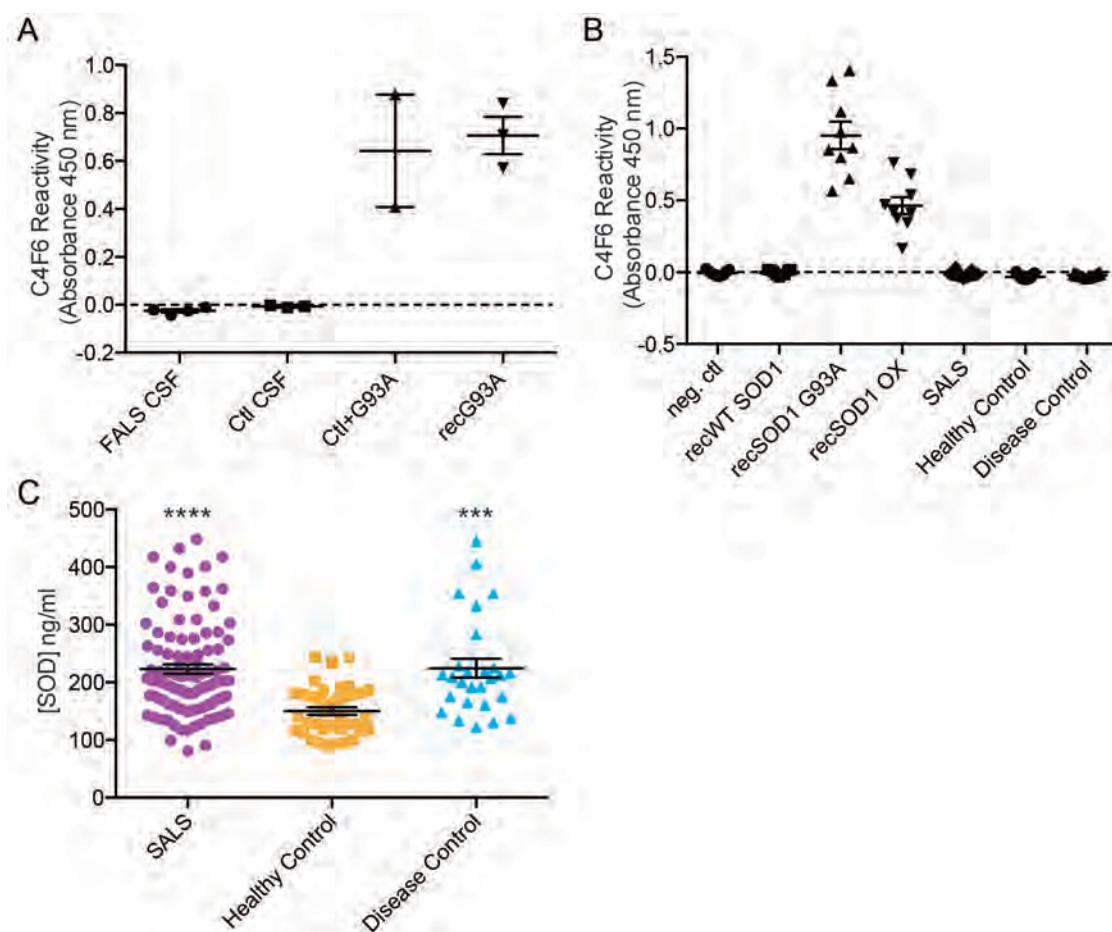


Figure III-2. Quantification of SOD1 in cerebrospinal fluid by ELISA. (A) The C4F6-based ELISA is unable to differentiate between CSF samples of SOD1-FALS patients harboring mutations (A4V, I113T, L9V) from controls (Ctl). Recombinant SOD1 G93A exogenously added to control CSF (Ctl+G93A) at 100 ng/mL is detectable with the C4F6-based ELISA. (B) Misfolded SOD1, as determined by the C4F6-based ELISA, is not detectable in CSF of ALS patients (SALS, n=105; Healthy Controls, n=39; Disease Controls, n=27). (C) Total SOD1 was quantified using a sandwich ELISA for samples described in (B). SALS and Disease Controls have a ~50% increase in total SOD1 in the CSF (****, $p < 0.0001$; ***, $p < 0.001$). No significant difference between SALS and disease controls was observed. Error bars indicate the standard error of the mean (SEM).

variants are not detectable at concentration levels approaching that of CSF (200 ng/mL, **Fig. III-1A**). The total concentration of SOD1, however, in SALS patients was significantly elevated to 48% above the mean of the HC group (150 ng/mL, HC; 222 ng/mL, SALS, **Fig. III-2C**). DCs are also elevated by 49%, suggesting this could be a general response to the increased level of oxidative stress seen among these diseases. These data are consistent with Winer and colleagues who found a 30% increase in SOD1 relative to the total protein in both SALS patients and other neurological disease controls compared with healthy controls in the CSF (Winer et al. 2013).

A subset of SALS patients' sera harbors misfolded SOD1

The C4F6-ELISA described above was employed to assess the extent of SOD1 misfolding in sera samples from SALS subjects. To establish the sensitivity of the assay in the context of sera, blood collected from FALS patients with an *SOD1* mutation was employed as a positive control. As described above for CSF, we were unable to differentiate the FALS-linked SOD1 from the HC sera in this assay (**Fig. III-3A**), likely due to the mutations we were able to obtain (A4V and L9V) that are not conducive to binding the C4F6 antibody at concentrations present in sera (**Fig. III-1A, III-2A**). Next, a cohort of SALS sera samples was selected for testing in the C4F6-ELISA based on published data demonstrating that these samples had elevated levels of anti-oxidized SOD1 antibodies that in turn correlated with longer survival (van Blitterswijk et al. 2011). Two out of the 11 SALS sera samples tested showed misfolded SOD1 elevated from baseline

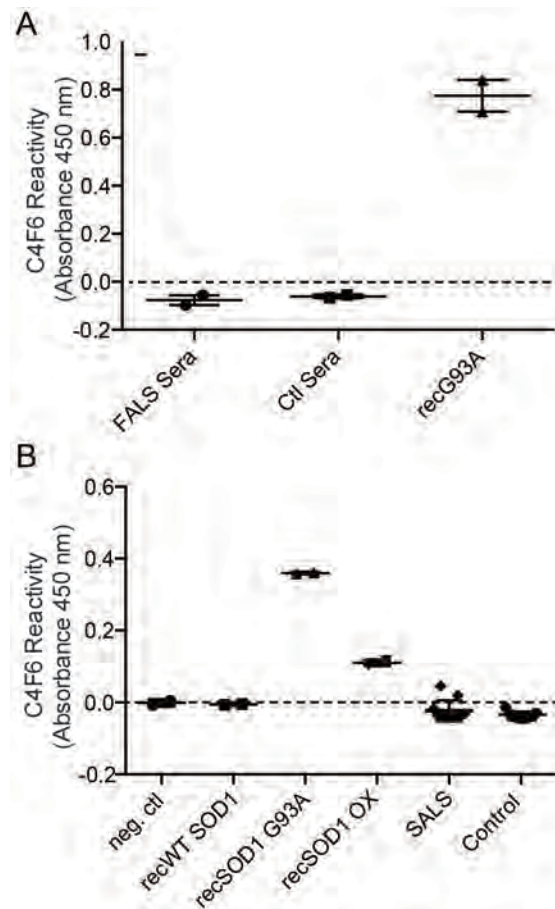


Figure III-3. Quantification of misfolded SOD1 in sera by ELISA. As described in **Figure III-2** for CSF, the C4F6-based ELISA was employed to identify misfolded SOD1 in patient sera. (A) The C4F6-ELISA is unable to differentiate sera of SOD1-FALS patients harboring mutations (A4V, L9V) from controls (Ctl). (B) Two out of 11 SALS patients' sera showed C4F6 reactivity above baseline compared to 0 out of 9 for the control cases. Error bars indicate SEM of the cohort. (recG93A, positive control; recWT SOD1, negative control).

(Fig. III-3B), suggesting sera may be a source of misfolded SOD1 in SALS. In contrast, no misfolded SOD1 was detected in control samples.

SOD1 isolated from SALS patients displays toxic properties

Previously published data demonstrates that SOD1 isolated from the spinal cord of sporadic ALS patients exhibits characteristics of FALS-linked mutant SOD1, such as inhibiting axonal transport (Bosco et al. 2010, Morfini G. A. et al. 2013). As an alternative approach to the C4F6-ELISA, we aimed to investigate whether or not SOD1 misfolding extended beyond the spinal cord of sporadic ALS patients using this same axonal transport assay. Briefly, this assay is performed by isolating the axoplasm of giant squid (*Loligo pealii*) and measuring fast axonal transport following the addition of SOD1 variants to the axoplasm. Previous studies have shown an inhibition of axonal transport in the presence of multiple ALS-linked SOD1 variants (Bosco et al. 2010, Morfini G. A. et al. 2013, Song et al. 2013). Here, we assessed the ability of human SOD1 (hSOD1) isolated from brain tissue to inhibit axonal transport, which would imply an aberrant form of SOD1 exists in these tissues. Although hSOD1 derived from CNS tissue cannot directly be utilized as a biomarker, determining which tissues harbor misfolded SOD1 in ALS patients will help to identify modes of SOD1 pathogenesis. To test this, hSOD1 was purified from the cortex of frozen post-mortem tissue. As a positive and negative control, hSOD1 was also purified from the spinal cord tissue of SALS patients as well as from healthy controls, respectively, in parallel with the purification of SOD1 from brain tissue. Isolated

squid axoplasm was perfused with pooled hSOD1 immunopurified from three sporadic ALS patient cortices and monitored using video microscopy. Consistent with previous results, SALS-linked hSOD1 isolated from the spinal cord inhibited axonal transport, while hSOD1 derived from control spinal cord tissue did not (**Fig. III-4A,B**). Interestingly, SALS-linked hSOD1 isolated from brain tissue also inhibited anterograde axonal transport (**Fig. III-4C**), extending the implications of SOD1 misfolding beyond the diseased spinal cord.

No conformational differences in SOD1 from SALS patients detected by limited proteolysis

Being that hSOD1 purified from spinal cord tissue in SALS, but not controls, inhibited axonal transport, we aimed to identify if this toxicity was due to an altered conformation of SALS-linked hSOD1 in human tissue. To assess the structural integrity of hSOD1 in SALS samples, we employed a limited proteolysis experiment with endoproteinase K, as less structured proteins are more susceptible to the proteolysis. To establish the limited proteolysis assay, recombinant proteins were analyzed after an hour incubation with endoproteinase K (0 to 125 ng/ μ L) followed by western analysis with an anti-SOD1 antibody. For WT SOD1, the protein bands were further digested with increasing enzyme concentrations (**Fig. III-5A**). For the ALS-linked proteins SOD1 G93A and SOD1 A4V, an initial decrease in the protein band is observed at the lowest concentration of endoproteinase K, but this protein band remains constant with increasing enzyme concentration. At first glance, one might

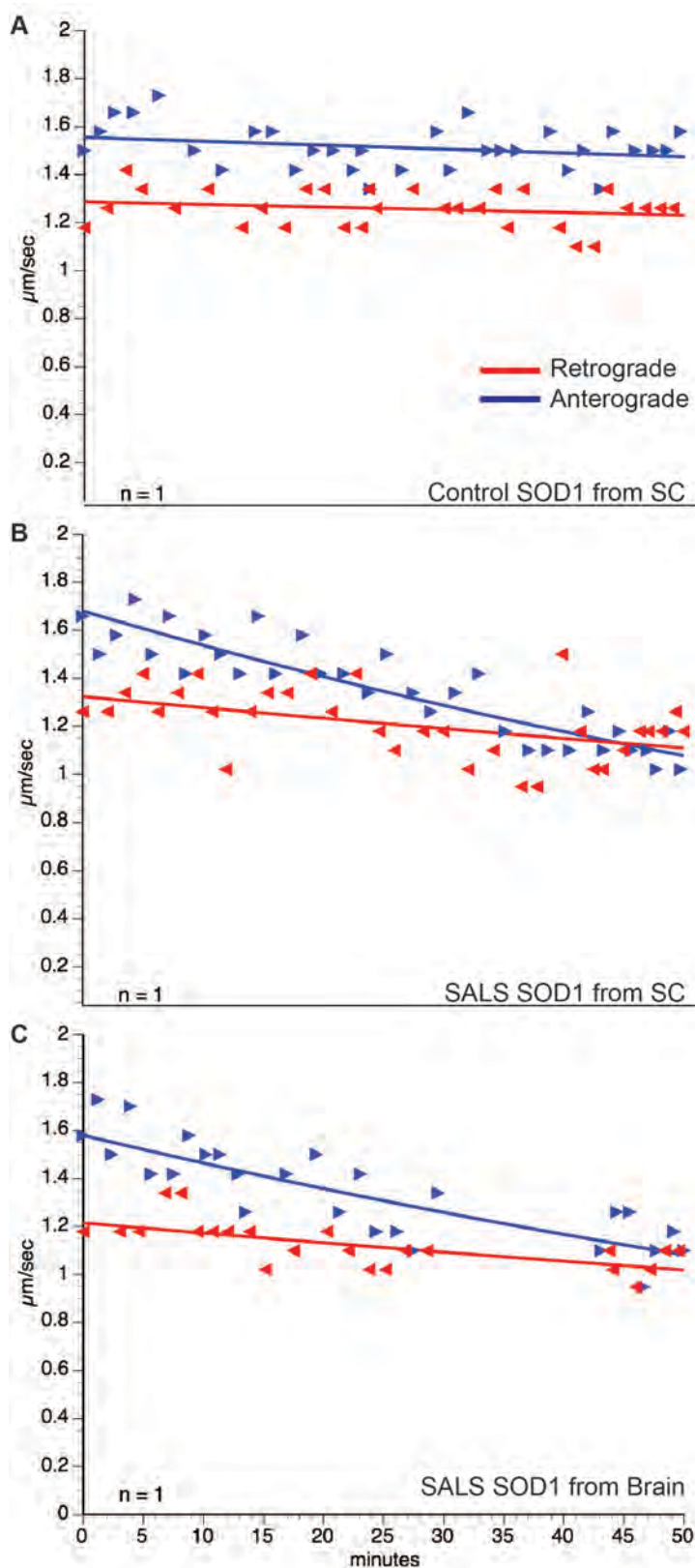


Figure III-4. hSOD1 immunopurified from brain and spinal cord of sporadic ALS patients inhibits axonal transport. Isolated squid axoplasm was perfused with $1.4 \mu\text{M}$ of the indicated SOD1 protein and the rates of vesicles transported across the axon were manually determined. (A) SOD1 immunopurified from control subjects has no effect on transport when perfused onto the squid axoplasm. Conversely, SOD1 isolated from both sporadic ALS spinal cord (B, SC) and brain (C) show transport inhibition.

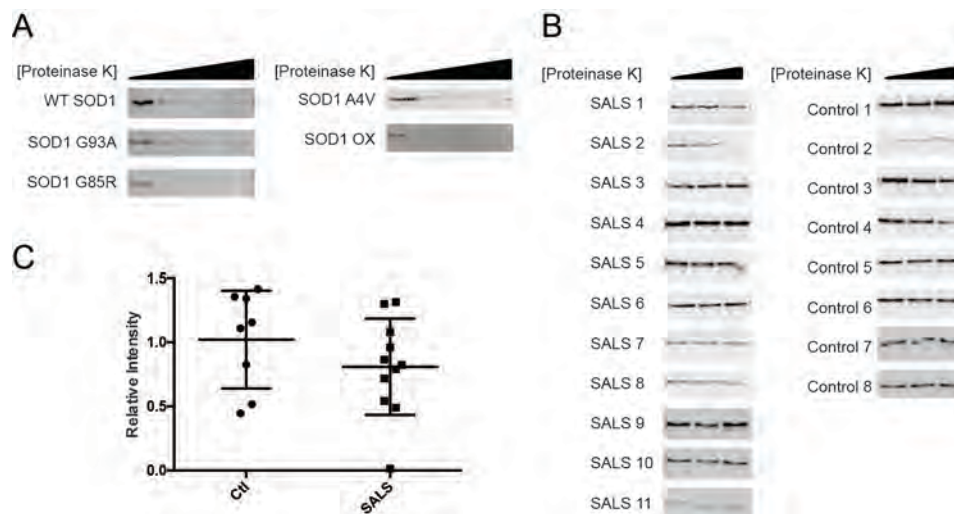


Figure III-5. Unaltered digestion patterns of SOD1 purified from SALS and control human tissue. (A) A representative western analysis of recombinant SOD1 variants digested with endoproteinase K (0 to 125 ng/ μ L) for 1 h and probed with anti-SOD1 (n=2). An enhanced susceptibility to proteolytic digestion for both SOD1 G85R and SOD1 OX compared to WT SOD1 suggests a decrease in stability. Both SOD1 G93A and A4V have similar digestion patterns to WT SOD1. (B) Limited proteolysis analysis, as described in (A), was employed to assess the structural integrity of human SOD1 purified from spinal cord tissue of SALS (n=11) and Control (n=8) cases. (C) Quantification of the amount of SOD1 digested with endoproteinase K (62.5 ng/ μ L; B, column 3) normalized to undigested (B, column 1).

suspect that these mutants have an increased stability compared to WT SOD1, but more likely enhanced aggregation of FALS-linked mutant SOD1 is protecting the protein from digestion. In support of this hypothesis, limited proteolysis is a technique that has been frequently employed for the assessment of protease resistant SOD1 aggregates (Furukawa et al. 2010, Chan et al. 2013). For SOD1 G85R and SOD1ox, the protein is digested at the lowest concentrations of endoproteinase K used, 15 ng/ μ L (**Fig. III-5A**, column 2), while WT SOD1 persists. Based on these preliminary experiments, digestion conditions of 0, 15, and 62 ng/ μ L were selected for analysis of SOD1 purified from human tissue.

SOD1 purified from human spinal cord tissue was assessed with the limited proteolysis assay described above to evaluate structural integrity. Grad et al. found that treatment with proteinase K of spinal cord homogenates from SALS and FALS patients resulted in a decrease of misfolded SOD1. The misfolded SOD1 was quantified by subsequent immunoprecipitation with a misfolded SOD1-specific antibody, DSE2 (**Table I-1**, (Grad et al. 2014)). In the present study, we aimed to identify the effects of limited proteolysis on total hSOD1 purified from spinal cord homogenates. No significant differences, as determined by a *t*-test, in digestion patterns were observed in SALS hSOD1 compared to controls (**Fig. III-5B,C**). Similarly, Grad and colleagues were unable to detect a substantial decrease in total SOD1 following proteinase K treatment when employing a pan-SOD1 antibody in place of DSE2 (Grad et al. 2014). The reason for the discrepancy between pan-SOD1 and misfolded specific SOD1 antibodies

is unclear. One possibility is a subpopulation of misfolded hSOD1 that is indiscernible when assessing the entire hSOD1 pool. Additionally, the endoproteinase K concentration employed in both studies may require further optimization. The as-isolated recombinant SOD1 from *E. coli* used in this study to optimize the protease concentration has a lower metal occupancy, which is known to decrease the stability of the protein (**Fig. II-3**, (Hayward et al. 2002, Stathopoulos et al. 2006)). It is quite possible that a higher concentration of enzyme would be required to tease out the differences in total hSOD1 isolated from human spinal cords, which are known to be fully metallated in the presence of the copper chaperone for SOD1, CCS (Wong P. C. et al. 2000, Rae et al. 2001, Banci et al. 2012b). In fact, Grad and colleagues found that increasing the proteinase K treatment to 20 mg/mL in control spinal cord homogenates had no effect on levels of WT SOD1 (Grad et al. 2014).

A subpopulation of SOD1 is greatly reduced in SALS

Being that limited proteolysis reveals no conformational differences between SALS hSOD1 and controls, we next employed 2D-gel electrophoresis (2D-GE) to identify unique modifications that may induce misfolding. SOD1 isolated from healthy human erythrocytes has been shown to contain multiple SOD1 species, partly due to the long half-life of these cells. These modification include deamidation (Shi Y. et al. 2013), phosphorylation (Wilcox et al. 2009), and glutathionylation (Wilcox et al. 2009). Both glutathionylation and deamidation enhance the aggregation propensity of WT SOD1 (Wilcox et al. 2009, Redler et

al. 2011, Shi Y. et al. 2013). These data suggest a higher abundance of these modified species *in vivo* could be detrimental. Moreover, an ideal biomarker source would be in the blood, as it is relatively non-invasive and simple to obtain. In light of this, we aimed to identify differential modifications on SOD1 in red blood cells (RBCs) from sporadic ALS patients compared to that of controls. All SALS patients included in this study represent earlier stages of disease with ALS functional rating scores (ALSFR) above 30 (**Table III-1**). To identify modifications that induce a charge shift in SOD1, we employed 2D-GE on RBC lysates from both SALS and controls. 2D-GE separates proteins by both isoelectric point (pI) and molecular weight allowing for an assessment of the charged species present in each sample. By doing a western analysis of the 2D-GE probed with anti-SOD1, we were able to identify multiple species of SOD1 present in RBC lysates (**Fig. III-6**). The species that migrates at a pI of “5.6” and molecular weight of 16 kDa likely represents unmodified SOD1, as the theoretical pI of SOD1 is 5.7. As illustrated in **Figure III-6**, modifications on SOD1 from RBCs in both SALS and control groups demonstrated high variability. This is likely due to the high amount of salts and proteins, such as albumin, present in these samples that may interfere with the isoelectric focusing, the first step of 2D-GE. In future studies, it will be vital to increase the number of washes and employ harsher pelleting strategies to further purify the RBC pellet prior to lysis and analysis by 2D-GE.

Table III-1. Characteristics of participants providing blood for SOD1 analysis.

Status [§]	Site of onset	sex	age	Months since onset	ALSFRS	Slow vital capacity (%)
control	N/A	M		N/A	N/A	N/A
control	N/A	M	49	N/A	N/A	N/A
control	N/A	F		N/A	N/A	N/A
control	N/A	F	60	N/A	N/A	N/A
control	N/A	F	57	N/A	N/A	N/A
control	N/A	M	58	N/A	N/A	N/A
control	N/A	F	50	N/A	N/A	N/A
control	N/A	M	63	N/A	N/A	N/A
control	N/A	F	32	N/A	N/A	N/A
SALS**	bulbar	M	70	23	ND	ND
SALS	lower left limb	F	72	41	ND	ND
SALS		M	45	28	34	77
SALS	upper limbs	M	63	15	37	200*
SALS	upper limbs	M	56	20	35	79
SALS	upper limbs	F	56	21	43	91
SALS**		M	53	18	37	71
SALS**	upper limbs	F	71	12	43	94
SALS	bulbar	M	31	23	37	76

*SVC is calculated based on height; subject is unable to stand up straight, therefore height is underestimated

N/A: not applicable; ND, not determined

**Negative for C9orf72 expansion; <30 repeats present

§Unless otherwise noted, no genetic testing was performed on participants

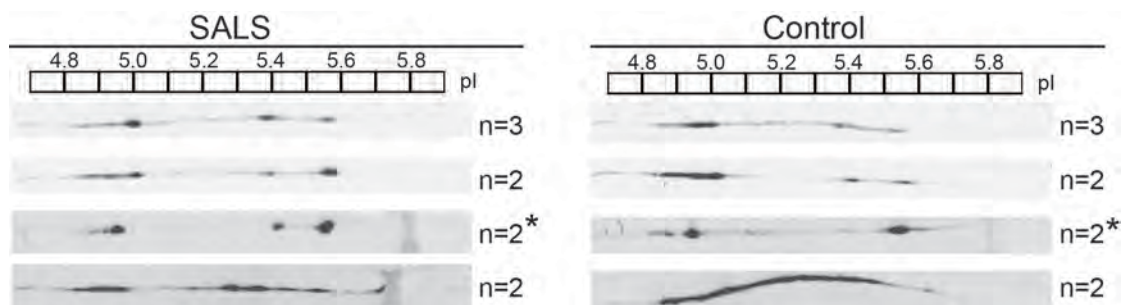


Figure III-6. Human red blood cells (RBC) contain modified SOD1 protein. A total of 300 μ g of protein lysate was subjected to 2D-GE western analysis probed with anti-SOD1. SOD1 ran at the expected MW of \sim 16 kDa. 2D-GE demonstrates the presence of multiple differentially charged species of SOD1 in both SALS (*left*) and Control (*right*) RBC lysates. The number (n) of patients pooled for each sample is shown with the estimated pI displayed above. *indicates sample subjected to immunoprecipitation and mass spectrometry analysis.

As an alternative approach, the presence of misfolded SOD1 in RBCs was assessed by employing the C4F6-ELISA, as described above for CSF and sera. No misfolded SOD1 was detected in control or SALS patient derived RBC lysate (data not shown). This data suggests that the misfolded SOD1 detected by C4F6 is either not present or at concentrations lower than the limit of detection in these samples. This does not preclude the possibility that a different misfolded species is present, as multiple antibodies have been generated that recognized different regions of SOD1 exposed upon misfolding (**Table I-1, Fig. I-3** (Jonsson et al. 2004, Urushitani et al. 2006, Rakhit et al. 2007, Gros-Louis et al. 2010, Kerman et al. 2010)).

To further elucidate the potential differential modifications in SALS and control RBCs, immunoprecipitated SOD1 from RBC lysate from SALS (n=2) and controls (n=2) was digested with trypsin and analyzed by mass spectrometry. Sequence coverage of 100% was observed for both pooled SOD1 samples. Consistent with previously published data, deamidation at N26D was present in the control group (**Fig. III-7A**) (Shi Y. et al. 2013), as well as the SALS group (data not shown). A novel phosphorylation site at T135 was also observed in both groups (**Fig. III-7B**), but further validation is required as the immunoprecipitated SOD1 was washed with phosphate buffered saline (0.01 M

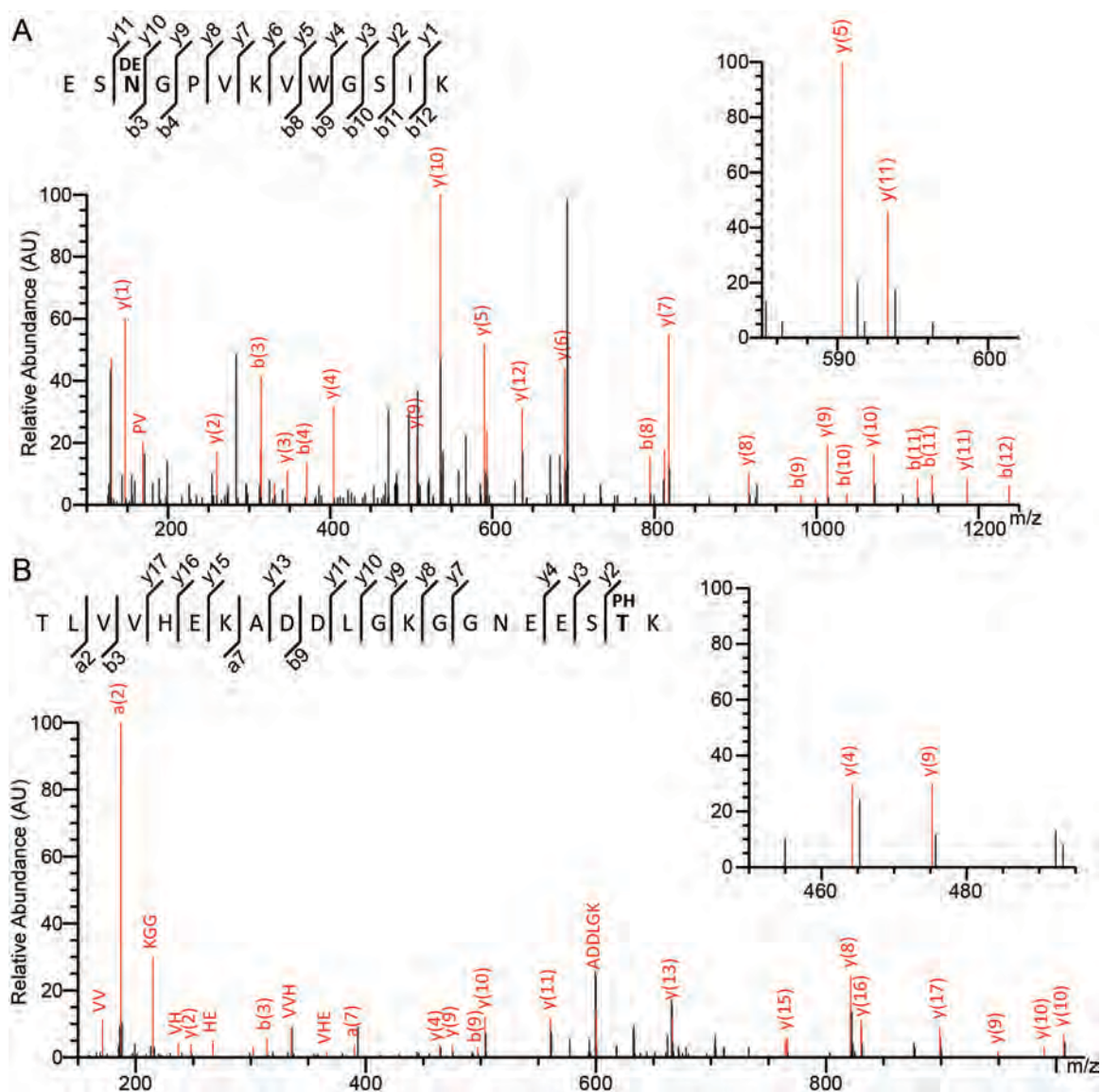


Figure III-7. Phosphorylation and deamidation are present on SOD1 isolated from RBCs. Immunoprecipitated SOD1 (Fig. III-6, *) was subjected to mass spectrometry analysis to identify the modifications present. Two samples were pooled for SALS and Ctl cohorts. Representative spectra of modifications identified in both SALS pool and Ctl pool are shown. Insets demonstrate ion coverage of the indicated modification, allowing for the amino acid assignment. Sequence and sequence coverage is displayed above. The monoisotopic peaks of y, a, and b-ions assigned to the indicated peptide are illustrated in orange. Both SOD1 IP'd from SALS (n=2) and Ctl (n=2) RBCs contained deamidation at N26 (DE, A) and phosphorylation at T135 (PH, B).

PBS, 0.01% Tween20) which may have induced artificial phosphorylation. Phosphorylation has been previously observed at other sites, T2 and T59/S58, neither of which were identified in these samples (Wilcox et al. 2009). Unfortunately, quantification of phosphorylation by mass spectrometry is highly unreliable because of variability in the phosphate bond breaking during ionization and further enrichment may be required to identify differential phosphorylation (Quan and Liu 2013).

In addition to RBCs, another source that could harbor misfolded SOD1 species are peripheral blood mononuclear cells (PBMCs), which can be isolated from total blood by centrifugation techniques (see Materials and Methods). PBMCs constitute about 1% of the total cells in blood and include multiple white blood cells such as monocytes and lymphocytes (Mantovani et al. 2009). PBMCs reflect many of the same pathological hallmarks of ALS as seen in other cell types such as altered calcium homeostasis, increased oxidative stress, and decreased levels of Bcl-2 (Curti et al. 1996, Cova et al. 2006, Nardo et al. 2009). To assess the extent of differential modifications of SOD1 in PBMCs isolated from SALS and control patients, the same 2D-GE technique was employed as described above for RBCs. Blood samples for both RBCs and PBMCs were drawn simultaneously from the same cohorts (**Table III-1**). However, contrary to RBCs, the 2D-GE blots of SOD1 from PBMCs had only 3 prominent spots (**Fig. III-8**). Both PBMCs from control (n=9) and SALS (n=9) subjects have an abundant SOD1 species at pI of ~5.6 (**Figure III-8A**). This SOD1 species,

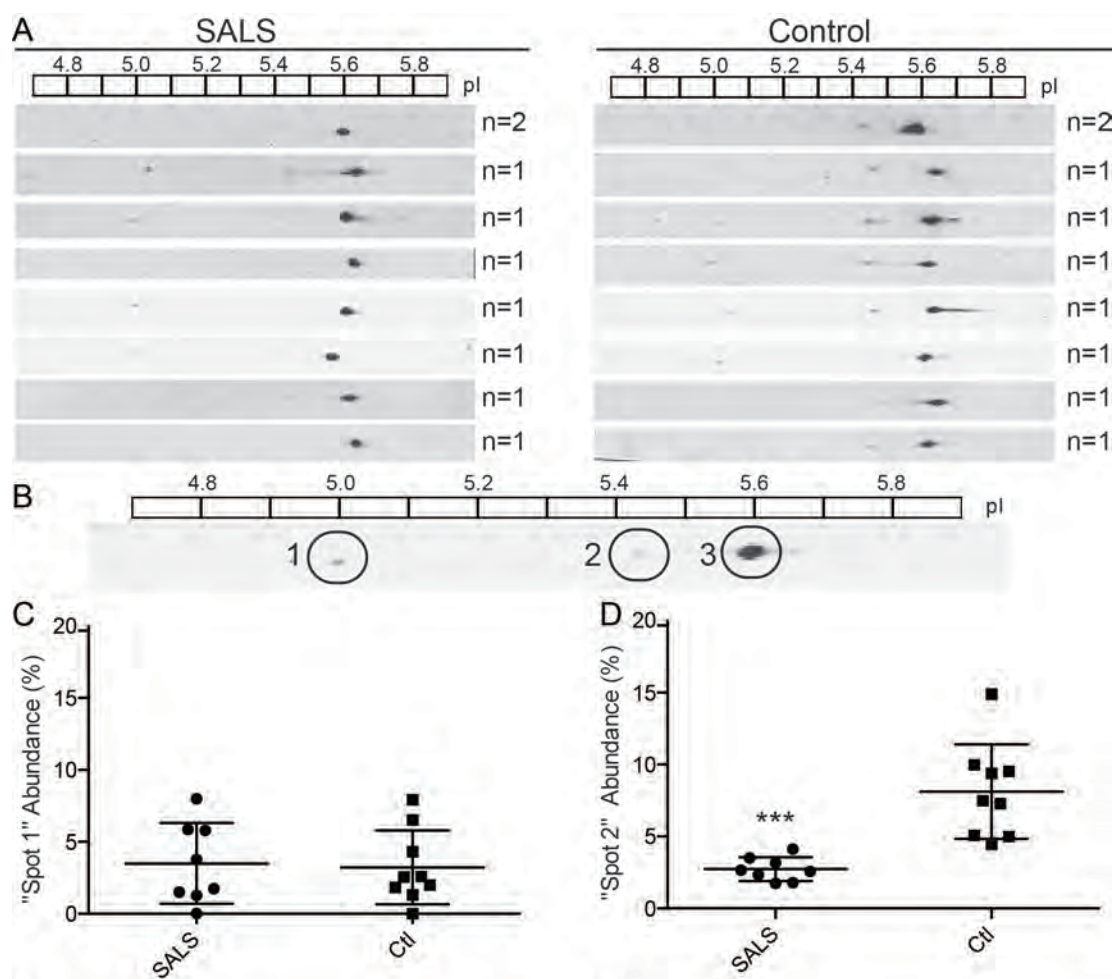


Figure III-8. PBMCs isolated from control cases harbor an SOD1 species greatly reduced in SALS. (A) Western analysis probed with anti-SOD1 of 2D-GE of PBMC lysate from SALS (left) and control (right) isolated from blood. Estimated pI, based on the isoelectric focusing strip used, is displayed above. The number of patients (n) pooled for each gel sample is shown. (B) A representative 2D-GE as described in (A) to demonstrate the method used for quantification. (C,D) Quantification of the relative abundance of “Spot 1” and “Spot 2” normalized to the total SOD1 (Spot 1 + Spot 2 + Spot 3). “Spot 2” is significantly decreased in SALS compared to control (Ctl, $p=0.0004$). Statistics were determined by an unpaired t-test (***, $p<0.001$; $n=9$). No significant difference for “Spot 1” quantification.

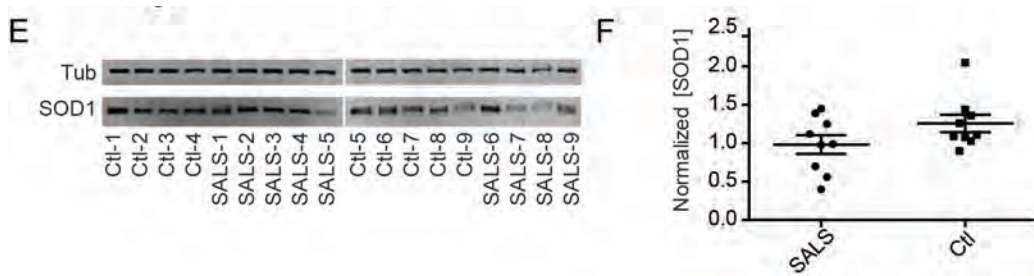


Figure III-8 continued. PBMCs isolated from control cases harbor an SOD1 species greatly reduced in SALS. (E) PBMC lysate was subjected to western analysis to determine the relative SOD1 abundance (Tub, α -tubulin). (F) Quantification of (E) by densitometry was performed and SOD1 was normalized to the loading control, tubulin. These data demonstrate no significant difference in the abundance of SOD1 observed between SALS and healthy controls.

designated as “Spot 3” (**Figure III-8B**), signifies the major species of SOD1 present in PBMCs (90-95% of total SOD1), and likely represents unmodified SOD1 with a theoretical pI of 5.7. The SOD1 species at pI 5.0 (Spot 1) appeared in a subset of both control and SALS patients, with no significant overrepresentation in either cohort (**Fig. III-8C**). The SOD1 species at pI 5.4 (Spot 2), however, is significantly overrepresented in control compared to SALS subjects and accounts for $8.1 \pm 1.1\%$ and $2.7 \pm 0.3\%$ of total SOD1, respectively (**Fig. III-8D**). Both Spot 1 and Spot 2 correspond to SOD1 with a modification that leads to a net change in charge, either a loss of a positive charge or the gain of a negative charge relative to Spot 3. No significant change in the relative levels of total SOD1 was observed (**Fig. III-8E,F**).

An over-oxidized SOD1 species is present in SALS PBMCs

Immunoprecipitated SOD1 from pooled PBMCs (n=9 SALS, n=9 Ctl), as described above for RBCs, was subjected to mass spectrometry analysis to identify Spot 2 that was overrepresented in controls. First, it was vital to confirm that Spot 2 was immunoprecipitated by the monoclonal anti-SOD1 antibody employed, since we aimed to identify this species by mass spectrometry. As illustrated by 2D-GE followed by western blotting (**Fig. III-9A**), Spot 2 (pI 5.4) is immunoprecipitated from Control PBMC lysate. Of note, the antibody used for the immunoprecipitation (Pierce) differs from those used to probe SOD1 in the western analysis (AbCam and (Taylor et al. 2007)), confirming by 3 independent anti-SOD1 antibodies that Spot 2 is SOD1 and not cross-reactivity with another

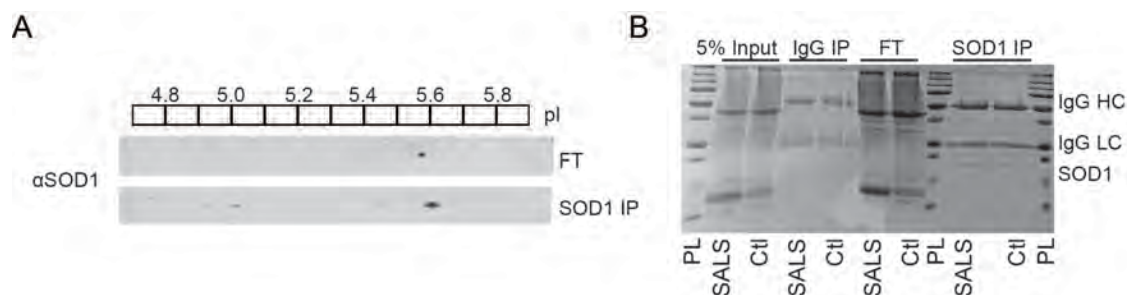


Figure III-9. Immunoprecipitated SOD1 from Control PBMCs contains Spot 2. (A,B) Immunoprecipitation of SOD1 from PBMCs for mass spectrometry analysis. (A) 2D-GE probed with anti-SOD1 confirms that the SOD1 species at pI 5.4 is depleted from the flow-through lysate (FT, top) and present in the immunoprecipitated sample (bottom). (B) Immunoprecipitated SOD1 was subjected to Coomassie SDS PAGE. SOD1 is seen in anti-SOD1 IP, but not the IgG control. This 16 kDa species was excised, digested with trypsin and subjected to mass spectrometry.

protein.

The low abundance of Spot 2 precluded our ability to isolate it from total SOD1 for mass spectrometry analysis. Instead, to determine protein modifications that induce the shift of SOD1 by 2D-GE, total SOD1 was immunoprecipitated and subjected to SDS-PAGE followed by Coomassie. The 16 kDa SOD1 species (**Fig. III-9B**) was excised, digested with trypsin, and analyzed by mass spectrometry. Sequence coverage of 100% was observed for SOD1 in both SALS (n=9) and Ctl (n=9) pooled samples. Overall, SALS SOD1 contained more oxidized amino acid residues than control SOD1. Since oxidative stress is a known hallmark of ALS, these results are not surprising (Carri et al. 2015). The oxidation of Pro13 and Phe20, for example, was only identified in SALS SOD1 on the peptide spanning Gly10 to Lys23 (**Table III-2**). It is also worth noting that oxidation of Lys122 was observed only in the SALS SOD1 pool (6.7% of Tyr116-Lys128). Lysine oxidation inhibits ubiquitination and, in turn could interfere with regulation of protein turnover (Spasser and Brik 2012).

Moreover, an increase in the total relative abundance of peptides with oxidized amino acids (H, W, P, D, N, F, K) was observed (all peptides weighted equally; SALS, 3.7%; Ctl, 1.6%; **Table III-2**). This percentage is calculated by weighting all peptides equally. In other words, 100% oxidation would indicate every peptide identified by mass spectrometry has at least one oxidized residue within it. This is a conservative calculation that does not consider the relative

Table III-2. Relative abundance of SOD1 peptides identified by Mass Spectrometry.

Peptide	% Relative Abundance ¹		% Oxidized ¹	
	Cti	SALS	Cti	SALS
1-ATKAVCVLK-9	0.011	0.127	ND	ND ²
4-AVCVLKGDGPVQGIINFEQK-23	2.688	0.206	0.2	33.9
4-AVCVLKGDGPVQGIINFEQKESNGPVK-30	7.610	ND	ND	ND
10-GDGPVQGIINFEQK-23	21.381	22.024	ND	0.3
10-GDGPVQGIINFEQKESNGPVK-30	6.144	ND	ND	ND
10-GDGPVQGIINFEQKESNGPVKVVWGSIK-36	0.284	ND	ND	ND
24-ESNGPVK-30	0.016	0.045	ND	ND
24-ESNGPVKVVWGSIK-36	11.752	1.411	0.5	23.1
37-GLTEGLHGFHVHEFGDNTAGCTSAGPHFNPLSR-69	16.325	2.113	5.3	12.4
70-KHGGPKDEER-79	0.002	0.001	ND	ND
76-DEERHVGDLGNVTADK-91	0.042	ND	ND	ND
80-HVGDLGNVTADK-91	0.006	11.341	29.4	ND
80-HVGDLGNVTADKDGADVSIEDSVISLSGDHCIIGR-115	2.141	1.586	ND	3.0
92-DGADVSIEDSVISLSGDHCIIGR-115	1.067	0.141	0.2	ND
116-TLVVHEK-122	0.002	0.006	ND	ND
116-TLVVHEKADDLGK-128	1.676	0.046	ND	9.1
116-TLVVHEKADDLGKGGNEESTK-146	0.965	ND	ND	ND
123-ADDLGKGGNEESTK-146	0.025	0.002	ND	ND
128-GGNEESTK-136	0.005	0.012	ND	ND
137-TGNAGSR-143	0.006	0.008	ND	ND
137-TGNAGSRLACGVIGIAQ-153	0.164	0.195	ND	ND
144-LACGVIGIAQ-153	27.661	60.717	ND	ND
		Total:³	1.6%	3.7%

¹Represents the percentage of relative abundance for oxidized precursors/total relative abundance for that individual peptide

²ND, not detected

³Represents the total percent of oxidized precursors with all peptides equally weighted

⁴The percentage of the peptide's total precursor intensity normalized to sum of all SOD1 total precursor intensities identified in sample

abundance of individual peptides. For example, 72% of the total oxidation found in the Ctl SOD1 pool is attributed to the peptide spanning His80 to Lys91, which was uniquely over-oxidized in controls compared to SALS. However, this is misleading as the His80 to Lys91 peptide was significantly underrepresented in the control SOD1 (Relative Abundance: SALS, 11.3%; Ctl, 0.006%; **Table III-2**). The underrepresentation of this peptide in controls is likely skewing the percentage of oxidation present, as His80 to Arg115, a peptide that has the His80 to Lys91 sequence within it, contains no sites of oxidation with a much greater relative abundance (2.1%). Thus, this suggests that i) there is an unidentified modification on His80 to Lys91 in the control pool that is precluding its identification or ii) a modification on the terminal lysine is inhibiting the tryptic digestion.

Likewise, the total calculated oxidation present in the SALS pool (3.7%) is misleading. Approximately 23.1% of the peptide spanning Glu24 to Lys36 is oxidized in the SALS SOD1 pool, while only 0.5% is oxidized in the control pool. For the SALS SOD1 pool, Trp32 oxidation (Trp32ox) within Glu24-Lys36 contributes to more than 90% of the oxidation observed (**Table III-2, Fig. III-10**). Glu24 to Lys36 is the only peptide identified that contains this Trp32 within it, suggesting that 21% of the SOD1 population from the SALS pool contains Trp32ox. Assuming similar ionization efficiencies between the oxidized and non-oxidized Glu24-Lys36 peptides, this data implies that 21% of all SOD1 protein immunoprecipitated is aberrantly oxidized at this tryptophan residue. Trp32 is

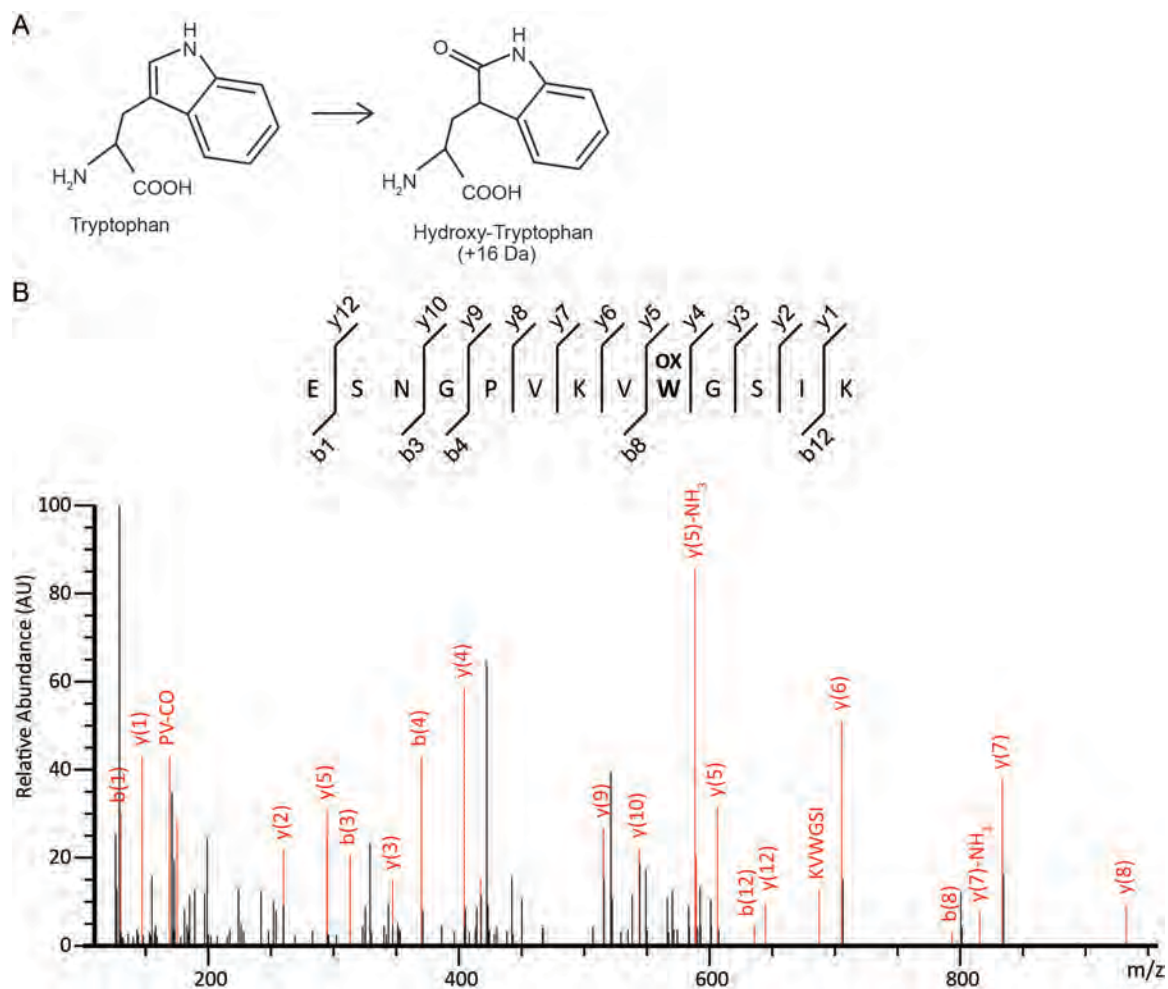


Figure III-10. Tryptophan oxidation at residue 32 of SOD1 is elevated in SALS PBMCs. Immunoprecipitated SOD1 from both SALS ($n=9$) and Ctl ($n=9$) PBMCs as described in **Fig. III-9**, were subjected to mass spectrometry analysis to identify protein modifications. (A) Tryptophan is readily oxidized resulting in its conversion to hydroxy-tryptophan, among other oxidation products, which increases the MW by 16 Da. (B) The peptide spanning Glu24 to Lys36 contains an oxidized tryptophan residue present on SOD1 immunoprecipitated from both SALS ($\geq 21\%$) and control ($\leq 0.5\%$) pools. A representative spectrum of the oxidation of tryptophan (Trp32) to hydroxy-tryptophan from SALS pooled SOD1 sample is shown. The sequence coverage is displayed above (OX, oxidized tryptophan). The monoisotopic peaks of y, a, and b-ions assigned to the indicated peptide are illustrated in orange.

implicated in FALS-linked mutant SOD1 pathogenesis, suggesting Trp32ox may be the first direct link to a common pathogenic mechanism of SOD1 in both SALS and FALS (Zhang H. et al. 2003, Taylor et al. 2007, Grad et al. 2011). Whether all 9 SALS samples that were pooled for this analysis contain this 21% oxidation or if it is higher in a subset of patients remains to be determined.

Another interesting differential modification present on SOD1 in PBMCs is histidine oxidation to 2-oxo-histidine, a modification induced by metal-catalyzed oxidation ((Rakhit et al. 2002, Uchida 2003), **Fig III-11A**). This modification was previously reported to occur in the active site of SOD1 (Uchida and Kawakishi 1994, Kurahashi et al. 2001, Rakhit et al. 2002). In fact, 2-oxo-histidine was observed in both the SOD1 from the control and SALS cohorts (**Fig. III-11B**). Specifically, in the peptide spanning Gly37 to Arg69, oxidation was observed at His46 and His48, both of which coordinate Cu(II) in the active site (Selverstone Valentine et al. 2005). Since these histidines are in the active site of SOD1, their oxidation likely results in inactivation of the protein (Fucci et al. 1983, Smith C. D. et al. 1991, Berlett and Stadtman 1997, Selverstone Valentine et al. 2005). Further, the percentage of total oxidation of the peptide spanning Gly37 to Arg69 was enhanced in SALS, as indicated by the relative abundance (SALS, 12.4%; Ctl, 5.3%; **Table III-2**), with at least 60% of the oxidation attributed to oxidized histidine residues.

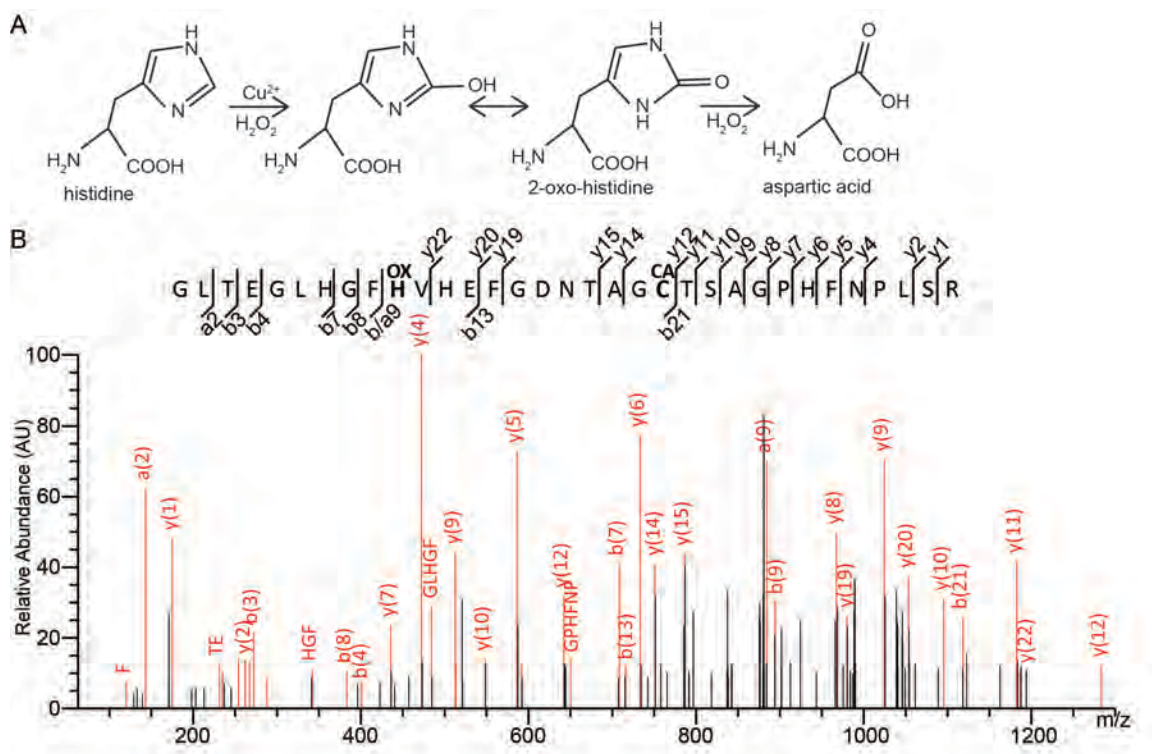


Figure III-11. Histidine oxidation to 2-oxo-histidine is present on PBMCs isolated from control and SALS samples. Immunoprecipitated SOD1 from both SALS (n=9) and Ctl (n=9) PBMCs as described in **Fig. III-9**, were subjected to mass spectrometry analysis to identify protein modifications. (A) Histidine is converted to 2-oxo-histidine in the presence of reactive oxygen species and further converted to aspartic acid under prolonged exposure and/or degradation. (B) The peptide spanning Gly37 to Arg69 contains multiple oxidized residues such as His46 and His48. A representative spectrum of the oxidation of histidine (His46) to 2-oxo-histidine from SALS pooled SOD1 sample is shown. His46 oxidation is present in both SALS and control pooled SOD1 samples. The sequence coverage is displayed above (OX, oxidized histidine; CA, carbamidomethyl adduct). The monoisotopic peaks of y, a, and b-ions assigned to the indicated peptide are illustrated in orange.

Within the same peptide discussed above, Gly37 to Arg69, the conversion of His46 to aspartic acid, was uniquely observed in SOD1 isolated from controls. The conversion of histidine to aspartic acid represents a ring-ruptured form of 2-oxo-histidine that may be a product of histidine degradation (**Fig. III-11A, III-12**,(Dean et al. 1989, Uchida 2003)). The aspartic acid residue at position 46 is expected to induce a charge shift like that observed for the SOD1 species at pI 5.4 (Spot 2) identified in the 2D-GE western analysis (**Fig. III-8**). In fact, the theoretical pI of the histidine to aspartic acid conversion is 5.4. The discrepancy in the quantification of Spot 2 by 2D-GE (8.1%) and His46Asp in mass spectrometry (0.1% of the total precursor intensity of the peptide) is likely due, at least in part, to the decreased ionization efficiency of a peptide with increased negative charge.

One possibility for why the histidine to aspartic acid conversion is observed in controls and not the SALS groups could be the overrepresentation of the peptide in the mass spectrometer (i.e. lower concentration could result in loss of detection). In fact, the total SOD1 injected into the mass spectrometer was 2-fold higher in control SOD1 (Ctl, 1.8×10^{11} ; SALS, 8.99×10^{10}). To address this issue, the relative abundance of each peptide was quantified using the total intensity of the precursor ion (**Table III-2**). The SOD1 peptide Gly37 to Arg69 was overrepresented in controls compared to SALS (Relative Abundance: Ctl, 16.325; SALS, 2.113). Nonetheless, if the histidine substitution to aspartic acid were present at similar percentages in the SALS SOD1, it would likely be

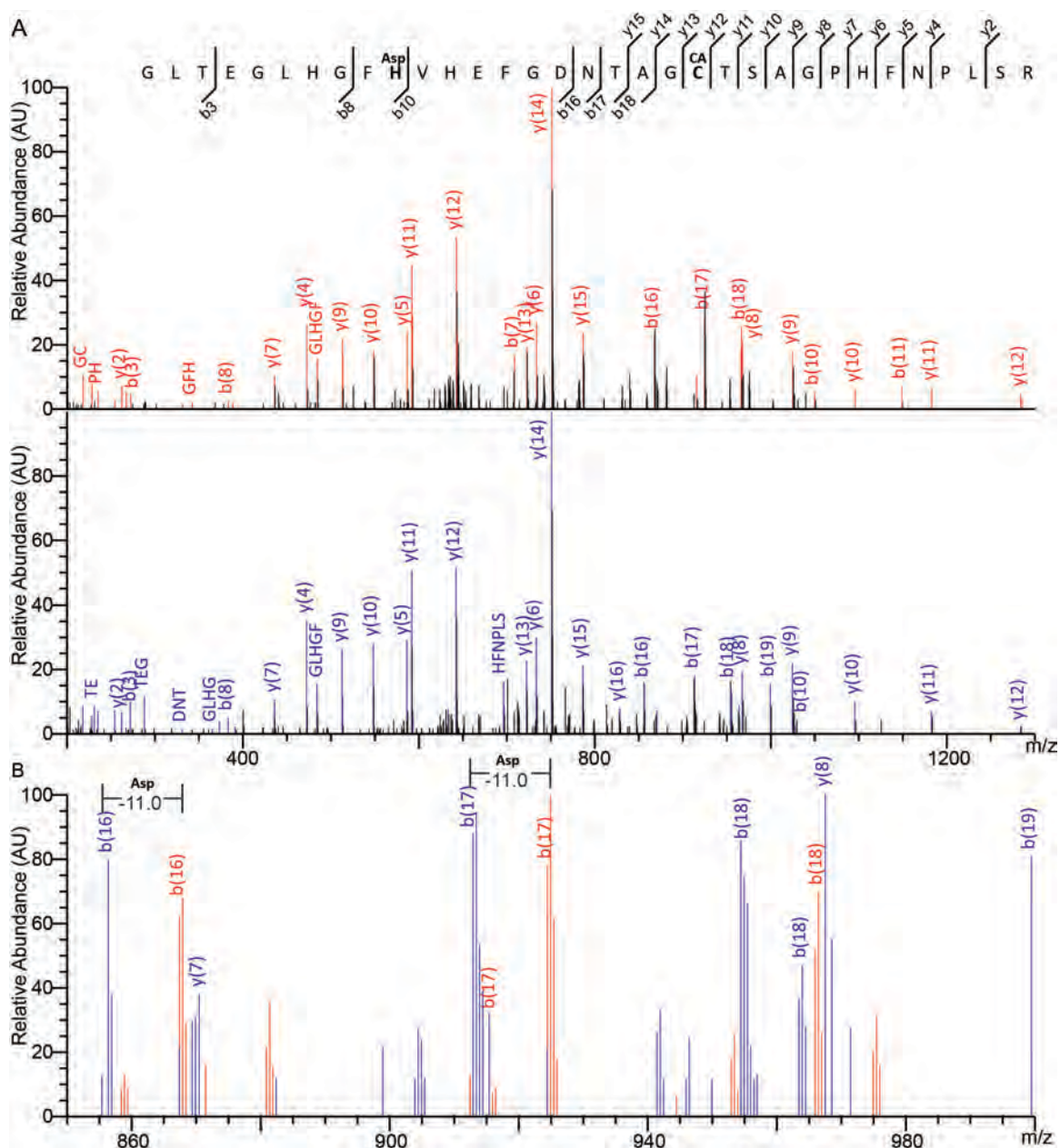


Figure III-12. Histidine oxidation to aspartic acid is unique to SOD1 in PBMCs isolated from controls. (A) The MS/MS spectra of the peptide identified as Gly37-Arg69. A carbamidomethyl modification is present in both samples on Cys57, which is an artifact of sample preparation (CA). Representative spectra with (Ctl, bottom; blue) and without (SALS, top; orange) the His46 to aspartic acid conversion are shown. The monoisotopic peaks of y, a, and b-ions assigned to the indicated peptide are illustrated in orange and blue, respectively. Note the similarity between the two spectra (sequence coverage displayed above).

Figure III-12 continued. Histidine oxidation to aspartic acid is unique to SOD1 in PBMCs isolated from controls. (B) The conversion of histidine to aspartic acid results in a loss of -22.01 Da at His46 (Actual Mass of Gly37-Arg69 peptide: His46, 3518.62 Da, Asp46, 3496.61 Da; $3518.62 - 3496.61 = -22.01$). A zoomed in overlay of the spectra with (Ctl, blue) and without (SALS, red) the amino acid substitution highlights the peak shifts present on b-ions (b(16), b(17)) that include residue 46, the site of histidine conversion to aspartic acid. These data demonstrate the change of -22.01 observed with the aspartic acid substitution ($-22.01/2 = -11.0$).

detectable with a total precursor intensity of 10^6 . It was not, however, detectable in the SALS SOD1 pool. Repeating the injection with higher concentrations of SALS SOD1 or doing a targeted mass spectrometry approach is required to confirm these findings. Moreover, these data represent a single set of immunoprecipitated SOD1 from control and SALS pools and a replicate analysis with new blood samples will be required to confirm the differences in peptide abundance and the differential modifications.

Discussion

The structural loosening that results from SOD1 misfolding induced by mutations and/or other environmental factors could make SOD1 more susceptible to adverse modification(s) (See **Chapter II**). Thus, in this study, we aimed to devise a mechanism to identify misfolded SOD1 in the context of sporadic ALS in order to exploit it as a biomarker. We employed C4F6, a misfolded SOD1-specific antibody, to detect misfolded SOD1 in CSF, sera, PBMCs and RBCs. Consistent with previous findings, total SOD1 is elevated in the CSF of both SALS and neurological controls (**Fig. III-2**, (Winer et al. 2013)), likely due to the oxidative stress found in these neurological disorders (**Fig. III-2**) (Christen 2000, Gilgun-Sherki et al. 2004, Carri et al. 2015). The nonspecific increase of SOD1 protein in neurodegenerative diseases renders SOD1 protein levels a weak biomarker in the context of ALS.

Misfolded SOD1, as detected by the C4F6-ELISA, was found in the sera of 2 out of 11 SALS patients selected based on their elevated levels of SOD1ox

antibodies. Although this data is intriguing, a larger cohort of both SALS and healthy controls is required to quantify the extent of this misfolding in sera and its relationship to disease. In contrast, misfolded SOD1 was not identified in RBCs, PBMCs (data not shown), or CSF samples from SALS (**Fig. III-2**). C4F6 may not be the optimal misfolded SOD1-specific antibody for detection in complex samples. First, the apparent K_d of SOD1 binding to C4F6 is relatively low (**Table II-1**), in the low micromolar range. This suggests that in complex mixtures, C4F6 will be competing with other SOD1 binding proteins, with C4F6 less favored to bind SOD1. Also, at the concentrations of SOD1 present in CSF (100-200 ng/mL) and Sera (10-70 ng/mL), C4F6 is reaching its detection limit, as it is unable to differentiate a subset of misfolded SOD1 (A4V and G85R) from WT SOD1 (**Fig. III-1**). Developing antibodies with a higher affinity to misfolded SOD1 will likely have greater diagnostic and therapeutic potential. It is also possible that misfolded SOD1 is not present in all biofluids and tissues. We have shown that toxic SOD1 is in the spinal cord and brain tissue, as indicated by axonal transport inhibition, but whether or not this misfolded SOD1 extends to the CSF and RBCs is unknown at this time. The presence of an over-oxidized SOD1 species in PBMCs, however, supports the presence of misfolded SOD1 in these samples.

By subjecting spinal cord derived hSOD1 to limited proteolysis with endoproteinase k, we aimed to assess the structural integrity of SALS-linked hSOD1 compared to controls. In this study, we assessed the susceptibility of the entire population of SOD1 to proteolysis and found no difference in digestion

patterns between hSOD1 from SALS and healthy controls (**Fig. III-5**). The fact that hSOD1 isolated from the spinal cord demonstrates signs of toxicity through axonal transport inhibition, argues for the presence of misfolded SOD1. Whether this species is more susceptible to proteolytic digestion is unknown. Previous studies demonstrated the susceptibility of a subpopulation of misfolded SOD1, immunoprecipitated by DSE2 (**Table I-1**), to limited proteolysis (Grad et al. 2014). In the current study, only the total population of SOD1 was assessed, which does not rule out the possibility of a subpopulation of SOD1 present in the spinal cord that may be more destabilized in this cohort as well, as suggested by the Cashman study (Grad et al. 2014). Another possibility is an enhanced aggregation propensity of SALS-purified SOD1, increasing the oligomeric SOD1 species resulting in proteolytic resistance under the conditions assessed.

Peripheral blood mononuclear cells (PBMCs) are a vital immune system defense and could be a biomarker source for ALS, as they recapitulate many aspects of disease. PBMCs isolated from ALS patients, for example, demonstrate increased oxidative stress and signs of excitotoxicity such as altered calcium homeostasis and glutamate receptor expression (Curti et al. 1996, Pouloupoulou et al. 2005, Nardo et al. 2009). In fact, when PBMCs are exposed to misfolded SOD1, they secrete pro-inflammatory cytokines (Fiala et al. 2010). In this study, we identified an SOD1 species at pI 5.4 greatly reduced in SALS patients compared to controls in PBMCs. Likely, a modification is present in controls that is lacking in the SALS SOD1 causing the shift in pI observed.

Another possibility is an additional modification on SALS SOD1 that shifts the species back to the “5.6” pI, while the modification originally causing the shift to 5.4 remains. Alternatively, there could be a slower formation or a more efficient clearing of this species of pI 5.4 in SALS patients.

PBMCs represent a mixed population of white blood cells consisting of mainly lymphocytes and monocytes (Ratts and Weng 2012). These cell types can be further divided into subclasses with the ratio of cell types varying between individuals. One possibility for the lack of this SOD1 species in the SALS population could be a PBMC cell type expressing these species that is underrepresented in diseased individuals. In fact, SALS patients have demonstrated an altered subpopulation of CD3+T lymphocytes, which is the major cell type present in PBMCs. Even though the total percentage of CD3+ T cells is unchanged, the subpopulations are shifted resulting in an increase in CD4+ T helper cells and a decrease in CD8+ T cytotoxic cells relative to controls (Mantovani et al. 2009). In this scenario, it remains to be determined if CD8+ T cytotoxic cells are the population that express the 5.4 SOD1 species.

By analyzing SOD1 immunoprecipitated from both SALS and control PBMCs by mass spectrometry, we were able to identify an over-oxidized form of SOD1 unique to SALS-linked SOD1. This over-oxidized form of SOD1 would likely not induce a pI shift by 2D-GE, as the majority of oxidized residues do not reduce the charge of SOD. Additionally, the mass difference of oxidation is too small to detect by SDS-PAGE and western analysis. In support of this

differentially modified SOD1 species, previously published data identified an over-oxidized species of SOD1 in immortalized lymphocytes, the major constituents of the PBMC population, derived from SALS patients (Guareschi et al. 2012). An increase in protein oxidation that correlates with aging has also been observed (Smith C. D. et al. 1991). In fact, aging, oxidative stress, and inflammation are implicated in an increased production of reactive oxygen species (Berlett and Stadtman 1997) and a decrease in activity of the hydrogen peroxide scavenger, catalase (Alper 1998, Tsay et al. 2000). SOD1 is responsible for converting the reactive oxygen species, O_2^- , to oxygen and hydrogen peroxide (H_2O_2). However, in the absence of downstream peroxidases to convert H_2O_2 to non-reactive species, or an overload of produced H_2O_2 , H_2O_2 can accumulate and participate in metal-catalyzed oxidation resulting in the production of toxic hydroxyl radicals, $\bullet OH$. These toxic hydroxyl radicals can induce histidine oxidation, among many other oxidation products.

The increase in oxidation of the SALS SOD1 pool has three major plausible sources. First, the increase in overall oxidative stress evident in ALS (Barber and Shaw 2010, Pollari et al. 2014, Carri et al. 2015) could be inducing this over-oxidized state. Second, a decrease in the structural integrity of SOD1 could enhance susceptibility of the protein to oxidative modifications. As an alternative route to limited proteolysis, one could test this by performing H/D exchange followed by mass spectrometry on immunopurified SOD1 from PBMCs to identify regions of SOD1 with enhanced flexibility. Third, a deficiency in protein

turnover could result in the accumulation of over-oxidized SOD1 species. This could be tested by pulse-chase radiolabeling of newly synthesized proteins to assess the half-life of SOD1 in PBMCs, as PBMCs can be cultured for short periods of time (Cova et al. 2006). These theories are not mutually exclusive. The amount of protein oxidation is thought to be a balance between the rate of protein oxidation and protein turnover. A decrease in protein degradation, for example, would likely increase the amount of oxidized species present. Supporting this hypothesis, the two major mechanisms involved in protein turnover, the ubiquitin proteasome system (UPS) and autophagy, are compromised in ALS (Ferrucci et al. 2011). In fact, lysine oxidation, as seen at Lys122 in SALS SOD1 from PBMCs, would interfere with SOD1 turnover via the UPS and/or autophagy if it functions as a ubiquitination site, as ubiquitination would be inhibited (Basso et al. 2006, Kabuta et al. 2006, Spasser and Brik 2012). Bioinformatics sites have identified Lys122 as a non-ubiquitination site (<http://www.jci-bioinfo.cn/iUbiq-Lys>). Lys122 may still function as a ubiquitination site, as consensus sequences for ubiquitination are lacking and Lys136, a known ubiquitination site of SOD1, was identified as a non-ubiquitination site as well (Basso et al. 2006). Previous studies have demonstrated that even non-canonical sites of ubiquitination, such as cysteine (Spasser and Brik 2012) are oxidized in WT SOD1 in the presence of hydrogen peroxide (Bosco et al. 2010). Unfortunately, the extent of oxidation on cysteine residues in PBMC SOD1 was unable to be determined because the alkylation and reduction steps employed

during sample preparation for mass spectrometry are expected to eliminate the presence of these species. Generally, oxidized proteins are degraded more rapidly by a ubiquitin-independent proteasome pathway, but the accumulation of oxidized SOD1 in SALS PBMCs suggests an impairment of this pathway as well (Shringarpure et al. 2003). Together, these data suggest an inefficient/altered turnover of SOD1 in sporadic ALS. This does not necessarily translate to an increase in the overall level of SOD1 protein, as SOD1 expression is regulated by multiple mechanisms (Milani et al. 2011, Milani et al. 2013). In fact, published data suggests a decrease in total SOD1 in PBMCs, although this was not observed in the work presented in this chapter (**Fig. III-8**, (Cova et al. 2006, Gagliardi et al. 2010)).

Interestingly, Trp32 was found to be over-oxidized in SOD1 isolated from SALS PBMCs compared to controls (**Table III-2, Fig. III-10**). This tryptophan residue is directly implicated in FALS-linked SOD1 pathogenesis. Trp32 is not required for toxicity of FALS-linked SOD1 variants as mice expressing mouse SOD1 G86R, a model lacking Trp32, develop an ALS-like phenotype, suggesting other mechanisms are involved in SOD1 pathogenesis as well (Ripps et al. 1995). However, multiple studies have suggested the Trp32 residue contributes to toxicity and misfolding of human SOD1. For example, oxidation-induced aggregation of WT SOD1 requires the presence and oxidation of Trp32 to proceed (Zhang H. et al. 2003). In immortalized cell lines, the propagation of SOD1 misfolding by FALS-linked SOD1 is prevented when Trp32 is replaced

with a serine (Grad et al. 2011). Moreover, the toxicity due to FALS-linked SOD1 expression in cultured motor neurons is ameliorated when Trp32 is mutated to a phenylalanine (Taylor et al. 2007). The heightened oxidation of Trp32 specifically on SOD1 from SALS PBMCs suggests SALS-linked SOD1 may contribute to ALS pathogenesis in a similar manner.

One potential modification responsible for the SOD1 species observed at pI 5.4 is the oxidation of His46 to produce aspartic acid. Being that aspartic acid is negatively charged, this conversion from histidine induces a reduction in pI like that observed for the SOD1 in control samples by 2D-GE (**Fig. III-8**). Histidine is known to be one of the primary targets of metal catalyzed oxidation (Dean et al. 1989, Schoneich 2000, Uchida 2003), and as such, the oxidation of this amino acid is not surprising. In fact, the oxidation of histidine to 2-oxo-histidine that was identified in both the SALS and control pooled SOD1 samples has been previously identified in SOD1 from bovine and human erythrocytes (Uchida and Kawakishi 1994, Rakhit et al. 2002). One can imagine the unique susceptibility of histidines in SOD1 to be oxidized, as the majority of the histidines coordinate zinc and copper in the active site, which in the presence of H₂O₂, can participate in metal-catalyzed oxidation (**Fig. III-11**). Further, SOD1 isolated from bovine erythrocytes subjected to amino acid composition analysis demonstrated a decrease of histidine and an increase in aspartic acid after exposure to H₂O₂ (Uchida and Kawakishi 1994). The conversion of histidine to aspartic acid in the control SOD1 pool only, however, is surprising especially since an overall

increase in oxidation is seen in the SALS SOD1 pool (**Table III-2**). One theory is that this difference may signify a change in the cellular environment of PBMCs in SALS compared to controls. For example, oxidation of SOD1 by other methods *in vitro*, such as CuCl_2 and ascorbic acid, results in a decrease in the histidine composition, like what is seen for H_2O_2 induced oxidation, but has no effect on aspartic acid composition (Rakhit et al. 2002). These data suggest that the oxidized SOD1 products may be indirect evidence of altered oxidative species present inside the cell. A second theory is that the ring-ruptured product of oxidized histidine, aspartic acid, is an early step in the degradation of SOD1. In fact, the ring-opening products of histidine have been proposed to be products of degradation as they are downstream events of 2-oxo-histidine (Dean et al. 1989, Uchida 2003). Therefore, the conversion of histidine to aspartic acid found enriched in SOD1 from control PBMCs could be evidence of a protein degradation pathway compromised in SALS. Further, the over-oxidized SOD1 species present in SALS PBMCs, which is likely misfolded (Rakhit et al. 2002, Rakhit et al. 2004), may interfere with protein clearance mechanisms directly by triggering ER stress through an interaction with Derlin-1, similar to what is seen for FALS-linked SOD1 variants (Nishitoh et al. 2008).

This is the first study to demonstrate differential species of SOD1 in SALS PBMCs compared to controls. The 5.4 SOD1 species identified by 2D-GE provides a direct link between altered SOD1 homeostasis and sporadic ALS. Future studies aimed at evaluating the SOD1 species in sera and PBMCs of

SALS patients over time will help us discover the role of this protein in disease progression. Further study is required to identify if this connection is unique to ALS, or if it has a more global application with other neurodegenerative and inflammatory diseases.

Materials and Methods

SOD1 protein expression and purification- See **Chapter II**, Materials and Methods for details on protein purification.

Sandwich ELISA for misfolded SOD1- A 384-well high binding plate (Greiner, #781061) was coated with 12.5 μ l/well of C4F6 antibody at 9 μ g/ml in phosphate buffered saline (PBS) and incubated at 4°C for 16 h. The plate was washed by submersion 3x in phosphate buffered saline, tween20 (0.01 M PBS, 0.05% tween20) followed by a blocking step with 25 μ L/well of 5% BSA in PBS for 1 h at room temperature. Following the blocking period, the plate was washed 1x with PBST and recombinant SOD1, CSF, sera or lysate were added in a dilution series (1, 1:2, 1:4, 1:8) and incubated for 1 h at room temperature. The plate was then washed 3x with PBST and the primary antibody, anti-SOD1 (AbCam, ab79390), was added at 1:1000 in PBST, incubated for 1 h at room temperature. The plate was then washed 3x in PBST and probed with poly HRP-conjugated anti-Rabbit (Fisher, PI32260) at 1:10,000 in PBST for 1 h at room temperature. After washing 3x with PBST, 25 μ L of TMB substrate (SurModics, TMBS-0100-01) was added to each well for 30 min. The reaction was quenched by adding 25

μ L/well of Stop Solution (SurModics, LSTP-0100-01). Absorbance at 450 nm was detected with a 384-well plate reader (Safire).

Sandwich ELISA for total SOD1- For total SOD1 calculations, ELISA was performed essentially as described above with the following exceptions. The coating antibody was anti-SOD1 at 1: 40 and the detection antibody was HRP conjugated anti-SOD1 at 1:1000 (eBioscience, BMS222MST).

Isolation and lysis of RBCs and PBMCs- All SALS samples were processed with a healthy control in parallel. RBCs and PBMCs were processed from the same blood draw from the same individual. Blood samples were collected using standard venipuncture technique in yellow top tubes containing 22 g/L Trisodium Citrate, 8 g/L Citric Acid, 24.5 g/L Dextrose. For RBCs, 8 mL of blood was centrifuged in a 15 ml conical tube for 15 min at 300 ruff. Then, the cells were washed with 12 ml of Hank's Balanced Salt Solution (HBSS; Invitrogen, 14025076) and spun for 15 min at 300 rcf. Supernatant was removed and the cell pellet was resuspended in 500 μ L of lysis buffer (25 mM Tris, pH 7.8) and sonicated for 5 sec at 10% at 4°C. The lysed RBCs were then centrifuged at 13,000 rpm for 15 min at 4°C. The supernatant was aliquoted and stored at -80°C.

For PBMCs, 4 mL lymphoblast separation solution (Lonza, 17-829F) was added to an isolation tube (Greiner, 163290P) and spun at 1000 rcf for 1 min for tube priming. Then, 5 ml blood was added slowly to the upper layer of the tube

and spun at 1600 rcf for 30 minutes. Immediately following centrifugation, the mononuclear cell layer was collected with a Pasteur Pipette and transferred to a 15 ml conical tube and spun at 300 rcf for 15 min. Cells were washed with 12 ml of HBSS and mixed by inverting tube 5 times. The PBMCs were centrifuged for 15 minutes at 300 RCF. The supernatant was removed and the cells were resuspended in 200 μ l of lysis buffer (25 mM Tris, pH 7.8) and sonicated for 5 sec at 10% at 4°C. The cell lysate was Centrifuged at 13,000 rpm for 15 min at 4°C. Aliquoted supernatant was stored at -80°C. Lysates were processed within one week by 2D-GE analysis. Lysates were processed within one month for immunoprecipitation and mass spectrometry analysis.

Immunoblots- For denaturing western analyses, samples were diluted in 6x sample buffer (Boston Bioproducts, BP-111R). Samples were separated by PAGE with 15% Tris-acrylamide gels in 1% SDS, 25 mM Tris, 192 mM glycine and transferred to PVDF membrane (Millipore) in 25M Tris, 192 mM glycine. Membranes were blocked for 1h in Odyssey blocking buffer (LI-COR). Primary antibodies were incubated at 4°C overnight at the following dilutions: (pan-SOD1(Taylor et al. 2007), 1:500; anti- α tubulin (Sigma), 1:5000; anti-SOD1 (AbCam, ab79390), 1:50,000). The blots were incubated for 1 h with fluorophore-conjugated secondary antibodies (LI-COR) prior to visualization by the Odyssey Infrared Imaging System (LI-COR). The Odyssey infrared imaging software (LI-COR) was used for densitometry calculations.

2-D Gel Electrophoresis- Samples were mixed with rehydration buffer (8 M Urea, 1.5% CHAPS, 50 mM DTT, 0.2% Bio-lytes (Bio-Rad, 1632097), trace amounts of Bromophenol Blue) and separated by isoelectric focusing on a pH strip range 4.7-5.9 (BioRad, 163-2025 (discontinued); suggest 163-2017 as alternative). The following parameters were used after a 12 h passive rehydration:

Step 1: 250 V for 15 min
Step 2: 2000 V hours
Step 3: 8000 V for 2 hours
Step 4: 500 V hold

Upon completion of focusing, strips were moved to rehydration trays containing 500 μ l of equilibration buffer (6 M Urea, 2% SDS, 0.375 M Tris, 20% Glycerol, 150 mM DTT) for 5 min. The strips were then secured in gel with agarose sealing solution (1% agarose, 1% SDS, 25 mM Tris, 192 mM glycine) and subjected to SDS-PAGE in a 15% Tris-acrylamide gels in 1% SDS, 25 mM Tris, 192 mM glycine. Where applicable, the gels were then transferred to a PVDF membrane for 16 h at 30 V at 4°C. Membranes were blocked for 1 h in Odyssey blocking buffer (LI-COR). Primary antibodies were incubated for 3 h at the following dilutions: anti-SOD1(Taylor et al. 2007); anti-SOD1 (AbCam, 1:50,000). The blots were incubated for 1 h with fluorophore-conjugated secondary antibodies (LI-COR) prior to visualization by the Odyssey Infrared Imaging System (LI-COR). The Odyssey infrared imaging software (LI-COR) was used for densitometry calculations.

Mass spectrometry analysis of immunoprecipitated SOD1- Protein G Dynabeads (Invitrogen, 10004D) were coated with mouse IgG (Sigma, I5381) for preclearing of lysate) and anti-SOD1 (Pierce, LFMA0023) for immunoprecipitation. Approximately 1400 µg (RBC) or 350 µg (PBMC) of lysate diluted in PBST was added to 50 µL mouse IgG coated beads, rotating at room temperature for 1 h. The precleared lysate was removed and added to anti-SOD1 coated beads for 2 h rotating at room temperature. SOD1 was boiled off the beads with 50 µL of 3x SDS Page loading buffer and subjected to SDS-PAGE and stained with coomassie. Tryptic (Promega) in-gel digest was performed essentially as described (Shevchenko et al. 2006). Extracted peptides were lyophilized and resuspended in 16 µL of 5% acetonitrile in 0.1% trifluoroacetic acid immediately prior to injection on LC/MS/MS. A 4.0 µL aliquot was directly injected onto a custom packed 2cm x 100µm C₁₈ Magic 5µm particle trap column. Peptides were then eluted and sprayed from a custom packed emitter (75µm x 25cm C₁₈ Magic 3µm particle) with a linear gradient from 95% solvent A (0.1% formic acid in water) to 35% solvent B (0.1% formic acid in acetonitrile) in 45 minutes at a flow rate of 300 nanoliters per minute on a Waters Nano Acquity UPLC system. Data dependent acquisitions were performed on a Q Exactive mass spectrometer (Thermo Scientific) according to an experiment where full MS scans from 300-1750 m/z were acquired at a resolution of 70,000 followed by 10 MS/MS scans acquired under HCD fragmentation at a resolution of 17,500 with an isolation width of 1.6 Da. Raw data files were processed with Proteome

Discoverer (version 1.4) with Mascot (Version 2.5, Matrix Science) using the human Uniprot database. An error tolerant search was employed to identify modifications present on SOD1 peptides. Scaffold was used to quantify the modified (oxidation, deamidation, carbidomethylation, N-term acetylation, phosphorylation) and unmodified peptides (false discovery rate (FDR), 1.3%) identified in the error tolerant search.

Axonal Transport Assay- Squid axoplasms were isolated and perfused with SOD1 essentially as previously described (Morfini G. et al. 2006). The isolated axoplasms were perfused with 1.4 μ M hSOD1 (pooled from 3 patients) and monitored for 50 min using live imaging as described (Morfini G. et al. 2006).

PREFACE TO CHAPTER IV:**Parts of this chapter appeared in:**

Rotunno, M.S., Bosco, D.A., “An emerging role for misfolded wild-type SOD1 in sporadic ALS pathogenesis.” *Frontiers in Cellular Neuroscience*. 2013, 7, 253.
Invited review.

CHAPTER IV: DISCUSSION

ALS is a devastating disease resulting in motor neuron degeneration, muscle atrophy, and paralysis. Although ALS is relatively rare, the lifetime risk is estimated at greater than one in 500, as it primarily targets the aged population (Alonso et al. 2009, Wijesekera and Leigh 2009). ALS is known to be a multifaceted disease with numerous contributing factors such as oxidative stress, excitotoxicity, protein aggregation, mitochondrial dysfunction and chronic inflammation (Wijesekera and Leigh 2009). The ALS community is starving for an effective treatment, as Riluzole, the only FDA approved drug to treat ALS, has minimal effects on survival (Miller et al. 2012).

A large number of mutations in SOD1 result in ALS pathogenesis, but the common “toxic” region among these species had not been determined prior to this study. Misfolding of ALS-linked mutant SOD1 has been well established through both its increased propensity to aggregate (Durham et al. 1997, Bruijn et al. 1998, Johnston et al. 2000, Stathopoulos et al. 2003, Furukawa et al. 2006, Wang Q. et al. 2008, Prudencio et al. 2009) Review: (Chattopadhyay and Valentine 2009), in-solution structural analyses (Shipp et al. 2003, Durazo et al. 2009, Molnar et al. 2009), and through the generation of misfolded SOD1-specific antibodies (Rakhit et al. 2007, Urushitani et al. 2007, Liu et al. 2009, Bosco et al. 2010, Forsberg et al. 2010, Gros-Louis et al. 2010, Grad et al. 2011, Brotherton et al. 2012, Fujisawa et al. 2012, Broering et al. 2013).

In addition to misfolding of SOD1 induced by ALS-linked mutations, aberrant post-translational modifications (PTMs) have been shown to result in major structural disturbances, a phenomenon that could result from the environmental/genetic factors involved in SALS pathology. Examples of such PTMs include oxidation of amino acid side chains (Ezzi et al. 2007, Fujiwara et al. 2007, Bosco et al. 2010, Chen X. et al. 2012b, Auclair et al. 2013b), lack of metal coordination (Ding and Dokholyan 2008, Banci et al. 2009, Durazo et al. 2009), and loss of the stabilizing intramolecular disulfide bridge (Chan et al. 2013).

The work presented in this dissertation provides preliminary data on methods of tracking misfolded and differentially modified forms of SOD1 in biofluids as a biomarker strategy for ALS. As discussed in **Chapter III**, finding a reliable biomarker for ALS is vital for patient stratification in clinical trials, early diagnosis, tracking patient response to therapeutics and for tracking disease progression (Robelin and Gonzalez De Aguilar 2014). With this in mind, it is necessary to repeat these preliminary studies with a larger cohort of ALS patients to verify the validity and reproducibility of the findings put forth in this dissertation.

In addition to exploiting SOD1 as a biomarker for ALS, the work presented in this dissertation has put forth stabilizing the zinc binding and electrostatic loops of misfolded SOD1 as a therapeutic target. Modified forms of SOD1, whether by mutations or aberrant post-translational modifications, result in a loosening of the

protein structure that further exposes the hydrophobic core (**Fig. I-1, IV-1**). This effect may increase SOD1's vulnerability to oxidation (**Table III-2**) and lead to a more promiscuous SOD1 protein, engaging in aberrant protein-protein interactions and/or tighter binding with normal protein-protein interactions thereby altering downstream effects (**Fig. I-4**). ALS-linked SOD1 has been shown to exhibit prion-like properties, similar to those of established prion proteins (Polymenidou and Cleveland 2011). In cell culture models, misfolded and aggregated SOD1 is secreted and taken up by surrounding cells, inducing misfolding and aggregation of endogenous, nonpathogenic SOD1 protein (Grad et al. 2011, Munch et al. 2011). Recently, spinal cord homogenates from paralyzed SOD1 G93A transgenic mice injected directly into the spinal cord of predisposed ALS mouse models have been shown to induce aggregation and progressive paralysis (Ayers et al. 2014). Stabilizing SOD1 in its proper fold and/or blocking this "toxic" region and inhibiting the exponential process of SOD1 misfolding could potentially curb disease progression in both sporadic and familial forms of ALS.

SOD1-Based Therapeutics

Being that SOD1 pathological aggregates are a downstream consequence of SOD1 misfolding, the presence of such aggregates in human post-mortem tissues and ALS-mice argues for a role of misfolded SOD1 in disease. As discussed earlier, there is evidence for misfolded SOD1 in both sporadic and familial ALS (see **Chapter I**). Strategies for neutralizing, decreasing, and

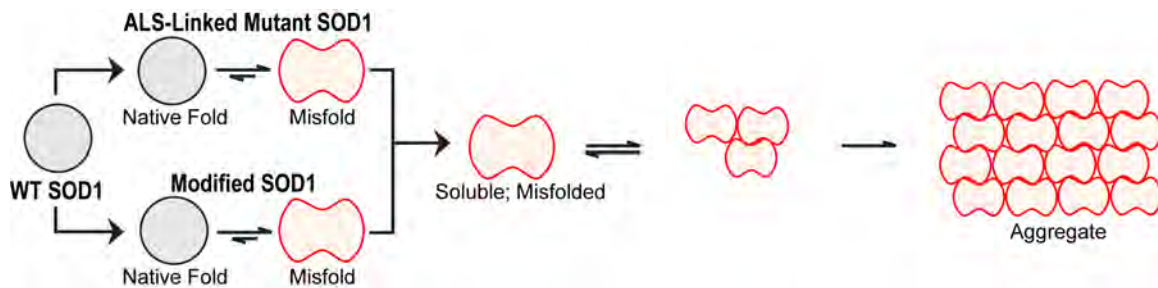


Figure IV-1. PTM-linked and FALS-linked SOD1 share a common misfolded conformation. We hypothesize that misfolded SOD1 results from both ALS-linked mutations and aberrant post-translational modifications. The term “misfolding” refers to the structural loosening of SOD1 due to a mutation and/or altered post-translational modification within a soluble form of the protein. Misfolded, soluble SOD1 can engage in aberrant protein-interactions and acquire new toxic functions (illustrated in **Figure I-4**). Misfolded SOD1 can also assemble into aggregates.

repairing this load of misfolded SOD1 species are being explored as potential therapies (**Fig. IV-2**).

Immunization Strategies Targeting SOD1

Studies from van Blitterswijk et al. suggest that longer survival is associated with ALS patients harboring antibodies directed at misfolded SOD1 (van Blitterswijk et al. 2011). In fact, immunization strategies targeting misfolded SOD1 species have had therapeutic outcomes in ALS mice. A passive immunization strategy with the D3H5 antibody that specifically reacts with misfolded SOD1 extended survival in G93A SOD1 transgenic mice (Gros-Louis et al. 2010)(**Fig I- 3, Table I-1**). A greater therapeutic impact was shown in active immunization trials with the SOD1 G37R transgenic mouse model, using both recombinant apo-SOD1 G93A (Urushitani et al. 2007) and the SEDI (SOD1 exposed dimer interface) peptide (Liu et al. 2012) as immunogens. Use of SEDI increased survival and delayed disease onset to a greater extent than the full-length SOD1 immunogen, likely due to specific targeting of a misfolded toxic epitope within mutant-SOD1 (Liu et al. 2009, Liu et al. 2012).

A more modern approach by Patel et al. demonstrated the effectiveness of a “chronic passive immunization” treatment (Patel et al. 2013). This approach involves the intrathecal delivery of a viral vector expressing a single chain antibody fragment derived from the D3H5 described above. The result is chronic

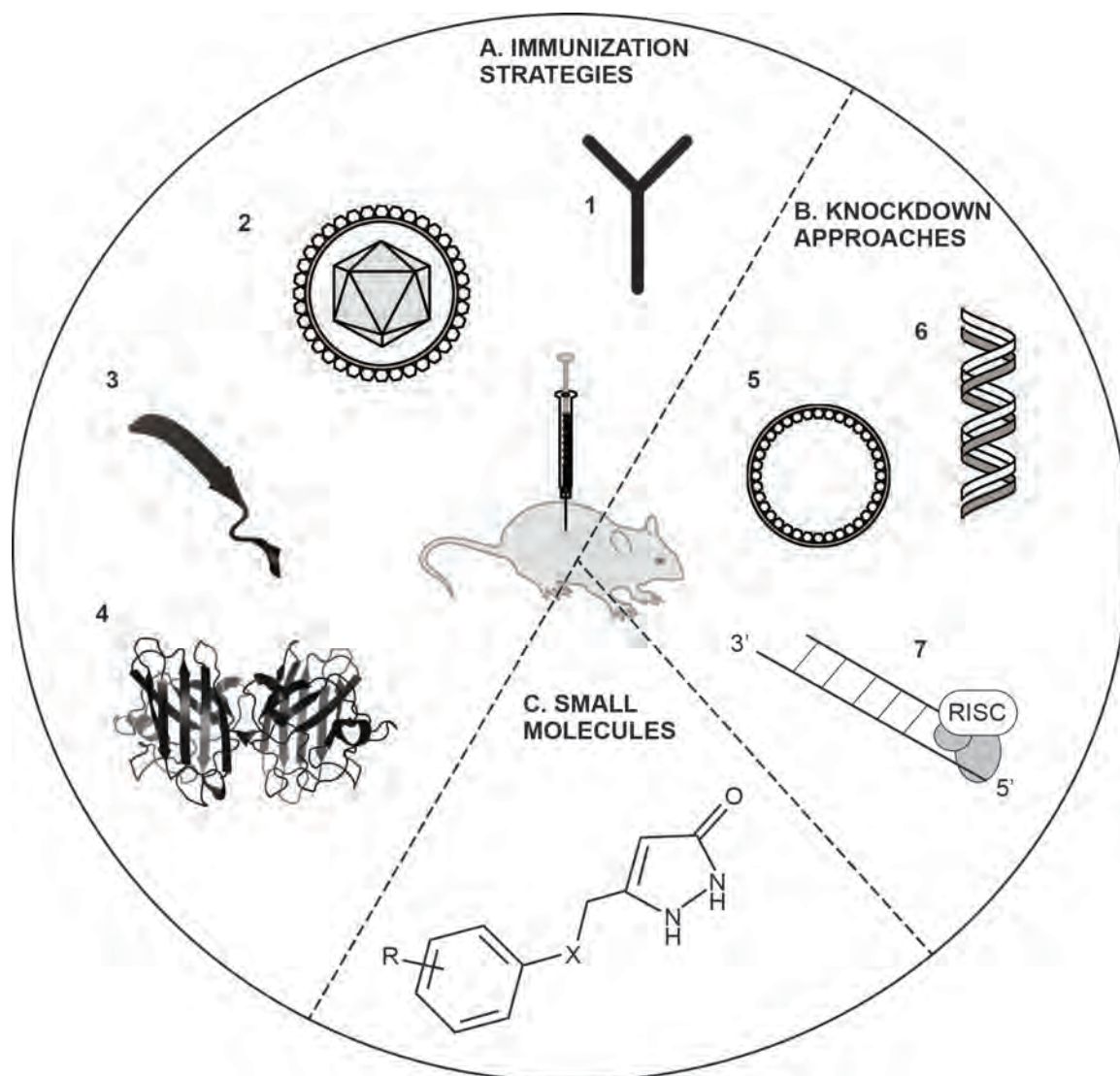


Figure IV-2. Therapeutic Strategies for SOD1-linked ALS. (A) Immunization strategies targeting misfolded SOD1. Passive immunization approaches include treatment with misfolded-SOD1 specific antibodies (1) and viral vectors to chronically express antibody fragments (2). Active immunization with either fragments of (3) or full-length (4) misfolded SOD1 are also being explored. (B) Knockdown approaches involving RNAi expressing viral vectors (5), antisense oligonucleotides (6, in clinical trials), and siRNA mechanisms (7) are being investigated. (C) Small molecules that repair and/or neutralize the load of misfolded SOD1 are currently in clinical trials.

expression of the variable region of a misfolded SOD1-specific antibody. The methodology requires more fine-tuning and optimization to increase consistency, but shows great promise as survival in SOD1 G93A transgenic mice was extended from 140 to 180 days upon treatment (Patel et al. 2013). These data suggest that immunization strategies directly targeting misfolded SOD1 could have therapeutic potential.

While these studies provide a direct correlation between misfolded SOD1 species and disease in mice, a survival benefit was not realized using humanized SOD1 antibodies in SOD1 transgenic mice (Broering et al. 2013). Going forward, immunotherapeutic strategies in humans may require the specific targeting of regions within SOD1 that are only exposed upon misfolding. Moreover, these regions should mediate some toxic effect *in vivo*, so that antibodies have the potential to neutralize or otherwise block that “toxic epitope”. The latter criterion is important in light of the fact that not all mutant-specific antibodies have produced a therapeutic outcome in SOD1 transgenic mice (Gros-Louis et al. 2010).

Decreasing Expression of SOD1

Studies underway are investigating the possibility of reducing the load of total SOD1 protein as a potential therapeutic target. Although the major school of thought is the gain-of-toxic function model for SOD1-induced ALS, there is increasing evidence that loss-of-function contributes to disease progression as

well (reviewed in (Saccon et al. 2013)), which argues against decreasing SOD1 expression as treatment. For example, the anti-oxidizing activity, although still functional, is decreased in the majority of FALS-linked SOD1 mutations (Borchelt et al. 1994, Robberecht et al. 1994).

Reducing the load of misfolded SOD1 could be a promising avenue, but could also increase neuronal susceptibility to degeneration in the absence of such a highly abundant anti-oxidizing enzyme. One can imagine in a disease such as ALS, where oxidative stress is elevated, that the lack of an abundant anti-oxidizing enzyme, like SOD1, could be detrimental. Mice lacking SOD1 protein, for example, have an increased sensitivity to neuronal injury (Reaume et al. 1996). This study implies that when faced with additional neuronal stress, which is evident in ALS pathology, SOD1 protein is required as part of the coping mechanism. In fact, evidence suggests oxidative stress increases with age (Smith C. D. et al. 1991). Oxidative stress is known to induce destabilization, aggregation, and reduced activity of SOD1, which could be one of the reasons for the age-related onset of ALS (Smith C. D. et al. 1991, Rakhit et al. 2004, Ezzi et al. 2007).

Altering SOD1 levels has been explored as a novel cancer therapeutic. In cell culture systems, SOD1 knockdown results in senescence and therefore has the potential to halt tumor growth, and even induces cell death in a cancer cell line (Blander et al. 2003). Tumors, however, have evidence of decreased SOD1

activity (Sun et al. 1993), which is linked to tumorigenesis. SOD1 deficient mice, for example, have a shorter lifespan caused by hepatocellular carcinomas, or liver tumors (Elchuri et al. 2005). In fact, overexpression of SOD1 has been proposed as a possible cancer treatment, as it has been shown to inhibit tumor growth (Bai et al. 1998, Zhang Y. et al. 2002). Hepatocellular carcinoma, one of the more common cancers, is likely caused by DNA damage induced by oxidative stress (Cardin et al. 2014). The liver has a unique susceptibility to spontaneous DNA mutations in SOD1-deficient mice. In contrast, the brain does not demonstrate an increase in spontaneous DNA mutations (Busuttill et al. 2005), which implies a CNS-specific knockdown of SOD1, in the context of ALS, might not have the same carcinoma-inducing effect.

Indeed, several ALS animal models expressing FALS-linked SOD1 have demonstrated the protective effects of SOD1 knockdown *in vivo* (Ralph et al. 2005, Smith R. A. et al. 2006, Wang L. et al. 2010). It is possible that a more selective knockdown in specific cell types could be beneficial while still maintaining the protective effect of SOD1 in other parts of the body. More specific targeting of SOD1 knockdown in select cell types such as Schwann, motoneuron, and astrocytes exhibit protective effects as well (Wang L. et al. 2012b, Dirren et al. 2015). Ideally, we could identify a method to specifically knockdown only the mutant allele, leaving the other allele to express native SOD1. Nevertheless, decreasing SOD1 expression is a therapy worth exploring as beneficial effects have been observed.

Small Molecules Targeting Misfolded SOD1

Another potential therapeutic method being explored is to target SOD1 with small molecules to either stabilize it in its dimeric form or neutralize the toxic properties (reviewed in (Limpert et al. 2013)). Being that misfolded SOD1 engages in multiple aberrant protein-protein interactions (**Fig. I-4**), high-throughput screens directed at disrupting them, such as the dynein-SOD1 interaction, are being explored (Zhang F. et al. 2007, Tang et al. 2012). In fact, we identified several small molecules that have the potential to repair misfolded SOD1 by employing the misfolded-specific antibody, C4F6 (described in **Appendix II**).

Monomeric SOD1 is thought to be a precursor to misfolding and aggregation. One route of targeting for therapeutics would be to find small molecules that can stabilize SOD1 in its dimeric state. Several *in silico* screens have been performed to identify such compounds. In the first *in silico* study, Ray et al. identified 100 compounds with a predicted high binding affinity to SOD1 dimer (Ray et al. 2005, Nowak et al. 2010). Of these initial hits, 15 were able to prevent dimer loss of mutant SOD1 *in vitro*. These compounds stabilized SOD1 as indicated by unfolding studies with guanidine-HCl. In follow-up *in vitro* studies, however, the aggregation of FALS-linked SOD1 was unaltered in the presence of these compounds, despite the fact that one of the compounds was found to bind SOD1 at an amino acid implicated in SOD1 pathogenesis, Trp32 (Wright et al. 2013).

Several studies have searched for small molecules that reverse the toxic properties of FALS-linked mutant SOD1 in cell culture systems (Benmohamed et al. 2011, Yang et al. 2013). Benmohamed et al. identified compounds that reduced MG132-induced toxicity and FALS-linked SOD1 aggregation (Benmohamed et al. 2011). The benefit of this type of screen over the completely *in vitro* approach with recombinant SOD1 protein is the ability to identify compounds that indirectly tweak the cell's coping mechanisms as opposed to only identifying compounds that directly bind SOD1 to interfere with aggregation. An aryloxanyl pyrazolone derivative, an optimized version of 1 of the 3 original chemical scaffolds identified, extends survival in an ALS mouse model (Benmohamed et al. 2011, Chen T. et al. 2012a). These compounds are currently being optimized to further enhance the pharmacokinetic properties (Zhang Y. et al. 2013) prior to clinical trials. Preferably, we can identify a therapeutic approach specifically targeting the misfolded SOD1 species, leaving WT unchanged. This is a challenging endeavor, as SOD1 is a homodimer, and dimeric species are likely a mixture of misfolded and normal WT SOD1 (Ganesan et al. 2008).

Other Promising Future Therapeutics

Multiple small molecules are being explored that target different aspects of disease such as decreasing excitotoxicity, conserving mitochondria, increasing neuronal survival, decreasing inflammation and increasing muscle function (Pandya et al. 2013). A variety of pathways are involved in ALS pathogenesis

and, as such, a more effective approach may be therapeutics used in combination to enhance the benefits of these compounds. Some of the more promising compounds are discussed herein.

There is ample evidence that excitotoxicity is linked to ALS pathology in cell culture models, transgenic models, and patients (Van Den Bosch et al. 2006). Even Riluzole, the only drug currently available to ALS patients, is thought to act as an anti-excitotoxic agent by decreasing extracellular glutamate (Martin et al. 1993). Beta-lactam antibiotics act by increasing the expression of glutamate transporter, GLT1, which protects against excitotoxicity (Rothstein et al. 2005). One clinical trial in progress is testing whether Ceftriaxone, a beta-lactam antibiotic, has any promising effects since it indirectly results in a decrease in glutamate. Preliminary data shows safety and efficacy, but long-term studies are unable to be interpreted, as too many patients left the trial. Therefore, further studies are required to determine the effects this treatment has on curbing disease progression ((Berry et al. 2013); <https://clinicaltrials.gov/ct2/show/NCT00349622?term=ALS+ceftriaxone&rank=1>).

Cell replacement therapy is another promising avenue being explored as a treatment for ALS (Thomsen et al. 2014). This can be further divided into two main approaches. The first is to replenish the depleted motor neurons with neuronal progenitor cells. This approach, although potentially very powerful, is quite challenging because these cells need to incorporate themselves into an

established complex network (Becker and Diez Del Corral 2015). The second approach is to deliver cells to serve as a support system for the motor neurons in jeopardy. Specifically, mesenchymal stem cells are being explored for this purpose and their safety has been established (Mazzini et al. 2009). Mesenchymal cells have been shown to promote neurotrophic factors and decrease gliosis in ALS mouse models (Vercelli et al. 2008, Sadan et al. 2009). Being that neuronal death and lack of muscle stimulation results in progressive paralysis in ALS, replacing and/or supporting the motor neurons through cell replacement therapy is a promising therapeutic approach. It is, however, important to proceed with caution as the chronic immune suppression regimen that accompanies these cell replacement therapies can have detrimental side effects to ALS patients (Thomsen et al. 2014).

Directly targeting the toxic properties displayed by ALS-linked neurons is a possible treatment for ALS as well. By investigating multiple iPSC-derived motor neuron cell lines, Wainger and colleagues demonstrated a hyperexcitability unique to ALS patient lines. By using retigabine, an FDA approved anticonvulsant for the treatment of epilepsy, a decrease in the hyperexcitability was observed. Treatment with retigabine also decreased signs of ER stress, a cellular response to unfolded/misfolded protein accumulation, such as reduced splicing of *XBP1* (Wainger et al. 2014).

A generalized increase in heat shock chaperones could prove protective in the cytotoxic environment of the CNS. Heat shock proteins represent a known coping mechanism of cells in a toxic environment. Arimoclomol, a known inducer of heat shock proteins, is currently in Phase III clinical trials for the treatment of FALS-linked SOD1 induced ALS (<https://clinicaltrials.gov/ct2/show/NCT00706147?term=Arimoclomol&rank=1>).

Arimoclomol enhances survival in a transgenic mouse model of ALS, even when treatment begins after symptom onset (Kieran et al. 2004).

As discussed below, protein misfolding and aggregation is a hallmark of ALS. In theory, the upregulation or enhancement of the cellular system that deal with this burden, such as the UPS and autophagy, could be exploited as a therapeutic approach. One such autophagy inducer, Tamoxifen, originates as a breast cancer drug. A patient with both ALS and breast cancer was prescribed Tamoxifen and appeared to have a milder case of ALS (<http://www.als.net/ALS-Research/Tamoxifen/ALS-Topics/>), launching an investigation into this drug as a treatment for motor neuron disease. Tamoxifen treatment results in both neuronal protection and a decrease in TDP43 inclusions in an FTL mouse model with TDP43 proteinopathy (Wang I. F. et al. 2012a). Now, Tamoxifen has passed phase II clinical trials and is currently recruiting for phase III (Traynor et al. 2006, Rubinsztein et al. 2007). Hopefully, over the next couple of years, a handful of these promising compounds will prove beneficial in

the treatment of ALS in patients and slow, halt, or even revert, the process of neurodegeneration and paralysis.

Protein Misfolding and ALS

Evidence of Altered Protein Homeostasis

Multiple mechanisms involved with maintaining protein homeostasis have been implicated in ALS. SOD1 is not, by far, the only ALS-associated protein incriminating protein misfolding and turnover in pathogenesis. In fact, the majority of ALS-linked mutations translate an aggregation prone form of the protein. This is evident in, for example, *in vitro* studies of SOD1, TDP43, and profilin-1, which demonstrate an accumulation of these proteins in the insoluble fraction of cellular lysates (Johnson et al. 2009, Prudencio et al. 2009, Wu et al. 2012). Most ALS-linked proteins, if not all, have been found in end-stage aggregates in the spinal cord of patients (reviewed in (Blokhuis et al. 2013)). These aggregates are commonly ubiquitinated and contain p62, both of which directly implicate the protein clearance mechanisms, UPS and autophagy (Seibenhener et al. 2004, Pankiv et al. 2007). Further, two proteins linked to inherited ALS, VCP and UBQLN2 are directly involved in protein degradation (Wojcik et al. 2006, Lee and Brown 2012). ALS mouse models demonstrate signs of both ER stress and proteasome malfunction (Kabashi et al. 2004, Prell et al. 2012, Gorrie et al. 2014). In fact, studies support an impairment of the proteasome in SALS patient spinal cord (Kabashi et al. 2012). Together, these data implicate impaired protein clearance mechanisms in ALS.

The Additive Effect of Aging

ALS is a disease primarily effecting the aging population. This is likely because of the breakdown of key systems that are involved with managing chronic stress. Aging tips the balance, decreasing the body's army of defense mechanisms, allowing for people who have kept their ALS-inducing factors at bay to begin to lose the battle (**Fig. IV-3**).

In vitro studies demonstrate a more rapid turnover of ALS-linked misfolded proteins, presumably as a coping mechanism (Kabuta et al. 2006, Farr et al. 2011, Araki et al. 2014), which suggests protein turnover mechanisms are vital to combat disease. In the process of aging under non-diseased conditions, protein oxidation is increased which adds to the load of misfolded proteins (Oliver et al. 1987, Smith C. D. et al. 1991). This increase in protein oxidation is a contributing factor to the decrease in select enzymatic activity, as seen for glutamine synthetase (Wolff and Dean 1986) that, mainly expressed in astrocytes, is responsible for maintaining extracellular glutamate levels and protecting surrounding cells from excitotoxicity (Suarez et al. 2002). The activity of catalase, a hydrogen peroxide scavenger, has also been shown to decrease with age (Alper 1998, Tsay et al. 2000). In addition to creating an environment that promotes protein modifications and misfolding, aging induces a decrease in efficiency of mechanisms that are involved in their reparation and degradation (Martinez-Vicente et al. 2005, Cuervo 2008). The ability to transcribe chaperones, which are required to both repair damaged proteins and/or promote

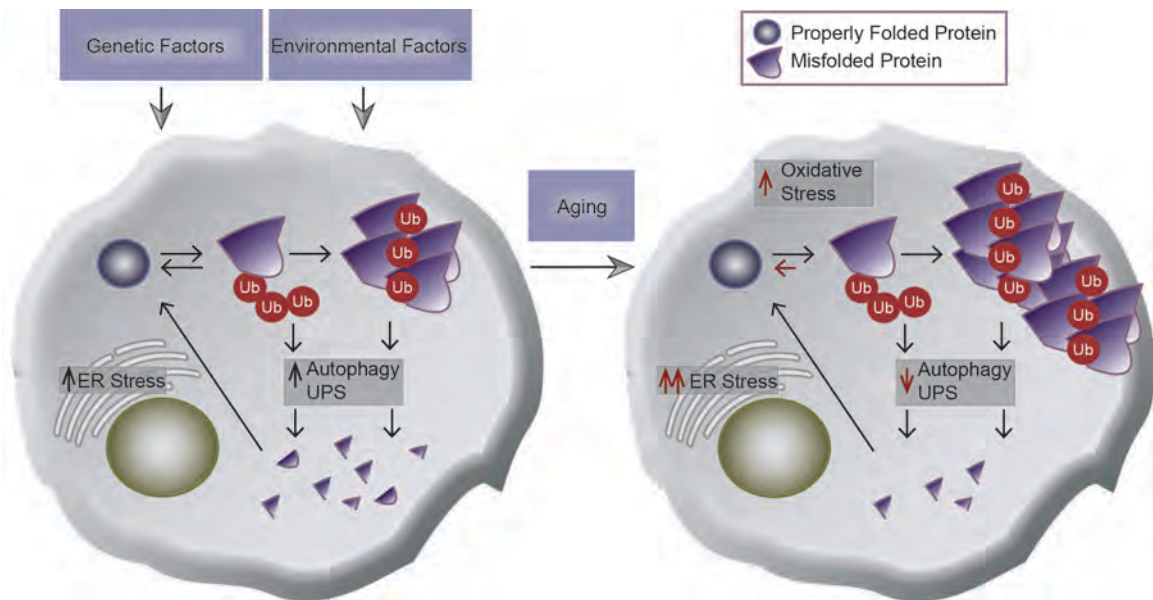


Figure IV-3. Protein misfolding, aging and ALS. Both genetic and environmental factors induce ALS-linked protein misfolding. The coping mechanisms, autophagy and UPS, counteract this stress by recycling damaged proteins. With age, these coping mechanisms decrease in efficiency, resulting in a build-up of protein misfolding and subsequently aggregation, both of which interfere with cellular homeostasis.

their degradation, declines with age (Calderwood et al. 2009). This, in turn, increases the load of misfolded proteins in the cell. The effects of this are detrimental, particularly in non-dividing cells such as neurons, wherein ameliorating this burden of damaged proteins through cell division is not an option. Protein clearance mechanisms are also severely compromised in aging systems. Chaperone-mediated autophagy, for example, decreases with age in both rats and cultured human fibroblasts (Cuervo and Dice 2000). Moreover, proteasome function declines with age (Saez and Vilchez 2014). One can easily imagine a disease, such as ALS, where protein misfolding is rampant, that fully functioning protein clearance and repairing pathways are essential for survival. By teasing out the mechanism of protein misfolding in the context of ALS, we can hope to develop therapeutics that tip the system back to maintaining proteostasis.

Conclusion

Since the discovery of the link of *SOD1* mutations to ALS in 1993 (Rosen et al. 1993), multiple studies have provided insight into disease pathogenesis and mechanisms. Studies suggest that *SOD1* misfolding extends far beyond the inherited form of ALS and targeting this species has great therapeutic potential. In fact, *SOD1* misfolding is induced by more than simply FALS-linked *SOD1* mutations. Misfolded *SOD1* is seen in spinal cord of patients harboring FALS-linked FUS variants as well as in SALS cases with TDP43 pathology (Bosco et al. 2010, Forsberg et al. 2010, Pokrishevsky et al. 2012). Although the direct

involvement of SOD1 in ALS pathogenesis remains controversial, the work presented in this dissertation supports a causative role for WT SOD1 in disease. To test this hypothesis, we need to investigate further the ability of aberrantly modified SOD1 species found in SALS to induce an ALS-like phenotype *in vivo* (See **Appendix I**). If misfolded SOD1 is directly involved in pathogenesis of both SALS and FALS, therapeutic targets directed at FALS-linked SOD1 have the potential to extend to SALS-linked SOD1 as well.

We now know protein misfolding, chronic inflammation, mitochondrial dysfunction, oxidative stress, impaired axonal transport, excitotoxicity and altered RNA metabolism are pathological hallmarks of disease (Barber and Shaw 2010, Sreedharan and Brown 2013). Next, we need to identify which of these pathways proactively trigger pathogenesis and how they can be exploited for therapeutic development.

PREFACE TO APPENDIX I

Alexandra Weiss performed the surgery wherein osmotic pumps were inserted into the mice with a catheter directly inserted into the intrathecal space of the spinal cord for protein delivery. Karin Green of the UMass proteomics and Mass Spectrometry facility analyzed fluorescently tagged SOD1 by mass spectrometry. All other work presented was performed by Melissa S. Rotunno.

APPENDIX I: Investigating a Causative Role for WT SOD1 in Sporadic ALS

The primary cause of sporadic ALS, as of now, is unknown. Since multiple neurodegenerative disease-associated proteins have been implicated in both familial and sporadic forms of disease, we are testing the hypothesis that modified forms of WT SOD1 play a causative role in sporadic ALS. Conformation-specific antibodies have been developed that preferentially bind to ALS-linked mutant over WT SOD1 (**Table I-1, Fig. I-3**). We found that these same antibodies recognize an oxidized form of SOD1 (SOD1ox), which exerts a mutant-like toxicity in several biological assays. Therefore, SOD1ox and mutant SOD1 proteins share a similar “toxic” conformation that is not formed by native WT SOD1 (**Chapter II**). We are investigating whether misfolded WT SOD1 proteins that exhibit an aberrant conformation, such as SOD1ox, can induce an ALS-like phenotype in mice as observed for FALS-linked SOD1 variants. The difficulty in developing such a model lies in the simple fact that mice cannot be transgenically engineered to express proteins with aberrant post-translational modifications. To overcome this limitation, we are exploring an alternative approach to assess toxicity utilizing osmotic pumps to chronically deliver SOD1 with aberrant PTMs to the spinal fluid of mice.

SOD1 variants exhibit prolonged stability in osmotic pumps- Prior to inserting osmotic pumps directly into mice, we aimed to assess the efficiency of delivery and the stability of SOD1 proteins inside these pumps over time. Being that oxidized SOD1 is a misfolded protein, we wanted to confirm the protein was

capable of being delivered through the catheter at the concentration expected and not lost by adherence to plastic tubing or aggregation.

Four 28-day osmotic pumps were filled (>100 μ l) with filter-sterilized protein (WT SOD1 and SOD1ox) at 1 mg/mL. These pumps deliver protein at a rate of 0.11 μ L/h. Oxidized SOD1 exhibiting various degrees of oxidation induced by increasing hydrogen peroxide exposure time (1, 4 and 24 h) were included in this analysis (SODox1, 1 h; SODox4, 4 h; SODox24, 24 h). The pumps were placed in 50 mL conical tubes containing 15 mL of phosphate buffered saline and placed at 37°C. Protein was extracted periodically from the end of the catheter and tested for activity and stability. SOD1 activity assays were carried out immediately after taking the sample. To assess SOD1 activity, a competition assay with cytochrome C was employed (Okado-Matsumoto and Fridovich 2001). Xanthine oxidase reacts with xanthine to produce superoxide, the natural substrate of SOD1. When cytochrome C reacts with xanthine, an increase in absorbance at 550 nm is observed. When SOD1 reacts with the superoxide to form hydrogen peroxide and water, no change in absorbance is observed (**Figure AI-1**).

Western blot samples were prepared and placed at -80°C and run simultaneously after the completion of the time course. As determined by western analysis, an initial decrease in SOD1 was seen for all samples between

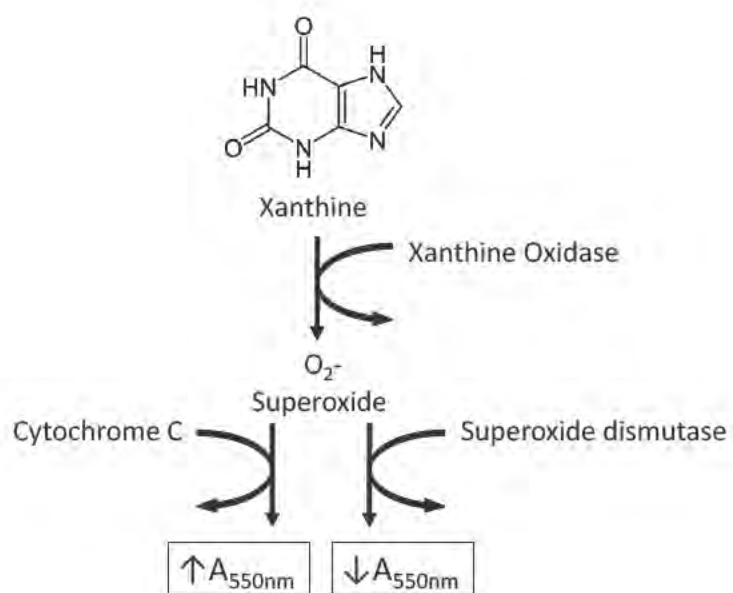


Figure AI-1. Schematic of SOD1 activity assay.

the initial setup (Day 0) and Day 3. Subsequently, the concentration of SOD1 remained stable over the 28-day period assessed (**Figure AI-2**).

As shown in **Figure AI-3**, the activity of SOD1 with the superoxide radical is maintained with minor fluctuations in the range of 80-100% of SOD1 at the start of the experiment. This data supports that the functionality of SOD1 is not impaired by a 28 d incubation at 37°C in osmotic pumps. It should be noted, however, that oxidized SOD1 dismutase activity is inherently impaired compared to WT SOD1 (**Fig. AI-4**).

Osmotic pumps effectively deliver SOD1 to the spinal cord of surgically implanted mice - Now that the stability of SOD1 has been established over a 28 d period in osmotic pumps, the next step was to assess the efficiency and efficacy of protein delivery to the intrathecal space of these mice. A pilot study was performed with 4 mice surgically implanted with osmotic pumps containing fluorescently tagged SOD1 (fluoro488-SOD1, n=3) or PBS (n=1) with the catheter directly inserted into the intrathecal space of the lumbar region. Fluorescently tagged SOD1 was used to differentiate between the human SOD1 delivered via osmotic pumps from that of endogenous mouse SOD1. To confirm SOD1 was conjugated to the fluorophore, the protein was subjected to mass spectrometry analysis (**Figure AI-5**). Unmodified WT SOD1 and SOD1ox24 have a molecular weight of 16,345 Da and 16,405 Da respectively. The modified WT SOD1 has molecular weights of 16,861 Da, 17,377 Da and 17,896 Da, which is

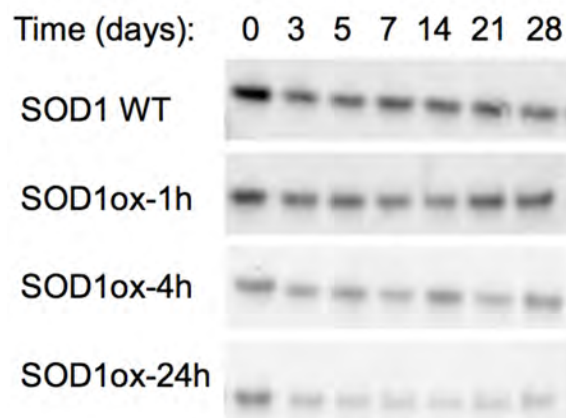


Figure AI-2. SOD1 proteins are stable for up to 28 days in osmotic pumps. Osmotic pumps were filled with the indicated protein (SOD1 WT, SOD1ox-1h, SOD1ox-4h, SOD1ox-24h) and placed at 37°C for 28 days. SOD1 samples were taken at the indicated time. The SOD1 was subjected to western analysis to assess solubility and stability of SOD1 over time. All SOD1 variants exhibited an initial decrease in concentration (compare 0 day to 3 day sample) that was maintained over the 28 day period.

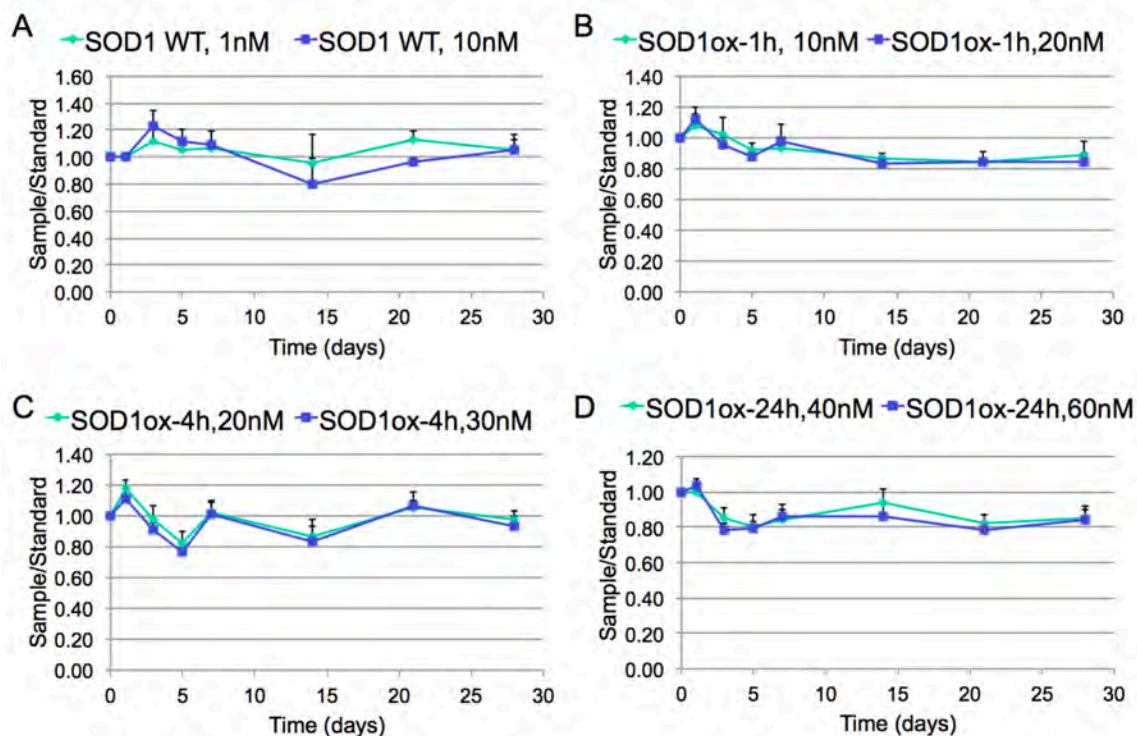


Figure A1-3. SOD1 proteins retain activity for 28 days in osmotic pumps.

Osmotic pumps were filled with protein (A, SOD1 WT; B, SOD1ox-1h; C, SOD1ox-4h; D, SOD1ox-24h) and placed at 37° for 28 days. Aliquots were taken at the indicated times, and tested in the SOD1 activity assay. All SOD1 variants (Sample) were normalized to activity at T=0 (Standard), with the relative activity illustrated. Results of assay show that both SOD1 WT and SOD1ox proteins retain activity, and thus appear stable, over the 28-day time course.

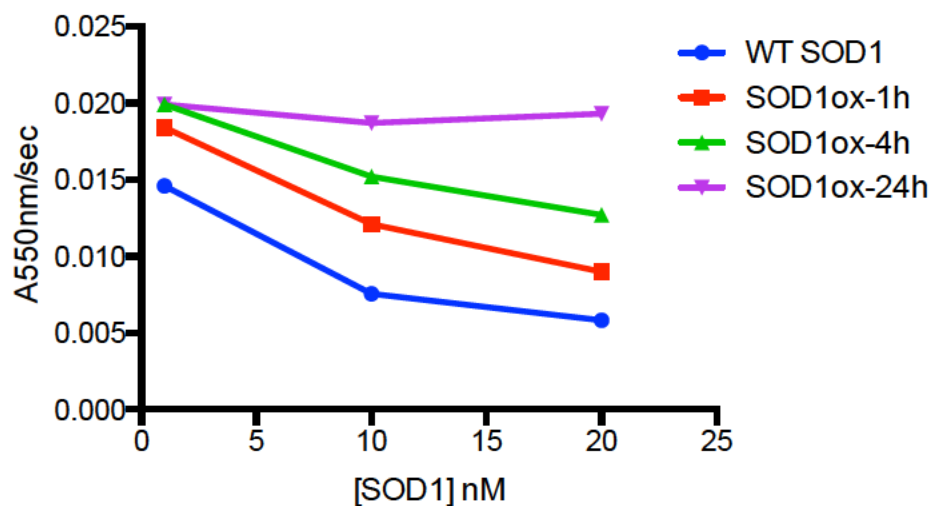


Figure AI-4. Oxidized SOD1 exhibits reduced activity compared to WT SOD1. The activity assay employed is a competitive assay where the greatest increase in A550 nm/sec translates to the least amount of activity, as SOD1's competitor, cytochrome C reacting with superoxide results in the absorbance increase. The activity of SOD1ox-24h does not increase as the concentration of SOD1 increases, suggesting SOD1ox-24h is unable to compete with cytochrome C to react with superoxide under these conditions. All other SOD1 variants (SOD1ox-4h, SOD1ox-1h, WT SOD1) tested show an increase in activity correlating with an increase in concentration. WT SOD1, which demonstrates the lowest amount of increase in A550 nm/sec displays the highest amount of dismutase activity. These data suggest a loss of SOD1 activity upon exposure to H₂O₂.

consistent with the addition of 1, 2, and 3 tags, respectively (**Figure AI-5A,B**). Each tag adds 516 Da to available primary amines. Modified SOD1ox has molecular weights of 16,923 Da, 17,441 Da, and 17,969 Da, which is also consistent with the addition of 1, 2, and 3 tags (**Figure AI-5C,D**). The mass spectrometry results indicate efficient modification of both WT SOD1 and SOD1ox with 1-3 modifications per monomer in >80% of the samples.

To allow for maximum signal, a 3-day pump was employed which delivers the solution at a rate of 1 $\mu\text{L/h}$. After the 3-day period, the mice were sacrificed and assessed for protein delivery in the lumbar, thoracic and cervical spinal cord regions by immunoblotting and immunofluorescence techniques. The lumbar and cervical regions were removed and homogenized, and 12.5 μg and 25 μg of lysates, respectively were loaded onto an SDS-PAGE for western analysis. The blot was probed with anti- fluoro488 for the detection of fluoro488-SOD1 and anti-actin as a loading control. As illustrated in **Figure AI-6A**, 2 out of the 3 mice contained fluoro488-SOD1 in the lumbar spinal cord. Only 1 out of the 3 mice contained fluoro488-SOD1 in the cervical spinal cord. The abundance of fluoro488-SOD1 in the thoracic region of the spinal cord was not assessed by Western analyses. Instead, the thoracic region was sectioned for immunofluorescence and fluoro488-SOD1 was detected utilizing the anti-fluoro488 antibody, which showed fluoro488-SOD1 in 1 out of 3 mice (**Fig. AI-6B**). This data suggests delivery of SOD1 to the spinal cord is possible, but the technique requires fine-tuning to increase the efficacy of delivery.

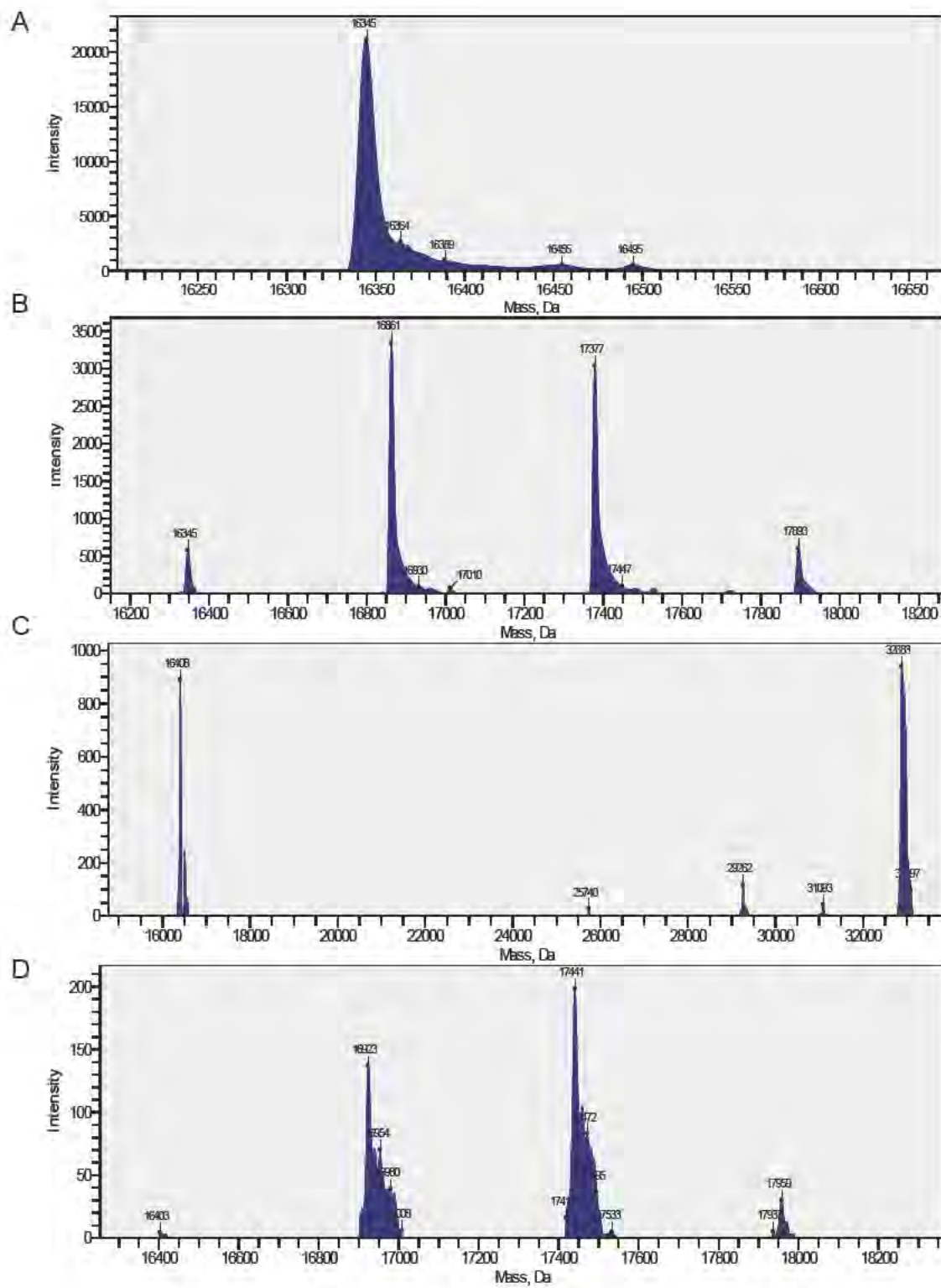


Figure AI-5. Mass spectrometry identifies Fluoro488-tagged species of SOD1. SOD1 proteins were subjected to LC-MS to identify the number of fluorescent tags covalently bound. (A) Analysis of unmodified WT SOD1 revealed one predominant species at 16,345 Da that is consistent with the actual mass (16,347 Da). This corresponds to the full length WT SOD1 with an additional “GPLGS” on the N-terminus that remains from the GST tag employed during purification. (B) WT SOD1 conjugated with Fluoro488 revealed 4 predominant species, unmodified (16,345 Da), WT SOD1 + 1 Fluoro488 (16,861 Da), WT SOD1 + 2 Fluoro488 (17,377 Da) and WT SOD1 + 3 Fluoro488 (17,893 Da). (C,D) Same analysis as described in (A) and (B) for unmodified (C) and modified (D) 24 h oxidized SOD1 subjected to mass spectrometry analysis.

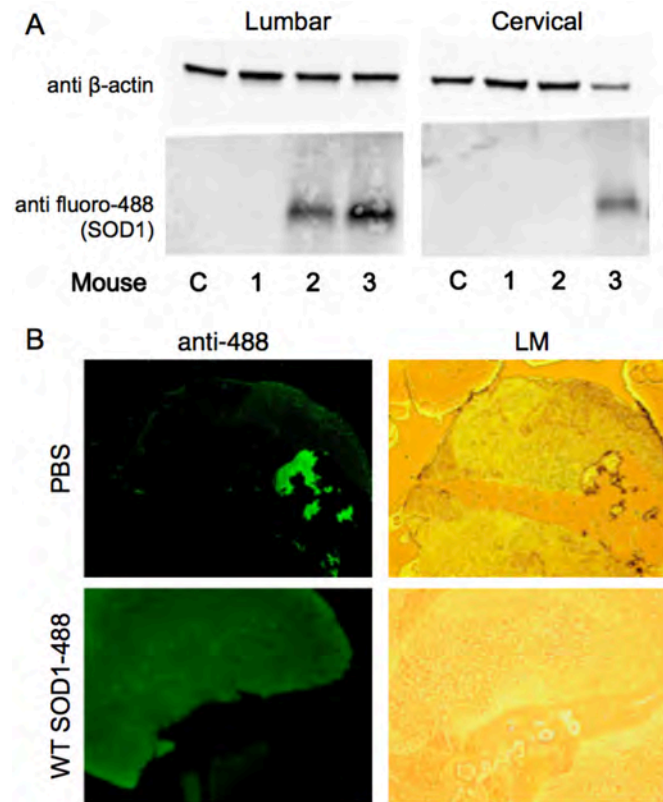


Figure A1-6. Osmotic pumps effectively deliver SOD1 protein to the spinal cord of implanted mice. An osmotic pump delivered SOD1 WT-Fluor488 to mice over a 3 day period. After 3 days, the mice were sacrificed and the spinal cord sectioned. (A) A Western analysis of homogenized lumbar (left) and cervical (right) spinal cord lysates confirmed the delivery of SOD1 WT-Fluor488 into the lumbar (mouse 2,3) and cervical (mouse 3) spinal cord. (B) SOD1 fluorescence is detected in thoracic spinal cord tissue sections from mice infused with SOD1 WT-Fluoro488 (LM=Light Microscopy).

Chronic delivery of misfolded SOD1 to mice results in no overt phenotype - To test the hypothesis that misfolded SOD1 delivered to the spinal cord of mice could result in an ALS-like phenotype, we filled 3 day osmotic pumps with SOD1 variants (PBS, n=3; WT SOD1, n=6; SOD1 G93A, n=3; SOD1 OX, n=8) at a concentration of 1.5 mg/ml. The weight of the mice was monitored over time and they were visually inspected for signs of paralysis. No other histological or diagnostic tests were performed. Approximately 9 months after surgical implantation of osmotic pumps, the mice revealed no visual signs of an ALS-like phenotype. Their weight continued to increase over the period assessed and no noticeable impairment was present (**Figure AI-7**).

Conclusion

Providing evidence that oxidized SOD1 can induce an ALS-like phenotype would be pivotal for ALS research, as it would demonstrate for the first time the ability of modified SOD1 to induce ALS pathology, bridging the gap between SALS and FALS. As of now, SOD1ox has been shown to be toxic when exogenously added to cultured cells (Ezzi et al. 2007, Rotunno et al. 2014). In addition, SOD1ox and WT SOD1 have been shown to be stable in osmotic pumps for >28 days and delivery to the spinal cord with these pumps is feasible. The chronic exposure of misfolded SOD1 to mice in this preliminary study did not elicit any ALS-like phenotype. This is likely because: 1) Post-translational modifications induced by hydrogen peroxide (such as SOD1ox) delivered to the

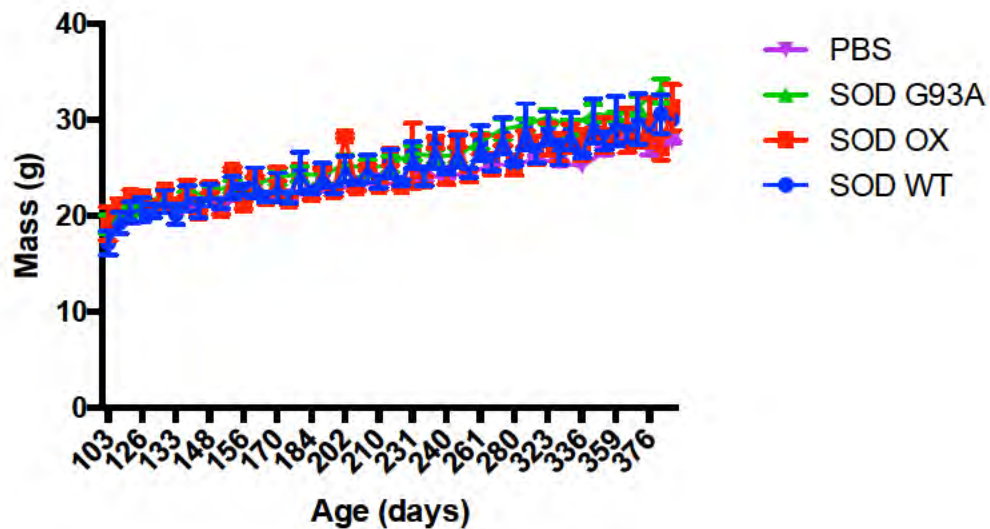


Figure AI-7. No decline in mass is observed for mice treated with SOD1 variants. Mice were surgically implanted with 3 day osmotic pumps filled with the indicated SOD1 variant or PBS. Body mass was monitored overtime for 9 months following the implantation. No decline in mass was observed for any of the cohorts.

spinal cord of mice is not sufficient to cause disease phenotype or 2) The SOD1 concentrations assessed were too mild and did not recapitulate that of transgenic mouse models vastly overexpressing mutant SOD1 (Rudick et al. 1982, Gurney et al. 1994). It is quite likely a higher concentration of SOD1 would be required to induce a disease phenotype, as these ALS transgenic mouse models have over 70 μg of mutant SOD1 present in their spinal cord. It is vital to determine the concentration of recombinant FALS-linked SOD1 variants, such as SOD1 G93A, required to induce an ALS-like phenotype using the osmotic pump system to develop a baseline to assess aberrantly modified SOD1. As described in **Chapter II**, SOD1 ^{$\Delta\text{IV}/\Delta\text{VII}$} represents the extreme, artificial case of misfolded SOD1, making it an interesting candidate to test for the ability to induce an ALS-like phenotype *in vivo* in this pump assay as well. Another avenue to explore would be to assess exacerbation of disease onset and progression of an established ALS mouse model when delivering SALS-linked SOD1 variants via osmotic pumps. As of now, the causative agent of sporadic ALS has not yet been established. Obtaining a mouse model would enhance research by providing a means to further study the disease mechanism as well as to develop novel therapeutic agents to fight SALS.

Materials and Methods

SOD1 Activity Assay- SOD1 activity assay was performed essentially as previously described (Okado-Matsumoto and Fridovich 2001). Activity Assay

Buffer was prepared to reach a final concentration of 50 mM potassium phosphate buffer, 230 μ M of Xanthine (Sigma, X7375-10G), and 100 μ M of cytochrome C (Sigma, C2506-100mg). The assay was carried out in a standard 96-well plate with 100 μ l of buffer per well, followed by the addition of the specified concentration of protein. Xanthine oxidase (Roche, #10110434001) was added to the wells at a concentration of 0.01 units/mL directly preceding the absorbance reading. Samples were shaken for 10 seconds prior to measuring the absorbance. Samples were read at 550 nm 12 times over a period of 5 minutes.

Preparation of protein for osmotic pumps – GST-tagged protein was purified essentially as previously described (Harper and Speicher 2011). The GST-tag was cleaved with preScission protease (GE Lifesciences, 27-0843-01). The SOD1 protein was concentrated to > 5 mg/mL and buffer exchanged to 0.1 M sodium bicarbonate at pH 8.3 for fluorescent tagging. Alexa Fluor 488 5-SDP ester was added to a final concentration of 0.5 mg/ml and the SOD1/tag mixture was incubated at room temperature for 2 h while rotating. Following the incubation, SOD1 was buffer exchanged into PBS.

Protein delivery with osmotic pumps – All SOD1 proteins were in phosphate buffered saline and filter sterilized through a 0.22 μ m (Millipore, SLGV004SL) filter prior to usage. The osmotic pumps (Alzet; 1003D, 3 d pumps; 1004, 28 d pumps) were filled with approximately 100 μ L of SOD1 with a 27G x 0.45”

syringe. A mouse intrathecal catheter (Alzet, #0007743) was attached to the top of the pump.

PREFACE TO APPENDIX II

The data presented in **Figure All-5** and **Table All-1** was performed by Ye Shang.

All other work presented was performed by Melissa S. Rotunno.

APPENDIX II: Reverting the ALS-linked Misfolded SOD1 to its Non-toxic Wild-Type Conformation

Amyotrophic lateral sclerosis (ALS) is a devastating neurodegenerative disease characterized by a loss of voluntary movement over time, typically resulting in death within 3-5 years of diagnosis. As of now, there is only weak treatment available, extending survival by a mere 3-6 months. Approximately 10% of ALS cases are inherited or familial (FALS), the majority of which are linked to mutations in *C9orf72* and *SOD1*. However, much less is known about the cause(s) of sporadic ALS (SALS) that account for 90% of ALS cases. FALS and SALS are clinically indistinguishable, suggesting similar mechanisms underlie both forms of this disease. SOD1 (Cu,Zn-superoxide dismutase), an anti-oxidizing enzyme, represents one factor common to FALS and SALS, distinguishing it as a plausible therapeutic target. Mutations in SOD1 cause ALS through a mechanism involving misfolding of the protein. Likewise, aberrant post-translational modifications can cause non-mutated, wild-type (WT) SOD1 to adopt a similar misfolded conformation. A portion of post-mortem SALS spinal cord tissues possess misfolded WT SOD1 that, when purified exhibits mutant-like neurotoxic properties such as axonal transport inhibition. Together, these observations support the hypothesis that WT SOD1 plays a pathogenic role in SALS, analogous to the role of mutant-SOD1.

A conformation specific antibody, C4F6, preferentially reacts with ALS-linked SOD1 variants in their native state (see **Chapter II**). C4F6 also recognizes aberrantly modified forms of WT-SOD1 that are present in post-mortem spinal

cord tissue from a subset of SALS patients not harboring a genetic mutation in *SOD1* (Bosco et al. 2010). C4F6 suppresses the axonal transport inhibition caused by SOD1 purified from SALS spinal cord tissue, while other anti-SOD1 antibodies do not. Together, these data suggest the epitope for C4F6 represents an exposed pathogenic motif within misfolded SOD1.

Instead of treating the downstream effects in patients with misfolded SOD1, we hypothesize that directly reverting ALS-linked SOD1 to its wild-type conformation will attenuate disease progression. Our studies aim to identify small molecules to repair misfolded SOD1, as indicated by a loss of C4F6 reactivity. Using high-throughput ELISAs, we identified several promising compounds with therapeutic potential, the most intriguing of which has been shown to bind and decrease SOD1 aggregation in a prior study (Banci et al. 2012a). Currently, we are investigating the ability of these compounds to repair SOD1 misfolding and curb the toxic properties of ALS-linked SOD1 in hopes of establishing an effective therapy for patients suffering from ALS.

Six small molecules have the potential to revert misfolded SOD1 to its WT-like fold. A sandwich ELISA (initial C4F6-ELISA) directed at misfolded SOD1 was used to identify compounds that could repair the protein. The C4F6 reactivity of SOD1 preincubated with compounds was quantified using the initial C4F6-ELISA (**Fig. All-1**). The compound library (LOPAC®1280, Sigma) consists of 1280 compounds that include pharmacologically active compounds and diverse chemical structures. Hits were identified as compounds that resulted in a

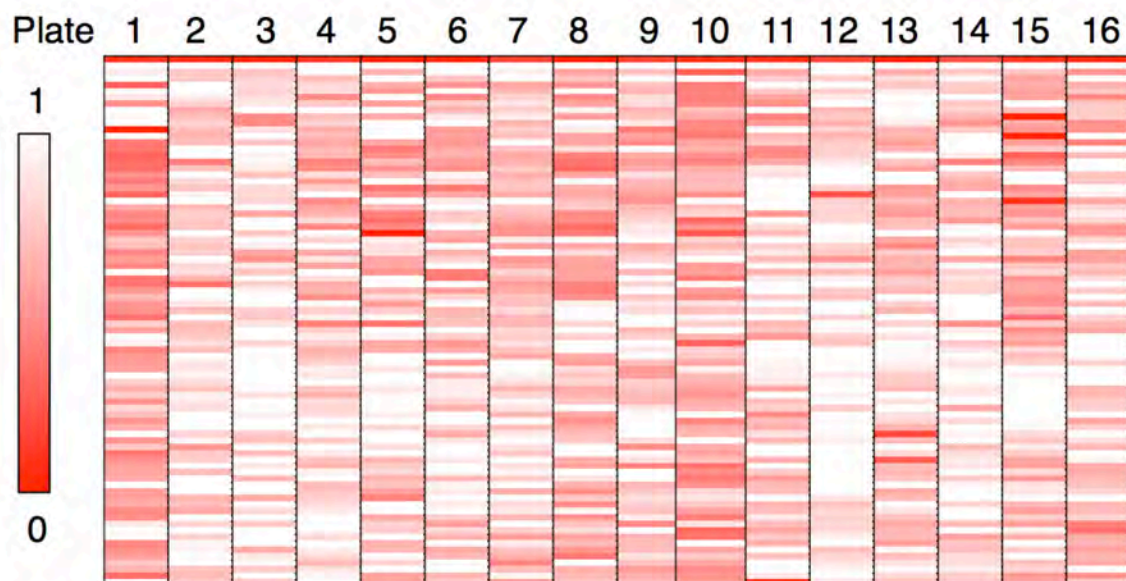


Figure All-1. Initial small molecule screen, LOPAC®1280, identifies six compounds capable of reducing C4F6-ELISA signal. The binding of SOD1 G93A, a misfolded form of SOD1, to C4F6 in the presence of 1280 different compounds was assessed by employing the initial C4F6-ELISA. C4F6 reactivity was normalized to SOD1 G93A alone, the negative control. The key to the left illustrates the color gradient used in the analyses, where 1 (white) indicates no change and 0 (red) indicates a complete loss of C4F6 binding. On the right, all 16 ELISA plates are illustrated with the color gradient indicating the change in C4F6 reactivity compared to SOD1 G93A alone. Each column represents a separate 96-well plate subjected to the initial C4F6-ELISA. Compounds with greater than 75% loss in C4F6 binding were considered lead compounds. Six compounds from this screen fit this criteria and were selected for additional analyses.

>75% reduction in C4F6 binding, when compared to SOD1 G93A reactivity alone. Six compounds were selected for further validation based on this criteria (**Figure All-1**).

Dose-response curve identifies one compound that reproducibly results in loss of C4F6 reactivity. The six initial compounds were tested in a dose-response curve to determine if the initial results in the screen were reproducible. One out of the six compounds, MRS2211 (Drug A, **Figure All-2**) showed reduction in C4F6-ELISA signal that correlated with increasing drug concentration. Being that MRS2211 contains a phosphate group on the molecule, one possibility is that the phosphate group is interfering with the alkaline phosphatase enzyme, as phosphate inhibits its activity. To eliminate this possibility, an identical ELISA was performed with this compound using horse radish peroxidase (HRP) conjugated anti-mouse as the secondary antibody instead of alkaline phosphatase. The HRP-based ELISA produced similar results where increasing concentrations of MRS2211 resulted in a decrease in C4F6 reactivity suggesting that the signal reduction is not due to interference in the alkaline phosphatase enzyme itself (**Figure All-3**). Next, we wanted to test whether or not MRS2211 produced a loss of C4F6 reactivity for other SOD1 variants as well. Dose-response curves with SOD1 G93A and G85R show that increasing concentrations of MRS2211 result in loss of ELISA signal (**Fig. All-4**). Despite the promising data produced by these ELISAs, we were unable to detect any binding between SOD1 G93A and MRS2211 with isothermal titration

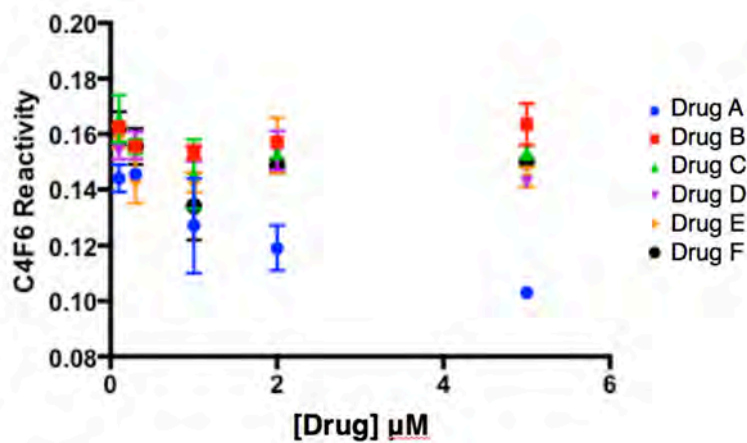


Figure All-2. Independent verification of lead compounds with a Dose-Response analysis. The ability of lead compounds to disrupt C4F6 binding to SOD1 G93A in the presence of the six initial lead compounds identified in the LOPAC®1280 screen was assessed by C4F6-ELISA with AP-conjugated antibody as the detection method (initial C4F6-ELISA). SOD1 G93A was pre-incubated with the indicated compounds prior to analyses. One (Drug A, MRS2211) out of the 6 initial hits demonstrated a reduction in SOD1 G93A binding to C4F6.

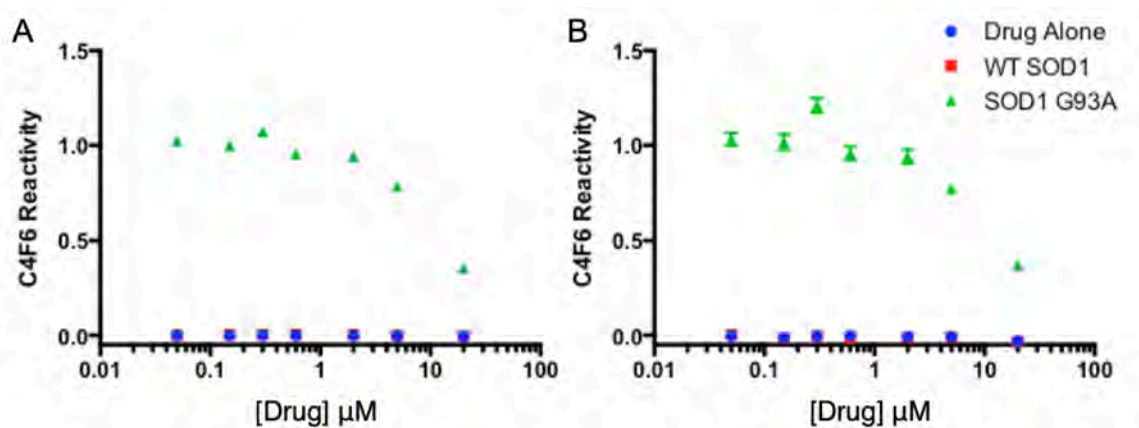


Figure AII-3. Verification of the lead compound, MRS2211, using an alternative sandwich ELISA approach. C4F6 reactivity assessed in the presence of either WT or SOD1 G93A with increasing concentrations of MRS2211. The optimized C4F6-ELISA was employed for verification. SOD1 G93A pre-incubated with MRS2211 induces a loss of C4F6 binding as demonstrated by both the alkaline phosphatase (A) and horseradish peroxidase (B) ELISA formats with an EC₅₀ of approximately 10 μM . This loss of C4F6 reactivity suggests MRS2211 has the potential to revert SOD1 G93A to a “WT-like” conformation.

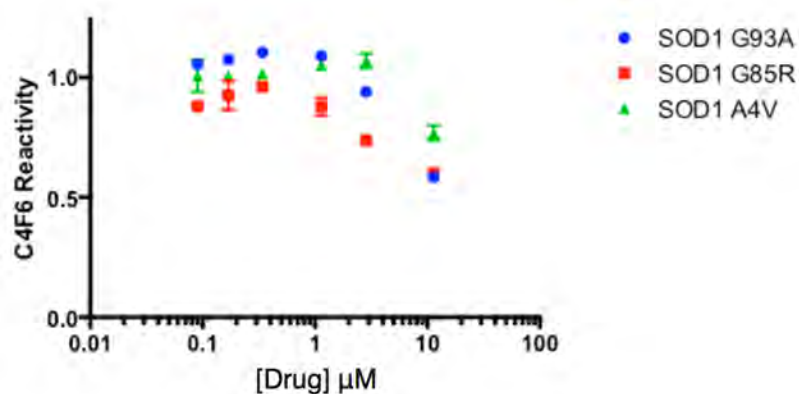


Figure All-4. MRS2211 attenuates C4F6 reactivity in all ALS-linked SOD1 variants tested. The optimized HRP C4F6-ELISA was employed to assess C4F6 reactivity of FALS-linked SOD1 variants in the presence of MRS2211. In addition to SOD1 G93A, both ALS-linked mutations SOD1 G85R and A4V demonstrate a reduction in C4F6 binding when pre-incubated with MRS2211 ([SOD]=0.3 μM).

calorimetry experiments (ITC) and, therefore, conclude that the drug was interfering with the coating antibody and not binding SOD1 directly.

Employing an optimized C4F6-ELISA to identify novel compounds with the potential to repair misfolded SOD1. The C4F6-ELISA employed in **Figure All-1** and **All-2** exhibited a high signal to noise ratio. This resulted in huge limitation of the initial compound screen to detect promising compounds (**Fig. All-1**). The sandwich C4F6-ELISA antibodies were further optimized to enhance the signal to noise ratio (compare the C4F6 reactivity values from **Figure All-2** (initial C4F6-ELISA, 0.16) and **Figure All-3** (optimized C4F6-ELISA, 1.0). Also, horseradish peroxidase was used as an enzymatic read-out in place of the alkaline phosphatase as it demonstrated less well-to-well variability. All told, these optimizations increased the signal to noise ration from 2:1 (initial C4F6-ELISA) to greater than 10:1 (optimized C4F6-ELISA, **Fig. III-1**). We repeated the same LOPAC screen as discussed above employing the optimized C4F6-ELISA to identify potential compounds to repair misfolded SOD1 G93A ([SOD1]=0.04 μ M, [Drug]=10 μ M). As illustrated in **Figure All-5**, a significant reduction in overall background was observed. The improved screen identified 9 potential candidates that resulted in a greater than 50% reduction in C4F6 reactivity (**Fig. All-5**). None of these 9 hits were identified in the initial compound screen (**Fig. All-1**). A dose-response curve with SOD1 G93A generated from these hits demonstrated a reproducible reduction in C4F6 reactivity in 7 out of the 9 compounds tested (**Fig. All-5B**). To eliminate the compounds that directly interfered with the ELISA

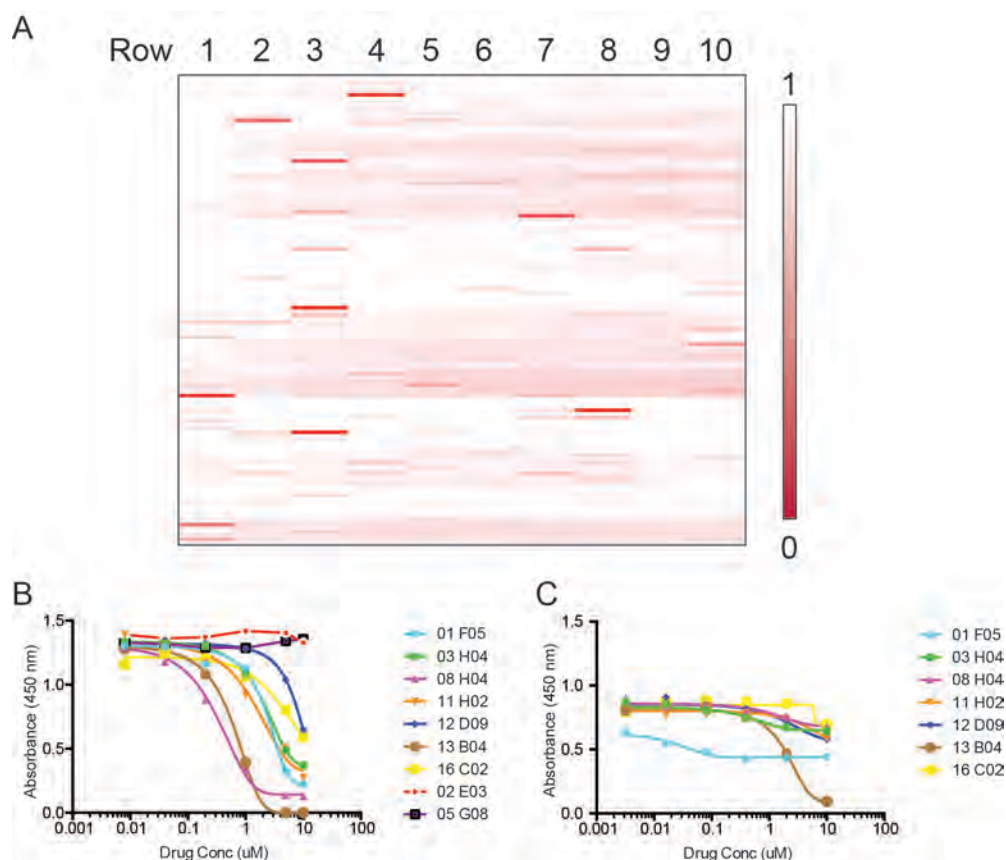


Figure AII-5. Optimized C4F6-ELISA identifies 6 potential compounds to repair misfolded SOD1. (A) A summary of the LOPAC screen for molecules that result in a loss of C4F6 binding (0, complete loss of C4F6 binding; 1, no change). All samples were normalized to SOD1 G93A alone, the negative control. “Hits” were compounds that resulted in a >50% decrease in signal compared to SOD1 G93A alone. (B) The initial 9 hits were tested in a dose-response curve with SOD1 G93A. Seven out of the 9 initial hits were able to decrease absorbance at 450 nm, suggesting a loss of C4F6 binding. (C) The confirmed 7 hits were tested in an ELISA with SOD1 G93A for total SOD1. Six out of 7 compounds had no effect on total SOD1 concentration. One compound resulted in a loss of total SOD1, suggesting that it is interfering with the ELISA itself and not repairing the SOD1 misfolding.

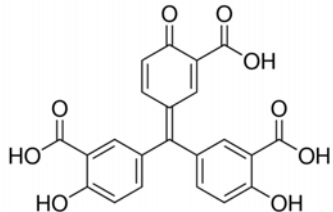
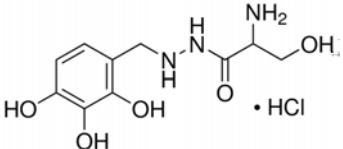
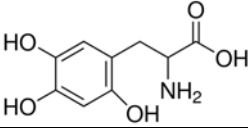
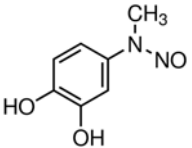
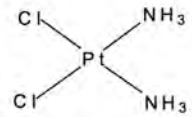
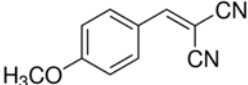
assay, we assessed these 7 compounds in an SOD1 ELISA with WT SOD1 that detects total SOD1 using an independent set of antibodies. One out of the 7 compounds, 13 B04, interfered with the detection of WT SOD1 in a dose-dependent manner (**Fig. AII-5C**). In summary, 6 compounds have been identified that have the potential to repair misfolded SOD1 but further testing, such as ITC, is required to assess the extent of SOD1 binding.

Discussion

In this preliminary study, six compounds have been identified with the potential to repair misfolded SOD1 (**Table AII-1**). With the exception of Cisplatin, all compounds contain a benzene ring with at least one hydroxyl group attached, suggesting this structural moiety is conducive to binding SOD1. The structural outlier, Cisplatin, is a known binder of SOD1 that interferes with the formation of high molecular weight SOD1 aggregates (Banci et al. 2012a). Cisplatin is also a common chemotherapy agent. In fact, the resistance of ovarian cancer cells to cisplatin-induced apoptosis is linked to an upregulation of the SOD1 protein (Brown D. P. et al. 2009, Kim et al. 2010).

It is important to further validate these compounds since a reduction in C4F6 reactivity does not definitively indicate a reparation of SOD1 misfolding. The possible reasons for a loss of C4F6 signal include i) binding and stabilizing the SOD1 protein thereby decreasing exposure of the C4F6 epitope, ii) binding to

Table All-1. Promising compounds identified in C4F6-ELISA LOPAC Screen

Compound	Rack #	C4F6-ELISA Signal Decrease (%)	
		Initial Screen	Validation
Aurintricarboxylic acid	01 F05	81.2	84.1
			
Benserazide hydrochloride	03 H04	72.3	64.4
			
6-hydroxy-DL-DOPA	08 H04	88.4	90.4
			
Methyl-3,4-dephostatin	11 H02	82.7	79.7
			
Cisplatin	12 D09	92.7	50.7
			
Tyrphostin 47	16 C02	51.2	52.9
			

SOD1 and inducing protein precipitation, iii) competing with C4F6 in the same binding pocket, with no effect on SOD1 conformation, iv) competing with the detection antibody for the same binding region on SOD1, or v) interfering with the coating of C4F6 directly onto the ELISA plate. Future studies are required to determine whether or not these compounds have the ability to repair misfolded SOD1 directly. Initially, ITC can be performed to determine the kinetics of this binding interaction. To test the extent these compounds repair and stabilize the fold of SOD1, we could assess the effects of the compounds on aggregation propensity, melting temperature, and urea denaturation of SOD1. We can also determine whether these compounds reduced the SOD1-induced activation of microglia, as described in **Chapter II**. We can determine if treatment with these compounds in *in vivo* ALS transgenic mouse models alters onset and progression of disease. Alternatively, approaches identifying proteins and/or genes with the ability to revert misfolded SOD1 to its wild-type conformation should be explored. One can imagine that employing siRNA screens for a loss of C4F6 binding in cell culture systems could be a powerful tool for identifying mechanisms that induce SOD1 misfolding in ALS.

Materials and Methods

C4F6-ELISA for initial small molecule screen - The plate was coated with a polyclonal anti-SOD1 (Binding Site, PC077). Then SOD1 G93A (0.3 μ M) pre-incubated with small molecules (5 μ M) were added to the plate and incubated for

1 h. Then C4F6 antibody at 0.6 $\mu\text{g}/\text{mL}$ was added to detect misfolded SOD1. Alkaline phosphatase (AP) conjugated or HRP-conjugated anti-mouse antibody was used to quantify the reaction. Absorbance at 450 nm was recorded.

C4F6-ELISA for optimized small molecule screen – See **Chapter III**, Materials and Methods for C4F6-ELISA protocol details. The screen was performed with SOD1 at a concentration of 0.04 μM and compound at 10 μM .

PREFACE TO APPENDIX III

My contribution to the published work was the purification of human SOD1 protein from human tissue using immunoprecipitation techniques described herein.

The following is reproduced with permission from:

Auclair, J.R., Johnson, J.L., Liu, Q., Salisbury, J.P., **Rotunno, M.S.**, Petsko, G.A., Ringe, D., Brown Jr., R.H., Bosco, D.A., Agar, J.N. "Post-translational Modification by Cysteine Protects Cu/Zn-Superoxide Dismutase from Oxidative Damage." *Biochemistry*. **2013**, 52, 6137-44.

Copyright 2013 American Chemical Society.

APPENDIX III: Post-translational modification by cysteine protects Cu/Zn-superoxide dismutase from oxidative damage.

Post-Translational Modification by Cysteine Protects Cu/Zn-Superoxide Dismutase from Oxidative Damage

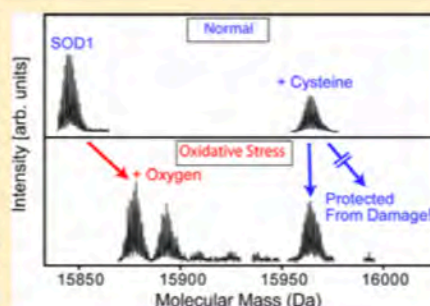
Jared R. Auclair,^{†,‡} Joshua L. Johnson,^{†,¶} Qian Liu,[†] Joseph P. Salisbury,^{†,‡} Melissa S. Rotunno,[‡] Gregory A. Petsko,[†] Dagmar Ringe,[†] Robert H. Brown, Jr.,[‡] Daryl A. Bosco,^{‡,§} and Jeffrey N. Agar^{*,†,‡}

[†]Departments of Biochemistry and Chemistry and Rosenstiel Basic Medical Sciences Research Center, Brandeis University, Waltham, Massachusetts 02454, United States

[‡]Department of Neurology and [§]Department of Biochemistry and Molecular Pharmacology, University of Massachusetts Medical School, Worcester, Massachusetts 01655, United States

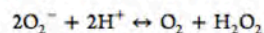
Supporting Information

ABSTRACT: Reactive oxygen species (ROS) are cytotoxic. To remove ROS, cells have developed ROS-specific defense mechanisms, including the enzyme Cu/Zn superoxide dismutase (SOD1), which catalyzes the disproportionation of superoxide anions into molecular oxygen and hydrogen peroxide. Although hydrogen peroxide is less reactive than superoxide, it is still capable of oxidizing, unfolding, and inactivating SOD1, at least in vitro. To explore the relevance of post-translational modification (PTM) of SOD1, including peroxide-related modifications, SOD1 was purified from postmortem human nervous tissue. As much as half of all purified SOD1 protein contained non-native post-translational modifications (PTMs), the most prevalent modifications being cysteinylations and peroxide-related oxidations. Many PTMs targeted a single reactive SOD1 cysteine, Cys₁₁₁. An intriguing observation was that unlike native SOD1, cysteinylated SOD1 was not oxidized. To further characterize how cysteinylations may protect SOD1 from oxidation, cysteine-modified SOD1 was prepared in vitro and exposed to peroxide. Cysteinylations conferred nearly complete protection from peroxide-induced oxidation of SOD1. Moreover, SOD1 that has been cysteinylated and peroxide oxidized in vitro comprised a set of PTMs that bear a striking resemblance to the myriad of PTMs observed in SOD1 purified from human tissue.



INTRODUCTION

Reactive oxygen species (ROS) are byproducts of aerobic metabolism and are also the primary products of certain oxidoreductases. For example, the incomplete reduction of oxygen to water during mitochondrial respiration can create both hydrogen peroxide (H₂O₂) and superoxide anion (O₂^{•-}). These byproducts are harmful to cells because they can alter protein conformation, disrupt enzyme function, and mutate DNA, among other things.^{1–3} A testament to the toxicity of ROS is the monocyte-resident oxidoreductase, NADPH oxidase (NOX), which generates the superoxide enzymatically to kill targeted cells, including microorganisms. Cells combat harmful ROS species with a multifaceted antioxidant defense mechanism that includes the metalloenzyme Cu/Zn superoxide dismutase (SOD1). SOD1 catalyzes the disproportionation of the superoxide anion as follows:⁴



Loss of SOD1 function leads to an increase in superoxide anions, causing negative effects, including cell death under conditions of oxygen stress. One potential mechanism for inactivation of SOD1 is via oxidation by its own reaction product, hydrogen peroxide. Indeed, modification by two (sulfenic acid) or three (sulfonic acid) oxygen atoms on SOD1

Cys₁₁₁ are well-established peroxide-mediated modifications in vitro⁵ and in vivo.⁶ Residue 111 is situated at the SOD1 dimer interface⁵ and is highly conserved, commonly serine. In humans, great apes, and a few other species, residue 111 is a cysteine. Cys₁₁₁ is highly reactive and has been shown to be modified by oxygen, copper,⁷ glutathione,^{8–10} and potentially cysteine.^{7,11,12}

Modification by an oxygen atom can be detrimental to SOD1 structure and function^{1–3} and has been implicated in diseases such as amyotrophic lateral sclerosis.¹³ In fact, sulfonic acid-modified SOD1 (three oxygen atoms) is the same form of SOD1 that Bosco et al. showed inhibits fast axonal transport in a similar fashion to SOD1 familial amyotrophic lateral sclerosis (FALS) variants.¹³ Here, we characterize post-translational modifications (PTMs) of SOD1 in situ, including peroxide- and cysteine-related modifications, and provide in vitro evidence that cysteinylations protects SOD1 from oxidative damage.

Received: May 15, 2013

Revised: July 30, 2013

Published: August 8, 2013

METHODS

SOD1 Purification from Human Tissue. Two purification protocols using distinct elution buffers and antibodies were used to investigate PTMs and their relative amounts in human tissue. The first purification protocol was previously described and used polyclonal rabbit antibodies raised in house against a mixture of native and modified (by both oxygen and sulfur adducts on Cys₁₁₁) SOD1 purified from human erythrocytes; elution was with 5% acetic acid.¹⁴ This protocol provides protein that can be directly infused into a mass spectrometer, avoiding lengthy liquid chromatography. In the second purification, SOD1 was isolated from human nervous tissue as previously described¹³ using a sheep polyclonal antibody raised against SOD1 from human erythrocytes and gentle elution buffer (reportedly 3 M MgCl₂ at roughly neutral pH). Frozen human nervous tissue was homogenized in lysis buffer (25 mM Tris, pH 7.8, supplemented with a protease inhibitor cocktail (Roche)) at 4 °C followed by centrifugation at 14 000 rpm, and this supernatant was applied to an individual immunoaffinity column. Columns were washed four times with 600 μ L (~20 column volumes total) of wash buffer (25 mM Tris, 100 mM NaCl, pH 7.8). SOD1 proteins were eluted with 2 \times 500 μ L of either 5% acetic acid (purification 1) or gentle antibody elution buffer (GEB), pH 6.6 (Pierce, 21027) (purification 2). To ensure that the purified samples contained a representative sampling of native and modified SOD1, we verified that SOD1 was immunodepleted from the homogenates. Following the first immunopurification, the column was re-equilibrated in lysis buffer, the depleted homogenates (flow-through) were reapplied, and the purifications were repeated in this way a total of three times. If protein was detected in a repeat purification (using MALDI-TOF MS; only the second purification occasionally contained minor amounts of SOD1), that purification was pooled with the first. Proteins eluted with GEB were buffer exchanged into 25 mM HEPES, pH 7.4, and concentrated to ~100 μ L, and the concentrations were determined by Western blot and densitometry (ImageJ) analyses with recombinant wild-type SOD1 standards. Proteins eluted with 5% acetic acid were used as purified. In addition, SOD1 was purified anaerobically in the presence or absence of iodoacetamide (10 mM), iodoacetic acid (4 mM), and S-methyl methanethiosulfonate (MMTS) (0.5 mM) to block any unreacted cysteine residues and to scavenge any free cysteine using an MBraun Unilab glovebox with oxygen levels below 10 ppm, monitored by diethyl zinc.

Recombinant SOD1 Expression and Purification. In *in vitro* studies, we used SOD1 overexpressed and purified from *S. cerevisiae*. The construct for expression of human SOD1 in *S. cerevisiae* was obtained through the generous gift of Dr. P. John Hart, Ph.D. (University of Texas Health Science Center, San Antonio, TX). Expression and purification was carried out as previously described.^{15,16} Briefly, each construct in the yeast expression vector YEp-351 was transformed into EGY118 Δ -SOD1 yeast and grown at 30 °C for 36–48 h. Cultures were pelleted, lysed using 0.5 mm glass beads and a blender, and subjected to a 60% ammonium sulfate cut. After ammonium sulfate precipitation, the sample was pelleted and the supernatant was diluted with 0.19 volumes of a low salt buffer (50 mM sodium phosphate, 150 mM sodium chloride, 0.1 M EDTA, 0.25 mM DTT, pH 7.0) to a final concentration of 2.0 M ammonium sulfate. This sample was then purified using a Phenyl Sepharose 6 Fast Flow (High Sub) hydrophobic

interaction chromatography column (GE Life Sciences) using a 300 mL linearly decreasing salt gradient from a high salt buffer (2.0 M ammonium sulfate, 50 mM sodium phosphate, 150 mM sodium chloride, 0.1 M EDTA, 0.25 mM DTT, pH 7.0) to the low salt buffer. Samples containing SOD1 were eluted between 1.6 and 1.1 M ammonium sulfate, pooled, and buffer exchanged to a 10 mM Tris, pH 8.0, buffer using Amicon Ultra-15 centrifugal filter units (Millipore). The protein was then loaded onto a Mono Q 10/100 anion exchange chromatography column (GE Life Sciences) and eluted using a 200 mL linearly increasing salt gradient from a low salt buffer (10 mM Tris, pH 8.0) to a high salt buffer (10 mM Tris, pH 8.0, 1 M sodium chloride). The gradient was run from 0 to 30% 10 mM Tris, pH 8.0, 1 M sodium chloride, and SOD1 eluted between 5 and 12% 10 mM Tris, pH 8.0, 1 M sodium chloride. SOD1 protein was quantified using the Bradford assay with yields of 6 mg/8L (0.75 mg/L) and confirmed by MALDI-TOF and FTMS analysis.

Direct Infusion ESI-FTMS and ESI-Ion Trap MS. Samples in 5% acetic acid were analyzed by direct infusion (Figures 1 and 2A), and the results were compared to LC-MS results (Figure 2B). For ESI-FTMS infusion experiments SOD1 was diluted to approximately 1 μ M concentration in 50% acetonitrile (ACN)/49.9% HPLC grade water/0.1% formic acid and infused (sprayed directly) into the FTMS using similar instrument acquisition parameters as described below. For ESI-ion trap infusion experiments, SOD1 was also diluted to approximately 1 μ M concentration in 40% ACN and infused (sprayed directly) into the Bruker Daltonics HCT Ultra ion trap with capillary voltage = -4000 V, skimmer 1 = 40 V, ICC on with a maximum accumulation time of 200 000 μ s.

RP-HPLC and FTMS. Purified SOD1 protein in GEB was analyzed using reversed-phase liquid chromatography and Fourier transform mass spectrometry as previously described.¹³ Briefly, reversed-phase liquid chromatography was performed using a 2-dimensional nanoflow rate liquid chromatography (Eksigent), a 5 mm, 300 μ m i.d. guard column (LC Packings, Part Number 160454), and a self-packed 14 cm, 100 μ m ID column with 5 μ m C₁₈ beads (unpacked from a larger Targa column). Buffer A consisted of 0.1% formic acid (v/v) in HPLC grade water and buffer B consisted of 0.1% formic acid (v/v) in 100% HPLC grade acetonitrile (v/v). Samples were diluted to a final formic acid concentration of 0.1% (v/v) and injected. Following injection, samples were washed on the guard column with 160 column volumes of buffer A (8 μ L min⁻¹), and eluted at 650 nL min⁻¹ using a 0–40% gradient over 30 min. Samples were introduced via a nanospray ion source with a dual ion funnel (Apollo II) connected to a 9.4 T hybrid quadrupole Fourier transform ion cyclotron resonance (FT-ICR, FTMS) mass spectrometer (Apex Q-94, Bruker Daltonics). External calibration of the *m/z* scale was performed using electrospray tuning mix (Agilent, G2431A) using peaks at *m/z* 622, 922, 1522, and 2122.

After desolvation, the ions were transferred from a source hexapole to the quadrupole mass filter where isolation could occur in a second hexapole (collision cell). Ions accumulated in the second hexapole were then transferred through the ion optics region of the instrument to the ICR cell. Frequency sweep excitation was followed by image charge detection. Important instrument operation parameters include source declustering potential = 40 V, hexapole 1 accumulation time = 0.1 ms, collision cell accumulation time = 1 s, time-of-flight = 1.8 ms (D2), sidekick extraction voltages = -1.0 V (EV1, EV2,

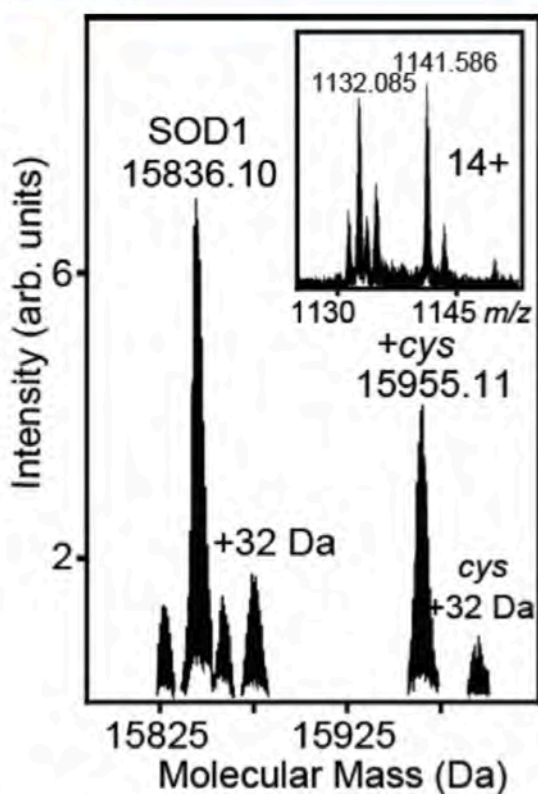


Figure 1. Cysteinylation, a prevalent post-translational modification of SOD1 in human nervous tissue. SOD1 was isolated from a nondiseased human spinal cord using an SOD1 antibody column, 50% acetonitrile was added to improve MS signal, and then the mixture was infused directly into the FTMS.¹⁴ Deisotoped and deconvoluted data for the entire mass range was analyzed, showing the monoisotopic mass for unmodified (15 836.10 Da) and modified (15 955.11 Da) SOD1, the delta mass being 119.01 Da, which is consistent with cysteinylation. Note that the solvents and declustering potentials used were such that native metals were not observed. Inset: 14+ charge state showing unmodified (m/z 1132.085) and modified (m/z 1141.586) apo SOD1. This data is representative of the eight human nervous tissue samples analyzed.

DEV2), RF excitation voltage = 130 V, and ICR trapping potential = 1.2 V. Intact protein masses were reconstructed using the deconvolution function from DataAnalysis (Bruker Daltonics, version 3.4), and monoisotopic masses were determined using the Snap II algorithm (Bruker Daltonics).

In Vitro Cysteinylation and Oxidation. Human SOD1 overexpressed and purified from *S. cerevisiae*, at either 0.1 or 1 μM concentration, was incubated with 40 μM L-cysteine overnight at room temperature and analyzed using direct infusion into the Fourier transform mass spectrometer. Oxidation was performed at room temperature for 4 h using 100 or 10 mM hydrogen peroxide. Time points were collected every hour and analyzed using direct infusion into the FTMS using similar parameters as described above. All samples were desalted using C_{18} -containing micropipet tips according to the manufacturer's protocol (Millipore) and diluted 1:3 in HPLC water prior to injection into the mass spectrometer.

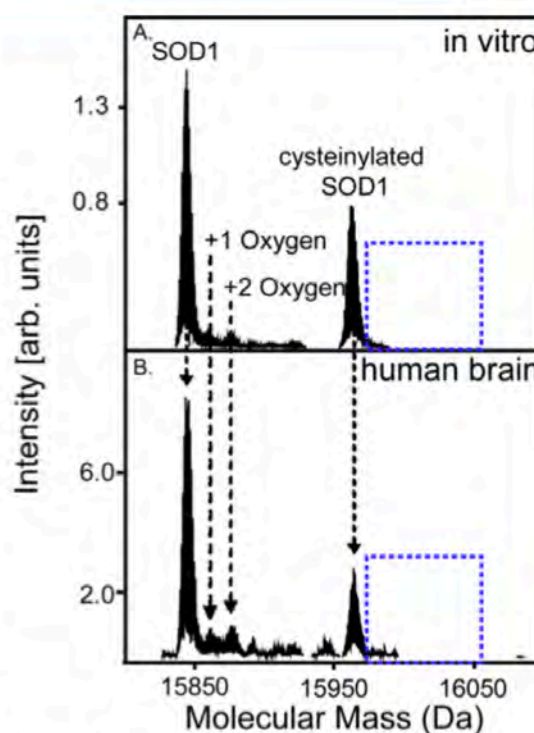


Figure 2. Cysteinylation and peroxide-mediated oxidations accounting for the majority of observed SOD1, purified from human tissue, post-translational modifications. (A) Spectra of SOD1 modified by cysteine (40 μM) and hydrogen peroxide (100 μM) 3.5 h after oxidation. SOD1 is modified by multiple oxygen atoms at this time point, whereas cysteine-modified SOD1 is not (dotted blue box). (B) Spectra of SOD1 purified from a human brain. SOD1 is oxidized with multiple oxygen atoms, whereas cysteine-modified SOD1 is not (dotted box). This is representative of the four additional samples analyzed using LC-MS.

Identification of Site of Cysteinylation Using Funnel Skimmer Dissociation (FSD). Cysteinylated SOD1 (1 μM) in a mixture of 5% acetonitrile and 0.1% formic acid was directly infused into a 9.4 T Bruker Daltonics Fourier transform mass spectrometry in nanospray mode. Skimmer 1 voltage was then increased from 40 to 120 V in 10 V increments in order to fragment the protein using diverse fragmentation channels (at low voltage, primarily mobile proton-directed, for example at proline residues; at higher voltages, primarily charge remote, for example at acidic residues¹⁷). Data were analyzed using Bruker Daltonics' DataAnalysis software.

RESULTS

SOD1 Purified from Human Brain and Spinal Cord Is Modified by Cysteine and Oxygen. SOD1 was immunopurified using rabbit polyclonal anti-SOD1 (each respective sample individually), from 10 nondiseased human and mouse nervous tissue samples (8 human and 2 mouse overexpressing human SOD1, brain and spinal cord), eluted using 5% acetic acid, and analyzed by direct infusion-Fourier transform mass spectrometry (Figure 1, human) or by direct infusion-ion trap mass spectrometry (Supporting Information Figure 1, mouse).

Cysteinylation of SOD1 was consistently the most prevalent PTM observed as peaks (e.g., the 14+ charge state at m/z 1141.586) corresponding to a deconvoluted and deisotoped monoisotopic mass of 15 955.11 Da, which is 119.01 Da larger than unmodified SOD1 (15 836.10 Da). A 119.01 Da modification is consistent with the molecular weight of cysteine with the two sulfhydryl hydrogen atoms liberated during disulfide bond formation (theoretical mass 119.01) between Cys₁₁₁ of SOD1 and free cysteine (Figure 1). In addition to cysteinylation, we observed modifications we putatively assigned as modification with one (15 851.40 Da) and two oxygen atoms (15 866.38 Da). The abundance of these putative oxidative modifications was too low to permit further characterization; however, oxidative modifications of Cys₁₁₁ and Trp₃₂ have been described previously.¹⁴

To further investigate PTMs by cysteine and oxygen, as well as their relative amounts, an additional four postmortem human brain samples were analyzed using a different purification method (different homogenization buffer, SOD1 antibodies, wash buffer, and elution buffer) and different preparative conditions (reversed-phase liquid chromatography–mass spectrometry [RPLC–MS]; Figure 2). Cysteinylation and oxidation were observed in all four samples (Figure 2B), although the percentage of total of Cys modified SOD1 appeared slightly lower in RPLC–MS analysis ($38\% \pm 7\%$ via RPLC–MS versus $48\% \pm 6\%$ via direct infusion). Reversed-phase chromatography generally increases the dynamic range of MS analysis, and as a result, additional modifications were detected in these samples. Therefore, the overall average cysteinylation observed in human nervous tissue (both direct infusion and RPLC–MS) was 41% (maximum cysteinylation observed was 62%; minimum cysteinylation observed was 22%). Notably, cysteinylation was not a prevalent modification in SOD1 purified from human blood by the first method¹⁴ but was reportedly observed in other purifications.^{11,12}

To determine if the extent of cysteine modification or oxidation depended upon purification methods—for example, if oxidative addition of free cysteine or thiol disulfide exchange with free cysteine—two additional controls were used. First, SOD1 was purified anaerobically. Second, SOD1 was homogenized anaerobically in the presence of iodoacetamide, iodoacetic acid, and *S*-methyl methanethiosulfonate (MMTS) to alkylate and scavenge any free cysteine as well as unmodified SOD1 Cys₁₁₁. Cysteinylation was observed in SOD1 purified anaerobically; however, there was approximately a 2-fold reduction in the amount observed compared to the amount of the samples purified aerobically. The cysteine alkylators and scavengers removed the majority of the cysteinylation, but a small amount was still present.

In summary, to investigate PTMs by cysteine and oxygen, we performed purifications (1) using different antibodies and elution conditions, (2) with and without liquid chromatography, (3) by aerobic and anaerobic methods, (4) with and without alkylation agent to block endogenous “free” cysteine from binding SOD1 during homogenization, and (5) from different tissues and organisms (human and mouse spinal cord and brain). Under the conditions tested here, the SOD1 purified from human and mouse tissue, but not from yeast, contained cysteinylated SOD1 (Table 1).

Majority of SOD1 Modifications Observed in Human Tissue Can Be Created In Vitro Using Cysteine and Peroxide. To determine if both the types and the relative amounts of modifications of SOD1 purified from human tissue

Table 1. Amount of SOD1 Cysteinylated Using Different Purification Procedures and from Different Sources

purification method	% cysteinylation	figure
polyclonal rabbit antibody	48	Figure 1
polyclonal sheep antibody	38	Figure 2B
elution: 5% acetic acid	48	Figure 1
elution: gentle elution buffer	38	Figure 2B
with liquid chromatography	38	Figure 2B
without liquid chromatography	48	Figure 1
aerobically	48	Figures 1, 2B
anaerobically		
with alkylating agent	1	
without alkylating agent	24	

protein source	% cysteinylation	figure
human nervous tissue	41	Figures 1, 2B
mouse nervous tissue	21	Supporting Information Figure 1
yeast	0	Figure 3A

could be recapitulated in vitro, SOD1 was incubated with a 40-fold molar excess of cysteine, which approximated the cysteinylation levels of postmortem SOD1. This sample was incubated with a 100-fold molar excess of peroxide (100 μ M) in a time course experiment. Following incubation with low levels of peroxide (the amount generated in 100 turnovers of peroxide) for 3.5 h, these in vitro samples resembled SOD1 purified from human tissue, indicating that many of the modifications observed in SOD1 purified from human samples are the result of modification by cysteine and peroxide (Figure 2).

Cysteine-Modified SOD1 Is Protected from Oxidation.

Human SOD1 expressed and purified from yeast cells was analyzed using a Fourier transform mass spectrometer (FTMS), which showed a peak consistent with native SOD1 (Figure 3A; note that acidic buffers and desolvation conditions were such that Cu and Zn could not be detected). Cysteinylated SOD1 was created in vitro as described above. Both native and cysteinylated SOD1 were observed, and the binding stoichiometry was approximately one cysteine per SOD1 dimer (Figure 3B), indicating that cysteinylation of one Cys₁₁₁ can potentially block cysteinylation of the adjacent Cys₁₁₁, presumably sterically.

To determine the extent to which in vitro cysteine modification protected SOD1 from peroxide-mediated modification, a sample containing both cysteine-modified SOD1 and the native protein was oxidized using 10 mM hydrogen peroxide in a time course study. After 2 h, the majority of native SOD1 protein was modified by two or three oxygen atoms. Conversely, only a small amount of cysteine-modified SOD1 was oxidized (Figure 3C; red dotted lines versus blue dotted lines), indicating near complete protection. In addition, 4 h after peroxide treatment, all the native SOD1 had been oxidized by two or three oxygen atoms (the native protein is no longer observed), whereas cysteine-modified SOD1 was not oxidized (Figure 3D; red dotted lines versus blue dotted lines).

Cysteinylation Occurred Specifically upon SOD1 Cys₁₁₁. PTMs are typically localized using endoproteinase digestion followed by LC–MS/MS analysis. In both MALDI–TOF fingerprinting and LC–MS/MS experiments, we observed cysteinylated peptides containing Cys₁₁₁ and localized this modification to Cys₁₁₁ using MS/MS data (Supporting Information Figures 2 and 3). This approach, however, was not

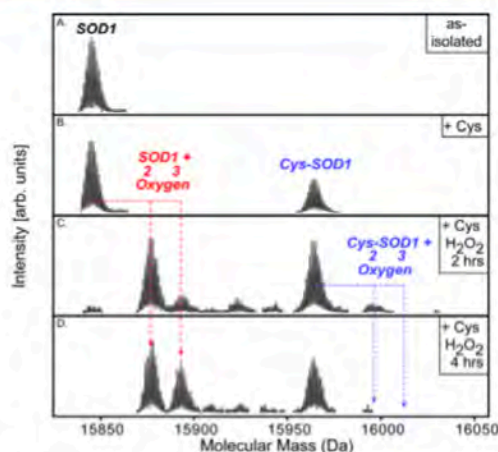


Figure 3. Cysteinylated SOD1 protecting SOD1 from oxidation. (A) Spectra of unmodified (as isolated) SOD1 (15 835.97 Da). (B) Spectra of SOD1 modified by cysteine (40 μM) (15 954.97 Da), which is consistent with the molecular weight of SOD1-cysteine (less two hydrogen atoms, forming cystine). (C and D) Taken from the time course of 10 mM peroxide-mediated oxidation of cysteinylated SOD1. (C) Spectra of cysteine-modified SOD1, oxidized using hydrogen peroxide, 2 h after oxidation. Most of the native SOD1 protein has been modified by two (sulfonic acid) (15 867.97 Da) or three (sulfonic acid) oxygen atoms (15 883.96 Da) (dotted red lines), whereas a small amount of cysteine-modified SOD1 is oxidized (dotted blue lines). (D) Spectra of SOD1 modified by cysteine and oxidized using hydrogen peroxide, 4 h after oxidation. All native SOD1 has been oxidized by two (15 867.97 Da) or three oxygen atoms (15 883.95 Da) (dotted red lines), whereas cysteine-modified SOD1 does not appear to be oxidized (dotted blue lines). In addition, the sulfonic acid modified SOD1 is the same form of SOD1 that Bosco et al. show inhibits fast axonal transport in a similar fashion to SOD1 FALS variants.¹³ These experiments were repeated in triplicate.

ideal for cysteinylated. Control experiments revealed that, following endoproteinase digestion, rapid scrambling of SOD1 disulfides occurred, including scrambling of the native disulfide (Cys_{57} and Cys_{146}) with Cys_6 and Cys_{111} . This necessitated a “top-down” MS approach, whereby fragmentation occurs within the mass spectrometer such that disulfide scrambling cannot normally occur.¹⁸ To localize the site of modification by cysteine, SOD1 was cysteinylated *in vitro* and analyzed via intact protein dissociation within the FTMS (Figure 4A). Cysteinylated SOD1 was fragmented in the FTMS using collisionally activated dissociation at the funnel-skimmer interface, yielding an abundant *b*-ion series (Figure 4B). The b_6 -ion and larger *b*-ions (fragments containing the N-terminus and Cys_6) fit the theoretical mass of unmodified Cys_6 (Figure 4C), and no modified peaks were observed (on the basis of *S/N*, as little as 2% of modified Cys_6 could have been detected). In addition, we observed a y_{139} -ion at a mass of 14 454.09 Da. This mass is consistent with a cysteinylated SOD1 *y*-ion containing C-terminal residues 16–153 and containing the intramolecular disulfide bond between residues 57 and 146 (Figure 4D). In summary, cysteine 57 and 146 are in a disulfide bond and are unable to be cysteinylated; we ruled out cysteinylated cysteine 6 using MS/MS data and observed a large cysteinylated C-terminal SOD1 fragment, consistent with cysteinylated Cys_{111} . In a sister publication (DOI 10.1021/bi400613h), we present the 3-dimensional structure of

cysteinylated SOD1, which is consistent with the results presented here, and also characterize the binding stoichiometry as 1 cysteinylated per SOD1 dimer.

DISCUSSION

Protein cysteinylated is not well-characterized, partially due to the practice of purifying/treating proteins in the presence of reducing agents such as DTT. It has, however, been observed in transthyretin (TTR), human serum albumin, and the k1 light chain from an amyloid patient.^{19,20} In addition, cysteinylated has been observed in *Bacillus subtilis* during oxidative stress treatment. Hochgrafe et al. suggest that cysteinylated may play a role in protecting cysteine residues from oxidation and irreversible damage in *Bacillus subtilis* and possibly other organisms.²¹

More than half of all the SOD1 protein isolated here from postmortem human nervous tissues contained PTMs, predominantly cysteinylated and oxidation. Cysteine-modified SOD1 was protected from peroxide mediated oxidation *in vitro*, and cysteinylated SOD1 purified from human tissue appears also to have been protected from oxidation. SOD1 that had been cysteinylated and peroxide oxidized *in vitro* was composed of a set of PTMs that bear a striking resemblance to the myriad of PTMs observed in SOD1 purified from human tissue (Figures 1 and 2), indicating peroxide and cysteine are among the major modifiers of SOD1.

Putative cysteinylated of SOD1 was observed *in vitro*⁷ and in preparations from blood^{11,12} on the basis of differences in intact protein mass, and in some cases, the modification was labile to reductants. Li et al.⁷ observe a modified SOD1 118 Da heavier than unmodified SOD1 that disappears with DTT treatment and concluded that the modification was cysteine. However, this change in mass of 118 Da is not consistent with the 119 Da increase in mass expected for a cysteine modification. In no previous studies were peptide digest or MSⁿ data provided to confirm that the modification was cysteine or to determine the site of modification. Here, using endoproteinase peptide mapping by MALDI-TOF MS, MSⁿ data of an LC-ESI-ion trap, and top-down MS, cysteinylated of SOD1 on residue 111 was confirmed. In addition, we suggest a possible role for SOD1 cysteinylated, namely protection from peroxide-mediated oxidation.

In anaerobic control experiments in the presence or absence of alkylating/thiol scavenging agents, we observed a reduction in the amount of cysteinylated, which is consistent with some of the modifications we observed from human tissue occurring during the homogenization process. Note that cysteinylated from cystine occurs via thiol-disulfide exchange and is redox neutral, whereas cysteinylated from cysteine requires the loss of two protons and two electrons (oxidation). Although treatment with alkylating agents/cysteine scavengers is a harsh treatment with the potential to remove cysteinylated,²² it did not do so in *in vitro* control experiments. Cysteinylated remained the most abundant PTM in the anaerobic (with no other chemicals) treatment.

An argument against nonenzymatic cysteinylated of SOD1 occurring during homogenization can be made on the basis of the cellular ratios of SOD1 to free cysteine/cystine (CSH/CSSC) and glutathione (GSH/GSSG). Although the amount of SOD1 is $\sim 10 \mu\text{M}$, the amount of cysteine inside the cell is approximately $2.5 \mu\text{M}$,^{23,24} and the amount of cystine is approximately $0.25\text{--}1.3 \mu\text{M}$.^{23,25–27} Given similarities in redox potential (E_0) for CSH/CSSC and GSH/GSSG (-0.22 and

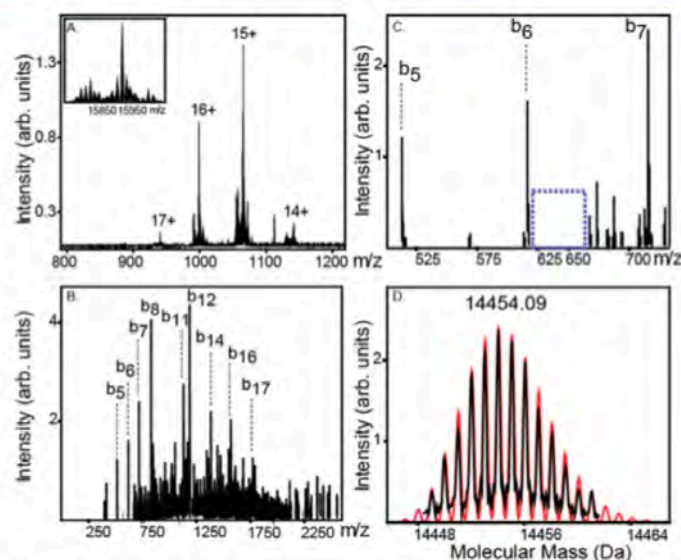


Figure 4. SOD1 Cys₁₁₁, the site of cysteinylation. (A) Mass spectrum of intact cysteinylated SOD1. (B) Fragmentation spectrum of cysteinylated SOD1 using funnel-skimmer dissociation with the N-terminal *b*-ion series labeled. (C) Zoom in of the *b*₆-ion (contains cysteine 6). No peak corresponding to a cysteinylated form of cysteine 6 is observed (approximately *m/z* 632; dotted blue box). (D) C-terminal fragment (*y*₁₃₉) of SOD1 (residues 16–153), which is consistent with the mass of a cysteinylated SOD1 fragment. The red lines are the theoretical isotopic distribution modeled using the simulated isotopic pattern parameter in DataAnalysis (Bruker) of cysteinylated *y*₁₃₉ (mass of *y*₁₃₉ plus 121.158 Da for cysteine, subtract two hydrogen atoms upon its non-native disulfide formation, and an additional two hydrogen atoms for the intramolecular disulfide).

–0.24 V,²⁸ respectively) and the 1000-fold higher concentration of glutathione in the brain (~1–2 mM GSH and ~8 μM GSSG^{29–31}), glutathionylation (not observed) is the most likely artifact of our purification. Furthermore, despite concentrations of cystine and cysteine being 50–100 times higher in plasma,³² we do not observe cysteinylated SOD1 in blood preparations¹⁴ (>50 purifications). On the other hand, cysteinylation was putatively assigned, though without MS/MS or protein digest confirmation, in other purifications.^{11,12} Thus, on the basis of the protein concentrations in the cell, the cysteine concentration, and their redox potential, it is likely cysteinylation can occur *in vivo*.

Despite treatment with large excesses of cysteine, only one cysteine was detected to be bound per SOD1 dimer, consistent with cysteinylation of SOD1 Cys₁₁₁ on one monomer blocking cysteinylation on the second monomer. This is probably due to the close proximity (~8–10 Å) of both cysteine residues in the dimer interface of SOD1;⁷ we were unable to model two cysteine residues per dimer without them overlapping or being strained. A sister publication characterizes the 3-dimensional structure of cysteinylated SOD1. Although the binding of free cysteine to one of SOD1's cysteine residues blocks the binding of a second cysteine, our data suggested it does not completely protect the adjacent Cys₁₁₁ (noncysteinylated Cys₁₁₁) from oxidation.

Dimer destabilization of SOD1 has been implicated in disease progression for amyotrophic lateral sclerosis (ALS),^{15,33–36} Oxygen-modified cysteine residues are negatively charged,³⁷ and if both Cys₁₁₁ are oxidized, there would be a coulombic impetus for destabilizing the SOD1 dimer. We, and others, have shown that oxidation of SOD1 by hydrogen peroxide is capable of destabilizing SOD1.^{1–3,13} In addition, the sulfonic acid modified SOD1 (three oxygen atoms per cysteine)

is the same form of SOD1 that Bosco et al. show inhibits fast axonal transport in a similar fashion to SOD1 FALS variants.¹³ Thus, by preventing oxidation of Cys₁₁₁, cysteinylation could ameliorate SOD1 dimer destabilization and minimize the formation of toxic SOD1 species. Under conditions of both oxidative stress and aging, there is both more cystine, which can cysteinylate SOD1 directly, and more oxygen to promote cysteine–SOD1 oxidative coupling. For example, cystine concentrations double with age (average of 52 μM at age 26; average of 105 μM at age 60²²). Cysteinylated SOD1 is therefore more likely to occur under conditions of both oxidative stress and aging and may be an adaptive modification.

■ ASSOCIATED CONTENT

Supporting Information

MS, MALDI-TOF, and LC–MS/MS figures further characterizing cysteinylation. This material is available free of charge via the Internet at <http://pubs.acs.org>.

■ AUTHOR INFORMATION

Corresponding Author

*J. N. Agar: e-mail, j.agar@neu.edu; phone, (617) 373-5909.

Present Addresses

¹(J.R.A., J.P.S., J.N.A.) Department of Chemistry and Chemical Biology and Pharmaceutical Sciences and the Barnett Institute, Northeastern University, Boston, Massachusetts 02115, United States.

[‡](J.L.J.) Novartis Institute for Biomedical Research, Cambridge, Massachusetts 02139, United States.

Funding

This work was supported in part by grants from National Institutes of Health (1R01NS065263-01 to J.N.A. and

1R01NS067206-02 to D.A.B.), ALS Therapy Alliance/CVS Pharmacy to D.A.B., and Fidelity Biosciences Research Initiative to G.A.P. and D.R.

Notes

The authors declare no competing financial interest.

ACKNOWLEDGMENTS

We thank Dr. P. John Hart for the generous gift of the YEP351-SOD1 plasmid and EGy118- Δ SOD1 yeast cells used to express SOD1 in this study. We thank Dr. Nathalie Y. R. Agar for providing the postmortem human cortex used in the anaerobic control experiments. We also thank the patients who donated the tissue used in these experiments. We also thank members of the Agar and Petsko/Ringe Laboratories for thoughtful discussions, insights, and critically reviewing this manuscript.

REFERENCES

- Keithley, E. M., Canto, C., Zheng, Q. Y., Wang, X., Fischel-Ghodsian, N., and Johnson, K. R. (2005) Cu/Zn superoxide dismutase and age-related hearing loss. *Hear. Res.* 209, 76–85.
- Phillips, J. P., Tainer, J. A., Getzoff, E. D., Boulianne, G. L., Kirby, K., and Hilliker, A. J. (1995) Subunit-destabilizing mutations in *Drosophila* copper/zinc superoxide dismutase: neuropathology and a model of dimer dysequilibrium. *Proc. Natl. Acad. Sci. U. S. A.* 92, 8574–8578.
- Woodruff, R. C., Phillips, J. P., and Hilliker, A. J. (2004) Increased spontaneous DNA damage in Cu/Zn superoxide dismutase (SOD1) deficient *Drosophila*. *Genome* 47, 1029–1035.
- McCord, J. M., and Fridovich, I. (1968) The reduction of cytochrome c by milk xanthine oxidase. *J. Biol. Chem.* 243, 5753–5760.
- Fujiwara, N., Nakano, M., Kato, S., Yoshihara, D., Ookawara, T., Eguchi, H., Taniguchi, N., and Suzuki, K. (2007) Oxidative modification to cysteine sulfonic acid of Cys111 in human copper-zinc superoxide dismutase. *J. Biol. Chem.* 282, 35933–35944.
- Choi, J., Rees, H. D., Weintraub, S. T., Levey, A. I., Chin, L. S., and Li, L. (2005) Oxidative modifications and aggregation of Cu,Zn-superoxide dismutase associated with Alzheimer and Parkinson diseases. *J. Biol. Chem.* 280, 11648–11655.
- Liu, H., Zhu, H., Eggers, D. K., Nersissian, A. M., Faull, K. F., Goto, J. J., Ai, J., Sanders-Loehr, J., Gralla, E. B., and Valentine, J. S. (2000) Copper(2+) binding to the surface residue cysteine 111 of His46Arg human copper-zinc superoxide dismutase, a familial amyotrophic lateral sclerosis mutant. *Biochemistry* 39, 8125–8132.
- Redler, R. L., Wilcox, K. C., Proctor, E. A., Fee, L., Caplow, M., and Dokholyan, N. V. (2011) Glutathionylation at Cys-111 induces dissociation of wild type and FALS mutant SOD1 dimers. *Biochemistry* 50, 7057–7066.
- Schinina, M. E., Carlini, P., Polticelli, F., Zappacosta, F., Bossa, F., and Calabrese, L. (1996) Amino acid sequence of chicken Cu, Zn-containing superoxide dismutase and identification of glutathionyl adducts at exposed cysteine residues. *Eur. J. Biochem.* 237, 433–439.
- Wilcox, K. C., Zhou, L., Jordon, J. K., Huang, Y., Yu, Y., Redler, R. L., Chen, X., Caplow, M., and Dokholyan, N. V. (2009) Modifications of superoxide dismutase (SOD1) in human erythrocytes: a possible role in amyotrophic lateral sclerosis. *J. Biol. Chem.* 284, 13940–13947.
- Nakanishi, T., Kishikawa, M., Miyazaki, A., Shimizu, A., Ogawa, Y., Sakoda, S., Ohi, T., and Shoji, H. (1998) Simple and defined method to detect the SOD-1 mutants from patients with familial amyotrophic lateral sclerosis by mass spectrometry. *J. Neurosci. Methods* 81, 41–44.
- Shimizu, A., Nakanishi, T., and Miyazaki, A. (2006) Detection and characterization of variant and modified structures of proteins in blood and tissues by mass spectrometry. *Mass Spectrom. Rev.* 25, 686–712.
- Bosco, D. A., Morfini, G., Karabacak, N. M., Song, Y., Gros-Louis, F., Pasinelli, P., Goolsby, H., Fontaine, B. A., Lemay, N., McKenna-Yasek, D., Frosch, M. P., Agar, J. N., Julien, J. P., Brady, S. T., and Brown, R. H., Jr. (2010) Wild-type and mutant SOD1 share an aberrant conformation and a common pathogenic pathway in ALS. *Nat. Neurosci.* 13, 1396–1403.
- Taylor, D. M., Gibbs, B. F., Kabashi, E., Minotti, S., Durham, H. D., and Agar, J. N. (2007) Tryptophan 32 potentiates aggregation and cytotoxicity of a copper/zinc superoxide dismutase mutant associated with familial amyotrophic lateral sclerosis. *J. Biol. Chem.* 282, 16329–16335.
- Doucette, P. A., Whitson, L. J., Cao, X., Schirf, V., Demeler, B., Valentine, J. S., Hansen, J. C., and Hart, P. J. (2004) Dissociation of human copper-zinc superoxide dismutase dimers using chaotrope and reductant. Insights into the molecular basis for dimer stability. *J. Biol. Chem.* 279, 54558–54566.
- Hayward, L. J., Rodriguez, J. A., Kim, J. W., Tiwari, A., Goto, J. J., Cabelli, D. E., Valentine, J. S., and Brown, R. H., Jr. (2002) Decreased metallation and activity in subsets of mutant superoxide dismutases associated with familial amyotrophic lateral sclerosis. *J. Biol. Chem.* 277, 15923–15931.
- Cobb, J. S., Easterling, M. L., and Agar, J. N. (2010) Structural characterization of intact proteins is enhanced by prevalent fragmentation pathways rarely observed for peptides. *J. Am. Soc. Mass Spectrom.* 21, 949–959.
- Kellie, J. F., Tran, J. C., Lee, J. E., Ahlf, D. R., Thomas, H. M., Ntai, I., Catherman, A. D., Durbin, K. R., Zamborg, L., Vellaichamy, A., Thomas, P. M., and Kelleher, N. L. (2010) The emerging process of Top Down mass spectrometry for protein analysis: biomarkers, protein-therapeutics, and achieving high throughput. *Mol. BioSyst.* 6, 1532–1539.
- Kleinova, M., Beigacem, O., Pock, K., Rizzi, A., Buchacher, A., and Allmaier, G. (2005) Characterization of cysteinylated of pharmaceutical-grade human serum albumin by electrospray ionization mass spectrometry and low-energy collision-induced dissociation tandem mass spectrometry. *RCM* 19, 2965–2973.
- Lim, A., Wally, J., Walsh, M. T., Skinner, M., and Costello, C. E. (2001) Identification and location of a cysteinyl posttranslational modification in an amyloidogenic kappal light chain protein by electrospray ionization and matrix-assisted laser desorption/ionization mass spectrometry. *Anal. Biochem.* 295, 45–56.
- Hochgrafe, F., Mostertz, J., Pother, D. C., Becher, D., Helmann, J. D., and Hecker, M. (2007) S-cysteinylated is a general mechanism for thiol protection of *Bacillus subtilis* proteins after oxidative stress. *J. Biol. Chem.* 282, 25981–25985.
- Johnson, J. M., Strobel, F. H., Reed, M., Pohl, J., and Jones, D. P. (2008) A rapid LC-FTMS method for the analysis of cysteine, cystine and cysteine/cystine steady-state redox potential in human plasma. *Clin. Chim. Acta* 396, 43–48.
- Sato, H., Tamba, M., Okuno, S., Sato, K., Keino-Masu, K., Masu, M., and Bannai, S. (2002) Distribution of cystine/glutamate exchange transporter, system x(c)-, in the mouse brain. *J. Neurosci.* 22, 8028–8033.
- Castagna, A., Le Grazie, C., Accordini, A., Giuliodori, P., Cavalli, G., Bottiglieri, T., and Lazzarin, A. (1995) Cerebrospinal fluid S-adenosylmethionine (SAME) and glutathione concentrations in HIV infection: effect of parenteral treatment with SAME. *Neurology* 45, 1678–1683.
- Araki, K., Harada, M., Ueda, Y., Takino, T., and Kuriyama, K. (1988) Alteration of amino acid content of cerebrospinal fluid from patients with epilepsy. *Acta Neurol. Scand.* 78, 473–479.
- Amesano, F., Banci, L., Bertini, I., Martinelli, M., Furukawa, Y., and O'Halloran, T. V. (2004) The unusually stable quaternary structure of human Cu,Zn-superoxide dismutase 1 is controlled by both metal occupancy and disulfide status. *J. Biol. Chem.* 279, 47998–48003.
- Lakke, J. P., and Teelken, A. W. (1976) Amino acid abnormalities in cerebrospinal fluid of patients with parkinsonism and extrapyramidal disorders. *Neurology* 26, 489–493.

- (28) Jocelyn, P. C. (1967) The standard redox potential of cysteine-cystine from the thiol-disulphide exchange reaction with glutathione and lipoic acid. *Eur. J. Biochem.* 2, 327–331.
- (29) Ratan, R. R., Murphy, T. H., and Baraban, J. M. (1994) Macromolecular synthesis inhibitors prevent oxidative stress-induced apoptosis in embryonic cortical neurons by shunting cysteine from protein synthesis to glutathione. *J. Neurosci.* 14, 4385–4392.
- (30) Slivka, A., Mytilineou, C., and Cohen, G. (1987) Histochemical evaluation of glutathione in brain. *Brain Res.* 409, 275–284.
- (31) Slivka, A., Spina, M. B., and Cohen, G. (1987) Reduced and oxidized glutathione in human and monkey brain. *Neurosci. Lett.* 74, 112–118.
- (32) Brigham, M. P., Stein, W. H., and Moore, S. (1960) The Concentrations of Cysteine and Cystine in Human Blood Plasma. *J. Clin. Invest.* 39, 1633–1638.
- (33) Auclair, J. R., Boggio, K. J., Petsko, G. A., Ringe, D., and Agar, J. N. (2010) Strategies for stabilizing superoxide dismutase (SOD1), the protein destabilized in the most common form of familial amyotrophic lateral sclerosis. *Proc. Natl. Acad. Sci. U. S. A.* 107, 21394–21399.
- (34) Hornberg, A., Logan, D. T., Marklund, S. L., and Oliveberg, M. (2007) The coupling between disulphide status, metallation and dimer interface strength in Cu/Zn superoxide dismutase. *J. Mol. Biol.* 365, 333–342.
- (35) Rakhit, R., Crow, J. P., Lepock, J. R., Kondejewski, L. H., Cashman, N. R., and Chakrabartty, A. (2004) Monomeric Cu,Zn-superoxide dismutase is a common misfolding intermediate in the oxidation models of sporadic and familial amyotrophic lateral sclerosis. *J. Biol. Chem.* 279, 15499–15504.
- (36) Rakhit, R., Robertson, J., Vande Velde, C., Horne, P., Ruth, D. M., Griffin, J., Cleveland, D. W., Cashman, N. R., and Chakrabartty, A. (2007) An immunological epitope selective for pathological monomer-misfolded SOD1 in ALS. *Nat. Med.* 13, 754–759.
- (37) Yarnell, A. (2009) Cysteine Oxidation New Chemical tools are poised to help scientists explore the roles of oxidized cysteine residues might play in biology. *Chem. Eng. News* 87, 38–40.

PREFACE TO APPENDIX IV

All work was performed by Melissa S. Rotunno.

APPENDIX IV: Cysteinylation of SOD1 may protect against misfolded SOD1

As described in detail in Appendix III, cysteinylation of SOD1 may be an *in vivo* mechanism to avoid the presence of misfolded SOD1 induced by oxidation. Cysteinylated SOD1 is less likely to be oxidized and demonstrates an increase in overall stability of the protein compared to oxidized SOD1 (Auclair et al. 2013a). To assess the extent of reparation of the fold of SOD1 induced by cysteinylation, SOD1 variants were cysteinylated, run on a native PAGE, and probed with the C4F6 antibody. The C4F6 antibody demonstrates a decrease in reactivity in SOD1 G93A, G85R, and Δ IV/ Δ VII upon cysteinylation (**Fig. AIV-1**). This supports the protective role of cysteinylation in SOD1 folding, described in **Appendix III**.

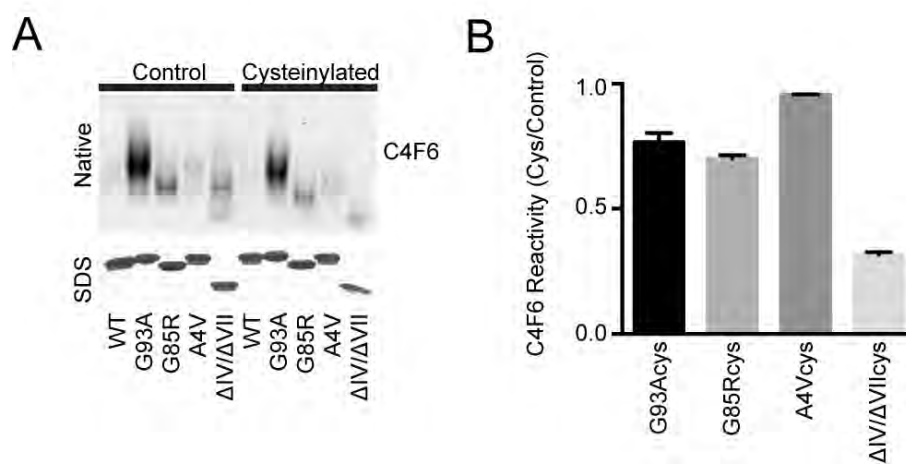


Figure AIV-1. Cysteinylation of recombinant SOD1 results in a decrease in C4F6 reactivity. (A) Recombinant SOD1 variants incubated with 4-fold molar excess of cysteine for 16 h were assessed for C4F6 reactivity by Native PAGE western analysis. Cysteinylation variants demonstrate a decrease in C4F6 reactivity. (B) Quantification of analysis described in (A) where each variant is normalized to the “no cys” counterpart.

References

Allen MJ, Lacroix JJ, Ramachandran S, Capone R, Whitlock JL, Ghadge GD, Arnsdorf MF, Roos RP, Lal R. 2011. Mutant SOD1 forms ion channel: implications for ALS pathophysiology. *Neurobiol Dis* 45:831-838.

Alonso A, Logroscino G, Jick SS, Hernan MA. 2009. Incidence and lifetime risk of motor neuron disease in the United Kingdom: a population-based study. *Eur J Neurol* 16:745-751.

Alper GS, Eser; Kanit, Lutfiye; Menten, Gulris; Ersoz, Biltan; Kutay, Fatma. 1998. Age-Related Alterations in Superoxide Dismutase and Catalase Activities in Rat Brain. *Tr. J. of Medical Sciences* 28:491-494.

Araki W, Minegishi S, Motoki K, Kume H, Hohjoh H, Araki YM, Tamaoka A. 2014. Disease-associated mutations of TDP-43 promote turnover of the protein through the proteasomal pathway. *Molecular neurobiology* 50:1049-1058.

Arnesano F, Banci L, Bertini I, Martinelli M, Furukawa Y, O'Halloran TV. 2004. The unusually stable quaternary structure of human Cu,Zn-superoxide dismutase 1 is controlled by both metal occupancy and disulfide status. *The Journal of biological chemistry* 279:47998-48003.

Auclair JR, Boggio KJ, Petsko GA, Ringe D, Agar JN. 2010. Strategies for stabilizing superoxide dismutase (SOD1), the protein destabilized in the most common form of familial amyotrophic lateral sclerosis. *Proc Natl Acad Sci U S A* 107:21394-21399.

Auclair JR, Brodtkin HR, D'Aquino JA, Petsko GA, Ringe D, Agar JN. 2013a. Structural consequences of cysteinylolation of Cu/Zn-superoxide dismutase. *Biochemistry* 52:6145-6150.

Auclair JR, Johnson JL, Liu Q, Salisbury JP, Rotunno M, Petsko GA, Ringe D, Brown Jr RH, Bosco DA, Agar JN. 2013b. Post-Translational Modification by Cysteine Protects Cu/Zn-Superoxide Dismutase From Oxidative Damage. *Biochemistry* 52:6137-6144.

Ayers JI, Fromholt S, Koch M, DeBosier A, McMahon B, Xu G, Borchelt DR. 2014. Experimental transmissibility of mutant SOD1 motor neuron disease. *Acta Neuropathol* 128:791-803.

Bahadorani S, Mukai ST, Rabie J, Beckman JS, Phillips JP, Hilliker AJ. 2013. Expression of zinc-deficient human superoxide dismutase in *Drosophila* neurons produces a locomotor defect linked to mitochondrial dysfunction. *Neurobiol Aging* 34:2322-2330.

Bai J, Zhu X, Zheng X, Wu Y. 1998. Overexpression of CuZnSOD gene suppresses the growth of hepatocellular cancer cell line HepG2. *Chin Med J (Engl)* 111:789-792.

Banci L, et al. 2012a. Interaction of cisplatin with human superoxide dismutase. *J Am Chem Soc* 134:7009-7014.

Banci L, Bertini I, Boca M, Calderone V, Cantini F, Girotto S, Vieru M. 2009. Structural and dynamic aspects related to oligomerization of apo SOD1 and its mutants. *Proceedings of the National Academy of Sciences of the United States of America* 106:6980-6985.

Banci L, Bertini I, Cantini F, Kozyreva T, Massagni C, Palumaa P, Rubino JT, Zovo K. 2012b. Human superoxide dismutase 1 (hSOD1) maturation through interaction with human copper chaperone for SOD1 (hCCS). *Proceedings of the National Academy of Sciences of the United States of America* 109:13555-13560.

Banci L, Bertini I, Cramaro F, Del Conte R, Viezzoli MS. 2003. Solution structure of Apo Cu,Zn superoxide dismutase: role of metal ions in protein folding. *Biochemistry* 42:9543-9553.

Banci L, Bertini I, Durazo A, Girotto S, Gralla EB, Martinelli M, Valentine JS, Vieru M, Whitelegge JP. 2007. Metal-free superoxide dismutase forms soluble oligomers under physiological conditions: a possible general mechanism for familial ALS. *Proc Natl Acad Sci U S A* 104:11263-11267.

Barber SC, Shaw PJ. 2010. Oxidative stress in ALS: key role in motor neuron injury and therapeutic target. *Free radical biology & medicine* 48:629-641.

Bartnikas TB, Gitlin JD. 2003. Mechanisms of biosynthesis of mammalian copper/zinc superoxide dismutase. *The Journal of biological chemistry* 278:33602-33608.

Basso M, Massignan T, Samengo G, Cheroni C, De Biasi S, Salmona M, Bendotti C, Bonetto V. 2006. Insoluble mutant SOD1 is partly oligoubiquitinated

in amyotrophic lateral sclerosis mice. *The Journal of biological chemistry* 281:33325-33335.

Becker CG, Diez Del Corral R. 2015. Neural development and regeneration: it's all in your spinal cord. *Development* 142:811-816.

Beckman JS, Estevez AG, Crow JP, Barbeito L. 2001. Superoxide dismutase and the death of motoneurons in ALS. *Trends Neurosci* 24:S15-20.

Beers DR, Henkel JS, Xiao Q, Zhao W, Wang J, Yen AA, Siklos L, McKercher SR, Appel SH. 2006. Wild-type microglia extend survival in PU.1 knockout mice with familial amyotrophic lateral sclerosis. *Proc Natl Acad Sci U S A* 103:16021-16026.

Beghi E, Logroscino G, Chio A, Hardiman O, Millul A, Mitchell D, Swingler R, Traynor BJ. 2010. Amyotrophic lateral sclerosis, physical exercise, trauma and sports: results of a population-based pilot case-control study. *Amyotroph Lateral Scler* 11:289-292.

Benmohamed R, Arvanites AC, Kim J, Ferrante RJ, Silverman RB, Morimoto RI, Kirsch DR. 2011. Identification of compounds protective against G93A-SOD1 toxicity for the treatment of amyotrophic lateral sclerosis. *Amyotroph Lateral Scler* 12:87-96.

Berlett BS, Stadtman ER. 1997. Protein oxidation in aging, disease, and oxidative stress. *The Journal of biological chemistry* 272:20313-20316.

Berry JD, et al. 2013. Design and initial results of a multi-phase randomized trial of ceftriaxone in amyotrophic lateral sclerosis. *PLoS One* 8:e61177.

Beyer K, Ariza A. 2013. Alpha-synuclein posttranslational modification and alternative splicing as a trigger for neurodegeneration. *Molecular neurobiology* 47:509-524.

Blander G, de Oliveira RM, Conboy CM, Haigis M, Guarente L. 2003. Superoxide dismutase 1 knock-down induces senescence in human fibroblasts. *The Journal of biological chemistry* 278:38966-38969.

Block ML, Zecca L, Hong JS. 2007. Microglia-mediated neurotoxicity: uncovering the molecular mechanisms. *Nat Rev Neurosci* 8:57-69.

Blokhuis AM, Groen EJ, Koppers M, van den Berg LH, Pasterkamp RJ. 2013. Protein aggregation in amyotrophic lateral sclerosis. *Acta Neuropathol* 125:777-794.

Borchelt DR, Lee MK, Slunt HS, Guarnieri M, Xu ZS, Wong PC, Brown RH, Jr., Price DL, Sisodia SS, Cleveland DW. 1994. Superoxide dismutase 1 with mutations linked to familial amyotrophic lateral sclerosis possesses significant activity. *Proc Natl Acad Sci U S A* 91:8292-8296.

Bosco DA, et al. 2010. Wild-type and mutant SOD1 share an aberrant conformation and a common pathogenic pathway in ALS. *Nat Neurosci* 13:1396-1403.

Braak H, Ludolph A, Thal DR, Del Tredici K. 2010. Amyotrophic lateral sclerosis: dash-like accumulation of phosphorylated TDP-43 in somatodendritic and axonal compartments of somatomotor neurons of the lower brainstem and spinal cord. *Acta Neuropathol* 120:67-74.

Broering TJ, et al. 2013. Identification of human monoclonal antibodies specific for human SOD1 recognizing distinct epitopes and forms of SOD1. *PLoS One* 8:e61210.

Brotherton TE, Li Y, Cooper D, Gearing M, Julien JP, Rothstein JD, Boylan K, Glass JD. 2012. Localization of a toxic form of superoxide dismutase 1 protein to pathologically affected tissues in familial ALS. *Proc Natl Acad Sci U S A* 109:5505-5510.

Brown DI, Griending KK. 2009. Nox proteins in signal transduction. *Free radical biology & medicine* 47:1239-1253.

Brown DP, Chin-Sinex H, Nie B, Mendonca MS, Wang M. 2009. Targeting superoxide dismutase 1 to overcome cisplatin resistance in human ovarian cancer. *Cancer Chemother Pharmacol* 63:723-730.

Brujin LI, et al. 1997. ALS-linked SOD1 mutant G85R mediates damage to astrocytes and promotes rapidly progressive disease with SOD1-containing inclusions. *Neuron* 18:327-338.

Brujin LI, Houseweart MK, Kato S, Anderson KL, Anderson SD, Ohama E, Reaume AG, Scott RW, Cleveland DW. 1998. Aggregation and motor neuron

toxicity of an ALS-linked SOD1 mutant independent from wild-type SOD1. *Science* 281:1851-1854.

Busuttill RA, Garcia AM, Cabrera C, Rodriguez A, Suh Y, Kim WH, Huang TT, Vijg J. 2005. Organ-specific increase in mutation accumulation and apoptosis rate in CuZn-superoxide dismutase-deficient mice. *Cancer Res* 65:11271-11275.

Butovsky O, et al. 2012. Modulating inflammatory monocytes with a unique microRNA gene signature ameliorates murine ALS. *J Clin Invest* 122:3063-3087.

Calderwood SK, Murshid A, Prince T. 2009. The shock of aging: molecular chaperones and the heat shock response in longevity and aging--a mini-review. *Gerontology* 55:550-558.

Cao X, et al. 2008. Structures of the G85R variant of SOD1 in familial amyotrophic lateral sclerosis. *The Journal of biological chemistry* 283:16169-16177.

Cardin R, Piciocchi M, Bortolami M, Kotsafti A, Barzon L, Lavezzo E, Sinigaglia A, Rodriguez-Castro KI, Rugge M, Farinati F. 2014. Oxidative damage in the progression of chronic liver disease to hepatocellular carcinoma: an intricate pathway. *World J Gastroenterol* 20:3078-3086.

Carri MT, Ferri A, Battistoni A, Famhy L, Gabbianelli R, Poccia F, Rotilio G. 1997. Expression of a Cu,Zn superoxide dismutase typical of familial amyotrophic lateral sclerosis induces mitochondrial alteration and increase of cytosolic Ca²⁺ concentration in transfected neuroblastoma SH-SY5Y cells. *FEBS Lett* 414:365-368.

Carri MT, Valle C, Bozzo F, Cozzolino M. 2015. Oxidative stress and mitochondrial damage: importance in non-SOD1 ALS. *Front Cell Neurosci* 9:41.

Chan PK, Chattopadhyay M, Sharma S, Souda P, Gralla EB, Borchelt DR, Whitelegge JP, Valentine JS. 2013. Structural similarity of wild-type and ALS-mutant superoxide dismutase-1 fibrils using limited proteolysis and atomic force microscopy. *Proc Natl Acad Sci U S A* 110:10934-10939.

Chattopadhyay M, Valentine JS. 2009. Aggregation of Copper-Zinc Superoxide Dismutase in Familial and Sporadic ALS. *Antioxid Redox Signal* 11:1603-1614.

Chen T, Benmohamed R, Kim J, Smith K, Amante D, Morimoto RI, Kirsch DR, Ferrante RJ, Silverman RB. 2012a. ADME-guided design and synthesis of aryloxanyl pyrazolone derivatives to block mutant superoxide dismutase 1 (SOD1) cytotoxicity and protein aggregation: potential application for the treatment of amyotrophic lateral sclerosis. *J Med Chem* 55:515-527.

Chen X, Shang H, Qiu X, Fujiwara N, Cui L, Li XM, Gao TM, Kong J. 2012b. Oxidative modification of cysteine 111 promotes disulfide bond-independent aggregation of SOD1. *Neurochemical research* 37:835-845.

Christen Y. 2000. Oxidative stress and Alzheimer disease. *Am J Clin Nutr* 71:621S-629S.

Cimini V, Ruggiero G, Buonomo T, Seru R, Sciorio S, Zanzi C, Santangelo F, Mondola P. 2002. CuZn-superoxide dismutase in human thymus: immunocytochemical localisation and secretion in thymus-derived epithelial and fibroblast cell lines. *Histochem Cell Biol* 118:163-169.

Coelho T, et al. 2013. Long-term effects of tafamidis for the treatment of transthyretin familial amyloid polyneuropathy. *J Neurol* 260:2802-2814.

Cova E, Cereda C, Galli A, Curti D, Finotti C, Di Poto C, Corato M, Mazzini G, Ceroni M. 2006. Modified expression of Bcl-2 and SOD1 proteins in lymphocytes from sporadic ALS patients. *Neurosci Lett* 399:186-190.

Cruts M, Gijselinck I, Van Langenhove T, van der Zee J, Van Broeckhoven C. 2013. Current insights into the C9orf72 repeat expansion diseases of the FTL/ALS spectrum. *Trends in neurosciences*.

Cuervo AM. 2008. Autophagy and aging: keeping that old broom working. *Trends Genet* 24:604-612.

Cuervo AM, Dice JF. 2000. Age-related decline in chaperone-mediated autophagy. *The Journal of biological chemistry* 275:31505-31513.

Curti D, Malaspina A, Facchetti G, Camana C, Mazzini L, Tosca P, Zerbi F, Ceroni M. 1996. Amyotrophic lateral sclerosis: oxidative energy metabolism and calcium homeostasis in peripheral blood lymphocytes. *Neurology* 47:1060-1064.

Dal Canto MC, Gurney ME. 1995. Neuropathological changes in two lines of mice carrying a transgene for mutant human Cu,Zn SOD, and in mice

overexpressing wild type human SOD: a model of familial amyotrophic lateral sclerosis (FALS). *Brain Res* 676:25-40.

Dal Canto MC, Gurney ME. 1997. A low expressor line of transgenic mice carrying a mutant human Cu,Zn superoxide dismutase (SOD1) gene develops pathological changes that most closely resemble those in human amyotrophic lateral sclerosis. *Acta Neuropathol* 93:537-550.

Danbolt NC, Storm-Mathisen J, Kanner BI. 1992. An [Na⁺ + K⁺]coupled L-glutamate transporter purified from rat brain is located in glial cell processes. *Neuroscience* 51:295-310.

Danielsson J, Awad W, Saraboji K, Kurnik M, Lang L, Leinartaite L, Marklund SL, Logan DT, Oliveberg M. 2013. Global structural motions from the strain of a single hydrogen bond. *Proc Natl Acad Sci U S A* 110:3829-3834.

Danielsson J, Kurnik M, Lang L, Oliveberg M. 2011. Cutting off functional loops from homodimeric enzyme superoxide dismutase 1 (SOD1) leaves monomeric beta-barrels. *The Journal of biological chemistry* 286:33070-33083.

de Beus MD, Chung J, Colon W. 2004. Modification of cysteine 111 in Cu/Zn superoxide dismutase results in altered spectroscopic and biophysical properties. *Protein science : a publication of the Protein Society* 13:1347-1355.

De Vos KJ, et al. 2007. Familial amyotrophic lateral sclerosis-linked SOD1 mutants perturb fast axonal transport to reduce axonal mitochondria content. *Hum Mol Genet* 16:2720-2728.

Dean RT, Wolff SP, McElligott MA. 1989. Histidine and proline are important sites of free radical damage to proteins. *Free Radic Res Commun* 7:97-103.

Dejesus-Hernandez M, et al. 2011. Expanded GGGGCC Hexanucleotide Repeat in Noncoding Region of C9ORF72 Causes Chromosome 9p-Linked FTD and ALS. *Neuron* 72:245-256.

Deng HX, et al. 2006. Conversion to the amyotrophic lateral sclerosis phenotype is associated with intermolecular linked insoluble aggregates of SOD1 in mitochondria. *Proc Natl Acad Sci U S A* 103:7142-7147.

Di Giorgio FP, Boulting GL, Bobrowicz S, Eggan KC. 2008. Human embryonic stem cell-derived motor neurons are sensitive to the toxic effect of glial cells carrying an ALS-causing mutation. *Cell Stem Cell* 3:637-648.

Di Giorgio FP, Carrasco MA, Siao MC, Maniatis T, Eggan K. 2007. Non-cell autonomous effect of glia on motor neurons in an embryonic stem cell-based ALS model. *Nat Neurosci* 10:608-614.

Ding F, Dokholyan NV. 2008. Dynamical roles of metal ions and the disulfide bond in Cu, Zn superoxide dismutase folding and aggregation. *Proceedings of the National Academy of Sciences of the United States of America* 105:19696-19701.

Dirren E, Aebischer J, Rochat C, Towne C, Schneider BL, Aebischer P. 2015. SOD1 silencing in motoneurons or glia rescues neuromuscular function in ALS mice. *Ann Clin Transl Neurol* 2:167-184.

Dobrowolny G, et al. 2008. Skeletal muscle is a primary target of SOD1G93A-mediated toxicity. *Cell Metab* 8:425-436.

Drachman DB, Frank K, Dykes-Hoberg M, Teismann P, Almer G, Przedborski S, Rothstein JD. 2002. Cyclooxygenase 2 inhibition protects motor neurons and prolongs survival in a transgenic mouse model of ALS. *Annals of neurology* 52:771-778.

Durazo A, Shaw BF, Chattopadhyay M, Faull KF, Nersissian AM, Valentine JS, Whitelegge JP. 2009. Metal-free superoxide dismutase-1 and three different ALS variants share a similar partially unfolded {beta}-barrel at physiological temperature. *The Journal of biological chemistry* 284:34382-34389.

Durham HD, Roy J, Dong L, Figlewicz DA. 1997. Aggregation of mutant Cu/Zn superoxide dismutase proteins in a culture model of ALS. *J Neuropathol Exp Neurol* 56:523-530.

Elam JS, et al. 2003. Amyloid-like filaments and water-filled nanotubes formed by SOD1 mutant proteins linked to familial ALS. *Nature structural biology* 10:461-467.

Elchuri S, Oberley TD, Qi W, Eisenstein RS, Jackson Roberts L, Van Remmen H, Epstein CJ, Huang TT. 2005. CuZnSOD deficiency leads to persistent and

widespread oxidative damage and hepatocarcinogenesis later in life. *Oncogene* 24:367-380.

Ermilova IP, Ermilov VB, Levy M, Ho E, Pereira C, Beckman JS. 2005. Protection by dietary zinc in ALS mutant G93A SOD transgenic mice. *Neurosci Lett* 379:42-46.

Estevez AG, Crow JP, Sampson JB, Reiter C, Zhuang Y, Richardson GJ, Tarpey MM, Barbeito L, Beckman JS. 1999. Induction of nitric oxide-dependent apoptosis in motor neurons by zinc-deficient superoxide dismutase. *Science* 286:2498-2500.

Ezzi SA, Urushitani M, Julien JP. 2007. Wild-type superoxide dismutase acquires binding and toxic properties of ALS-linked mutant forms through oxidation. *J Neurochem* 102:170-178.

Farr GW, Ying Z, Fenton WA, Horwich AL. 2011. Hydrogen-deuterium exchange in vivo to measure turnover of an ALS-associated mutant SOD1 protein in spinal cord of mice. *Protein science : a publication of the Protein Society* 20:1692-1696.

Ferrucci M, Fulceri F, Toti L, Soldani P, Siciliano G, Paparelli A, Fornai F. 2011. Protein clearing pathways in ALS. *Arch Ital Biol* 149:121-149.

Fiala M, et al. 2010. IL-17A is increased in the serum and in spinal cord CD8 and mast cells of ALS patients. *J Neuroinflammation* 7:76.

Forman HJ, Fridovich I. 1973. On the stability of bovine superoxide dismutase. The effects of metals. *The Journal of biological chemistry* 248:2645-2649.

Forsberg K, Andersen PM, Marklund SL, Brannstrom T. 2011. Glial nuclear aggregates of superoxide dismutase-1 are regularly present in patients with amyotrophic lateral sclerosis. *Acta neuropathologica* 121:623-634.

Forsberg K, Jonsson PA, Andersen PM, Bergemalm D, Graffmo KS, Hultdin M, Jacobsson J, Rosquist R, Marklund SL, Brannstrom T. 2010. Novel antibodies reveal inclusions containing non-native SOD1 in sporadic ALS patients. *PLoS One* 5:e11552.

Fucci L, Oliver CN, Coon MJ, Stadtman ER. 1983. Inactivation of key metabolic enzymes by mixed-function oxidation reactions: possible implication in protein turnover and ageing. *Proc Natl Acad Sci U S A* 80:1521-1525.

Fujisawa T, et al. 2012. A novel monoclonal antibody reveals a conformational alteration shared by amyotrophic lateral sclerosis-linked SOD1 mutants. *Annals of neurology* 72:739-749.

Fujiwara N, Nakano M, Kato S, Yoshihara D, Ookawara T, Eguchi H, Taniguchi N, Suzuki K. 2007. Oxidative modification to cysteine sulfonic acid of Cys111 in human copper-zinc superoxide dismutase. *The Journal of biological chemistry* 282:35933-35944.

Fukai T, Ushio-Fukai M. 2011. Superoxide dismutases: role in redox signaling, vascular function, and diseases. *Antioxid Redox Signal* 15:1583-1606.

Furukawa Y, Fu R, Deng HX, Siddique T, O'Halloran TV. 2006. Disulfide cross-linked protein represents a significant fraction of ALS-associated Cu, Zn-superoxide dismutase aggregates in spinal cords of model mice. *Proc Natl Acad Sci U S A* 103:7148-7153.

Furukawa Y, Kaneko K, Yamanaka K, Nukina N. 2010. Mutation-dependent polymorphism of Cu,Zn-superoxide dismutase aggregates in the familial form of amyotrophic lateral sclerosis. *The Journal of biological chemistry* 285:22221-22231.

Furukawa Y, Kaneko K, Yamanaka K, O'Halloran TV, Nukina N. 2008. Complete loss of post-translational modifications triggers fibrillar aggregation of SOD1 in the familial form of amyotrophic lateral sclerosis. *The Journal of biological chemistry* 283:24167-24176.

Furukawa Y, O'Halloran TV. 2005. Amyotrophic lateral sclerosis mutations have the greatest destabilizing effect on the apo- and reduced form of SOD1, leading to unfolding and oxidative aggregation. *The Journal of biological chemistry* 280:17266-17274.

Furukawa Y, Torres AS, O'Halloran TV. 2004. Oxygen-induced maturation of SOD1: a key role for disulfide formation by the copper chaperone CCS. *The EMBO journal* 23:2872-2881.

Gagliardi S, et al. 2010. SOD1 mRNA expression in sporadic amyotrophic lateral sclerosis. *Neurobiol Dis* 39:198-203.

Gal J, Chen J, Barnett KR, Yang L, Brumley E, Zhu H. 2013. HDAC6 regulates mutant SOD1 aggregation through two SMIR motifs and tubulin acetylation. *The Journal of biological chemistry* 288:15035-15045.

Galaleldeen A, Strange RW, Whitson LJ, Antonyuk SV, Narayana N, Taylor AB, Schuermann JP, Holloway SP, Hasnain SS, Hart PJ. 2009. Structural and biophysical properties of metal-free pathogenic SOD1 mutants A4V and G93A. *Archives of biochemistry and biophysics* 492:40-47.

Ganesan S, et al. 2008. Mutant SOD1 detoxification mechanisms in intact single cells. *Cell Death Differ* 15:312-321.

Georgiou G. 2002. How to flip the (redox) switch. *Cell* 111:607-610.

Gilgun-Sherki Y, Melamed E, Offen D. 2004. The role of oxidative stress in the pathogenesis of multiple sclerosis: the need for effective antioxidant therapy. *J Neurol* 251:261-268.

Gong YH, Parsadanian AS, Andreeva A, Snider WD, Elliott JL. 2000. Restricted expression of G86R Cu/Zn superoxide dismutase in astrocytes results in astrocytosis but does not cause motoneuron degeneration. *J Neurosci* 20:660-665.

Gordon PH, et al. 2007. Efficacy of minocycline in patients with amyotrophic lateral sclerosis: a phase III randomised trial. *Lancet Neurol* 6:1045-1053.

Gorrie GH, et al. 2014. Dendritic spinopathy in transgenic mice expressing ALS/dementia-linked mutant UBQLN2. *Proc Natl Acad Sci U S A* 111:14524-14529.

Grad LI, et al. 2011. Intermolecular transmission of superoxide dismutase 1 misfolding in living cells. *Proceedings of the National Academy of Sciences of the United States of America* 108:16398-16403.

Grad LI, et al. 2014. Intercellular propagated misfolding of wild-type Cu/Zn superoxide dismutase occurs via exosome-dependent and -independent mechanisms. *Proc Natl Acad Sci U S A* 111:3620-3625.

Graeber MB. 2010. Changing face of microglia. *Science* 330:783-788.

Graffmo KS, Forsberg K, Bergh J, Birve A, Zetterstrom P, Andersen PM, Marklund SL, Brannstrom T. 2013. Expression of wild-type human superoxide dismutase-1 in mice causes amyotrophic lateral sclerosis. *Human molecular genetics* 22:51-60.

Greenfield NJ. 2006. Using circular dichroism spectra to estimate protein secondary structure. *Nat Protoc* 1:2876-2890.

Gros-Louis F, Soucy G, Lariviere R, Julien JP. 2010. Intracerebroventricular infusion of monoclonal antibody or its derived Fab fragment against misfolded forms of SOD1 mutant delays mortality in a mouse model of ALS. *J Neurochem* 113:1188-1199.

Guareschi S, Cova E, Cereda C, Ceroni M, Donetti E, Bosco DA, Trotti D, Pasinelli P. 2012. An over-oxidized form of superoxide dismutase found in sporadic amyotrophic lateral sclerosis with bulbar onset shares a toxic mechanism with mutant SOD1. *Proc Natl Acad Sci U S A* 109:5074-5079.

Gurney ME, et al. 1994. Motor neuron degeneration in mice that express a human Cu,Zn superoxide dismutase mutation. *Science* 264:1772-1775.

Haidet-Phillips AM, et al. 2011. Astrocytes from familial and sporadic ALS patients are toxic to motor neurons. *Nature biotechnology* 29:824-828.

Haley RW. 2003a. Excess incidence of ALS in young Gulf War veterans. *Neurology* 61:750-756.

Haley RW. 2003b. Gulf war syndrome: narrowing the possibilities. *Lancet Neurol* 2:272-273.

Haley RW, Billecke S, La Du BN. 1999. Association of low PON1 type Q (type A) arylesterase activity with neurologic symptom complexes in Gulf War veterans. *Toxicol Appl Pharmacol* 157:227-233.

Handy CR, Krudy C, Boulis N, Federici T. 2011. Pain in amyotrophic lateral sclerosis: a neglected aspect of disease. *Neurol Res Int* 2011:403808.

Harper S, Speicher DW. 2011. Purification of proteins fused to glutathione S-transferase. *Methods Mol Biol* 681:259-280.

Harras MM, et al. 2008. SOD1 mutations disrupt redox-sensitive Rac regulation of NADPH oxidase in a familial ALS model. *The Journal of clinical investigation* 118:659-670.

Hart PJ, Liu H, Pellegrini M, Nersissian AM, Gralla EB, Valentine JS, Eisenberg D. 1998. Subunit asymmetry in the three-dimensional structure of a human CuZnSOD mutant found in familial amyotrophic lateral sclerosis. *Protein science : a publication of the Protein Society* 7:545-555.

Hayward LJ, Rodriguez JA, Kim JW, Tiwari A, Goto JJ, Cabelli DE, Valentine JS, Brown RH, Jr. 2002. Decreased metallation and activity in subsets of mutant superoxide dismutases associated with familial amyotrophic lateral sclerosis. *The Journal of biological chemistry* 277:15923-15931.

Ho YS, Gargano M, Cao J, Bronson RT, Heimler I, Hutz RJ. 1998. Reduced fertility in female mice lacking copper-zinc superoxide dismutase. *The Journal of biological chemistry* 273:7765-7769.

Homma K, Fujisawa T, Tsuburaya N, Yamaguchi N, Kadowaki H, Takeda K, Nishitoh H, Matsuzawa A, Naguro I, Ichijo H. 2013. SOD1 as a molecular switch for initiating the homeostatic ER stress response under zinc deficiency. *Mol Cell* 52:75-86.

Hornberg A, Logan DT, Marklund SL, Oliveberg M. 2007. The coupling between disulphide status, metallation and dimer interface strength in Cu/Zn superoxide dismutase. *J Mol Biol* 365:333-342.

Horner RD, et al. 2003. Occurrence of amyotrophic lateral sclerosis among Gulf War veterans. *Neurology* 61:742-749.

Hough MA, et al. 2004. Dimer destabilization in superoxide dismutase may result in disease-causing properties: structures of motor neuron disease mutants. *Proc Natl Acad Sci U S A* 101:5976-5981.

Johnson BS, Snead D, Lee JJ, McCaffery JM, Shorter J, Gitler AD. 2009. TDP-43 is intrinsically aggregation-prone, and amyotrophic lateral sclerosis-linked mutations accelerate aggregation and increase toxicity. *The Journal of biological chemistry* 284:20329-20339.

Johnston JA, Dalton MJ, Gurney ME, Kopito RR. 2000. Formation of high molecular weight complexes of mutant Cu, Zn-superoxide dismutase in a mouse

model for familial amyotrophic lateral sclerosis. *Proc Natl Acad Sci U S A* 97:12571-12576.

Jonsson PA, Ernhill K, Andersen PM, Bergemalm D, Brannstrom T, Gredal O, Nilsson P, Marklund SL. 2004. Minute quantities of misfolded mutant superoxide dismutase-1 cause amyotrophic lateral sclerosis. *Brain* 127:73-88.

Kabashi E, Agar JN, Strong MJ, Durham HD. 2012. Impaired proteasome function in sporadic amyotrophic lateral sclerosis. *Amyotroph Lateral Scler* 13:367-371.

Kabashi E, Agar JN, Taylor DM, Minotti S, Durham HD. 2004. Focal dysfunction of the proteasome: a pathogenic factor in a mouse model of amyotrophic lateral sclerosis. *J Neurochem* 89:1325-1335.

Kabashi E, Valdmanis PN, Dion P, Rouleau GA. 2007. Oxidized/misfolded superoxide dismutase-1: the cause of all amyotrophic lateral sclerosis? *Annals of neurology* 62:553-559.

Kabuta T, Suzuki Y, Wada K. 2006. Degradation of amyotrophic lateral sclerosis-linked mutant Cu,Zn-superoxide dismutase proteins by macroautophagy and the proteasome. *The Journal of biological chemistry* 281:30524-30533.

Kawamata T, Akiyama H, Yamada T, McGeer PL. 1992. Immunologic reactions in amyotrophic lateral sclerosis brain and spinal cord tissue. *Am J Pathol* 140:691-707.

Kayatekin C, Zitzewitz JA, Matthews CR. 2008. Zinc binding modulates the entire folding free energy surface of human Cu,Zn superoxide dismutase. *Journal of molecular biology* 384:540-555.

Kayatekin C, Zitzewitz JA, Matthews CR. 2010. Disulfide-reduced ALS variants of Cu, Zn superoxide dismutase exhibit increased populations of unfolded species. *Journal of molecular biology* 398:320-331.

Kerman A, Liu HN, Croul S, Bilbao J, Rogaeva E, Zinman L, Robertson J, Chakrabartty A. 2010. Amyotrophic lateral sclerosis is a non-amyloid disease in which extensive misfolding of SOD1 is unique to the familial form. *Acta Neuropathol* 119:335-344.

Kieran D, Hafezparast M, Bohnert S, Dick JR, Martin J, Schiavo G, Fisher EM, Greensmith L. 2005. A mutation in dynein rescues axonal transport defects and extends the life span of ALS mice. *J Cell Biol* 169:561-567.

Kieran D, Kalmar B, Dick JR, Riddoch-Contreras J, Burnstock G, Greensmith L. 2004. Treatment with arimoclolmol, a coinducer of heat shock proteins, delays disease progression in ALS mice. *Nat Med* 10:402-405.

Kiernan MC, Vucic S, Cheah BC, Turner MR, Eisen A, Hardiman O, Burrell JR, Zoing MC. 2011. Amyotrophic lateral sclerosis. *Lancet* 377:942-955.

Kim JW, Sahm H, You J, Wang M. 2010. Knock-down of superoxide dismutase 1 sensitizes cisplatin-resistant human ovarian cancer cells. *Anticancer Res* 30:2577-2581.

Kitamura A, Inada N, Kubota H, Matsumoto G, Kinjo M, Morimoto RI, Nagata K. 2014. Dysregulation of the proteasome increases the toxicity of ALS-linked mutant SOD1. *Genes Cells* 19:209-224.

Kostic V, Jackson-Lewis V, de Bilbao F, Dubois-Dauphin M, Przedborski S. 1997. Bcl-2: prolonging life in a transgenic mouse model of familial amyotrophic lateral sclerosis. *Science* 277:559-562.

Kriz J, Nguyen MD, Julien JP. 2002. Minocycline slows disease progression in a mouse model of amyotrophic lateral sclerosis. *Neurobiol Dis* 10:268-278.

Kuhle J, Lindberg RL, Regeniter A, Mehling M, Steck AJ, Kappos L, Czaplinski A. 2009. Increased levels of inflammatory chemokines in amyotrophic lateral sclerosis. *Eur J Neurol* 16:771-774.

Kurahashi T, Miyazaki A, Suwan S, Isobe M. 2001. Extensive investigations on oxidized amino acid residues in H₂O₂-treated Cu,Zn-SOD protein with LC-ESI-Q-TOF-MS, MS/MS for the determination of the copper-binding site. *J Am Chem Soc* 123:9268-9278.

Kuwahara S, Sato Y. 2013. [Retired American football players have a four times higher chance of getting Alzheimer disease or amyotrophic lateral sclerosis]. *Brain Nerve* 65:996-997.

Kwiatkowski TJ, Jr., et al. 2009. Mutations in the FUS/TLS gene on chromosome 16 cause familial amyotrophic lateral sclerosis. *Science* 323:1205-1208.

Lee DY, Brown EJ. 2012. Ubiquilins in the crosstalk among proteolytic pathways. *Biol Chem* 393:441-447.

Lehman EJ, Hein MJ, Baron SL, Gersic CM. 2012. Neurodegenerative causes of death among retired National Football League players. *Neurology* 79:1970-1974.

Lemire J, Mailloux R, Appanna VD. 2008. Zinc toxicity alters mitochondrial metabolism and leads to decreased ATP production in hepatocytes. *J Appl Toxicol* 28:175-182.

Liao B, Zhao W, Beers DR, Henkel JS, Appel SH. 2012. Transformation from a neuroprotective to a neurotoxic microglial phenotype in a mouse model of ALS. *Exp Neurol* 237:147-152.

Limpert AS, Mattmann ME, Cosford ND. 2013. Recent progress in the discovery of small molecules for the treatment of amyotrophic lateral sclerosis (ALS). *Beilstein J Org Chem* 9:717-732.

Lin CL, Bristol LA, Jin L, Dykes-Hoberg M, Crawford T, Clawson L, Rothstein JD. 1998. Aberrant RNA processing in a neurodegenerative disease: the cause for absent EAAT2, a glutamate transporter, in amyotrophic lateral sclerosis. *Neuron* 20:589-602.

Lindberg MJ, Normark J, Holmgren A, Oliveberg M. 2004. Folding of human superoxide dismutase: disulfide reduction prevents dimerization and produces marginally stable monomers. *Proc Natl Acad Sci U S A* 101:15893-15898.

Liu HN, Sanelli T, Horne P, Piro EP, Strong MJ, Rogaeva E, Bilbao J, Zinman L, Robertson J. 2009. Lack of evidence of monomer/misfolded superoxide dismutase-1 in sporadic amyotrophic lateral sclerosis. *Annals of neurology* 66:75-80.

Liu HN, Tjostheim S, Dasilva K, Taylor D, Zhao B, Rakhit R, Brown M, Chakrabarty A, McLaurin J, Robertson J. 2012. Targeting of monomer/misfolded SOD1 as a therapeutic strategy for amyotrophic lateral sclerosis. *J Neurosci* 32:8791-8799.

Lynch SM, Boswell SA, Colon W. 2004. Kinetic stability of Cu/Zn superoxide dismutase is dependent on its metal ligands: implications for ALS. *Biochemistry* 43:16525-16531.

Mackenzie IR, Feldman HH. 2005. Ubiquitin immunohistochemistry suggests classic motor neuron disease, motor neuron disease with dementia, and frontotemporal dementia of the motor neuron disease type represent a clinicopathologic spectrum. *J Neuropathol Exp Neurol* 64:730-739.

Maekawa S, Leigh PN, King A, Jones E, Steele JC, Bodi I, Shaw CE, Hortobagyi T, Al-Sarraj S. 2009. TDP-43 is consistently co-localized with ubiquitinated inclusions in sporadic and Guam amyotrophic lateral sclerosis but not in familial amyotrophic lateral sclerosis with and without SOD1 mutations. *Neuropathology : official journal of the Japanese Society of Neuropathology* 29:672-683.

Mandelkow EM, Schweers O, Drewes G, Biernat J, Gustke N, Trinczek B, Mandelkow E. 1996. Structure, microtubule interactions, and phosphorylation of tau protein. *Annals of the New York Academy of Sciences* 777:96-106.

Mantovani S, Garbelli S, Pasini A, Alimonti D, Perotti C, Melazzini M, Bendotti C, Mora G. 2009. Immune system alterations in sporadic amyotrophic lateral sclerosis patients suggest an ongoing neuroinflammatory process. *Journal of neuroimmunology* 210:73-79.

Martin D, Thompson MA, Nadler JV. 1993. The neuroprotective agent riluzole inhibits release of glutamate and aspartate from slices of hippocampal area CA1. *Eur J Pharmacol* 250:473-476.

Martinez-Vicente M, Sovak G, Cuervo AM. 2005. Protein degradation and aging. *Exp Gerontol* 40:622-633.

Mazzini L, Vercelli A, Mareschi K, Ferrero I, Testa L, Fagioli F. 2009. Mesenchymal stem cells for ALS patients. *Amyotroph Lateral Scler* 10:123-124.

McAlary L, Yerbury JJ, Aquilina JA. 2013. Glutathionylation potentiates benign superoxide dismutase 1 variants to the toxic forms associated with amyotrophic lateral sclerosis. *Sci Rep* 3:3275.

McCord JM, Fridovich I. 1969. Superoxide dismutase. An enzymic function for erythrocyte hemocuprein (hemocuprein). *The Journal of biological chemistry* 244:6049-6055.

Mendonca DM, Chimelli L, Martinez AM. 2006. Expression of ubiquitin and proteasome in motoneurons and astrocytes of spinal cords from patients with amyotrophic lateral sclerosis. *Neurosci Lett* 404:315-319.

Milani P, et al. 2013. Posttranscriptional regulation of SOD1 gene expression under oxidative stress: Potential role of ELAV proteins in sporadic ALS. *Neurobiol Dis* 60:51-60.

Milani P, Gagliardi S, Cova E, Cereda C. 2011. SOD1 Transcriptional and Posttranscriptional Regulation and Its Potential Implications in ALS. *Neurol Res Int* 2011:458427.

Miller RG, Mitchell JD, Moore DH. 2012. Riluzole for amyotrophic lateral sclerosis (ALS)/motor neuron disease (MND). *Cochrane Database Syst Rev* 3:CD001447.

Molnar KS, Karabacak NM, Johnson JL, Wang Q, Tiwari A, Hayward LJ, Coales SJ, Hamuro Y, Agar JN. 2009. A common property of amyotrophic lateral sclerosis-associated variants: Destabilization of the Cu/Zn superoxide dismutase electrostatic loop. *The Journal of biological chemistry* 284:30965-30973.

Mondola P, Annella T, Santillo M, Santangelo F. 1996. Evidence for secretion of cytosolic CuZn superoxide dismutase by Hep G2 cells and human fibroblasts. *Int J Biochem Cell Biol* 28:677-681.

Mondola P, Annella T, Seru R, Santangelo F, Iossa S, Gioielli A, Santillo M. 1998. Secretion and increase of intracellular CuZn superoxide dismutase content in human neuroblastoma SK-N-BE cells subjected to oxidative stress. *Brain Res Bull* 45:517-520.

Mondola P, Ruggiero G, Seru R, Damiano S, Grimaldi S, Garbi C, Monda M, Greco D, Santillo M. 2003. The Cu,Zn superoxide dismutase in neuroblastoma SK-N-BE cells is exported by a microvesicles dependent pathway. *Brain Res Mol Brain Res* 110:45-51.

Mondola P, Santillo M, Seru R, Damiano S, Alvino C, Ruggiero G, Formisano P, Terrazzano G, Secondo A, Annunziato L. 2004. Cu,Zn superoxide dismutase increases intracellular calcium levels via a phospholipase C-protein kinase C pathway in SK-N-BE neuroblastoma cells. *Biochem Biophys Res Commun* 324:887-892.

Morfini G, Pigino G, Szebenyi G, You Y, Pollema S, Brady ST. 2006. JNK mediates pathogenic effects of polyglutamine-expanded androgen receptor on fast axonal transport. *Nat Neurosci* 9:907-916.

- Morfini GA, et al. 2013. Inhibition of Fast Axonal Transport by Pathogenic SOD1 Involves Activation of p38 MAP Kinase. *PLoS One* 8:e65235.
- Morfini GA, et al. 2009. Axonal transport defects in neurodegenerative diseases. *J Neurosci* 29:12776-12786.
- Mulligan VK, Kerman A, Laister RC, Sharda PR, Arslan PE, Chakrabartty A. 2012. Early steps in oxidation-induced SOD1 misfolding: implications for non-amyloid protein aggregation in familial ALS. *J Mol Biol* 421:631-652.
- Munch C, Bertolotti A. 2010. Exposure of hydrophobic surfaces initiates aggregation of diverse ALS-causing superoxide dismutase-1 mutants. *Journal of molecular biology* 399:512-525.
- Munch C, O'Brien J, Bertolotti A. 2011. Prion-like propagation of mutant superoxide dismutase-1 misfolding in neuronal cells. *Proc Natl Acad Sci U S A* 108:3548-3553.
- Nagai M, Re DB, Nagata T, Chalazonitis A, Jessell TM, Wichterle H, Przedborski S. 2007. Astrocytes expressing ALS-linked mutated SOD1 release factors selectively toxic to motor neurons. *Nat Neurosci* 10:615-622.
- Nakamura C, Bromberg M, Bhargava S, Wicks P, Zeng-Treitler Q. 2012. Mining online social network data for biomedical research: a comparison of clinicians' and patients' perceptions about amyotrophic lateral sclerosis treatments. *J Med Internet Res* 14:e90.
- Nakano T, Nakaso K, Nakashima K, Ohama E. 2004. Expression of ubiquitin-binding protein p62 in ubiquitin-immunoreactive intraneuronal inclusions in amyotrophic lateral sclerosis with dementia: analysis of five autopsy cases with broad clinicopathological spectrum. *Acta Neuropathol* 107:359-364.
- Nardo G, Pozzi S, Mantovani S, Garbelli S, Marinou K, Basso M, Mora G, Bendotti C, Bonetto V. 2009. Nitroproteomics of peripheral blood mononuclear cells from patients and a rat model of ALS. *Antioxid Redox Signal* 11:1559-1567.
- Neumann M, et al. 2006. Ubiquitinated TDP-43 in frontotemporal lobar degeneration and amyotrophic lateral sclerosis. *Science* 314:130-133.

Nguyen MD, D'Aigle T, Gowing G, Julien JP, Rivest S. 2004. Exacerbation of motor neuron disease by chronic stimulation of innate immunity in a mouse model of amyotrophic lateral sclerosis. *J Neurosci* 24:1340-1349.

Nishitoh H, Kadowaki H, Nagai A, Maruyama T, Yokota T, Fukutomi H, Noguchi T, Matsuzawa A, Takeda K, Ichijo H. 2008. ALS-linked mutant SOD1 induces ER stress- and ASK1-dependent motor neuron death by targeting Derlin-1. *Genes Dev* 22:1451-1464.

Nowak RJ, Cuny GD, Choi S, Lansbury PT, Ray SS. 2010. Improving binding specificity of pharmacological chaperones that target mutant superoxide dismutase-1 linked to familial amyotrophic lateral sclerosis using computational methods. *J Med Chem* 53:2709-2718.

Okado-Matsumoto A, Fridovich I. 2001. Assay of superoxide dismutase: cautions relevant to the use of cytochrome c, a sulfonated tetrazolium, and cyanide. *Anal Biochem* 298:337-342.

Oliver CN, Ahn BW, Moerman EJ, Goldstein S, Stadtman ER. 1987. Age-related changes in oxidized proteins. *The Journal of biological chemistry* 262:5488-5491.

Panchaud A, Singh P, Shaffer SA, Goodlett DR. 2010. xComb: a cross-linked peptide database approach to protein-protein interaction analysis. *J Proteome Res* 9:2508-2515.

Pandya RS, Zhu H, Li W, Bowser R, Friedlander RM, Wang X. 2013. Therapeutic neuroprotective agents for amyotrophic lateral sclerosis. *Cell Mol Life Sci* 70:4729-4745.

Pankiv S, Clausen TH, Lamark T, Brech A, Bruun JA, Outzen H, Overvatn A, Bjorkoy G, Johansen T. 2007. p62/SQSTM1 binds directly to Atg8/LC3 to facilitate degradation of ubiquitinated protein aggregates by autophagy. *The Journal of biological chemistry* 282:24131-24145.

Pardo CA, Xu Z, Borchelt DR, Price DL, Sisodia SS, Cleveland DW. 1995. Superoxide dismutase is an abundant component in cell bodies, dendrites, and axons of motor neurons and in a subset of other neurons. *Proc Natl Acad Sci U S A* 92:954-958.

Pasinelli P, Belford ME, Lennon N, Bacskai BJ, Hyman BT, Trotti D, Brown RH, Jr. 2004. Amyotrophic lateral sclerosis-associated SOD1 mutant proteins bind and aggregate with Bcl-2 in spinal cord mitochondria. *Neuron* 43:19-30.

Patel P, Kriz J, Gravel M, Soucy G, Bareil C, Gravel C, Julien JP. 2013. Adeno-associated Virus-mediated Delivery of a Recombinant Single-chain Antibody Against Misfolded Superoxide Dismutase for Treatment of Amyotrophic Lateral Sclerosis. *Molecular therapy : the journal of the American Society of Gene Therapy*.

Pearce N, Gallo V, McElvenny D. 2015. Head trauma in sport and neurodegenerative disease: an issue whose time has come? *Neurobiol Aging* 36:1383-1389.

Pedrini S, Sau D, Guareschi S, Bogush M, Brown RH, Jr., Naniche N, Kia A, Trotti D, Pasinelli P. 2010. ALS-linked mutant SOD1 damages mitochondria by promoting conformational changes in Bcl-2. *Hum Mol Genet* 19:2974-2986.

Pickles S, Destroismaisons L, Peyrard SL, Cadot S, Rouleau GA, Brown RH, Jr., Julien JP, Arbour N, Velde CV. 2013. Mitochondrial damage revealed by immunoselection for ALS-linked misfolded SOD1. *Human molecular genetics* 22:3947-3959.

Pokrishevsky E, Grad LI, Yousefi M, Wang J, Mackenzie IR, Cashman NR. 2012. Aberrant localization of FUS and TDP43 is associated with misfolding of SOD1 in amyotrophic lateral sclerosis. *PLoS One* 7:e35050.

Polazzi E, Mengoni I, Caprini M, Pena-Altamira E, Kurtys E, Monti B. 2012. Copper-zinc superoxide dismutase (SOD1) is released by microglial cells and confers neuroprotection against 6-OHDA neurotoxicity. *Neurosignals* 21:112-128.

Pollari E, Goldsteins G, Bart G, Koistinaho J, Giniatullin R. 2014. The role of oxidative stress in degeneration of the neuromuscular junction in amyotrophic lateral sclerosis. *Front Cell Neurosci* 8:131.

Polymenidou M, Cleveland DW. 2011. The seeds of neurodegeneration: prion-like spreading in ALS. *Cell* 147:498-508.

Potter SZ, Valentine JS. 2003. The perplexing role of copper-zinc superoxide dismutase in amyotrophic lateral sclerosis (Lou Gehrig's disease). *Journal of*

biological inorganic chemistry : JBIC : a publication of the Society of Biological Inorganic Chemistry 8:373-380.

Poulopoulou C, Davaki P, Koliaraki V, Kolovou D, Markakis I, Vassilopoulos D. 2005. Reduced expression of metabotropic glutamate receptor 2mRNA in T cells of ALS patients. *Annals of neurology* 58:946-949.

Prell T, Lautenschlager J, Witte OW, Carri MT, Grosskreutz J. 2012. The unfolded protein response in models of human mutant G93A amyotrophic lateral sclerosis. *Eur J Neurosci* 35:652-660.

Prudencio M, Borchelt DR. 2011. Superoxide dismutase 1 encoding mutations linked to ALS adopts a spectrum of misfolded states. *Molecular neurodegeneration* 6:77.

Prudencio M, Hart PJ, Borchelt DR, Andersen PM. 2009. Variation in aggregation propensities among ALS-associated variants of SOD1: correlation to human disease. *Hum Mol Genet* 18:3217-3226.

Quan L, Liu M. 2013. CID, ETD and HCD Fragmentation to Study Protein Post-Translational Modifications. *Modern Chemistry and Applications* 1:1-5.

Radunovic A, Mitsumoto H, Leigh PN. 2007. Clinical care of patients with amyotrophic lateral sclerosis. *Lancet Neurol* 6:913-925.

Rae TD, Torres AS, Pufahl RA, O'Halloran TV. 2001. Mechanism of Cu,Zn-superoxide dismutase activation by the human metallochaperone hCCS. *The Journal of biological chemistry* 276:5166-5176.

Rakhit R, Crow JP, Lepock JR, Kondejewski LH, Cashman NR, Chakrabartty A. 2004. Monomeric Cu,Zn-superoxide dismutase is a common misfolding intermediate in the oxidation models of sporadic and familial amyotrophic lateral sclerosis. *The Journal of biological chemistry* 279:15499-15504.

Rakhit R, Cunningham P, Furtos-Matei A, Dahan S, Qi XF, Crow JP, Cashman NR, Kondejewski LH, Chakrabartty A. 2002. Oxidation-induced misfolding and aggregation of superoxide dismutase and its implications for amyotrophic lateral sclerosis. *The Journal of biological chemistry* 277:47551-47556.

Rakhit R, Robertson J, Velde CV, Horne P, Ruth DM, Griffin J, Cleveland DW, Cashman NR, Chakrabartty A. 2007. An immunological epitope selective for pathological monomer-misfolded SOD1 in ALS. *Nat Med* 13:754-759.

Ralph GS, et al. 2005. Silencing mutant SOD1 using RNAi protects against neurodegeneration and extends survival in an ALS model. *Nat Med* 11:429-433.

Ratts RB, Weng NP. 2012. Homeostasis of lymphocytes and monocytes in frequent blood donors. *Front Immunol* 3:271.

Ray SS, Nowak RJ, Brown RH, Jr., Lansbury PT, Jr. 2005. Small-molecule-mediated stabilization of familial amyotrophic lateral sclerosis-linked superoxide dismutase mutants against unfolding and aggregation. *Proc Natl Acad Sci U S A* 102:3639-3644.

Reaume AG, et al. 1996. Motor neurons in Cu/Zn superoxide dismutase-deficient mice develop normally but exhibit enhanced cell death after axonal injury. *Nat Genet* 13:43-47.

Redler RL, Fee L, Fay JM, Caplow M, Dokholyan NV. 2014. Non-native soluble oligomers of Cu/Zn superoxide dismutase (SOD1) contain a conformational epitope linked to cytotoxicity in amyotrophic lateral sclerosis (ALS). *Biochemistry* 53:2423-2432.

Redler RL, Wilcox KC, Proctor EA, Fee L, Caplow M, Dokholyan NV. 2011. Glutathionylation at Cys-111 induces dissociation of wild type and FALS mutant SOD1 dimers. *Biochemistry* 50:7057-7066.

Renton AE, Chio A, Traynor BJ. 2014. State of play in amyotrophic lateral sclerosis genetics. *Nature neuroscience* 17:17-23.

Renton AE, et al. 2011. A Hexanucleotide Repeat Expansion in C9ORF72 Is the Cause of Chromosome 9p21-Linked ALS-FTD. *Neuron* 72:257-268.

Rhee SG. 2006. Cell signaling. H₂O₂, a necessary evil for cell signaling. *Science* 312:1882-1883.

Richardson JS, Richardson DC. 2002. Natural beta-sheet proteins use negative design to avoid edge-to-edge aggregation. *Proc Natl Acad Sci U S A* 99:2754-2759.

Ringholz GM, Appel SH, Bradshaw M, Cooke NA, Mosnik DM, Schulz PE. 2005. Prevalence and patterns of cognitive impairment in sporadic ALS. *Neurology* 65:586-590.

Ripps ME, Huntley GW, Hof PR, Morrison JH, Gordon JW. 1995. Transgenic mice expressing an altered murine superoxide dismutase gene provide an animal model of amyotrophic lateral sclerosis. *Proc Natl Acad Sci U S A* 92:689-693.

Robberecht W, Sapp P, Viaene MK, Rosen D, McKenna-Yasek D, Haines J, Horvitz R, Theys P, Brown R, Jr. 1994. Cu/Zn superoxide dismutase activity in familial and sporadic amyotrophic lateral sclerosis. *J Neurochem* 62:384-387.

Robelin L, Gonzalez De Aguilar JL. 2014. Blood biomarkers for amyotrophic lateral sclerosis: myth or reality? *Biomed Res Int* 2014:525097.

Rodriguez JA, et al. 2005. Destabilization of apoprotein is insufficient to explain Cu,Zn-superoxide dismutase-linked ALS pathogenesis. *Proc Natl Acad Sci U S A* 102:10516-10521.

Rohrer JD, et al. 2015. C9orf72 expansions in frontotemporal dementia and amyotrophic lateral sclerosis. *Lancet Neurol* 14:291-301.

Rosen DR, et al. 1993. Mutations in Cu/Zn superoxide dismutase gene are associated with familial amyotrophic lateral sclerosis. *Nature* 362:59-62.

Rossi D, Brambilla L, Valori CF, Roncoroni C, Crugnola A, Yokota T, Bredesen DE, Volterra A. 2008. Focal degeneration of astrocytes in amyotrophic lateral sclerosis. *Cell Death Differ* 15:1691-1700.

Rothstein JD, et al. 1996. Knockout of glutamate transporters reveals a major role for astroglial transport in excitotoxicity and clearance of glutamate. *Neuron* 16:675-686.

Rothstein JD, Martin LJ, Kuncl RW. 1992. Decreased glutamate transport by the brain and spinal cord in amyotrophic lateral sclerosis. *N Engl J Med* 326:1464-1468.

Rothstein JD, et al. 2005. Beta-lactam antibiotics offer neuroprotection by increasing glutamate transporter expression. *Nature* 433:73-77.

Rothstein JD, Van Kammen M, Levey AI, Martin LJ, Kurlan RW. 1995. Selective loss of glial glutamate transporter GLT-1 in amyotrophic lateral sclerosis. *Annals of neurology* 38:73-84.

Rotunno MS, Auclair JR, Maniatis S, Shaffer SA, Agar J, Bosco DA. 2014. Identification of a misfolded region in superoxide dismutase 1 that is exposed in amyotrophic lateral sclerosis. *The Journal of biological chemistry* 289:28527-28538.

Rotunno MS, Bosco DA. 2013. An emerging role for misfolded wild-type SOD1 in sporadic ALS pathogenesis. *Front Cell Neurosci* 7:253.

Rubinsztein DC, Gestwicki JE, Murphy LO, Klionsky DJ. 2007. Potential therapeutic applications of autophagy. *Nat Rev Drug Discov* 6:304-312.

Rudick RA, Zirretta DK, Herndon RM. 1982. Clearance of albumin from mouse subarachnoid space: a measure of CSF bulk flow. *J Neurosci Methods* 6:253-259.

Rusina R, Ridzon P, Kulist'ak P, Keller O, Bartos A, Buncova M, Fialova L, Koukolik F, Matej R. 2010. Relationship between ALS and the degree of cognitive impairment, markers of neurodegeneration and predictors for poor outcome. A prospective study. *Eur J Neurol* 17:23-30.

Saccon RA, Bunton-Stasyshyn RK, Fisher EM, Fratta P. 2013. Is SOD1 loss of function involved in amyotrophic lateral sclerosis? *Brain* 136:2342-2358.

Sadan O, et al. 2009. Protective effects of neurotrophic factor-secreting cells in a 6-OHDA rat model of Parkinson disease. *Stem Cells Dev* 18:1179-1190.

Saez I, Vilchez D. 2014. The Mechanistic Links Between Proteasome Activity, Aging and Age-related Diseases. *Curr Genomics* 15:38-51.

Sampson JB, Beckman JS. 2001. Hydrogen peroxide damages the zinc-binding site of zinc-deficient Cu,Zn superoxide dismutase. *Archives of biochemistry and biophysics* 392:8-13.

Sasabe J, Chiba T, Yamada M, Okamoto K, Nishimoto I, Matsuoka M, Aiso S. 2007. D-serine is a key determinant of glutamate toxicity in amyotrophic lateral sclerosis. *The EMBO journal* 26:4149-4159.

Schoneich C. 2000. Mechanisms of metal-catalyzed oxidation of histidine to 2-oxo-histidine in peptides and proteins. *J Pharm Biomed Anal* 21:1093-1097.

Schousboe A, Waagepetersen HS. 2005. Role of astrocytes in glutamate homeostasis: implications for excitotoxicity. *Neurotox Res* 8:221-225.

Seetharaman SV, Prudencio M, Karch C, Holloway SP, Borchelt DR, Hart PJ. 2009. Immature copper-zinc superoxide dismutase and familial amyotrophic lateral sclerosis. *Experimental biology and medicine* 234:1140-1154.

Seibenhener ML, Babu JR, Geetha T, Wong HC, Krishna NR, Wooten MW. 2004. Sequestosome 1/p62 is a polyubiquitin chain binding protein involved in ubiquitin proteasome degradation. *Mol Cell Biol* 24:8055-8068.

Selverstone Valentine J, Doucette PA, Zittin Potter S. 2005. Copper-zinc superoxide dismutase and amyotrophic lateral sclerosis. *Annu Rev Biochem* 74:563-593.

Shaw BF, et al. 2008. Detergent-insoluble aggregates associated with amyotrophic lateral sclerosis in transgenic mice contain primarily full-length, unmodified superoxide dismutase-1. *The Journal of biological chemistry* 283:8340-8350.

Shaw PJ, Forrest V, Ince PG, Richardson JP, Wastell HJ. 1995. CSF and plasma amino acid levels in motor neuron disease: elevation of CSF glutamate in a subset of patients. *Neurodegeneration* 4:209-216.

Shevchenko A, Tomas H, Havlis J, Olsen JV, Mann M. 2006. In-gel digestion for mass spectrometric characterization of proteins and proteomes. *Nat Protoc* 1:2856-2860.

Shi P, Strom AL, Gal J, Zhu H. 2010. Effects of ALS-related SOD1 mutants on dynein- and KIF5-mediated retrograde and anterograde axonal transport. *Biochim Biophys Acta* 1802:707-716.

Shi Y, Rhodes NR, Abdolvahabi A, Kohn T, Cook NP, Marti AA, Shaw BF. 2013. Deamidation of asparagine to aspartate destabilizes Cu, Zn superoxide dismutase, accelerates fibrillization, and mirrors ALS-linked mutations. *J Am Chem Soc* 135:15897-15908.

Shipp EL, Cantini F, Bertini I, Valentine JS, Banci L. 2003. Dynamic properties of the G93A mutant of copper-zinc superoxide dismutase as detected by NMR spectroscopy: implications for the pathology of familial amyotrophic lateral sclerosis. *Biochemistry* 42:1890-1899.

Shringarpure R, Grune T, Mehlhase J, Davies KJ. 2003. Ubiquitin conjugation is not required for the degradation of oxidized proteins by proteasome. *The Journal of biological chemistry* 278:311-318.

Siklos L, Engelhardt JI, Alexianu ME, Gurney ME, Siddique T, Appel SH. 1998. Intracellular calcium parallels motoneuron degeneration in SOD-1 mutant mice. *J Neuropathol Exp Neurol* 57:571-587.

Smith CD, Carney JM, Starke-Reed PE, Oliver CN, Stadtman ER, Floyd RA, Markesbery WR. 1991. Excess brain protein oxidation and enzyme dysfunction in normal aging and in Alzheimer disease. *Proc Natl Acad Sci U S A* 88:10540-10543.

Smith RA, et al. 2006. Antisense oligonucleotide therapy for neurodegenerative disease. *The Journal of clinical investigation* 116:2290-2296.

Song Y, Nagy M, Ni W, Tyagi NK, Fenton WA, Lopez-Giraldez F, Overton JD, Horwich AL, Brady ST. 2013. Molecular chaperone Hsp110 rescues a vesicle transport defect produced by an ALS-associated mutant SOD1 protein in squid axoplasm. *Proceedings of the National Academy of Sciences of the United States of America* 110:5428-5433.

Spasser L, Brik A. 2012. Chemistry and biology of the ubiquitin signal. *Angew Chem Int Ed Engl* 51:6840-6862.

Spreux-Varoquaux O, Bensimon G, Lacomblez L, Salachas F, Pradat PF, Le Forestier N, Marouan A, Dib M, Meininger V. 2002. Glutamate levels in cerebrospinal fluid in amyotrophic lateral sclerosis: a reappraisal using a new HPLC method with coulometric detection in a large cohort of patients. *J Neurol Sci* 193:73-78.

Sreedharan J, et al. 2008. TDP-43 mutations in familial and sporadic amyotrophic lateral sclerosis. *Science* 319:1668-1672.

Sreedharan J, Brown RH, Jr. 2013. Amyotrophic lateral sclerosis: Problems and prospects. *Annals of neurology* 74:309-316.

Stathopoulos PB, Rumfeldt JA, Karbassi F, Siddall CA, Lepock JR, Meiering EM. 2006. Calorimetric analysis of thermodynamic stability and aggregation for apo and holo amyotrophic lateral sclerosis-associated Gly-93 mutants of superoxide dismutase. *The Journal of biological chemistry* 281:6184-6193.

Stathopoulos PB, Rumfeldt JA, Scholz GA, Irani RA, Frey HE, Hallewell RA, Lepock JR, Meiering EM. 2003. Cu/Zn superoxide dismutase mutants associated with amyotrophic lateral sclerosis show enhanced formation of aggregates in vitro. *Proc Natl Acad Sci U S A* 100:7021-7026.

Steinebach OM, Wolterbeek HT. 1993. Effects of zinc on rat hepatoma HTC cells and primary cultured rat hepatocytes. *Toxicol Appl Pharmacol* 118:245-254.

Stewart HG, Mackenzie IR, Eisen A, Brannstrom T, Marklund SL, Andersen PM. 2006. Clinicopathological phenotype of ALS with a novel G72C SOD1 gene mutation mimicking a myopathy. *Muscle Nerve* 33:701-706.

Strange RW, Antonyuk S, Hough MA, Doucette PA, Rodriguez JA, Hart PJ, Hayward LJ, Valentine JS, Hasnain SS. 2003. The structure of holo and metal-deficient wild-type human Cu, Zn superoxide dismutase and its relevance to familial amyotrophic lateral sclerosis. *J Mol Biol* 328:877-891.

Strange RW, Yong CW, Smith W, Hasnain SS. 2007. Molecular dynamics using atomic-resolution structure reveal structural fluctuations that may lead to polymerization of human Cu-Zn superoxide dismutase. *Proc Natl Acad Sci U S A* 104:10040-10044.

Suarez I, Bodega G, Fernandez B. 2002. Glutamine synthetase in brain: effect of ammonia. *Neurochem Int* 41:123-142.

Sun Y, Oberley LW, Oberley TD, Elwell JH, Sierra-Rivera E. 1993. Lowered antioxidant enzymes in spontaneously transformed embryonic mouse liver cells in culture. *Carcinogenesis* 14:1457-1463.

Sundaramoorthy V, Walker AK, Yerbury J, Soo KY, Farg MA, Hoang V, Zeineddine R, Spencer D, Atkin JD. 2013. Extracellular wildtype and mutant SOD1 induces ER-Golgi pathology characteristic of amyotrophic lateral sclerosis in neuronal cells. *Cell Mol Life Sci* 70:4181-4195.

Suzumura A, Mezitis SG, Gonatas NK, Silberberg DH. 1987. MHC antigen expression on bulk isolated macrophage-microglia from newborn mouse brain:

induction of Ia antigen expression by gamma-interferon. *Journal of neuroimmunology* 15:263-278.

Svensson AK, Bilsel O, Kayatekin C, Adefusika JA, Zitzewitz JA, Matthews CR. 2010. Metal-free ALS variants of dimeric human Cu,Zn-superoxide dismutase have enhanced populations of monomeric species. *PLoS One* 5:e10064.

Svensson AK, Bilsel O, Kondrashkina E, Zitzewitz JA, Matthews CR. 2006. Mapping the folding free energy surface for metal-free human Cu,Zn superoxide dismutase. *J Mol Biol* 364:1084-1102.

Takeuchi S, et al. 2010. Induction of protective immunity by vaccination with wild-type apo superoxide dismutase 1 in mutant SOD1 transgenic mice. *J Neuropathol Exp Neurol* 69:1044-1056.

Tanaka K, et al. 1997. Epilepsy and exacerbation of brain injury in mice lacking the glutamate transporter GLT-1. *Science* 276:1699-1702.

Tang X, Seyb KI, Huang M, Schuman ER, Shi P, Zhu H, Glicksman MA. 2012. A high-throughput screening method for small-molecule inhibitors of the aberrant mutant SOD1 and dynein complex interaction. *J Biomol Screen* 17:314-326.

Taylor DM, Gibbs BF, Kabashi E, Minotti S, Durham HD, Agar JN. 2007. Tryptophan 32 potentiates aggregation and cytotoxicity of a copper/zinc superoxide dismutase mutant associated with familial amyotrophic lateral sclerosis. *The Journal of biological chemistry* 282:16329-16335.

Thomsen GM, Gowing G, Svendsen S, Svendsen CN. 2014. The past, present and future of stem cell clinical trials for ALS. *Exp Neurol* 262 Pt B:127-137.

Tikka T, Fiebich BL, Goldsteins G, Keinanen R, Koistinaho J. 2001. Minocycline, a tetracycline derivative, is neuroprotective against excitotoxicity by inhibiting activation and proliferation of microglia. *J Neurosci* 21:2580-2588.

Tiwari A, Liba A, Sohn SH, Seetharaman SV, Bilsel O, Matthews CR, Hart PJ, Valentine JS, Hayward LJ. 2009. Metal deficiency increases aberrant hydrophobicity of mutant superoxide dismutases that cause amyotrophic lateral sclerosis. *The Journal of biological chemistry* 284:27746-27758.

Tiwari A, Xu Z, Hayward LJ. 2005. Aberrantly increased hydrophobicity shared by mutants of Cu,Zn-superoxide dismutase in familial amyotrophic lateral sclerosis. *The Journal of biological chemistry* 280:29771-29779.

Tomkins J, Banner SJ, McDermott CJ, Shaw PJ. 2001. Mutation screening of manganese superoxide dismutase in amyotrophic lateral sclerosis. *Neuroreport* 12:2319-2322.

Traynor BJ, Bruijn L, Conwit R, Beal F, O'Neill G, Fagan SC, Cudkovic ME. 2006. Neuroprotective agents for clinical trials in ALS: a systematic assessment. *Neurology* 67:20-27.

Tsay HJ, Wang P, Wang SL, Ku HH. 2000. Age-associated changes of superoxide dismutase and catalase activities in the rat brain. *J Biomed Sci* 7:466-474.

Turner BJ, Atkin JD, Farg MA, Zang DW, Rembach A, Lopes EC, Patch JD, Hill AF, Cheema SS. 2005. Impaired extracellular secretion of mutant superoxide dismutase 1 associates with neurotoxicity in familial amyotrophic lateral sclerosis. *J Neurosci* 25:108-117.

Turner MR, Abisgold J, Yeates DG, Talbot K, Goldacre MJ. 2010. Head and other physical trauma requiring hospitalisation is not a significant risk factor in the development of ALS. *J Neurol Sci* 288:45-48.

Turner MR, Cagnin A, Turkheimer FE, Miller CC, Shaw CE, Brooks DJ, Leigh PN, Banati RB. 2004. Evidence of widespread cerebral microglial activation in amyotrophic lateral sclerosis: an [¹¹C](R)-PK11195 positron emission tomography study. *Neurobiol Dis* 15:601-609.

Uchida K. 2003. Histidine and lysine as targets of oxidative modification. *Amino Acids* 25:249-257.

Uchida K, Kawakishi S. 1994. Identification of oxidized histidine generated at the active site of Cu,Zn-superoxide dismutase exposed to H₂O₂. Selective generation of 2-oxo-histidine at the histidine 118. *The Journal of biological chemistry* 269:2405-2410.

Urushitani M, Ezzi SA, Julien JP. 2007. Therapeutic effects of immunization with mutant superoxide dismutase in mice models of amyotrophic lateral sclerosis. *Proc Natl Acad Sci U S A* 104:2495-2500.

Urushitani M, Sik A, Sakurai T, Nukina N, Takahashi R, Julien JP. 2006. Chromogranin-mediated secretion of mutant superoxide dismutase proteins linked to amyotrophic lateral sclerosis. *Nat Neurosci* 9:108-118.

Valentine JS, Hart PJ. 2003. Misfolded CuZnSOD and amyotrophic lateral sclerosis. *Proc Natl Acad Sci U S A* 100:3617-3622.

van Blitterswijk M, et al. 2011. Anti-superoxide dismutase antibodies are associated with survival in patients with sporadic amyotrophic lateral sclerosis. *Amyotroph Lateral Scler* 12:430-438.

Van Den Bosch L, Tilkin P, Lemmens G, Robberecht W. 2002. Minocycline delays disease onset and mortality in a transgenic model of ALS. *Neuroreport* 13:1067-1070.

Van Den Bosch L, Van Damme P, Bogaert E, Robberecht W. 2006. The role of excitotoxicity in the pathogenesis of amyotrophic lateral sclerosis. *Biochim Biophys Acta* 1762:1068-1082.

Vance C, et al. 2009. Mutations in FUS, an RNA processing protein, cause familial amyotrophic lateral sclerosis type 6. *Science* 323:1208-1211.

Vande Velde C, Miller TM, Cashman NR, Cleveland DW. 2008. Selective association of misfolded ALS-linked mutant SOD1 with the cytoplasmic face of mitochondria. *Proc Natl Acad Sci U S A* 105:4022-4027.

Vassall KA, Stathopoulos PB, Rumfeldt JA, Lepock JR, Meiering EM. 2006. Equilibrium thermodynamic analysis of amyotrophic lateral sclerosis-associated mutant apo Cu,Zn superoxide dismutases. *Biochemistry* 45:7366-7379.

Vercelli A, Mereuta OM, Garbossa D, Muraca G, Mareschi K, Rustichelli D, Ferrero I, Mazzini L, Madon E, Fagioli F. 2008. Human mesenchymal stem cell transplantation extends survival, improves motor performance and decreases neuroinflammation in mouse model of amyotrophic lateral sclerosis. *Neurobiol Dis* 31:395-405.

von Lewinski F, Keller BU. 2005. Ca²⁺, mitochondria and selective motoneuron vulnerability: implications for ALS. *Trends Neurosci* 28:494-500.

Wainger BJ, et al. 2014. Intrinsic membrane hyperexcitability of amyotrophic lateral sclerosis patient-derived motor neurons. *Cell Rep* 7:1-11.

Wang IF, Guo BS, Liu YC, Wu CC, Yang CH, Tsai KJ, Shen CK. 2012a. Autophagy activators rescue and alleviate pathogenesis of a mouse model with proteinopathies of the TAR DNA-binding protein 43. *Proc Natl Acad Sci U S A* 109:15024-15029.

Wang L, Deng HX, Grisotti G, Zhai H, Siddique T, Roos RP. 2009. Wild-type SOD1 overexpression accelerates disease onset of a G85R SOD1 mouse. *Hum Mol Genet* 18:1642-1651.

Wang L, Grisotti G, Roos RP. 2010. Mutant SOD1 knockdown in all cell types ameliorates disease in G85R SOD1 mice with a limited additional effect over knockdown restricted to motor neurons. *J Neurochem* 113:166-174.

Wang L, Pytel P, Feltri ML, Wrabetz L, Roos RP. 2012b. Selective knockdown of mutant SOD1 in Schwann cells ameliorates disease in G85R mutant SOD1 transgenic mice. *Neurobiol Dis* 48:52-57.

Wang Q, Johnson JL, Agar NY, Agar JN. 2008. Protein aggregation and protein instability govern familial amyotrophic lateral sclerosis patient survival. *PLoS Biol* 6:e170.

Watanabe M, Dykes-Hoberg M, Culotta VC, Price DL, Wong PC, Rothstein JD. 2001. Histological evidence of protein aggregation in mutant SOD1 transgenic mice and in amyotrophic lateral sclerosis neural tissues. *Neurobiol Dis* 8:933-941.

Wijesekera LC, Leigh PN. 2009. Amyotrophic lateral sclerosis. *Orphanet J Rare Dis* 4:3.

Wilcox KC, Zhou L, Jordon JK, Huang Y, Yu Y, Redler RL, Chen X, Caplow M, Dokholyan NV. 2009. Modifications of superoxide dismutase (SOD1) in human erythrocytes: a possible role in amyotrophic lateral sclerosis. *The Journal of biological chemistry* 284:13940-13947.

Williamson TL, Cleveland DW. 1999. Slowing of axonal transport is a very early event in the toxicity of ALS-linked SOD1 mutants to motor neurons. *Nat Neurosci* 2:50-56.

Winer L, et al. 2013. SOD1 in cerebral spinal fluid as a pharmacodynamic marker for antisense oligonucleotide therapy. *JAMA Neurol* 70:201-207.

Witan H, Gorlovoy P, Kaya AM, Koziollek-Drechsler I, Neumann H, Behl C, Clement AM. 2009. Wild-type Cu/Zn superoxide dismutase (SOD1) does not facilitate, but impedes the formation of protein aggregates of amyotrophic lateral sclerosis causing mutant SOD1. *Neurobiology of disease* 36:331-342.

Witan H, Kern A, Koziollek-Drechsler I, Wade R, Behl C, Clement AM. 2008. Heterodimer formation of wild-type and amyotrophic lateral sclerosis-causing mutant Cu/Zn-superoxide dismutase induces toxicity independent of protein aggregation. *Human molecular genetics* 17:1373-1385.

Wojcik C, Rowicka M, Kudlicki A, Nowis D, McConnell E, Kujawa M, DeMartino GN. 2006. Valosin-containing protein (p97) is a regulator of endoplasmic reticulum stress and of the degradation of N-end rule and ubiquitin-fusion degradation pathway substrates in mammalian cells. *Mol Biol Cell* 17:4606-4618.

Wolff SP, Dean RT. 1986. Fragmentation of proteins by free radicals and its effect on their susceptibility to enzymic hydrolysis. *Biochem J* 234:399-403.

Wong M, Martin LJ. 2010. Skeletal muscle-restricted expression of human SOD1 causes motor neuron degeneration in transgenic mice. *Hum Mol Genet* 19:2284-2302.

Wong PC, Waggoner D, Subramaniam JR, Tessarollo L, Bartnikas TB, Culotta VC, Price DL, Rothstein J, Gitlin JD. 2000. Copper chaperone for superoxide dismutase is essential to activate mammalian Cu/Zn superoxide dismutase. *Proc Natl Acad Sci U S A* 97:2886-2891.

Wright GS, Antonyuk SV, Kershaw NM, Strange RW, Samar Hasnain S. 2013. Ligand binding and aggregation of pathogenic SOD1. *Nat Commun* 4:1758.

Wu CH, et al. 2012. Mutations in the profilin 1 gene cause familial amyotrophic lateral sclerosis. *Nature* 488:499-503.

Yamanaka K, Chun SJ, Boillee S, Fujimori-Tonou N, Yamashita H, Gutmann DH, Takahashi R, Misawa H, Cleveland DW. 2008. Astrocytes as determinants of disease progression in inherited amyotrophic lateral sclerosis. *Nat Neurosci* 11:251-253.

Yang YM, et al. 2013. A small molecule screen in stem-cell-derived motor neurons identifies a kinase inhibitor as a candidate therapeutic for ALS. *Cell Stem Cell* 12:713-726.

Yi JH, Hazell AS. 2006. Excitotoxic mechanisms and the role of astrocytic glutamate transporters in traumatic brain injury. *Neurochem Int* 48:394-403.

Yoshida S, Mulder DW, Kurland LT, Chu CP, Okazaki H. 1986. Follow-up study on amyotrophic lateral sclerosis in Rochester, Minn., 1925 through 1984. *Neuroepidemiology* 5:61-70.

Zelko IN, Mariani TJ, Folz RJ. 2002. Superoxide dismutase multigene family: a comparison of the CuZn-SOD (SOD1), Mn-SOD (SOD2), and EC-SOD (SOD3) gene structures, evolution, and expression. *Free radical biology & medicine* 33:337-349.

Zhang B, Tu P, Abtahian F, Trojanowski JQ, Lee VM. 1997. Neurofilaments and orthograde transport are reduced in ventral root axons of transgenic mice that express human SOD1 with a G93A mutation. *J Cell Biol* 139:1307-1315.

Zhang F, Strom AL, Fukada K, Lee S, Hayward LJ, Zhu H. 2007. Interaction between familial amyotrophic lateral sclerosis (ALS)-linked SOD1 mutants and the dynein complex. *The Journal of biological chemistry* 282:16691-16699.

Zhang H, Andrekopoulos C, Joseph J, Chandran K, Karoui H, Crow JP, Kalyanaraman B. 2003. Bicarbonate-dependent peroxidase activity of human Cu,Zn-superoxide dismutase induces covalent aggregation of protein: intermediacy of tryptophan-derived oxidation products. *The Journal of biological chemistry* 278:24078-24089.

Zhang R, Gascon R, Miller RG, Gelinas DF, Mass J, Hadlock K, Jin X, Reis J, Narvaez A, McGrath MS. 2005. Evidence for systemic immune system alterations in sporadic amyotrophic lateral sclerosis (sALS). *Journal of neuroimmunology* 159:215-224.

Zhang R, Miller RG, Gascon R, Champion S, Katz J, Lancero M, Narvaez A, Honrada R, Ruvalcaba D, McGrath MS. 2009. Circulating endotoxin and systemic immune activation in sporadic amyotrophic lateral sclerosis (sALS). *Journal of neuroimmunology* 206:121-124.

Zhang Y, Benmohamed R, Huang H, Chen T, Voisine C, Morimoto RI, Kirsch DR, Silverman RB. 2013. Arylazanylpyrazolone derivatives as inhibitors of mutant superoxide dismutase 1 dependent protein aggregation for the treatment of amyotrophic lateral sclerosis. *J Med Chem* 56:2665-2675.

Zhang Y, Zhao W, Zhang HJ, Domann FE, Oberley LW. 2002. Overexpression of copper zinc superoxide dismutase suppresses human glioma cell growth. *Cancer Res* 62:1205-1212.

Zhao W, Beers DR, Henkel JS, Zhang W, Urushitani M, Julien JP, Appel SH. 2010. Extracellular mutant SOD1 induces microglial-mediated motoneuron injury. *Glia* 58:231-243.

Zhu S, et al. 2002. Minocycline inhibits cytochrome c release and delays progression of amyotrophic lateral sclerosis in mice. *Nature* 417:74-78.